YEDITEPE UNIVERSITY
GRADUATE SCHOOL OF NATURAL AND APPLIED SCIENCES

DEVELOPMENT OF A LOW-COST OPTICAL DEVICE FOR IMAGING LATERAL FLOW NITROCELLULOSE MEMBRANES

A Thesis Submitted
by
Seda Aksoy

In Partial Fulfillment
of the Requirements for the Degree of
Master of Science
in
Biomedical Engineering

Supervisor
Assoc. Prof. Dr. Gökhan Ertaş

Istanbul - 2024

DEVELOPMENT OF A LOW-COST OPTICAL DEVICE FOR IMAGING LATERAL FLOW NITROCELLULOSE MEMBRANES

by

Seda Aksoy

Approved by:

Assoc. Prof. Dr. Gökhan Ertaş
(Yeditepe University) ....
(Thesis Supervisor)

Assoc. Prof. Dr. Bilge Güvenç Tuna ....
(Yeditepe University)

Prof. Dr. Atadan Tunacı
(Istanbul University) ....

DATE OF APPROVAL: ..../..../20...

DECLARATION OF ORIGINALITY

I hereby declare that this thesis is my own work and that all information in this thesis has been obtained and presented following academic rules and ethical conduct. I have fully cited and referenced all material and results as required by these rules and conduct, and this thesis study does not contain any plagiarism. The necessary permissions have been obtained if any material used in the thesis requires copyright. No material from this thesis has been used to award another degree.

To the best of my knowledge and belief, it contains no material previously published or written by another person nor material accepted for the award of any other degree except where due acknowledgment has been made in the text.

I accept all kinds of legal liability that may arise in cases contrary to these situations.

Seda Aksoy

Signature

ABSTRACT

DEVELOPMENT OF A LOW-COST OPTICAL DEVICE FOR IMAGING LATERAL FLOW NITROCELLULOSE MEMBRANES

Lateral flow nitrocellulose membranes are commonly used in full assay designs. They provide a suitable surface for loading the detection particles without decreasing the adsorption ability. In point-of-care applications, various diseases can be detected by an optical reader imaging the fluorescently dyed disease markers. Therefore, there is a need for a low-cost optical reader device for imaging the membranes with fluorescent dyes. In this study, two versions of the optical reader are developed for imaging nitrocellulose membranes, including fluorescein sodium salt and rhodamine B dyes. The preliminary device is mainly composed of a minicomputer, a stand-alone camera, two different power light-emitting diodes matching the spectral characteristics of the dyes, an optical filter, and additional electronic components. The preliminary version underscores the need for further refinements to improve image quality and portability, leading to the development of the final version. The portable final optical reader, powered by the batteries, is designed using a minicomputer with improved features and a high-quality camera. The components of both readers are positioned and housed by the designed mechanical components. Also, the device operation is controlled by the developed graphical user interface. The samples are prepared by loading the different concentration solutions of fluorescein sodium salt and rhodamine B dyes onto the membranes. The prepared samples are imaged in both versions of the optical reader. According to the measured mean intensity values, the green and red channels are the primary channels for fluorescein sodium salt and rhodamine B, respectively. The captured images of the dyes, especially rhodamine B, are partially affected by the excitation lights from the power light-emitting diodes. During the experiments, the environmental conditions that the samples are exposed to, are monitored and recorded from the sensor. The designed compact and lightweight optical reader with the dimensions of $13{\times}14{\times}24 cm^3$ (W×H×L) raises the usability of devices across various settings, from clinical laboratories to field applications. In the future, the optimization of the imaging settings and sample properties, re-imaging of the new samples with unused membranes, and validation of the results will be carried out to improve the reliability and repeatability of the optical reader.

ÖZET

YANAL AKIŞLI NİTROSELÜLOZ MEMBRANLARIN GÖRÜNTÜLENMESİNE YÖNELİK DÜŞÜK MALİYETLİ OPTİK CİHAZIN GELİŞTİRİLMESİ

Yanal akışlı nitroselüloz membranlar, tam tahlil tasarımlarında yaygın olarak kullanılır. Adsorpsiyon kabiliyetini azaltmadan tespit partiküllerinin yüklenmesi için uygun bir yüzey sağlarlar. Bakım noktası uygulamalarında, floresanla boyanmış hastalık hücrelerini görüntüleyen bir optik okuyucu ile çeşitli hastalıklar tespit edilebilir. Bu nedenle floresan boya içeren membranların görüntülenmesi için düşük maliyetli bir optik okuyucu cihazına ihtiyaç duyulmaktadır. Bu çalışmada nitroselüloz membranların görüntülenmesi için floresein sodyum tuzu ve rodamin B boyalarını içeren optik okuyucunun iki versiyonu geliştirilmiştir. Okuyucu cihazın ilk versiyonu temel olarak bir mini bilgisayar, bağımsız bir kamera, boyaların spektral özelliklerine uygun, birbirinden farklı iki güçlü ışık yayan diyot, bir optik filtre ve ek elektronik bileşenlerden oluşur. İlk versiyon, görüntü kalitesini ve taşınabilirliği iyileştirmek için daha fazla iyileştirme yapılması ihtiyacını vurgular ve bu da son sürümün geliştirilmesine yol açar. Pillerle çalışan taşınabilir final optik okuyucu, geliştirilmiş özelliklere sahip bir mini bilgisayar ve yüksek kaliteli bir kamera kullanılarak tasarlanmıştır. Her iki okuyucunun bileşenleri tasarlanan mekanik bileşenler tarafından konumlandırılır ve muhafaza edilir. Ayrıca cihazın çalışması geliştirilen grafiksel kullanıcı arayüzü ile kontrol edilmektedir. Numuneler, floresein sodyum tuzu ve rodamin B boyalarının farklı konsantrasyondaki çözeltilerinin membranlara yüklenmesiyle hazırlanır. Hazırlanan numuneler optik okuyucunun her iki versiyonunda da görüntülenmiştir. Ölçülen ortalama yoğunluk değerlerine göre yeşil ve kırmızı kanallar sırasıyla floresan sodyum tuzu ve rodamin B için birincil kanallardır. Floresan boya görüntüleri uyarma ışıklarından kısmen etkilenir. Deneyler sırasında numunelerin maruz kaldığı ortam koşulları izlenmekte ve kayıt altına alınmaktadır. 13x14x24cm^3 (G×Y×U) boyutlarındaki tasarlanmış kompakt ve hafif optik okuyucu, klinik laboratuvarlardan saha uygulamalarına kadar çeşitli ortamlarda cihazın kullanılabilirlğini arttırır. Gelecek çalışmalarda, görüntüleme ayarlarının ve numune özelliklerinin optimizasyonu, yeni numunelerin kullanılmamış membranlarla yeniden görüntülenmesi ve sonuçların doğrulanması gerçekleştirilecektir.

ACKNOWLEDGEMENTS

I am profoundly grateful for the support and guidance I have received throughout this study. First and foremost, I extend my deepest appreciation to my supervisor, Assoc. Prof. Dr. Gökhan Ertaş, whose expertise, understanding, and patience added considerably to my experience. His willingness to give his time so generously has been very much appreciated. I want to express my sincere gratitude to the Scientific and Technological Research Council of Turkey (TUBITAK) for their support through the 1004 Center of Excellence Support Program (Project ID: 20AG011). This work has been made possible in part by their funding. Special thanks are extended to Prof. Dr. Gülderen Yanıkkaya Demirel, the coordinator of the project, for her invaluable support throughout this research endeavor. I am also grateful to her assistant, Furkan Aydın, for his exceptional assistance, expertise, and guidance in sample preparation processes. Their contributions have been instrumental in the success of this project. I extend my gratitude to Assoc. Prof. Dr. Bilge Güvenç Tuna and her PhD student, Dilara Durdabak for nitrocellulose membrane preparation within the study. I am also thankful to Muhammed Mehdi Menteş, the research assistant at the Department of Biomedical Engineering, Yeditepe University, for his tremendous support and assistance, especially in 3D drawings. I would like to express my gratitude to Gülay Tanik, and Batuhan Akdağcı, for their unwavering support and encouragement throughout this endeavor. Their presence and belief in my work have been a constant source of strength and motivation. Lastly, but certainly not least, I would like to thank my mother and my sister, whose love, support, and encouragement have been my greatest strengths throughout my life.

TABLE OF CONTENTS

LIST OF FIGURES

LIST OF TABLES

LIST OF ABBREVIATIONS

CCD	Charge-coupled device
CMOS	Complementary metal-oxide-semiconductor
CRP	C-reactive protein
CSI	Camera serial interface
CW	Center wavelength
Cy5	Cyanine 5
DSI	Display serial interface
ELISA	Enzyme-linked immunosorbent assay
FITC	Fluorescein isothiocyanate
FoV	Field of view
FS	Fluorescein sodium salt
GND	Ground
GPIO	General purpose input output
GUI	Graphical user interface
hCG	Human chorionic gonadotropin
HDMI	High-definition multimedia interface
I2C	Inter-Integrated Circuit
ISO	International organization for standardization
LED	Light-emitting diode
LFA	Lateral flow immunoassay
NoIR	No-infrared
PLA	Polylactic acid
RB	Rhodamine B
RGB	Red-green-blue
ROI	Region-of-interest
RPM	Rotation per minute
SCL	Serial clock
SDA	Serial data
SMD	Serial-mount device
USB	Universal serial bus

1. INTRODUCTION

Nitrocellulose membrane is commonly used in the lateral flow assays (LFAs) [1]. The membranes are the critical part of the assays since they serve as the reaction area where the analytes, particles, and specific molecules are loaded. They adsorb protein molecules at very high levels and provide a suitable surface for loading particles without decreasing the adsorption ability [2]. The LFAs with nitrocellulose membranes offer improved specificity, versatility, affordability, and sensitivity for the detection of diseases [3]. They are widely employed in environmental monitoring [4], food safety analysis [5], drug testing [6], and medical diagnostics, especially for use in point-of-care applications [7, 8]. The detection particles on the membrane are adapted for the diagnosis of various diseases, including cardiac diseases [9], cancer markers [10, 11], infectious diseases [12-14], as well as genetic diseases [15-16]. The LFAs consisting of nitrocellulose membranes were originally produced for color-based evaluations without an expert or a specialized reader device [17]. This could cause some wrong interpretations or false readings by the user errors. Therefore, the design of a specialized optical reader has been a keen interest in recent years [18,19]. With the help of the readers, the existence or the amount of the target molecules, like a disease marker or fluorescent label, are detected objectively [20]. The optical reader device is designed based on the preferred detection method applied to the membranes [21].

The lateral flow nitrocellulose membranes are imaged using different detection methods such as colorimetric [22], chemiluminescence [23], magnetic interactions [24], surface-enhanced Raman scattering analysis [25], electrochemical [26], and fluorescence [27, 28]. Among them, fluorescence-based imaging is favored for its higher sensitivity [29]. The fluorescent detection label, like nanoparticles, quantum dots, or fluorescent dyes, is selected based on their spectral characteristics, including emission and excitation light wavelengths. Fluorescent dyes are the most popular option for labeling the target molecules on the membranes and can be adapted to any disease-specific molecules for disease detection. Meanwhile, the most commonly voted dyes are obtained by using Fluorescein sodium salt and rhodamine B. The design of the optical reader depends on the spectral characteristics of the selected fluorescent dyes. Each fluorescent dye emits a fluorescence light of a specific wavelength when exposed to a light of a different specific wavelength [30]. Therefore, the main components of an optical reader are a light source and a light detector for imaging the fluorescent dyes. A stable and well-controlled light source ensures adequate excitation of the fluorescent dye and enhanced fluorescence emission [31]. Meanwhile, a fine-tuned light detector with good sensitivity ensures the detection of the light emitted by the dye. A photodiode, photomultiplier tube, or camera can be used as a light detector. Photodiodes or photomultiplier tubes offer single-point measurements and are limited in their spatial resolution while the cameras are more versatile and user-friendly approaches [32]. The camera-based optical reader can perform rapid, multiple, and efficient detection of different fluorescent dyes by simultaneously imaging the entire membrane [33]. Smartphone cameras are a popular choice, but they vary widely in terms of sensor size, resolution, and lens quality, and not all camera settings can be controlled or standardized across different smartphones [34, 35]. Therefore, the reproducibility, consistency, and reliability of the membrane imaging results can be affected. Additionally, the data extraction from images captured is very limited, as the smartphones are designed for general photography and they need to be optimized for specific requirements for the imaging of fluorescent dye-loaded membranes [36]. In contrast, standalone camera-based optical readers are finely tuned and programmed for specific imaging requirements, offering greater control over the imaging settings and data analysis capabilities [37-41].

This study aims the development a low-cost standalone optical reader housing a camera for imaging the membranes, two power LEDs for excitation of the different concentration levels of fluorescein sodium salt and rhodamine B dyes, an optical dual band-pass filter for imaging of the fluorescent dyes, mechanical components for appropriate positioning of the LEDs, camera, filter and additional electronics. During imaging, the environmental conditions that the membranes are being exposed to are monitored by the reader. Software is also developed to present a graphical user interface for guiding the user, controlling the operation of the reader, and setting the imaging parameters. The key contributions of this study are explained as follows:

- A low-cost, portable, and compact optical reader that eliminates the need for complex instrumentation, unlike the conventional readers that are comparably expensive and need a laboratory environment for operation.

- Use of power LEDs as the light source eliminates the need for complex instrumentation, unlike the readers that house lasers.

- Use of a dedicated dual band-pass filter to simply optical filtering in imaging the fluorescein sodium salt and rhodamine B dyes, unlike the conventional readers that house more complex and larger filtering setups.

- Use of dedicated software, not only to operate the reader as of conventional readers, but also to guide the user during imaging, to present different settings for making, and to inform the user about the environmental conditions that the sample is exposed to.

- Use of a very advanced but low-cost minicomputer, not only to control the operation of the reader but also to make the reader possible to serve as an internet of things or a cloud-based system enabling transfer of imaging results via Bluetooth or an internet connection to a designated server.

2. BACKGROUND INFORMATION

This section provides an overview of the fundamental concepts relevant to the development and applications of lateral flow assays and optical readers discussed in this thesis. Typical design of fluorescence-based optical readers is further investigated.

2.1. LATERAL FLOW ASSAYS

Lateral flow assays (LFAs) emerged in the late 1960s, were used for monitoring serum proteins, and later adapted in 1976 for detecting human chorionic gonadotropin produced during pregnancy in urine for human pregnancy tests. The LFA technology has evolved since the early 1980s [42-44]. Recently, LFAs have been widely used for their simplicity, portability, rapidity, and cost-effectiveness without the need for specialized equipment or trained personnel [45, 46]. These assays are produced using either nucleic acids or antibodies as recognition elements and rely on specific antibody-antigen interactions since they utilize antibodies for the detection target [47]. They are extensively employed in medical diagnostics and point-of-care test kits for detecting drugs [48-50], vitamins [51, 52], hormones [53], diseases [54], viruses [55-57], cancer markers [58], and mycotoxins [91]. Moreover, they can be adapted to diverse platforms like spectroscopy [59] and electrochemistry [60], enabling quantitative measurements. These advancements are steering LFAs towards becoming versatile platforms capable of delivering accurate results akin to lab-based technologies while retaining simplicity, portability, affordability, and rapid testing advantages.

2.1.1. Structure

An LFA is composed of several overlapping components: a sample pad, conjugation pad, nitrocellulose membrane, and absorbent pad (see Figure 2.1). The porous sample, conjugate, and absorbent pads require a backing to be in line with the nitrocellulose membrane and need accurate bed volume and thickness adjustment for housing the sample. On the nitrocellulose membrane, there exists a test line (T) to detect the presence of the target analyte, and a control line (C) to validate the correct functioning of the assay [61].

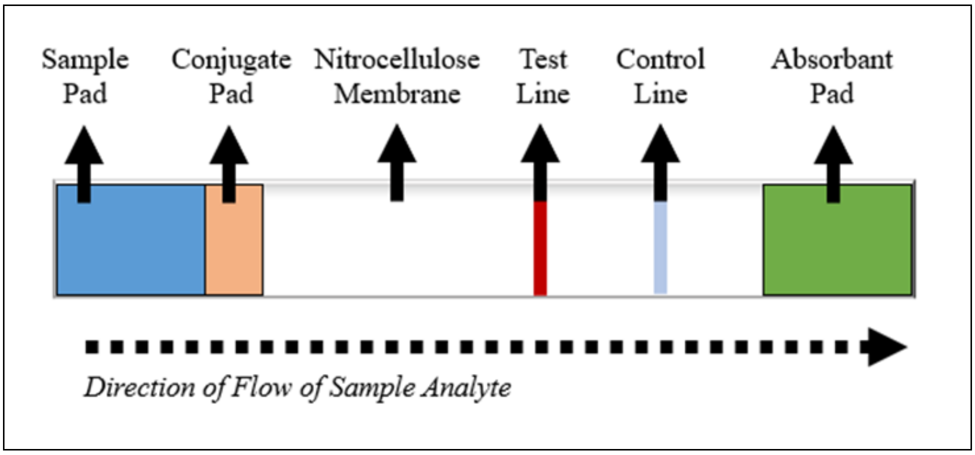

Figure 2.1. The physical layout of a typical lateral flow assay [62].

LFAs are designed with a simple "flow-through" architecture that allows for the movement of the sample and reagents by capillary action, requiring no external pumps or complex equipment. The flow of the sample is controlled to move unidirectionally from the sample pad through the conjugate pad, across the membrane, and finally to the absorbent pad. The capillary action within the membrane and absorbent pad draws the sample through the various components, ensuring proper interaction between the labeled molecules and the captured analytes. The dimensions and positioning of the pads and membrane are optimized to achieve efficient flow and capture of the analyte to obtain reliable results [63].

The “sample pad” acts as the point of entry for the specimen, like blood, urine, saliva, or another bodily fluid. The pad aids in controlling the flow rate of the sample to ensure it moves smoothly through the test, so it is responsible for the controlled discharge of the sample to the conjugation pad. Also, it controls the inconsistencies of chemical content to assess correct analyte concentrations. The “conjugate pad” contains labeled biosensing molecules or particles that are designed to bind specifically to the target analyte. These labels are often colloidal gold, fluorescent particles, enzymes, or other markers conjugated to antibodies or molecules that recognize the target analyte. When the sample reaches the conjugation pad, it releases conjugate molecules from the surface immediately. The release of the molecules should be fast and consistent, which is based on the homogenous suspension of the molecules in the pad. The reason for this is the moving action of the detection particles to the fastest flow rates. The homogeneity may be achieved using spraying or a dispensing mechanism to ensure equal dispersion of the conjugate molecules, thus achieving uniform flow with fewer artifacts. The “nitrocellulose membrane” has a strong protein adsorptive ability due to its hydrophobic nature and houses all the components of the assay. It captures molecules like antibodies, antigens, etc., that bind to specific target analytes, and the interaction between the captured target analyte and the labeled molecules from the conjugate pad is observed in this pad. The capillary flow rate of the membrane is unique and is defined according to the pore size and porosity properties of the membrane as well as manufacturing conditions (80-185sec/40mm, on average). These rates are important for the sensitivity, specificity, and stability of the LFA assessment [64]. The “absorbent pad” is positioned at the end of the assay and serves as a fluid trap by absorbing the processed or excess fluid using its pores, preventing the backflow action of the fluid onto the nitrocellulose membrane, thus eliminating the false-positive test readings. The sample fluid continues to flow until this pad is full [66-68].

LFAs are generally placed in plastic cassettes for easy transportation and to protect the assay from physical impacts. The thickness of the plastic cassette is directly affected by the thickness of the porous pads. On the upper face of the cassette, there is a round “sample hole” for administering the sample and a rectangular “observation window” to monitor light emission from the membrane under light excitation, as seen in Figure 2.2.

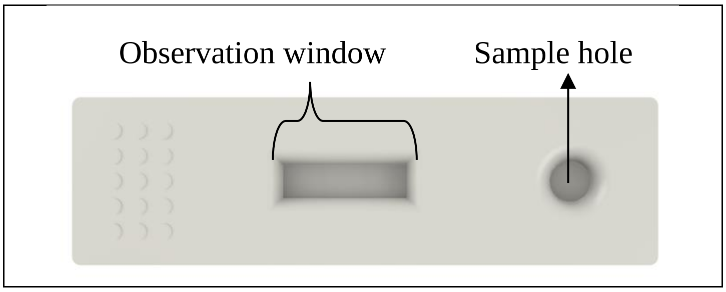

Figure 2.2. White-colored plastic cassette for LFA housing

2.1.2. Format

LFAs can be categorized into sandwich and competitive formats. In sandwich format, two different molecules specifically bind to distinct epitopes on the target molecule. One of these molecules is immobilized on the membrane (detection conjugate), while the other molecule is labeled with a fluorescent marker. The sandwiching technique provides the formation of a visible signal at the T line as the target analyte is placed between the detection conjugate and the T line. In this format, test line intensity is directly correlated with the target analyte concentration. In a competitive assay, there is competition between the labeled molecule and the target analyte. This resulted from immobilized detection conjugates, which are limited in the T line. More target analytes bounded to binding sites result in fewer labeled molecules to the conjugates in the T line. Therefore, T-line signal intensity inversely correlates with the target analyte concentration [69].

2.1.3. Detection Labels

Detection labels in the LFAs serve as markers to present the existence or absence of the target analyte in the sample [70]. Common labels are colloidal gold nanoparticles, colloidal carbon nanoparticles, quantum dots, upconversion nanoparticles, bioluminescent particles, and fluorescent dyes [71]. In contrast to their bulk state, materials at the nanoscale exhibit behavior that is favorable for biosensing applications. They have unique properties with their high surface-to-volume ratio and optical qualities like light scattering/absorption or fluorescence light emission [72, 73].

Colloidal gold nanoparticles are affordable, highly stable, and easy to use. Antibodies or antigens are used with these nanoparticles to achieve specific binding to the target analyte, which generates a visible T line. In this way, the target analyte detection is easily illustrated without additional equipment [74]. The nanoparticles are functionalized with molecules specific to the target analyte. Their unique optical properties allow them to produce a signal upon binding to the target, allowing for visual or instrumental detection. When compared to other labels, they require more waiting time to generate results. Colloidal carbon is appreciated for its stability, improved color contrast, and potential for enhancing assay sensitivity [75]. Quantum dots offer highly stable, bright, and tunable emissions and provide highly sensitive and multiplexed detection, allowing for the simultaneous detection of multiple analytes within a single LFA [76]. Upconversion nanoparticles convert lower-energy excitation light (such as near-infrared light) into higher-energy emission light (such as visible light). The emitted light still exists even if the excitation light is turned off. These nanoparticles provide increased signal-to-noise ratios and decreased background interference [77]. Bioluminescent markers utilize enzymes or proteins that generate light through chemical reactions and are conjugated to molecules that bind specifically to the target analyte [78]. Upon binding, the enzymatic reaction produces luminescence, enabling sensitive and specific detection with low background noise. Fluorescent dyes provide enhanced sensitivity and multiplexing capabilities by emitting fluorescence light of a specific wavelength when excited by a certain wavelength of excitation light. They deliver accurate detection and quantification of the target analyte in the sample. Fluorophore-based LFAs are highly sensitive and can determine labels at lower concentrations, but emitted weak light needs to be detected by a special optical system [79, 80]. They depend on the interaction between disease biomarkers and labeled capture molecules like antibodies to generate fluorescence light. The specific excitation and emission wavelengths are changeable according to the fluorescent dye as listed in Table 2.1 and may slightly vary from batch to batch within the same production lime.

Table 2.1. Attributes for commercial fluorescent dyes [80].

Fluorescent Dye	**Excitation wavelength (nm)**	**Emission wavelength (nm)**	**Stability**	**Fluorescence Intensity**	**Size**
Fluorescein Sodium Salt	450 - 490	510 - 527	Moderate	High	Small
Rhodamine B	540 - 590	600 - 650	Moderate	High	Small
Tetramethylrhodamine	545 - 555	572 - 582	Moderate	High	Small
Alexa Fluor 488	495	519	High	Very High	Medium
Cy3	550	570	High	High	Medium
Cy5	649	670	High	Very High	Medium
Phycoerythrin	565	578	Low	Very High	Large
Allophycocyanin	650	660	Moderate	High	Large
Texas Red	595	615	High	High	Medium
R-Phycoerythrin	565	578	Low	Very High	Large

2.1.4. Fluorescence-based Lateral Flow Assays

Fluorescence-based LFAs represent an advancement in diagnostic technology, offering heightened sensitivity, specificity, and potential for quantitative analysis compared to traditional LFAs. Unlike traditional colorimetric methods, the fluorescence method enables quantitative detection for lower concentrations of target analytes [81, 82]. Fluorescent labels are utilized to emit fluorescence light when exposed to excitation light of a specific wavelength for the detection of disease-related markers in patient blood or saliva samples. Different labels may be used for the detection of multiple diseases in one assay. Diagnostic test results are provided by the fluorescent labels conjugated to capture molecules that emit fluorescence when a target analyte exists [83]. Fluorescent dyes are employed as labels for the detection of various diseases, including hormonal [84], cardiac [85], cancer [86], autoimmune [87], allergen testing [88], and infectious diseases. The most common use of LFA is for the detection of infectious diseases, either virus or bacteria-oriented, in point-of-care applications [89]. Influenza [90], HIV [91], tuberculosis [92], malaria [93], and dengue fever [94] are the detected infections. Recently, LFAs have been used for the diagnosis of COVID-19 by detecting severe acute respiratory syndrome coronavirus 2 (SARS-CoV-2) [95, 96]. For this use, the LFA is modified to contain fluorescently labeled antibodies specific to SARS-CoV-2 antigens. When the sample is introduced to the LFA, it moves through the T and C regions. If the sample contains this virus, the antigen-antibody interaction occurs at the T region, and the fluorescence is emitted. Also, the antibodies bind to the fluorescent markers at the C region, indicating the test has worked correctly. Though a dedicated reader device is required to detect and quantify the fluorescence light [97], available commercial fluorescence analyzer products are still utilized for the purpose [98]. There is a need for low-cost optical readers for quantitative analysis of fluorescence-based LFAs, especially the ones utilizing fluorescein sodium salt and rhodamine B dyes.

2.2. OPTICAL READERS FOR LATERAL FLOW ASSAYS

The selection of an appropriate technology for the reader depends on the type of detection technique used [99]. Techniques such as colorimetry, chemiluminescence, and fluorescence are frequently utilized in optical readers. On the other hand, complex optical readers, such as spectroscopic readers [100], have been developed to capture and analyze color from multiple materials, while simple optical readers can be settled for a dedicated material [101].

2.2.1. Colorimetry-Based Readers

Colorimetric-based readers rely on the detection of the color change modulated by colloidal gold or colored latex beads. When the target analyte exists in the biological sample, these molecules accumulate and produce a visible color in the T region of the assay. This method is suitable for qualitative assessment where sensitivity is not a precedence [102]. Readers are simple and sometimes not necessary, as the naked eye can also be useful. Common examples are pregnancy and some infectious disease tests [103, 104].

2.2.2. Chemiluminescence-Based Readers

In chemiluminescence-based readers, the light emission is triggered by a chemical reaction between a specific substrate and label material on the assay without requiring any excitation light. Low levels of analyte can be detected with high sensitivity. The lack of an external light source makes the reader low-cost. The readers are widely used for hormone testing and the detection of infectious diseases [105, 106].

2.2.3. Fluorescence-Based Readers

Fluorescence-based readers rely on the signals from fluorescent labels as an indicator of the presence or absence of a target analyte in the sample. The sample dropped on the assay can be human blood or saliva that migrates through the assay by capillary action and encounters specific reagents pre-loaded at the T and C regions of the assay. The T region containing fluorescently labeled specific antibodies binds to the related antigens in the sample if they exist. When excited by a specific light source, the resulting complex emits fluorescence light, which is proportional to the concentration target analyte in the sample. The C region includes antibodies or other molecules capturing any remaining labeled molecules and serves as a built-in control to ensure the detection is valid. The visual information, usually in the form of lines on the regions, is captured and converted into quantitative data by the fluorescence-based reader, which typically houses a light source for the excitation, optical filters to distinguish the emitted fluorescence from the excitation light, and a light detector to sense the emitted fluorescence [107-109]. Figure 2.3 shows the typical instrumentation for the reader. The reader is expected to meet several requirements, such as enhanced sensitivity, specificity, accuracy, fast readout speed, and low cost and power consumption [110, 111].

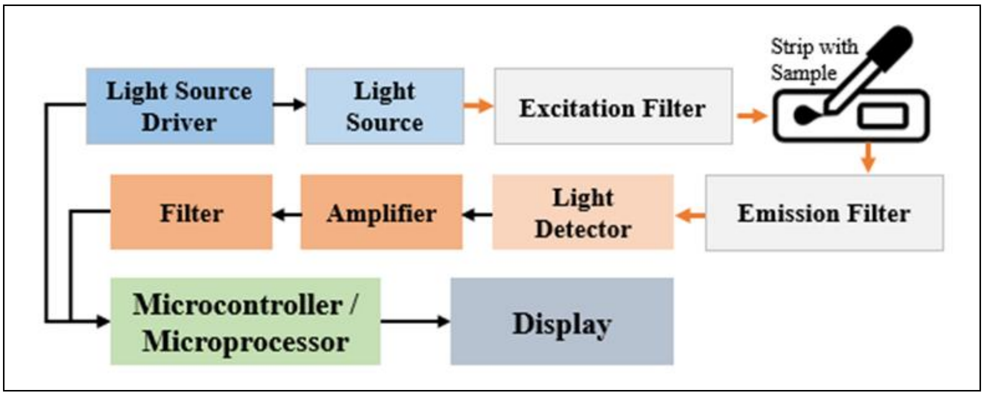

Figure 2.3. Typical instrumentation of a fluorescence-based reader.

2.2.4. Light Source

A light source is used to excite the fluorescent label on the assay. It is selected according to the wavelength, intensity, and stability of the light generated, and the size of the component to fulfill the spectral characteristics of the target fluorescent molecule and the placement of the reader. Light-emitting diodes, lasers, xenon, and arc lamps are the widely used types of light sources [112].

Light-emitting diodes (LEDs) are highly stable and compact light sources. The light of a broader spectral range is generated for the excitation of the target molecule. Narrow-band customized LEDs can also be manufactured to exactly match the fluorescent material characteristics, but this raises the production cost. Commercially available LEDs may emit light in the wavelengths from 410 nm to 980 nm [113]. Power LEDs are advanced versions of standard LEDs designed to handle more electrical power and emit a higher intensity of light. Despite the high power consumption, the power LEDs are relatively compact and have a long operational life of more than 25,000 hours [114].

Lasers generate highly focused and intense light of a specific wavelength from 150 nm to 10000 nm, which may be set by varying the applied current. A narrow light output makes them ideal for the excitation and detection of fluorescent molecules in the assays. Low-power lasers are small in size and preferable in portable readers. High-power lasers are large and require a power supply with a high-power rating, which holds increased space in readers that limits the portability. Lasers are much more expensive than LEDs. [115].

Xenon and arc lamps produce light by passing an electric current through a gas-filled tank. They are widely utilized as broad-spectrum light sources but may be customized for generating light of specific wavelengths with some cost. Although they have a lot in common, xenon lamps generate more uniform light with higher stability when compared to arc lamps [116, 117].

2.2.5. Light Detector

Light detectors are responsible for capturing the light reflected or emitted from the test strip and converting it into an electrical signal. Similar to light sources, light detectors are also preferred based on the fluorescence technology and labeling material. They are placed to align with the test and control lines of the strip for more accurate detections. Different light detectors, including photodiodes, photomultiplier tubes, charge-coupled device cameras, or complementary metal-oxide-semiconductor cameras, have been used [118].

Photodiodes are semiconductor devices operating based on the photoelectric effect. In these detectors, photons striking the diode produce electron-hole pairs. This generates electric current proportional to the detected light. They are sensitive and fast while highly precise outputs are produced. In optical LFA readers, the light intensity reflected by the LFA or transmitted through is quantitatively detected by using this type of detector [119].

Photomultiplier tubes operate based on a photoelectric effect similar to photodiodes, but they are more sensitive to light. Photocathode releases electrons when exposed to light and a series of electrodes, called dynodes, aid amplification of the signal. Amplified electrons reaching the anode generate a current proportional to the light signal. Photomultiplier tubes can handle a broad range of light intensities, allowing for accurate readings across various concentrations. However, their complexity, cost, and the need for high-voltage power supplies can be limiting factors, making them more implementable for laboratory-based assessments rather than point-of-care applications [120].

Charge-coupled devices (CCDs) are image sensors employed in digital cameras, scanners, and various scientific instruments. They house an array of “coupled” capacitors accumulating an electric charge responding to detect light intensity and generate high-quality images with low noise. Each element in the array corresponds to a pixel in the captured image. CCDs exhibit good performance since their response to detected light is highly linear for quantitative evaluations in both bright and dark regions of the LFA. As opposed to these benefits, they are expensive and need high power for the operation [121].

Complementary metal-oxide-semiconductor (CMOS) sensors consist of an array of photodetector cells that convert photons into electrical signals and are integrated into the cameras, generating images. Each photodetector cell corresponds to a pixel in the image. The signals from the sensor are converted into digital data, incorporating noise reduction and signal amplification. The digital data is translated into a readable format like a numeric value. CMOS cameras are very small and may generate images rapidly; therefore, they are suitable for portable and fast imagers. They are cheaper and cost-effective compared to other sensors like CCDs and offer high-resolution imaging with low power consumption, which makes them particularly beneficial in point-of-care applications [122].

2.2.6. Optical Components

Optical components in the readers are lenses, collimators, mirrors, and filters. Lenses focus and direct excitation light onto the assay and then harvest the transmitted or reflected light from the assay to direct it toward the detector. There are two types of lenses: Concave and convex. Concave lenses disperse the light or correct optical aberrations, while convex lenses converge the light onto the assay strip or focus the reflected or emitted light onto the detector. The quality of a lens and its arrangement affect the clarity and focus level of the image [123]. Optical collimators narrow down the light beam, ensuring that the trajectories are parallel and less divergent to provide uniform and directional beams for the excitation of the fluorescent molecules. They are made of various surface types. Specific degree surfaces are tailored to provide a precise angle of light dispersion, hollow-shaped surfaces are designed to manipulate the light path uniquely, blurring surfaces are used to soften and diffuse the light beam, and bead surfaces consist of numerous tiny, bead-like structures on their surface. The beads on the surface refract and scatter the excitation light, resulting in a more uniform and broad-spread illumination for the assay [124]. Optical mirrors change the direction of light to fit compact designs or to ensure optimal illumination. Dichroic mirrors divide light into different wavelengths and reflect or transmit specific wavelengths while allowing others to pass through, facilitating multicolor or multiplex light detections [125].

Optical filters allow certain wavelengths of light to pass through while blocking other wavelengths to improve the specificity, accuracy, and sensitivity of light detection. Long-pass filters transmit longer wavelengths while eliminating shorter wavelengths. Short-pass filters allow the passage of shorter wavelengths while blocking others. Band-pass filters allow passing through a specific range of wavelengths while blocking the remaining wavelengths. Notch filters prevent a specific range of wavelengths from passing through and allow transmission of remaining wavelengths. [126]. Optical filters may be used for both excitation and emission filtering. Excitation filters are for better excitation of the fluorescent molecules on the assay by blocking unwanted wavelengths from reaching the assay, which may lead to non-specific excitation and reduced specificity. Emission filters selectively allow only the light emitted by the fluorescent molecule on the assay to reach the detector, which reduces background noise and increases the signal-to-noise ratio.

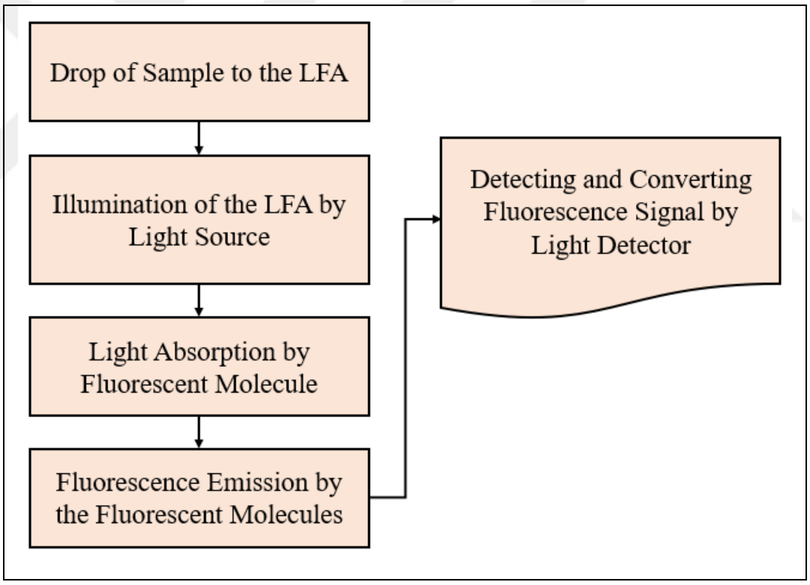

Figure 2.4. Working principle of an optical LFA reader.

2.2.7. Working Principle

A typical working principle of an optical lateral flow assay reader is illustrated in Figure 2.4. The process begins with the administration of the biological sample to the assay. If the sample includes the target analyte, the target molecule binds to the labeled molecules at the T region of the assay, and the remaining molecules bind at the C region of the assay. The assay is illuminated by a light source emitting light at a specific wavelength that is capable of exciting the fluorescent molecules [127]. Fluorescent molecules absorb the coming light and then become excited to a higher energy state. The molecules tend to return to their ground state so that they emit the fluorescence light at a specific wavelength. The emitted light is passed through an optical filter that passes the emitted light only to reach the light detector. The light detector detects the emitted light and converts it into a signal or an image, which is proportional to the concentration of the target analyte in the sample [128]. Recently, smartphone cameras or standalone cameras have been used as light detectors [129, 130].

2.2.8. Use of Fluorescence-Based Readers in Medicine

There is a widespread use of fluorescence-based readers in medicine, but there exists an increased interest in developing “new” readers implementing the advancing technology. One of the pioneer readers has been developed for the detection of Salmonella spp. and Escherichia coli [131]. Fluorescein isothiocyanate is excited by a 480 nm LED, and the camera of a smartphone captures the emitted fluorescence. An optical bandpass filter is used to capture only the emitted fluorescence signal, and a lens is utilized to acquire high-quality images. The reader can detect low pathogen concentrations (< 105 cfu/ml). An alternative option for the reader that utilizes a 980 nm laser as the light source is also developed for the detection of Salmonella spp [132].

A reader has been proposed for the detection of influenza A [40]. A 470 nm LED is used for the excitation of the fluorescent material. Plastic color filters are utilized for both filtering the excitation and emission light. The excitation filter is attached to the camera of a smartphone, while the emission filters centered at 580 nm and 650 nm are positioned between the reflectors covered with aluminum sheets. The images captured by the camera are processed to obtain intensity measurements.

A reader has been developed for the detection of dengue fever [133]. The Nokia Lumia 1020 smartphone camera optical filters and a 365 nm LED with a 5W power rating are positioned in a 3D printed black platform. The LED light is filtered by a 425 nm short-pass filter positioned 60-degree angle to the LFA, which is used to excite quantum dots. A 624±40 nm band-pass filter filters the emitted light. A plano-convex lens is placed just in front of the smartphone camera for distance adjustment. The ISO100 and 8 ms exposure time are considered for imaging. Captured images are analyzed using ImageJ Software to measure light intensity. The reader may quantify as low as 0.15 ng/ml of the molecules.

A reader is proposed to detect analytes using a method that relies on color changes instead of fluorescence light. [134]. The light is generated by a table lamp with 27 W and 36 W power ratings. A smartphone camera with a resolution of 4032 × 3024 pixels is used for imaging. The resulting images are segmented, and the mean intensity from the red channel of the images is calculated for evaluation. A machine learning model processing the ratio of T region to C region signal intensity is developed to assess the analyte quantity. An Android application controls all the components, capturing, and analysis processes.

A reader has been developed for the detection of salmonella and hepatitis B diseases [135]. A 980 nm laser, a CMOS camera of a smartphone, a dichroic mirror, and an optical filter are employed, as illustrated in Figure 2.5. The dichroic mirror is positioned at a 45-degree angle for precise reflection of the emitted fluorescence while allowing transmission of the 980 nm excitation light to the LFA. The reader is portable, compact, and lightweight (900 g). A reader is designed for the detection of the influenza virus [136]. A 365 nm LED with a 3W power rating is used to excite the fluorophore, and a smartphone camera with an aspherical lens is used for fluorescence detection. A long-pass filter with a cut-off wavelength of 410 nm is placed in front of the camera lens. The levels are reported to be determined with a better sensitivity when compared to traditional microscope results.

A reader design is done to detect human chorionic gonadotrophin and aflatoxin B1 [137]. The reader houses a CMOS camera of a smartphone with a macro lens, a 340 nm LED with a 610 nm optical band-pass filter, and a 555 nm LED with a 640 nm optical band-pass filter for the detections. Reflective aluminum foil tape is used to reflect the excitation light by the LEDs to the observation window of the LFA. The emitted fluorescence light intensities from the T and C lines on the LFA are quantified. The device achieves a detection range of 10 to 5000 mIU/mL human chorionic gonadotrophin and 5 to 4000 pg/mL aflatoxin B1. A reader has been proposed for the detection of prostate-specific antigens in cancer diagnosis [138]. A smartphone is utilized for both image acquisition via its CMOS camera and image analysis by using an Android application. The flash lamp of the smartphone is used for the excitation of the fluorescent molecule. With ISO100 and 3 s exposure time for imaging, the reader may detect very low concentrations of the antigen (0.1 ng/mL).

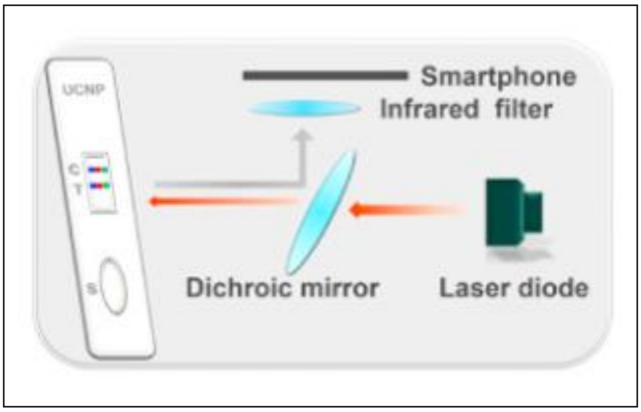

Figure 2.5. Illustration of the reader [135].

A portable reader is proposed for testing ELISA (Enzyme-Linked ImmunoSorbent Assay) plates [139]. It incorporates a smartphone camera with a convergent lens and a 400 nm long-pass filter for imaging. A 365 nm surface-mount device LED, four white LEDs, and a band-pass filter are also used to excite fluorescent material on the plates. The plates are moved with the help of a step motor. The reader operation is controlled by an Android application.

The Fujirebio Lumipulse G1200 is a fully automated reader that detects various fluorescent markers associated with various diseases [140]. The system utilizes a disposable cartridge containing the reagents and a fluorescence detection system to measure the concentration of the markers. It has a built-in xenon flash lamp and a photomultiplier tube, which allows analysis of different assays for oncology, syphilis, thyroid, and fertility.

The PorFloR is a lightweight and compact reader for the detection of mercaptopropionic acid-capped cadmium telluride quantum dots [141]. The reader employs 370 nm LEDs to excite the dots which results in a red fluorescence light emitted at 630 nm wavelength. The emitted light is detected by a photodiode array with red, green, blue, and clear filters and a current-to-frequency conversion mechanism (i.e., TCS3200). The reader operation is controlled by a specifically programmed Arduino Nano board. All the components are housed and isolated in a 3D-printed pyramid-shaped body. Different concentration levels of the quantum dots have been tested, and the results are compared with a commercial plate reader. There has been a linear relationship between the quantum dots' concentration and the emitted fluorescence light intensity.

Feice reader device is developed for the early detection of cardiac disease using double-layered microspheres as the fluorescent material. Incorporating Nile-red dye within the microspheres enhances stability and reduces background noise due to its higher emission wavelength. The concentrations as low as 0.016 ng/mL are detected by the reader [142]. Gmate is a reader that is designed to analyze a wide range of LFAs for various diseases [143, 144]. It has an internal rechargeable battery and can wirelessly send and analyze data to a mobile device such as a smartphone or tablet. A 470 nm LED is employed for the excitation of fluorescein isothiocyanate dye, and a photodiode is used to detect the emitted fluorescence. The reader utilizes a graphical user interface featuring button-based navigations. The device is small and lightweight, making it easy to transport and handle. It has been used for different detection purposes, especially for Hemoglobin A1c detection for patients with diabetes.

A portable reader has been designed for inflammation detection by measuring c-reactive protein levels in human blood samples [39]. Two lasers that provide light emission at 532 nm and 650 nm wavelengths are used to excite Alexa Fluor 532 and Alexa Fluor 647 dyes. Light-shaping diffusers are placed in front of the lasers to increase the homogeneity and uniformity of the generated light. Fluorescence signals by Alexa 532 and Alexa 647, which are at 554 nm and 665 nm wavelengths, are detected by a CMOS camera (Sony IMX219-NoIR) with a special multi-band pass filter attachment. An exposure time of 0.5 ms is reported to be sufficient for the detection of fluorescence light emission in low protein levels.

A reader has been suggested for the detection of the Alexa Fluor 647 dye with peak excitation and emission wavelengths of 640 nm and 665 nm, respectively [41]. The reader can image four assays simultaneously, reducing analysis time and human interaction. Four power LEDs with a wavelength of 630nm are utilized for the excitation of the dyed analytes. A monochrome camera with a resolution of 6.4 megapixels performs imaging. A lens and an optical band-pass filter passing wavelengths from 655 nm to 721 nm are attached to the camera for better detection of the fluorescent signal. The volume ratios of the T and C lines are calculated. Repeatability across the slots of the LFAs demonstrated a coefficient of variation of less than 6%.

The Quidel Sofia 2 reader is to detect different infectious diseases such as influenza, and respiratory syncytial virus. (see Figure 2.6) [145-147]. It houses a photodiode detector and an ultraviolet LED. The LED is capable of generating light at a range of wavelengths, which makes it more multipurpose. The reader employs single-use, disposable assay cartridges pre-loaded with the necessary reagents.

Figure 2.6. The Quidel Sofia 2 reader [145].

A standalone reader has been designed to detect the biomarker hs-CRP for cardiovascular disease diagnosis [148]. The reader houses a 530 nm LED to excite gold nanoparticles and a 5-megapixel CMOS camera for imaging. The system achieves a high detection accuracy and is able to detect low levels of hs-CRP (< 5 mg/L). Another standalone reader is developed to detect the biomarkers of the infectious diseases, human immunodeficiency virus antibody, hepatitis B virus surface antigen, hepatitis C virus antibody, and Treponema pallidum antibody [149]. A 365 nm LED with a 70 mW power rating is positioned at a 45-degree incident angle to the LFA. The emitted fluorescence light is passed through a slit and a band-pass optical filter with a range of 615±30 nm and a diameter of 1.25 cm. A photodiode, coupled with the signal amplifiers and an analog-to-digital converter, is used to capture the light. A mechanism implemented using a step motor rotates the cassette holding the LFA for better positioning. The results are presented on a touch-screen display. The operation of the reader is controlled by an STM32 microcontroller.

Standalone readers are equipped with dedicated cameras, which offer better functionalities in configuring imaging parameters when compared to smartphone camera-integrated readers. On the other hand, many readers do not monitor the environmental conditions that the lateral flow assays are being exposed to during imaging.

3. MATERIALS AND METHOD

Two standalone optical readers are developed to image fluorescein sodium salt and rhodamine B fluorescent dyes injected into the lateral flow nitrocellulose membranes in the current study. The preliminary reader consists of a minicomputer, an optical filter, a camera, two light sources, a display, a temperature-humidity sensor, and additional electronic elements and 3D-designed mechanical components. The final reader includes improved versions of these components and is portable (unlike the preliminary reader). Both readers feature user-friendly graphical user interfaces that simplify imaging by guiding the user. The readers are tested with nitrocellulose membranes treated with varying concentrations of fluorescein sodium salt and rhodamine B dyes.

3.1. NITROCELLULOSE MEMBRANES AND FLUORESCENT DYES

A raw nitrocellulose membrane with a capillary flow rate between 90 and 150 s/4cm and a thickness of 200 μm with 100 μm polystyrene backing material (FF80HP, Whatman, UK) is used to prepare various membranes at the Biophysics Department at Yeditepe University according to the protocol described by Durdabak et al. [150]. The membranes are treated with a 1% skim milk solution for an hour while being agitated at room temperature to block potential non-specific binding sites. Subsequently, they are washed three times with 1X phosphate-buffered saline to remove excess blocking agents and other residues, ensuring a clean surface for further application. Next, they are dried at 37 °C for a minimum of two hours, solidifying the blocking layer and preparing the surface. Finally, the membranes are stored at +4 °C to maintain their integrity and functionality till use.

A fluorescein sodium salt dye with an excitation center wavelength of 488 nm and emission center wavelength of 515 nm (923.D01, ISOLAB Chemicals, Germany), and a rhodamine B dye with an excitation center wavelength of 554 nm and emission center wavelength of 630 nm (964.D01, ISOLAB Chemicals, Germany) are used. Various concentrations of fluorescein sodium salt and rhodamine B solutions are prepared by dissolving the respective dye powders in distilled water, following a serial dilution method.

First, a 10 mM main stock of the raw fluorescein sodium salt with a molecular weight of 376.27 g/mol is synthesized. A mass of 18 mg of fluorescein sodium salt is weighed and then dissolved in 5 mL of distilled water in a container. The container is next subjected to vortexing to ensure complete dissolution and a homogeneous solution. Subsequent to vortexing, the solution undergoes sonication for two minutes to agitate particles for a uniform solution. Second, a ten mM main stock of the raw rhodamine B with a molecular weight of 479.02 g/mol is prepared by dissolving 23 mg of rhodamine B dye in 5 mL of distilled water. The solution is vortexed and sonicated for two minutes to achieve solubilization of the rhodamine B particles. Once prepared, these two solutions serve as the starting point for each fluorescent dye for the subsequent serial dilution steps.

Serial dilution is performed to prepare fluorescent dye solutions at varying concentrations. The main stock solution of both dyes, at a concentration of 10 mM and a volume of 5 mL, is serially diluted to produce 1 mM, 100 μM, 10 μM, 1 μM, and 100 nM concentration levels, as illustrated in Figure 3.1. An initial volume of 50 μL of the 10 mM main stock solution is transferred into a new tube, to which 270 μL of distilled water is added, resulting in a 1 mM solution after thorough manual mixing (see Figure 3.2). This dilution step is repeated sequentially. Subsequently, 30 μL of the 1 mM solution is added to 270 μL of distilled water to achieve a 100 μM solution. This procedure is repeated with 30 μL from the preceding concentration mixed with 270 μL of distilled water to create subsequent solutions of 10 μM, 1 μM, and 100 nM concentrations. All these steps are repeated for both fluorescein sodium salt and rhodamine B dyes.

Further dilution is performed using the remaining 4 mL volume for each fluorescent dye. A base stock solution of 100 μM concentration is produced by execution of two-step dilution. The first step involves the addition of 30 μL of the 10 mM main stock solution to 270 μL of distilled water, resulting in a 1 mM intermediate solution. In the second step, 300 μL of the 1 mM intermediate solution was further diluted with 2700 μL of distilled water to obtain 3000 μL of the final base stock solution at 100 μM concentration.

The 100 μM solution serves as the starting point for subsequent dilutions to achieve a range of concentrations between 10-100 μM. 270 μL of the 100 μM base stock is combined with 30 μL of distilled water to obtain a 90 μM solution. This process is repeated with the volume of the base stock decreased by 30 μL and the volume of distilled water increased by 30 μL. Subsequently, 80-10 μM solutions are obtained (see Table 3.1 and Figure 3.3). The resulting solutions are then carefully dispensed onto the nitrocellulose membranes prepared.

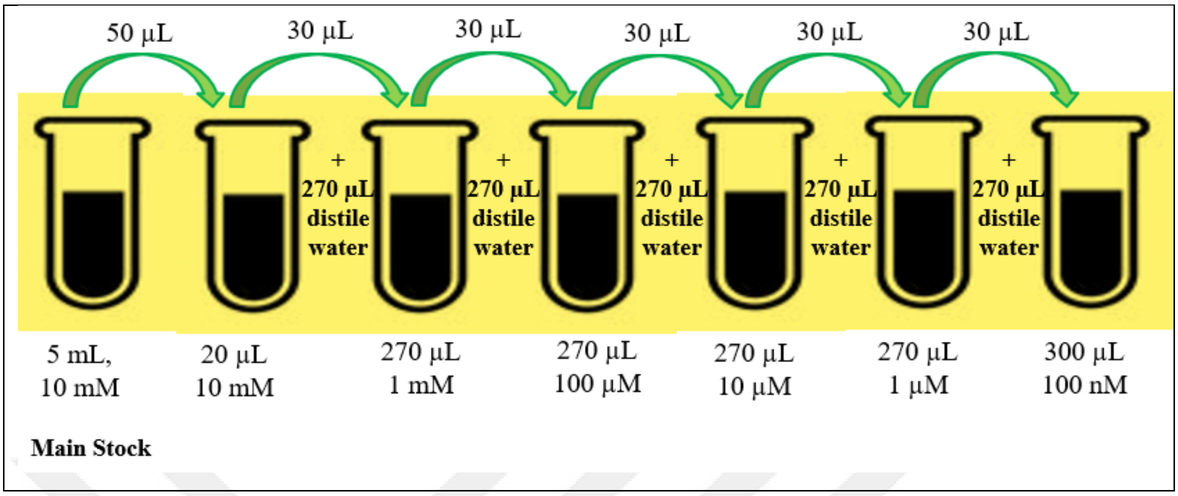

Figure 3.1. Serial dilution to prepare dye solutions at varying concentrations.

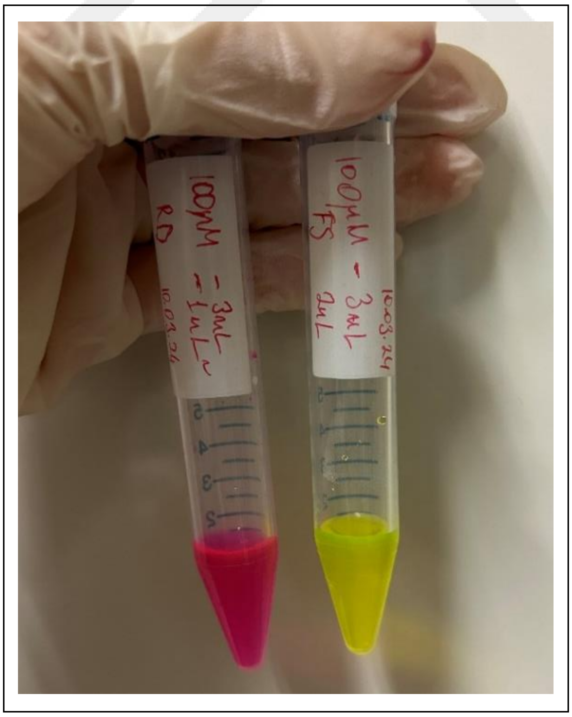

Figure 3.2. 100 µM base sample for rhodamine B and fluorescein sodium salt dyes.

Table 3.1. Dilution steps for the dye concentrations from 90 and 10 µM.

Target Dye Concentration (µM)	Formulation	
	Dye volume (µL) *	Distilled water volume (µL)
90	270	30
80	240	60
70	210	90
60	180	120
50	150	150
40	120	180
30	90	210
20	60	240
10	30	270

* Dye with 100 µM concentration

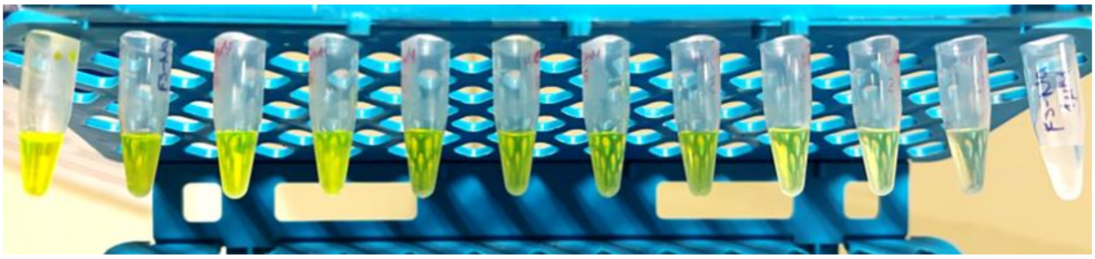

(a)

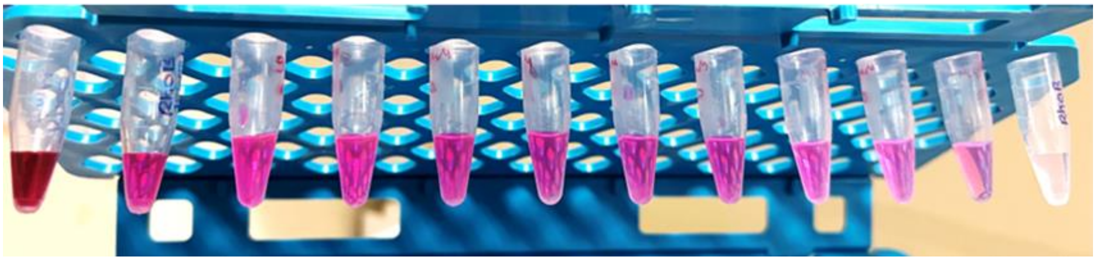

(b)

Figure 3.3. Solution with different concentrations of (a) Fluorescein sodium salt and (b) Rhodamine B dyes.

3.2. PRELIMINARY OPTICAL READER

The preliminary optical reader houses a mini-computer, two different light sources with voltage regulators, a camera, an optical filter, a touchscreen display, a temperature-humidity sensor, and additional electronic components. The block diagram of the reader is seen in Figure 3.4. A graphical user interface is developed for user interaction and controlling the operation of the device.

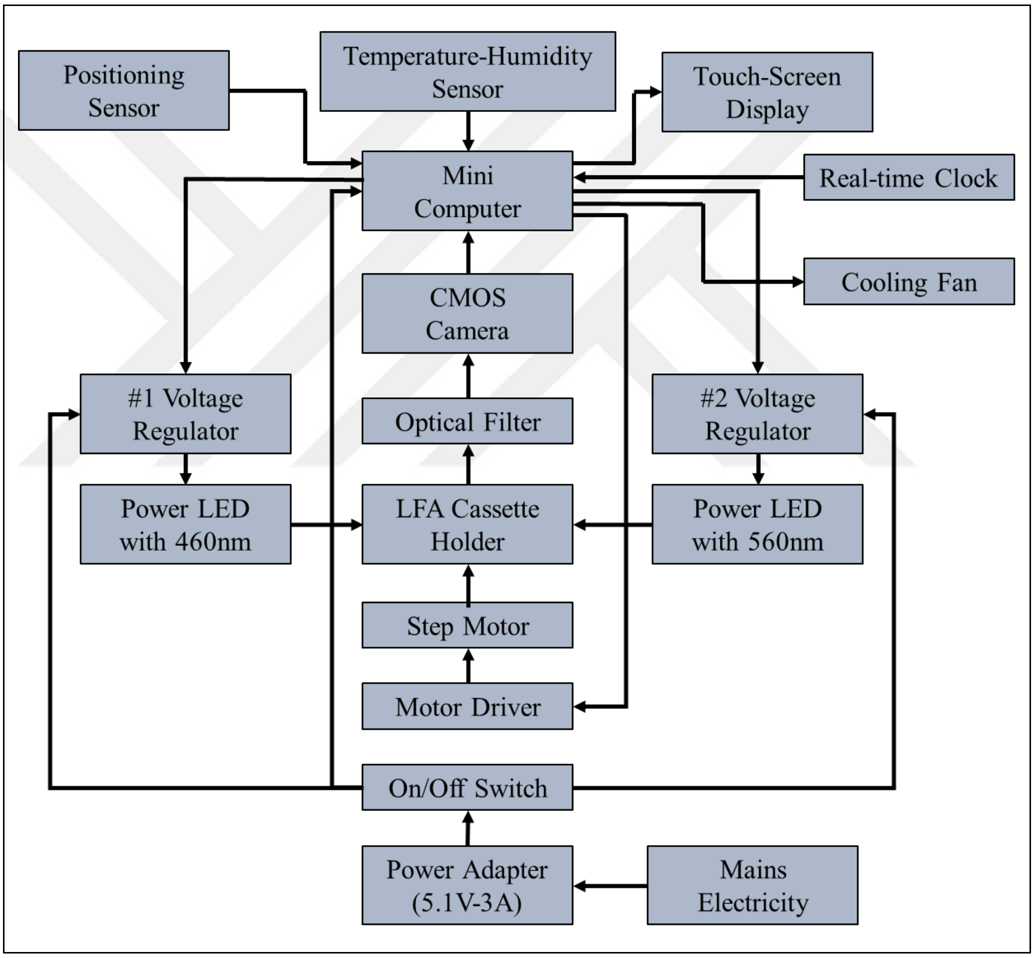

Figure 3.4. Block diagram of the preliminary optical reader.

3.2.1. Minicomputer

A single-board minicomputer, Raspberry Pi 4B-4GB (Raspberry Pi Foundation, UK), is utilized for controlling all the electronic components as well as performing the tasks for imaging lateral flow assays. It operates on the Debian GNU/Linux 11 Bullseye operating system and offers a variety of opportunities for computerization, data processing, and integration of other devices and peripherals. It has two micro-HDMI ports allowing for dual-screen setups at varying resolutions, two USB 3.0 ports allowing for rapid data transfer, and two USB 2.0 ports for additional peripherals. It is equipped with a full-speed Gigabit Ethernet port in addition to its wireless connection for internet and network connectivity. It includes a camera serial interface and a display serial interface port, allowing the device to connect to a range of cameras and touch-screen displays (Figure 3.5.). The device has a 40-pin general-purpose input-output header that gives support to multiple communication protocols, including up to six UART, six I2C, and five SPI connections, offering extensive possibilities for hardware expansion and development. A 5.1V 3A power adapter powers the minicomputer via its C-type USB port controlled by an on/off switch.

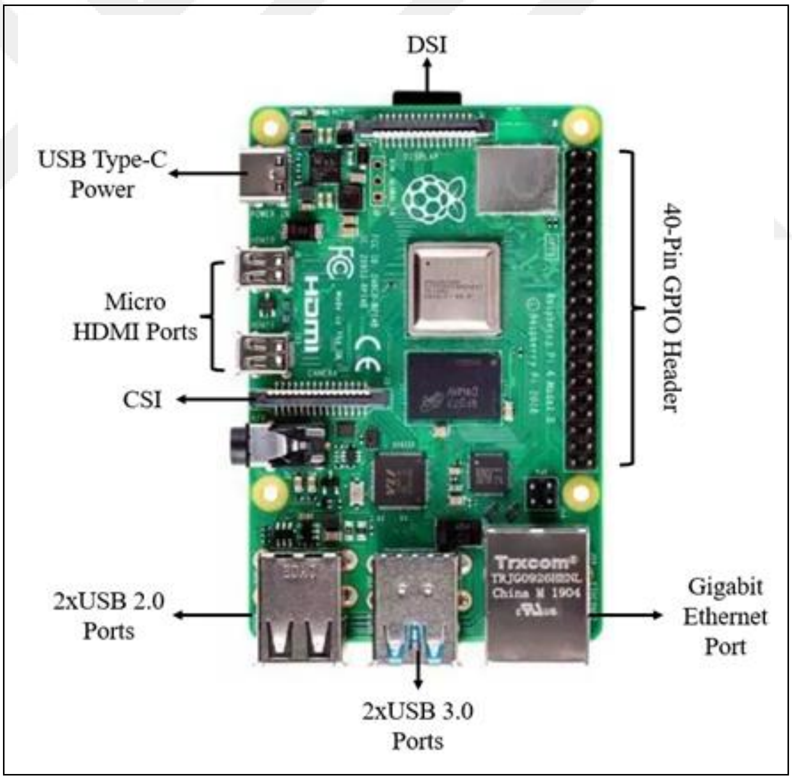

Figure 3.5. Raspberry Pi 4B minicomputer [151].

3.2.2. Light Source

Power LEDs are preferred in the developed optical reader because of their low cost, portability, and low power consumption while generating a broad range of wavelengths with a long operational life. A blue power LED (460nm, 3W) (DSTK3300, HQG, China) is employed to match the excitation light wavelength characteristic for the fluorescein sodium salt dye, while a green power LED (560nm, 3W) (Starsealand, China) is used to match the excitation light wavelength characteristic for the rhodamine B dye (Figure 3.6). The LEDs are soldered onto the star-shaped printed circuit board, which is made of aluminum substrate for excellent thermal conductivity, dissipating the heat generated by the power LED during operation, thereby preventing overheating and prolonging the life of the LED. Additionally, extruded aluminum heatsinks are attached to the back of the board for further cooling. A beads collimator is attached to each power LED to achieve more uniform and broad-spread illumination of the membranes.

The power LEDs are characterized using an experimental setup assembled with the USB4000-VIS-NIR spectrometer (Ocean Optics Inc., USA) connected to the computer via a USB cable, interfacing with SpectraSuite software for data analysis (see Figure 3.7). A fiber optic cable with an attached homogenizing probe is linked to the spectrometer. The probe tip is inserted into a custom 3D-printed hollow-shaped apparatus developed. At the opposite end of this apparatus, the power LED being tested is positioned 5 cm away from the probe to ensure consistent light capture. The spectrometer is configured with an integration time of 100 ms and an average of 5 scans per measurement. During tests, a set of fixed dc voltages is supplied to each power LED by using an adjustable DC laboratory power supply unit (GPS-4303, GW Instek, Republic of China)

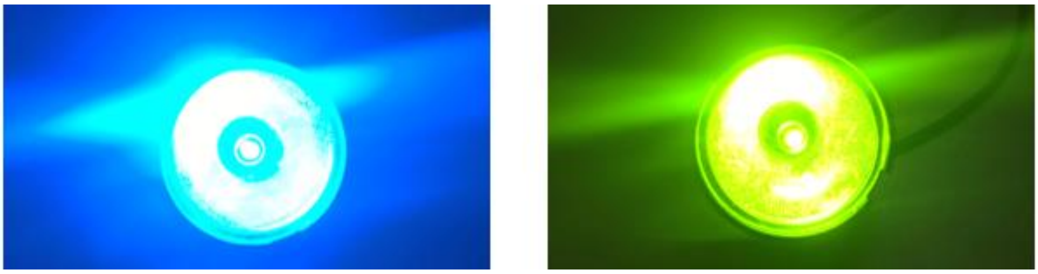

(a) (b)

Figure 3.6. Power LEDs with center wavelengths of (a) 460 nm and (b) 560 nm with 5-degree collimator attachment.

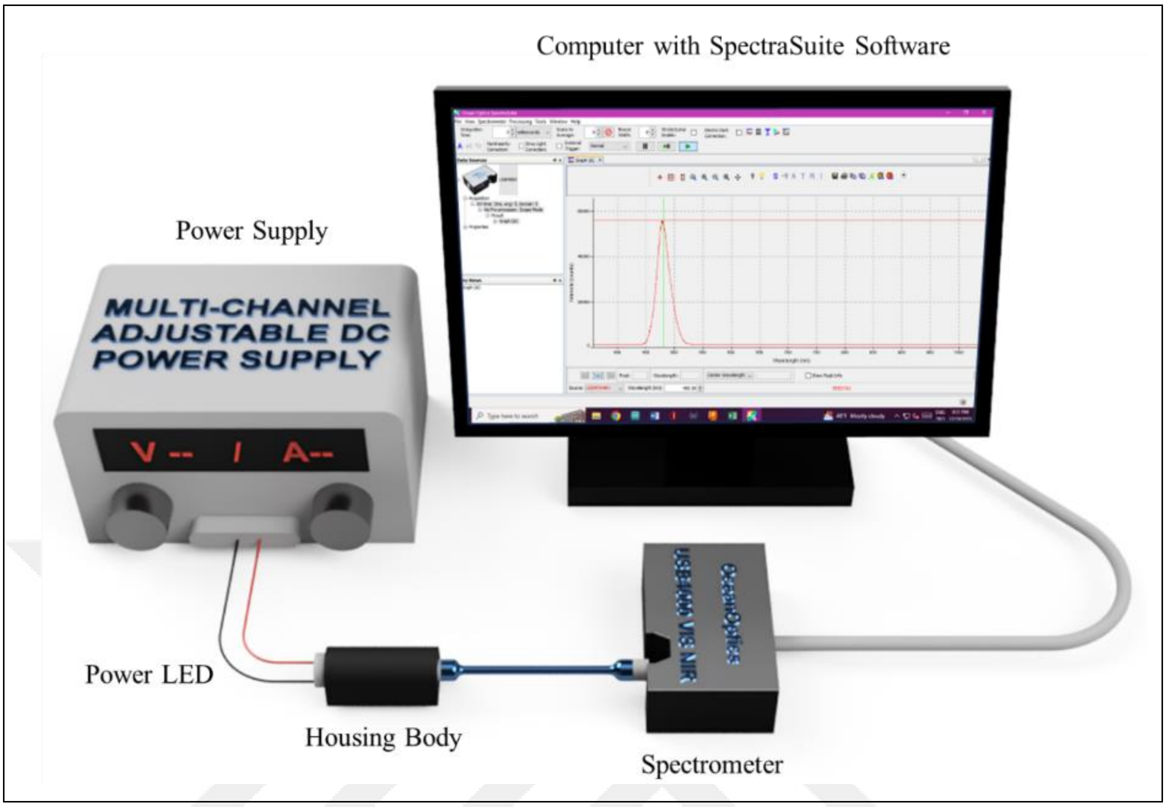

Figure 3.7. Experimental setup for power LED characterization.

The power LEDs are operated by using a fixed supply voltage by two voltage regulator modules. For each LED, an adjustable LM2596S step-down DC-DC voltage regulator module is employed to provide a fixed voltage and to turn the LED on and off during and before/after imaging. The module accepts input voltages between 4 and 35 Vdc and outputs voltages from 1.23 to 30 Vdc. The LM2596S voltage regulator has five pins [115]. The VIN pin is the power input for the voltage regulator, the Output pin serves as the terminal of the switch, cycling between a high and a low voltage relative to VIN, the Ground pin is the reference point, The Feedback pin monitors the output voltage to regulate and maintain a constant output despite fluctuations in the load or input voltage, and the ON/OFF pin (logic pin) allows external control of the regulator's power state, enabling the output power to be turned on or off. The logic pins (ON/OFF, pin 5) of the voltage regulators are connected to the separate GPIO pins of the minicomputer over 10 kΩ pull-up resistors to turn the power LEDS on and off. The output voltages are finely tuned using the onboard trim pot to provide 2.5V to both power LEDs, while the regulators are fed by a 5.1V 3A adapter over a power on/off switch.

3.2.3. Camera

A compact and lightweight CMOS camera, Raspberry Pi NoIR Camera V2 (Raspberry Pi Foundation, UK), is used as the light detector in the reader developed (25 mm × 23 mm × 9 mm, and 3 g) (Figure 3.8). It is compatible with minicomputers equipped with CSI ports. The NoIR version differentiates from the traditional version since it is without an infrared filter. The camera features a Sony IMX219 sensor that captures high-resolution static images at a resolution of 3280 × 2464 pixels. The IMX219 sensor supports 10-bit imaging with SRGGB10 Bayer format and 8-bit imaging with Bayer formats of XBGR8888, XRGB8888, RGB888, and BGR888.

3.2.4. Optical Filter

An optical dual band-pass filter (87-233, EdmundOptics Inc., USA) is integrated into the developed reader to refine the light reaching the camera by suppressing the reflected light initially produced by the power LEDs. The filter features two different center wavelengths with narrow bandwidths: 512 ± 23 nm for the fluorescein sodium salt emission at 515 nm and 630 ± 91 nm for the rhodamine B emission at 630 nm. It boasts a transmission rate of > 90%, ensuring that sufficient light within the bandwidths is allowed. It has a 12.5 mm diameter and operates at a 0-degree angle of incidence. The substrate of the filter is Fused Silica (Corning 7980), known for its high purity and optical clarity, ensuring minimal light dispersion. The surface is treated with a hard coating, maintaining an optical density of ≥ 6.0 for effective blocking of unwanted light. Housed within a black anodized ring, the filter mount thickness is 3.5±0.1 mm, while the substrate thickness is 2.00 ±0.25 mm.

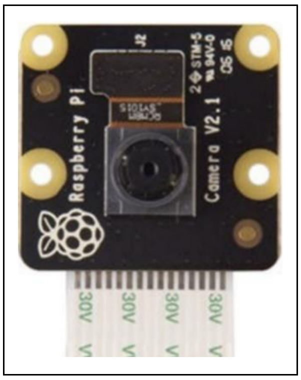

Figure 3.8. Raspberry Pi V2 NoIR camera module [152].

The optical filter is characterized using the setup illustrated in Figure 3.9. A deuterium-tungsten source (DT-MINI-2GS, Ocean Optics Inc., USA) generating a broad spectrum of light (450-900 nm), visible, and NIR regions, is employed for comprehensive spectral analysis of the optical filter. The light from the source is transmitted through a fiber optic cable (Ocean Optics Inc., USA) to the optical dual band-pass filter placed in the sample holder mechanism for fixed positioning. The modified light spectrum is channeled back through another fiber cable to the USB4000-VIS-NIR spectrometer (Ocean Optics Inc., USA), which can detect light with wavelengths 356-1055 nm. The measurement data by the spectrometer is transferred to a computer and processed to discern the spectral attributes of the optical filter using Spectra Suite software (Ocean Optics Inc., USA) with 100 ms integration time and five measurement averaging.

Figure 3.10 illustrates the layout of the camera, the optical filter, and the imaging area. The camera is placed five centimeters away from the laminar flow assay for proper focusing of the observation window of the assay.

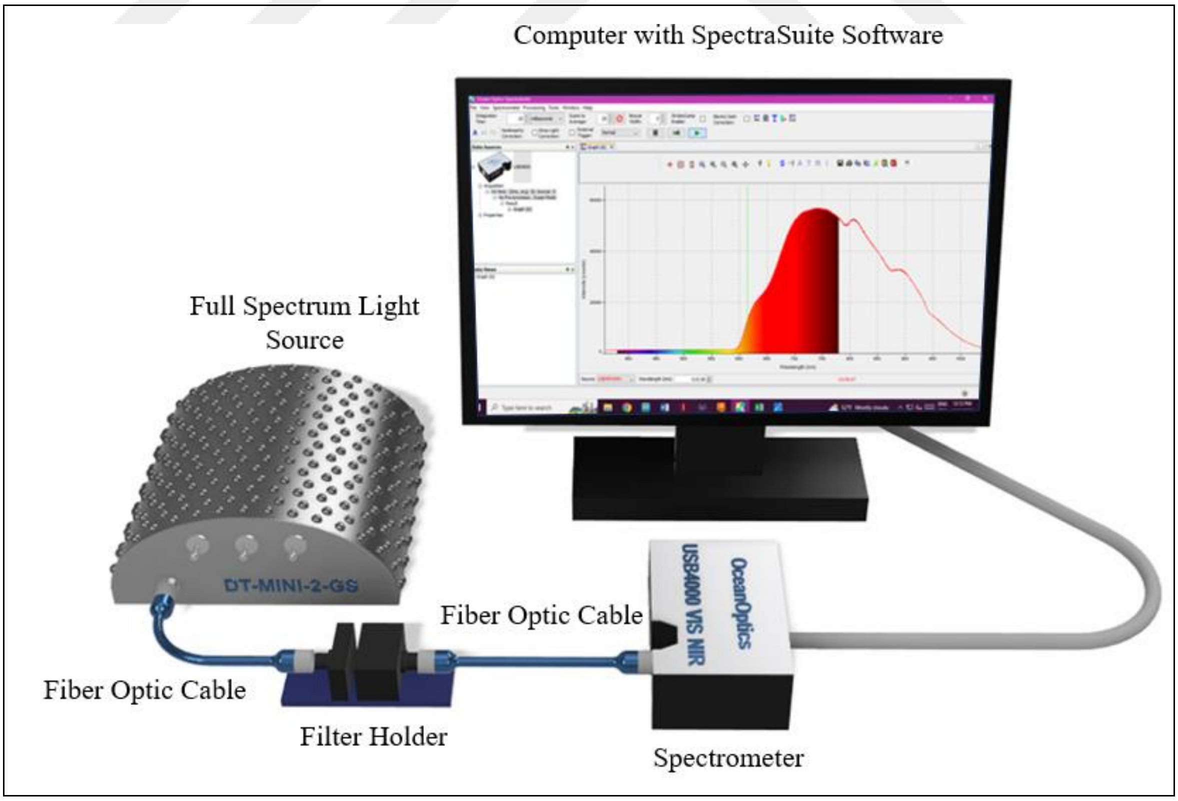

Figure 3.9. Experimental setup for characterization of the optical filter.

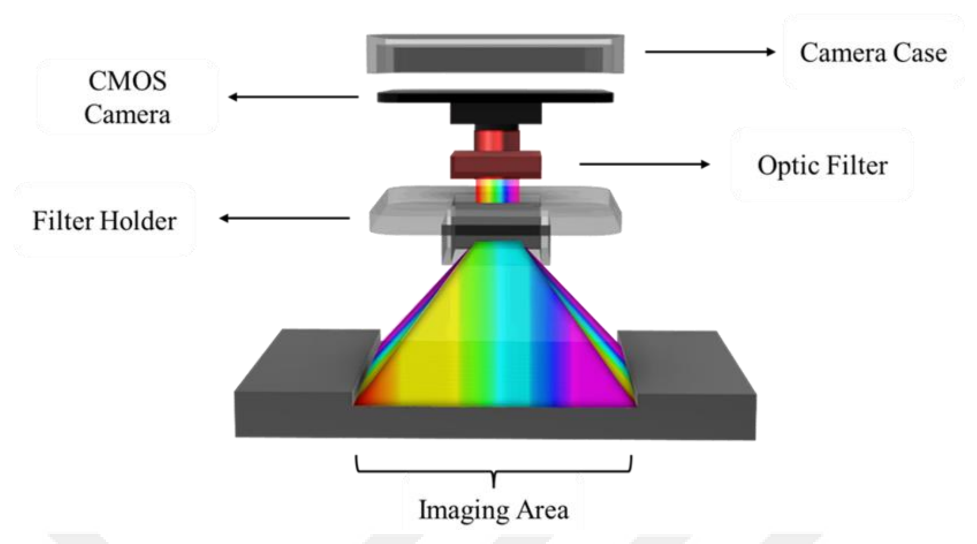

Figure 3.10. Layout of the imaging optics in the preliminary reader.

3.2.5. Touch-Screen Display

A 5-inch colored capacitive HDMI touch-screen display (Waveshare, China) is used to provide a direct and intuitive way for the user to interact with the reader via a graphical user interface developed. It boasts a hardware resolution of 800×480 and supports 5-point touch control with a tempered glass panel (See Figure 3.11). The display is connected to the minicomputer via its HDMI port to the micro-HDMI port of the minicomputer. An additional micro-to-USB cable is connected to the USB port of the minicomputer for powering and serial data transfer of the touch-screen.

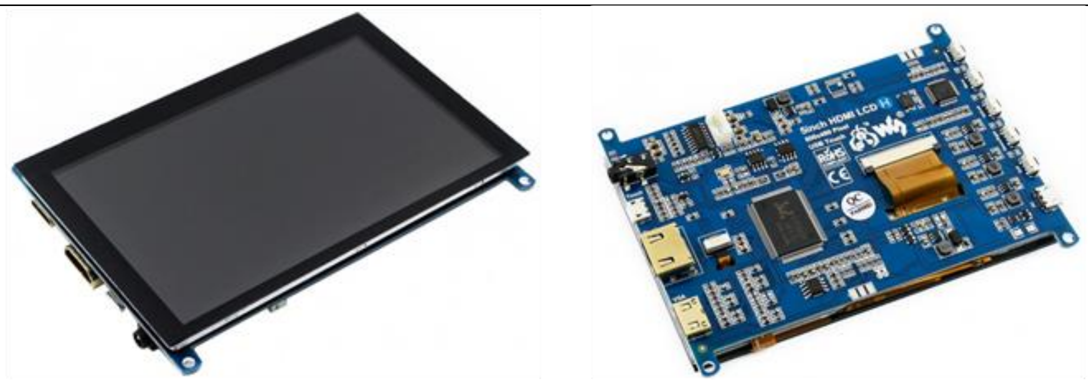

(a) (b)

Figure 3.11. HDMI touchscreen display. (a) Top, and (b) Bottom views [154].

3.2.6. Temperature and Humidity Sensor

A temperature-humidity sensor, HTU21D (SparkFun Electronics, USA), is used to monitor the environmental temperature and humidity that the laminar flow assay is being exposed to during imaging. The sensor consumes only 2.7 μW power and completes a single measurement in five seconds. It is equipped with built-in 4.7 kΩ pull-up resistors for I²C communications and is easily integrable into the minicomputer via its pins that are VCC for powering by 3.3 V on the minicomputer, GND as ground, and SDA and SCL pins for I²C communication via address 0x40 (see Figure 3.12).

3.2.7. Real-time Clock

A real-time clock module (DS3231, Maxim Integrated Inc., USA) is connected using its GPIO header and configured/activated by the terminal. The module is powered by a 3.3V pin of the minicomputer, and set to communicate with the minicomputer via I2C protocol (address: 0x68). The module has a 3 V Li-ion battery (CR-1220) for time and date backups.

3.2.8. Other Electronics

A DC fan motor that operates at 5V DC and 150 mA (4010S5H, MER Inc., China) is integrated into the top of the minicomputer for cooling. A power adapter rated at 5.1 V and 3 A, is employed to energize the entire electronic components of the reader. A power on/off switch (Swion, China) equipped with an LED is employed to cut this power connection.

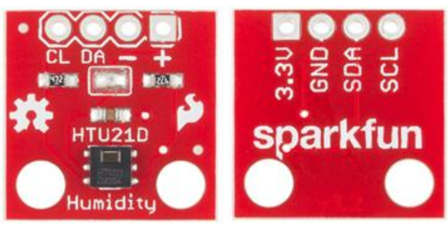

(a) (b)

Figure 3.12. HTU21D humidity sensor module. (a) Top, and (b) Bottom views [153].

3.2.9. Mechanical Components

The mechanical components are a darkroom, motorized sliding tray, and reader enclosure. These components are designed on Autodesk Fusion 360 software (Autodesk Inc., USA) and produced using a 3D printer (E2, Raise3D, USA) and black 1.75mm polylactic acid filament (Premium Red, Raise3D, USA).

The darkroom is to position the power LEDs, the CMOS camera, the optical dual band-pass filter, and the cassette case as presented in Figure 3.13. The LEDs are installed on either side and angled at 40 degrees toward the cassette, which allows for optimal illumination of the observation window of the assay. The LED beams are channeled through trapezoid-shaped apertures for the selective and independent excitation of the dyes and for preventing the light from the LED light reflected from the cassette. The camera is mounted perpendicularly 5 cm away from the cassette and aligned with the observation window of the cassette to capture high-fidelity images. The optical dual band-pass filter is affixed in front of the camera lens using a specially printed filter holder, which aligns light rays to strike the filter surface perpendicularly. The periphery of the camera lens is housed in a black case to absorb unwanted light and reduce the penetration of the incidental light to the camera lens aperture from side angles. The physical appearance of the dark room is seen in Figure 3.14.

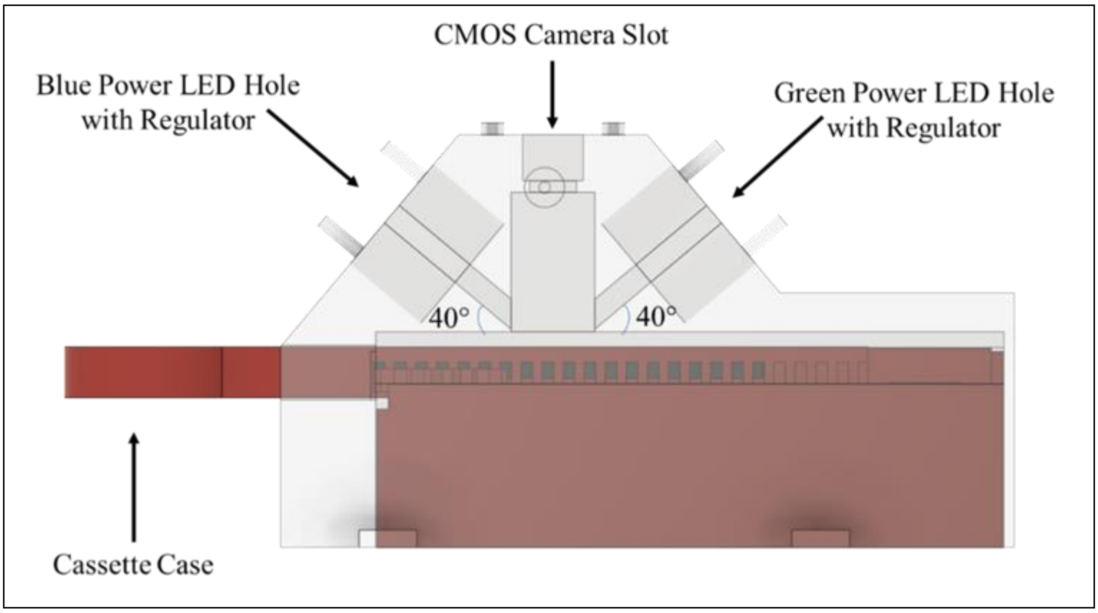

Figure 3.13. Darkroom of the preliminary reader.

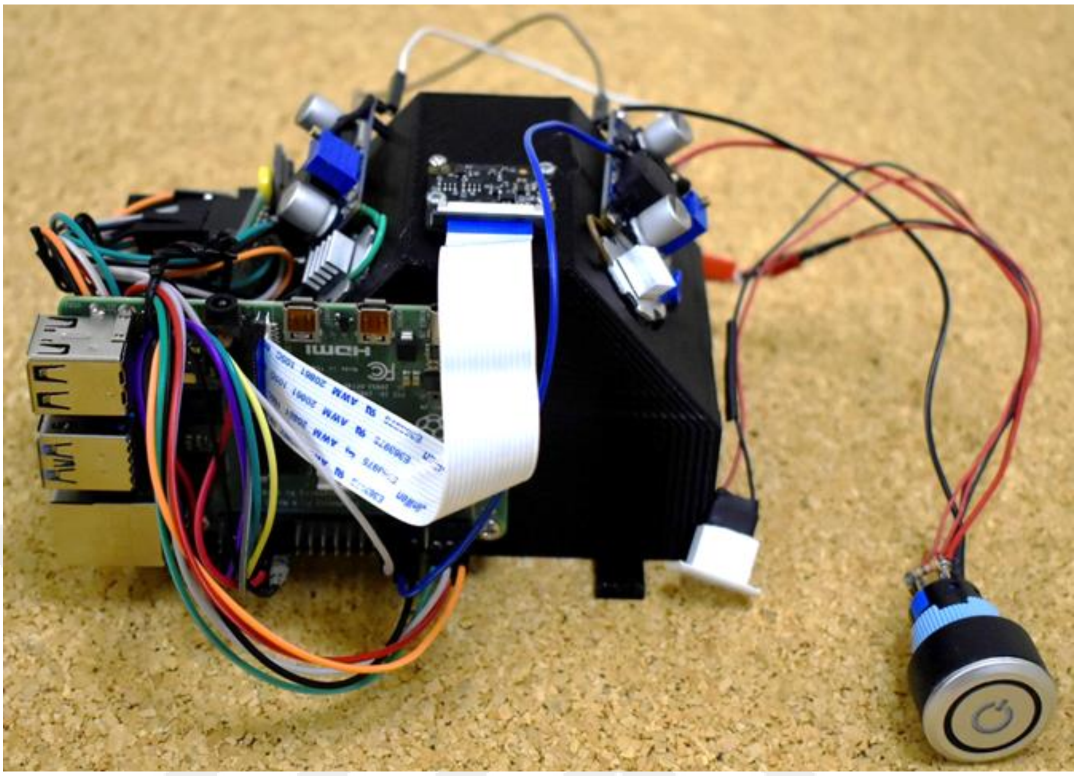

Figure 3.14. The physical appearance of the darkroom with the attached electronic hardware of the preliminary reader.

The motorized sliding tray is to ease the insertion and ejection of the cassette. A unipolar stepper motor (28BYJ-48) is used to control the movement and speed of the sliding tray that serves as a holder for the cassette. The motor operates at a nominal voltage of 5V DC, provides a fine step resolution for proper positioning, and runs quietly. The motor is controlled by a driver circuit (ULN2003AN) to get digital signals using its four input pins connected to the GPIO pins of the minicomputer and is set up with a step delay of 1 ms for smooth movement. A mechanic gear links the motor to the tray for forward and reverse movements, and a sensor detects the full insertion of the tray. Figure 3.15 shows the placement of these components on the tray.

The reader enclosure provides further maintenance of conditions like temperature and humidity inside the reader, thereby blocking threats to the functional stability of the reader. It features a display holder, a hole for the insertion of the on/off switch, and four mini drawers for keeping unused cassettes (Figure 3.16). Additionally, it includes a fan exhaust aperture for air-flowing. The physical appearance of the device is exhibited in Figure 3.17.

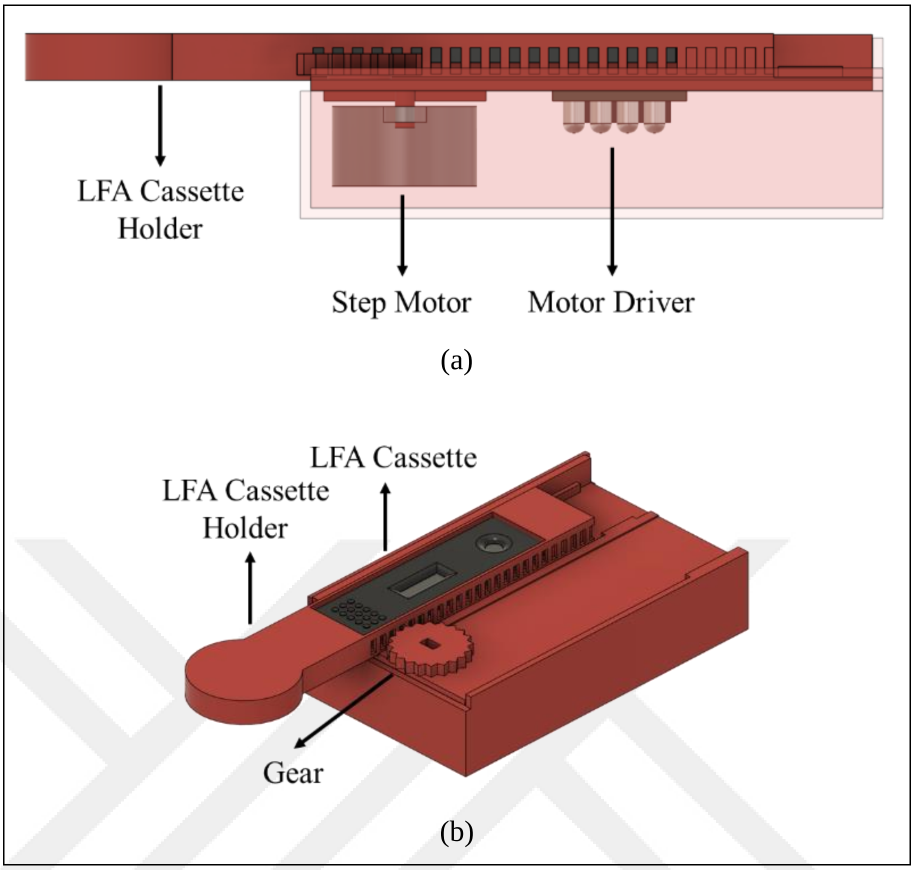

Figure 3.15. Motorized sliding tray. (a) Side, and (b) Top views.

Figure 3.16. Enclosure drawing for the preliminary reader.

(a) (b)

Figure 3.17. The physical appearance of the preliminary reader.
(a) Front, and (b) Side views.

3.2.10. Software

Dedicated software is developed for the reader using Python programming language (Python Software Foundation, USA). The software includes initialization settings of the camera, power LEDs, and other electronic components as well as a user-friendly graphical user interface. The graphical user interface is designed using the Guizero library in Python and includes a title box and many text boxes, panels, combo boxes, icons, buttons, and sliders, as seen in Figure 3.18:

- The title box is to show “YUBME: LFA Reader v2024.1” at the top,
- A power icon is displayed at the top-left corner to turn the reader off,
- A text box is next to the power icon to display the temperature and humidity in the units of degree Celcius (°C) and percent relative humidity (%RH) taken every two seconds,
- Another text box is on the left to display the directive status messages to the user,

- The panel named “Imaging Mode” has a combo box to select the imaging mode as “Pre-Imaging” or “Post-Imaging,”
- The panel named “Settings” has three sliders to set the light emission time, camera exposure time, and gain. The emission time can be set between 1-10 seconds; the exposure time may be set between 10-300 ms, and the gain can be set between 1-10.
- The text box at the button-left corner displays the date and time delivered from the real-time clock in the “DD/MM/YY – hh: mm” format,
- The button named “Insert” is to get the cassette holder into the reader by moving the sliding tray forward,
- The button named “Image” is for image acquisition and saving the images in PNG files while saving the metadata in TXT files. Once an image is captured, it is displayed on the right. The images are tagged with ‘Pre-T’, Pre-C’, ‘Post-T’, and ‘Post-C’ labels. T letter indicates that the image is from the T line, and C letter marks that the image is from the C line on the assay,
- The buttın named “Set ROI” is to place a rectangular region of interest on each of the captured images according to the selected position of the top-middle point of each rectangle by the sliders,
- The button named “Process” is for generating histogram plots within the defined ROI regions in addition to the mean intensity plot, which represents the calculated mean intensity of the green channel for the fluorescein sodium salt while of the red channel for the rhodamine B dye,
- The button named “Eject” is to eject the cassette holder by moving the sliding tray backward.

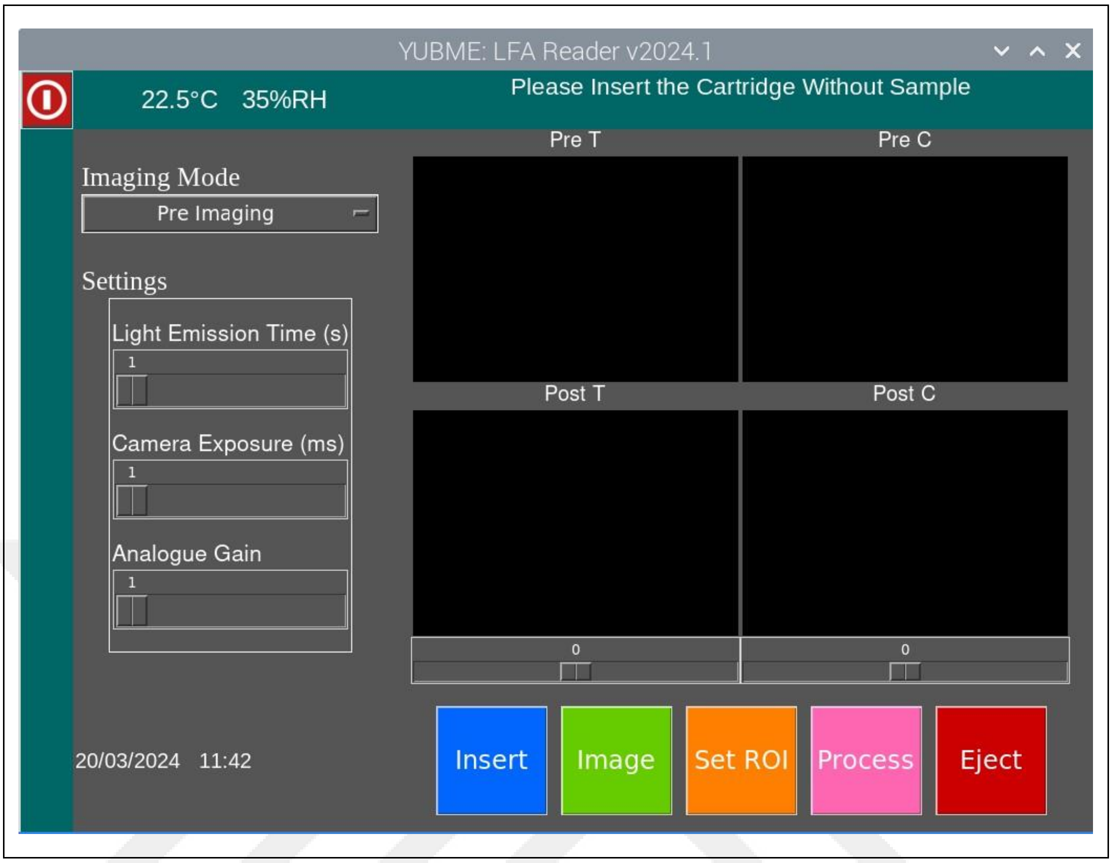

Figure 3.18. The graphical user interface of the preliminary reader.

During image acquisition, the CMOS camera is managed through the Picamera2 library. The primary camera resolution is set to 3280×2464 pixels, ensuring detailed image capture, while a concurrent area of 620×430 pixels. This facilitates real-time monitoring and previewing without computational overload. Display settings favor this low-resolution stream for efficiency. The imaging area is larger than the observation window of the cassette, but the targeted fluorescein sodium salt and rhodamine B dye regions on the assay are imaged separately. Therefore, the imaging area is cropped to focus on these regions separately. Manual control over exposure time and analog gain allows for adaptable image capturing across varying lighting or imaging conditions and enhances image consistency. Automatic white balance and auto-exposure are intentionally disabled, granting greater precision and avoiding inconsistencies due to automatic adjustments. Image compression is set to off, prioritizing maximal image quality and detail retention. The auto-adjusted parameters are turned off to eliminate the inconsistencies between measurements.

The image-capturing step follows the activation of the power LEDs. The images are captured using the configured camera settings. The images show focused fluorescein sodium salt and rhodamine B regions. They are exhibited in the corresponding sections according to the selected imaging mode. They are named according to these properties and taken timestamps while saving in .png format. Moreover, the metadata of each captured image is saved in .txt format. For future experiments, the region of interest describing the area where the dyes are expected to appear is placed on the read images by using the Imageio.V3 library. The ROIs are positioned according to the set slider value for the top-middle point of the rectangles with specified dimensions (width, height) to fit into the regions separately. The ROIs provide focus on the isolation of targeted regions from the rest of the imaged area. This ensures that subsequent image processing and analysis are focused solely on the fluorescein sodium salt and rhodamine B regions. Adjusted ROIs are also visually highlighted on the images using the Matplotlib patches library by drawing the colored rectangles around the defined ROIs. This visual cue verifies and ensures that the correct areas are considered. The images with ROIs are also saved in .png format for further analysis.

The colorful ROI images of T and C regions are read and analyzed separately for color and intensity levels within their color channels red (R), green (G), and blue (B). Histograms are produced by separating the image data into R, G, and B channels and calculating the frequency of each pixel intensity within these channels for future analysis. They are produced for both imaged dye regions to quantify variations in color and intensity. The histograms for both fluorescein sodium salt and rhodamine B regions allow for a comparative analysis. Histograms are shown as plots consisting of a horizontal axis representing pixel intensities in each color channel separately and a vertical axis illustrating the number of pixels in counts. In this analysis, normalized histograms exhibit each pixel intensity in the horizontal axis, ranging from 0 to 255, and their existence probability in the vertical axis. Probability is a measure of how often a particular intensity value occurs in the extracted ROI region. The production of the width and height of the interested image calculates the total number of pixels in the related ROI region. The probability is calculated as in Equation 3.1.

$$Probability\ (\%) = \frac{Number\ of\ pixels\ with\ specific\ intensity}{Total\ number\ of\ pixels} \times 100\% \qquad (3.1)$$

The peaks in the histogram indicate the most common intensities within the related ROI. For example, a peak near the lower end of the intensity spectrum suggests that the region is predominantly dark. Moreover, the contrast of the images is examined by evaluating the spread of the histograms. When the image is mostly of a similar intensity, its histogram shows a narrow spread, meaning there is low contrast in the image. On the other hand, the image consisting of a broad range of intensities demonstrates a wide spread in their histograms, indicating the high contrast levels. The mean parameter is considered a significant indicator for the quantification of the visual outputs since it correlates with the target analyte concentration. The extracted ROI images are converted to arrays for calculation of the mean values using the NumPy library in Python. The mean value for each array is calculated by the division of the pixels sum by the number of pixels. The G channel is considered for fluorescein sodium salt for mean value calculation. The mean value for the rhodamine B dye is calculated from the R channel. The resulting values are represented as plots for both dye region ROIs. These processing tools are featured on the developed software, but they are aimed to be used in future experiments for a full assay evaluation.

ImageJ open-source software is used to view and analyze the captured images in the current study. The software is equipped with a multitude of plugins designed for image analysis, including but not limited to histogram generation and mean intensity measurement. A histogram plot showing the distribution of the pixels in every channel is produced for each captured image. The minimum and maximum image intensities and the mean and standard deviation of the image intensities are calculated for the whole image. The ROI is set manually on the image, and the mean pixel value is calculated within the related channel instead of within the whole image. The mean value is calculated within the related channel by dividing the sum of the pixel values within the ROI by the area of the ROI.

3.2.11. Operating Procedure

The flowchart for the operating procedure of the preliminary reader is shown in Figure 3.19. The reader initiates with the configuration of general-purpose input/output pins, motor movements, and the activation and reading of the temperature-humidity sensor and real-time clock. The camera is configured as the main capturing mode implementing 8-bit RGB image data capturing. The GUI is presented on the screen with the status message “Please Insert the cartridge”. In parallel, continuous sensor readings for temperature and humidity are conducted, and real-time clock readings are obtained and shown on the GUI. Upon user interaction, the GUI, which includes buttons and sliders, allows for the selection of various imaging modes and parameters.

The “Pre-Imaging” mode is selected as the default (Post-imaging mode is for future experiments). The “Settings” for the image acquisition are adjusted on the GUI. The “Light Emission Time” determines the amount of time between 1-10 seconds that sets the LED on time (Default: 1 second). The “Camera Exposure” is the time that the camera is exposed to light in ms from 10 to 300 (Default: 10 ms). The “Analogue Gain” indicates the analog gain of the camera, adjustable between 1-10 (Default: 1). The cassette with the assay is placed into the cassette holder, and the sliding tray is activated when the “Insert” button is clicked. The tray stops moving when the holder is fully inserted. Image acquisition is started by clicking the “Image” button. The image acquisition begins with the camera opening, followed by an 8-second delay for waiting for the camera to prepare and apply the configured inherent settings. For imaging of fluorescein sodium salt, the 460 nm power LED is turned on for “Light emission time” in seconds. The status message of “Imaging T line” is shown. The image of fluorescein sodium salt is next captured. The power LED is turned off, and the status message is updated as “T line imaging completed.” The metadata of the imaging is saved in TXT format. The captured raw image with a resolution of 3280×2464 pixels is cropped to 620×430 pixels, and the resultant image is saved in 24-bit PNG format. The image is displayed in the Pre-T region panel. The procedure is repeated for rhodamine B imaging using the 560 nm power LED. The captured image for rhodamine B is presented in the Pre-C region panel. The ‘Set ROI’ and ‘Process’ buttons are added to the GUI for further processing in the future. The ROI rectangles with the dimensions of 120x670 pixels are set using a slider widget for both images. The slider position for each image is adjusted 580 pixels to the left and 580 pixels to the right from the zero point which is the default for the top-middle point of the ROI rectangle. After adjusting ROI positions in the x-axis, the “Process” button can be clicked to process the image. The process function reads the saved images for fluorescein sodium salt and rhodamine B and generates histogram and mean plots in .png format within the set ROI rectangles. The ‘Eject’ button is to eject the cassette holder and the status message “Insert the cartridge for imaging” is displayed after an ejection.

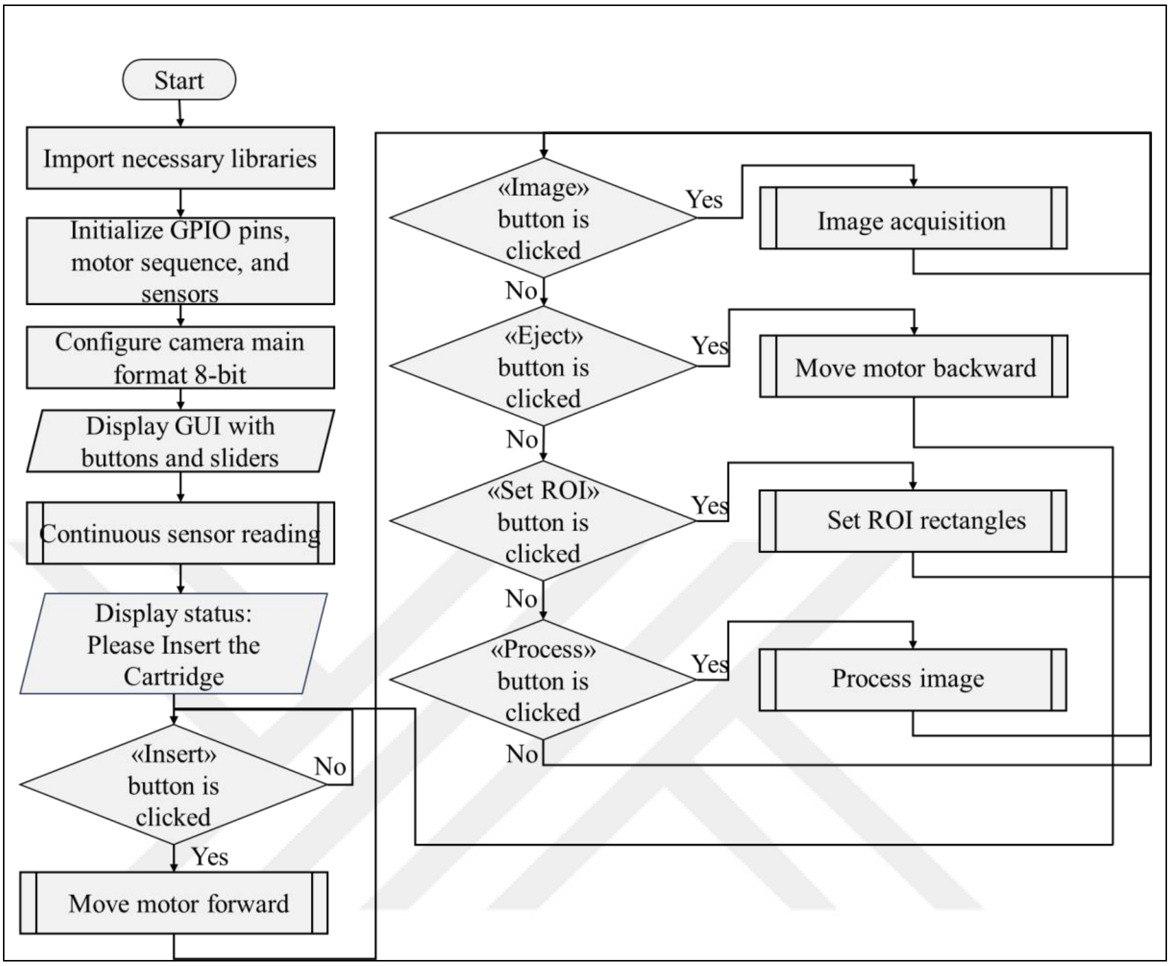

Figure 3.19. Flowchart for the working procedure of the preliminary reader.

3.3. FINAL OPTICAL READER

The final optical reader is developed to improve image quality and device performance by using an advanced CMOS camera, temperature-humidity sensor, and touch-screen display. In addition, this device is powered by batteries instead of mains electricity. Figure 3.20 shows the block diagram of the final optical reader. The software developed for the preliminary is modified for the “new” camera, display sensor, and camera, and the graphical user interface is updated for the resolution of the new display.

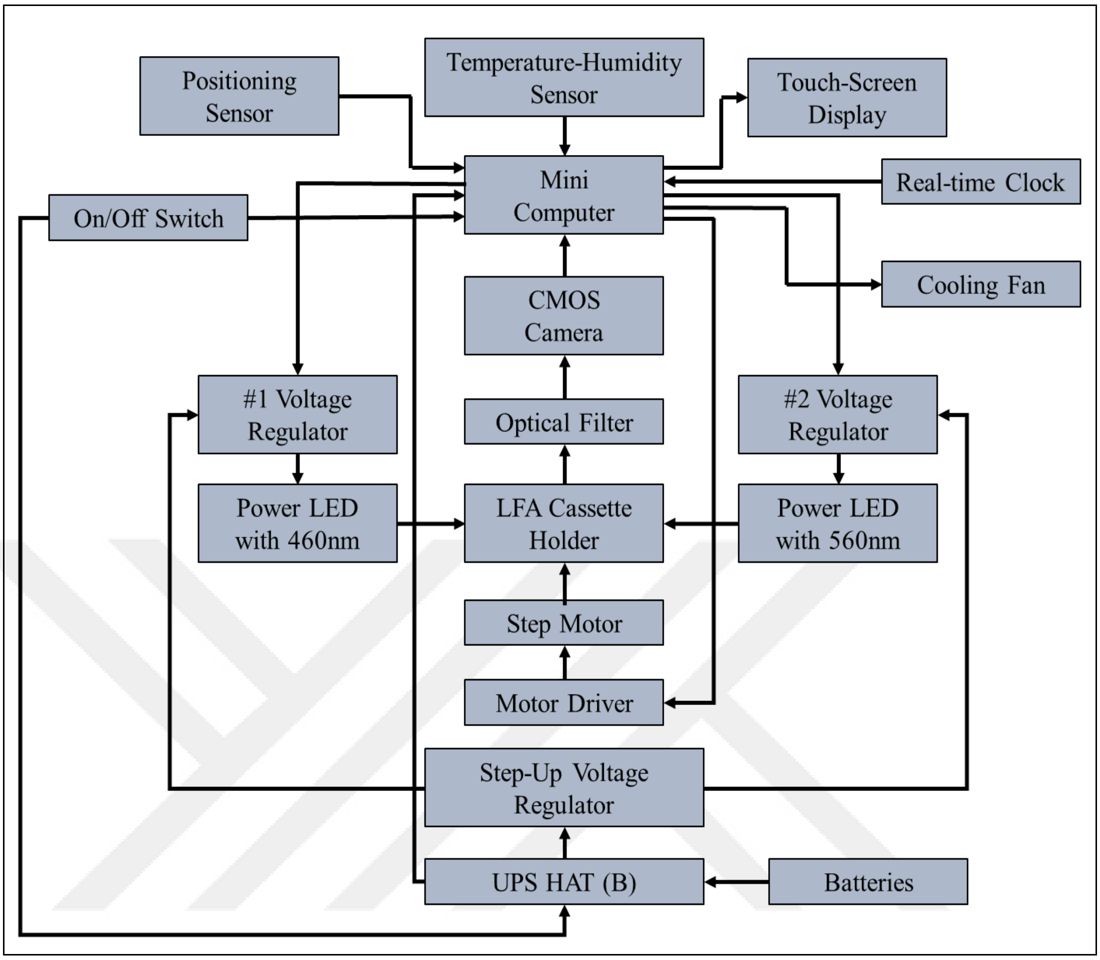

Figure 3.20. Block diagram of the final reader.

3.3.1. Minicomputer

In the final optical reader, Raspberry Pi 4B 8 GB is used instead of the Raspberry Pi 4B 4 GB employed in the preliminary reader. The minicomputer has 4 GB more RAM and 64 GB memory capacity. This is preferred for more data storage and faster response time while running more sophisticated algorithms.

3.3.2. Light Source

The backups of the 460 nm and 560 nm power LEDs employed in the preliminary reader are used, but 5-degree collimators are attached to the LEDs to narrow the spread of the light emitted by the power LEDs in the final reader. Each power LED is powered by its dedicated voltage regulator module as in the preliminary reader, but the voltage outputs of the models are tuned for better performance: The 460 nm power LED is powered by 3.3 Vdc and dissipates ~1.75 W. The 560 nm power LED is powered by 2.7 Vdc and dissipates ~1.82 W. To get the voltage regulator modules to operate better, the LM2577S adjustable DC-DC step-up voltage regulator module is embedded in the reader. This module can accept the input voltage from 3.5 Vdc to 35 Vdc and the output voltage is adjustable between 4 Vdc and 35 Vdc while delivering a rated current of up to 3A. [157]. It has a high conversion efficiency, around 92%, so it minimizes the energy loss during the voltage step-up process. It includes short-circuit protection through current limiting and automatic recovery.

The regulator module is fed by the 5V voltage from the UPS HAT and provides 8.5V output to both step-down voltage regulators. In addition to the step-up voltage regulator, the same type of step-down voltage regulator is employed to provide the required voltages to the power LEDs. The 100kΩ pull-up resistors are connected between their logic pins and input voltage (IN+) pins to control the turning on and turning off of the power LEDs. The logic pins of the regulators for the 460nm and 560nm power LEDs are connected to the GPIO 17 and GPIO 18 pins of the minicomputer. The 8.5V output of the step-up voltage regulator feeds the step-down voltage regulators. The output voltages are finely tuned using the onboard trim pot. The voltage regulators assigned as outputs in the developed code are initially turned off.

3.3.3. Camera

Arducam IMX477 HQ camera (Arducam, China), is employed for imaging the nitrocellulose membranes in the final reader (Figure 3.21). The module is equipped with a 12.3-megapixel IMX477 sensor and represents a significant upgrade from the 8-megapixel IMX219 sensor. It provides an enhanced resolution of 12.3 megapixels within an optical format of 1/2.3 inches image area (diagonal 7.9 mm). It can capture high-resolution static images at 4056 (H) x 3040 (V) pixels with a pixel size of 1.55 um × 1.55 um. It enables the capture of high-detail images essential for reliable imaging. The camera is interfaced through a 2-lane MIPI CSI connection to the Raspberry Pi minicomputer using a 15-pin flex cable (AOKIN, China). Furthermore, it features an interchangeable M12 lens mount system to replace M12 lenses with any degree. The FoV and focal length parameters are changeable based on the attached M12 lens degree. The manual focus capability by adjusting the lens position, provides the customization of the camera focus based on the imaging distance. The camera module comes with an integrated IR-cut filter between the sensor and the lens. In the implementation, this filter is removed to make the camera no-infrared (NoIR), and an M12 lens with 20^{o} is preferred. The RAW data format of the IMX477 sensor is 12-bit Bayer, and the captured images by the camera can be saved as 8-bit, 10-bit, and 12-bit. 8-bit and 10-bit images. For the IMX477 HQ camera, there are several 8-bit image formats available, including XBGR8888, XRGB8888, RGB888, and BGR888, as same as the IMX219 Raspberry Pi V2 camera. Additionally, a 10-bit image format, SRGGB10, and a 12-bit format, SRGGB12, are also provided. These formats lead to very high color depth.

Table 3.2 lists the major features of the Arducam IMX477 HQ camera and the Raspberry Pi IMX219 V2 camera for comparison. The IMX477 camera, with its higher resolution, larger optical format, and interchangeable lens system, offers a more flexible and higher-performance solution for applications requiring superior image quality and adaptability.

Figure 3.21. Arducam IMX477 HQ camera [158].

Table 3.2. Comparison of the cameras

Feature	IMX219	IMX477
Resolution	8 MP	12.3 MP
Optical Format	1/4"	1/2.3"
Active Pixels	3280(H) x 2464(V)	4056(H) x 3040(V)
Pixel Size	1.4 µm x 1.4 µm	1.55 µm x 1.55 µm
Lens Mount	Fixed Focus Lens	M12 Mount (Interchangeable)
Field of View	Fixed	Varies with lens
Raw Image Data	10-bit	12-bit

3.3.4. Optical Filter

An optical dual band-pass filter, which is identical to the optical filter of the preliminary reader, is placed between the camera sensor and the M12 lens holder by using a 3D-printed lens holder produced specifically. The filter position minimizes the potential for optical aberrations for uniform filtering. Figure 3.22 illustrates the layout of the camera, the optical filter, and the imaging area. The camera is placed five centimeters away from the laminar flow assay for proper focusing of the observation window of the assay.

3.3.5. Touch-Screen Display

A 5-inch capacitive touch-screen display (DSI LCD, Waveshare, China) is utilized in the final optical reader (Figure 3.23). The display incorporates a DSI interface, eliminating the need for the two external cables typically required for powering and activating touch functionality in HDMI displays. Therefore, the DSI interface provides both powering and communication of the display. It is connected to the DSI port of the minicomputer. It boasts a hardware resolution of 800×480 pixels. Moreover, the display supports up to 5-point touch, depending on the operating system, which enhances user interaction and allows for more complex touch-based commands. The screen transfers serial data by I2C communication with the minicomputer.

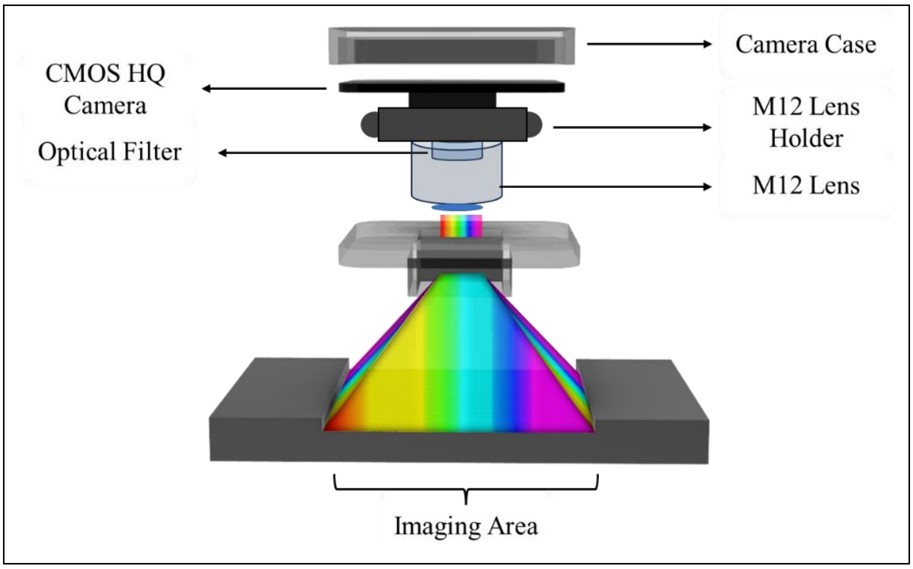

Figure 3.22. Layout of the imaging optics in the final reader.

(a) (b)

Figure 3.23. DSI touchscreen display. (a) Bottom, and (b) Top views [160].

3.3.6. Temperature, Humidity and Pressure Sensor

A temperature-humidity-pressure sensor, BME280 (Bosch Sensortec, Germany), is used to achieve accurate readings of the environmental temperature, humidity, and also atmospheric pressure that the assay is being exposed to during imaging. It is equipped with built-in 10 kΩ pull-up resistors for I²C communications that integrate it into the minicomputer via its pins: VCC for powering by 3.3 V on the minicomputer, GND as ground, and SDA and SCL pins for I²C communication via address 0x76 (see Figure 3.24).

3.3.7. Real-time Clock

A real-time clock module (DS3231, Maxim Integrated Inc., USA) is connected using its GPIO header and configured/activated by the terminal. The module is powered by a 3.3V pin of the minicomputer, and set to communicate with the minicomputer via I2C protocol (address: 0x68). The module has a CR-1220 3 V Li-ion battery for time and date backups.

(a) (b)

Figure 3.24. BME280 humidity sensor module. (a) Top and (b) Bottom views [159].

3.3.8. Uninterruptible Power Supply

An uninterruptible power supply module (Waveshare UPS HAT B for Raspberry Pi) is used to power the final reader. The module provides a reliable 5 Vdc power supply with real-time monitoring of the battery voltage, current, power, and remaining capacity by I2C communication (address:0x42). It supports an 8.4V 2A charger for recharging two 18650 Li-ion batteries that may accommodate a total capacity of 5200 mAh. The four pogo pins of the module are ground, I2C clock (SCL), serial data (SDA), and 5V output, which are wired to the minicomputer aligning pins (see Figure 3.25). The 5V output and ground pins are also connected to the input pins of the step-up voltage regulator LM2577S. The power switch on the module is removed, and the two pins of the switch are wired to the selected on/off switch for turning on/off the minicomputer and step-up voltage regulator.

3.3.9. Other Electronics

A DC fan motor that operates at 5Vdc / 150 mA (4010S5H, MER Inc., China) is integrated for improved cooling. A power adapter rated at 8.4 V and 2 A, is employed to energize the entire electronic components. A power on/off switch (Swion, China) equipped with an LED is employed to cut this power connection. The schematic diagram for the electronic components in the final optical reader is shown in Figure 3.26.

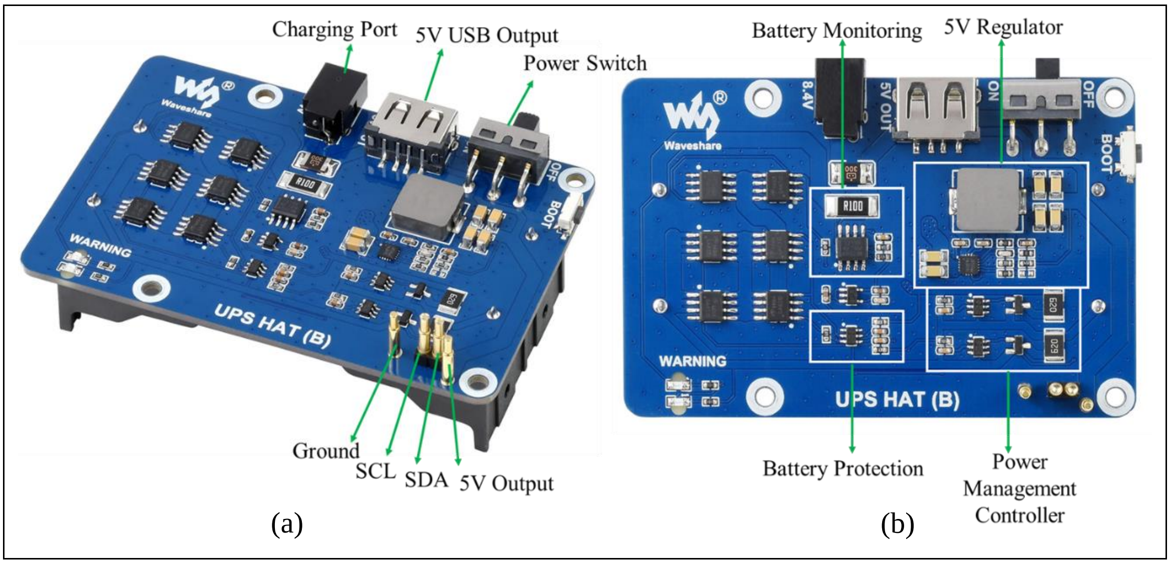

Figure 3.25. Uninterruptible power supply module (a) Side, and (b) Top views [156].

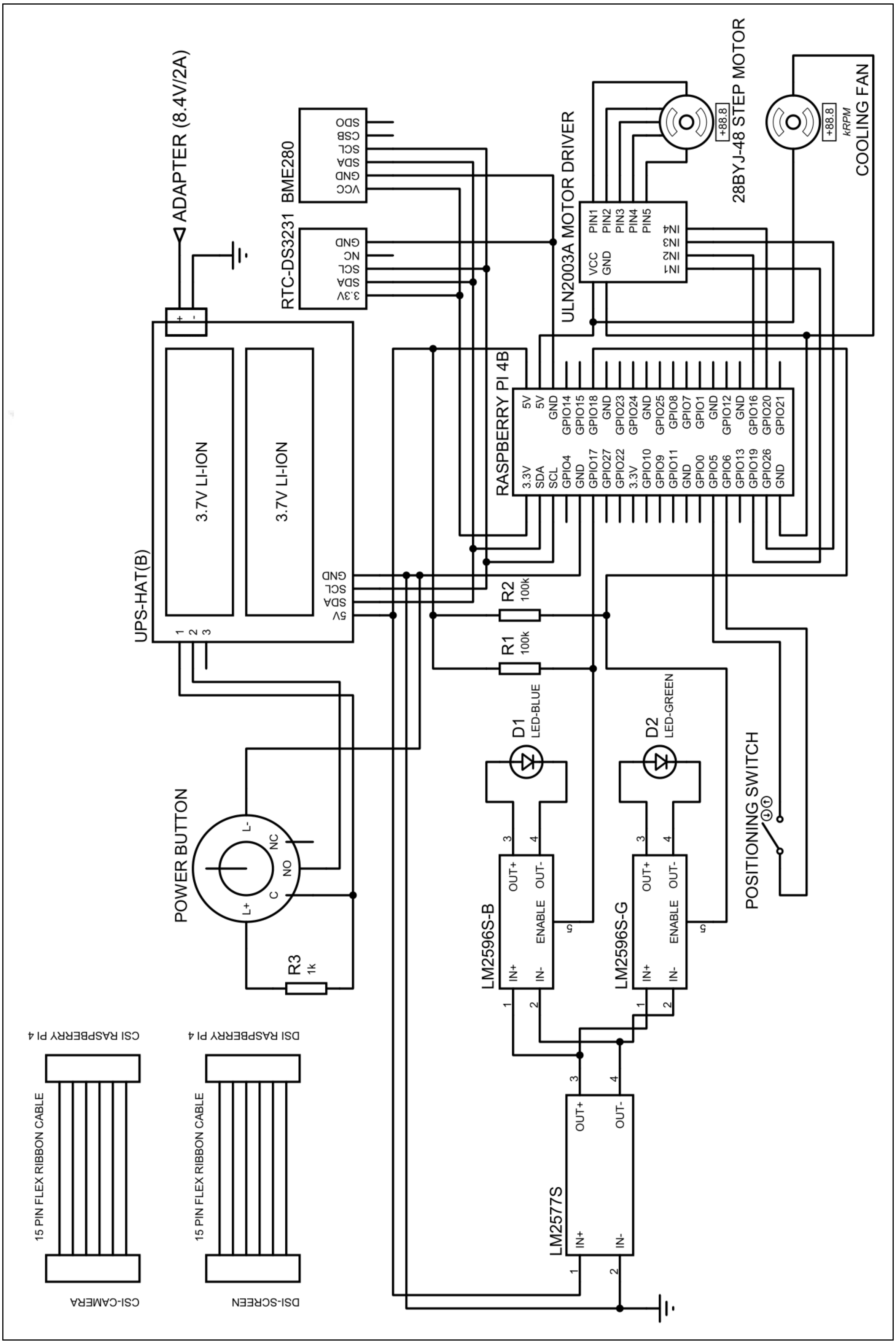

Figure 3.26. Schematic diagram of the final reader.

3.3.10. Mechanical Components

The mechanical components in the final reader are designed on the Autodesk Fusion 360 software (Autodesk Inc., USA) to ensure proper operation and durable construction in addition to precise placement of the components. A PLA filament with a thickness of 1.75 mm (Kimya, France) is used for manufacturing the main body. The black-colored darkroom is redesigned for positioning the camera, power LEDs, the optical dual band-pass filter, and a cassette within the designed sliding tray in addition to a hole for a laser light source for future experiments (Figure 3.27). Similar to the preliminary, the power LEDs are installed on either side and angled at 40 degrees toward the cassette. The beams are channeled through trapezoid-shaped apertures. The CMOS camera is mounted perpendicular to the cassette. The optical filter is placed between the camera sensor and the 20° M12 lens by using a 3D-printed M12 lens holder. The camera aperture is widened for the M12 lens when compared to the preliminary device. A modified enclosure for protection and maintaining the functionality and portability of the device is designed and printed using 1.75mm white and green PLA filament (Filamentum, Czechia). The enclosure has an aperture for the replacement of the DSI touch-screen display and a hole for the on/off switch (Figure 3.29). Similar to the preliminary device, it features a fan exhaust aperture for air-flowing. The physical appearance of the device is exhibited in Figure 3.30.

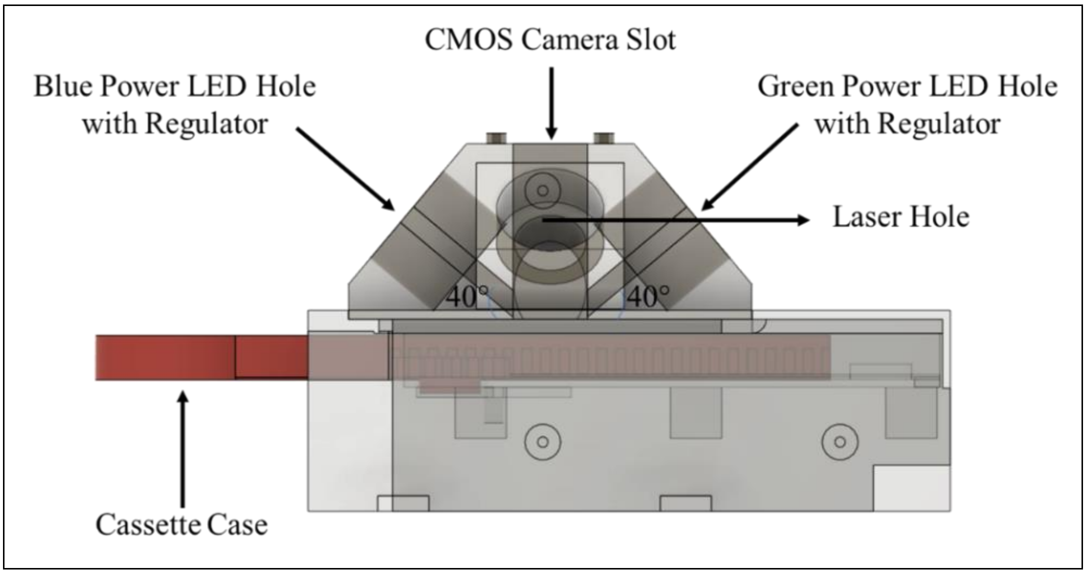

Figure 3.27. Darkroom of the final reader.

The motorized sliding tray consisting of the same components, a 28BYJ-48 unipolar stepper motor, a ULN2003AN motor driver, and the designed mechanical components, is reproduced for movement and positioning of the cassettes. The same movement sequence is applied for adjustment of its moving action. The electronics are integrated into the mechanical components designed on Autodesk Fusion 360 software (Autodesk Inc., USA) and produced using a 3D printer (E2, Raise3D, USA). A gear is positioned for sliding the cassette holder with rectangle wholes in a similar way applied in the preliminary. The designed motorized sliding tray for the optical reader is exhibited in Figure 3.28.

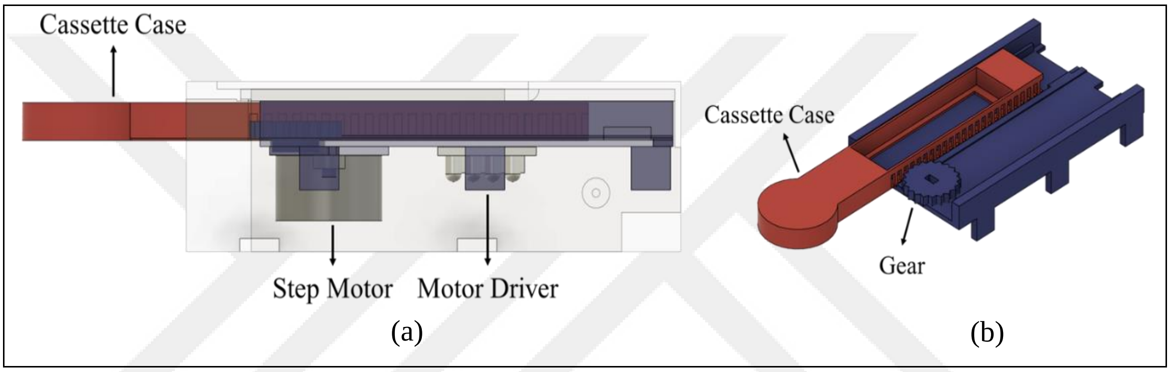

Figure 3.28. Sliding tray of the final reader. (a) Side, and (b) Top views.

Figure 3.29. Enclosure drawing of the final reader.

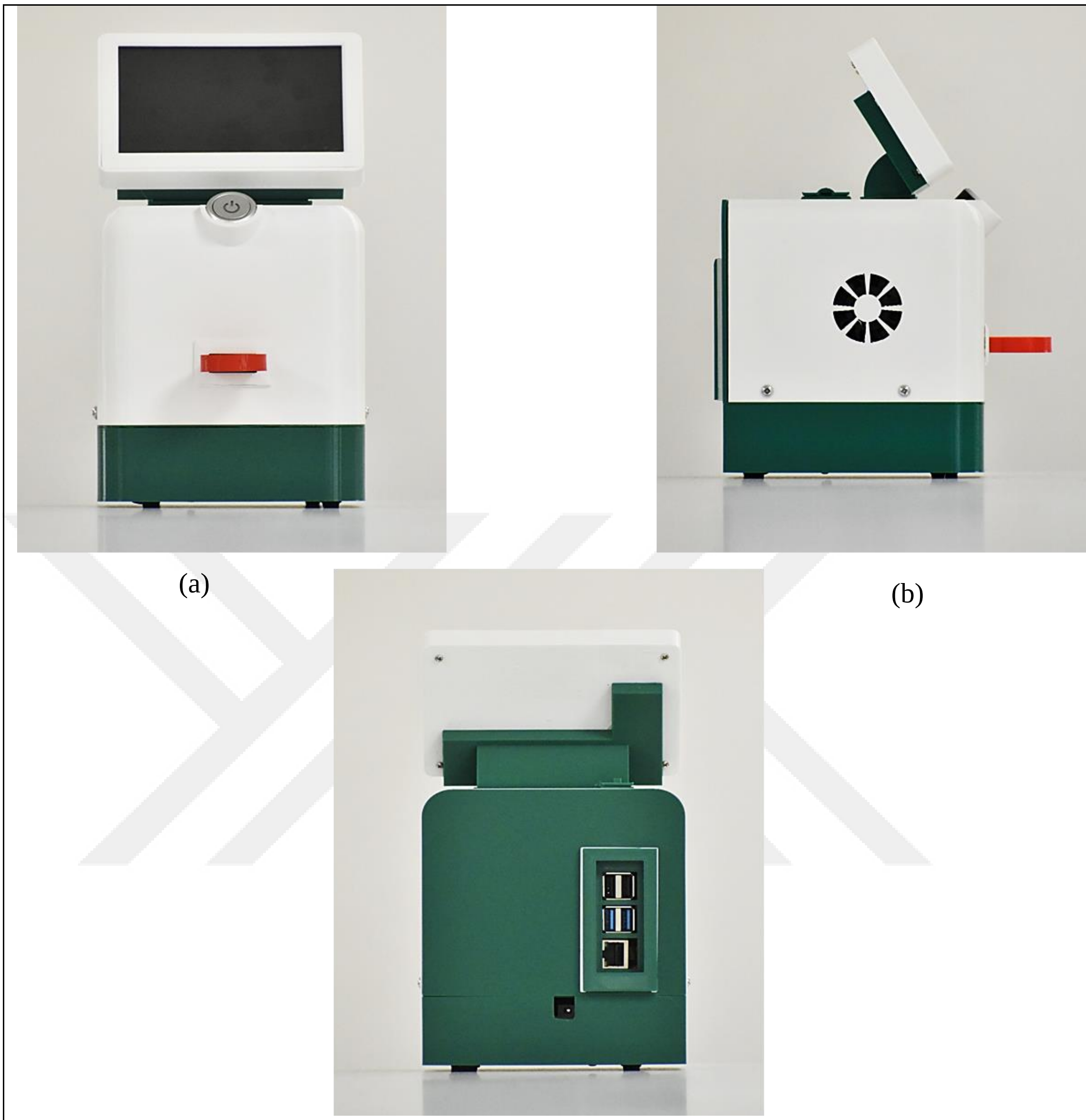

(a) (b) (c)

Figure 3.30. Physical appearance of the final reader. (a) Front, (b) Side, and (c) Back views.

3.3.11. Software

In the final reader, the changed components require some modifications in the developed code. The pressure, temperature, and humidity sensor, BME280, needs the “bme280” library of the python to work properly. Also, a library, “Adafruit_ina219”, is imported for the INA219 sensor for monitoring the status of the batteries. In the preliminary, the 8-bit images are generated and saved. In the final optical reader software, the imaging format is adjusted to the 'SRGGB12' raw format. In this way, higher-quality image data are captured for processing capabilities. In the final optical reader, the images are cropped. Also, the captured images are converted from Bayer RGGB format to the RGB format and cropped by the cv2 (OpenCV) library of Python instead of the PIL library. The metadata of the captured images is now saved with the Picamera2 library instead of the PIL (PngInfo) library. Apart from these changes, the device’s operation steps are the same within the software. The related code is written in the Python3 scripts on the Python environment (Python Software Foundation, USA). Each part of the developed software is explained in the following parts.

The previously designed GUI is adapted to the used DSI touch-screen display by changing the size of the application window, and the used widgets. The window size for the HDMI touch-screen display is adjusted according to the DSI touch-screen display. The modified version of the GUI layout can be seen in Figure 3.31. Some additional features resulting from the altered temperature sensor and added UPS are also visualized on the GUI. These changes are as follows:

- The altitude is calculated from the pressure readings by the BME280, and the calculated altitude in meters is shown in the sensor box next to the relative humidity. The altitude is calculated according to the Equation 3.2. where P0 is the reference atmospheric pressure at sea level (1013.25 hPa), P is the current atmospheric pressure measured by the BME280, 1/5.257 is a constant rate of temperature change with altitude and constant composition of the atmosphere, T is the read temperature by BME280 in Kelvin, and 0.0065 is the rate at which temperature in Kelvin, decreases with an increase in altitude.

$$Altitude\ (m) = \left(\left(\frac{P0}{P}\right)^{\frac{1}{5.257}} - 1\right) * \frac{T}{0.0065} \tag{3.2}$$

- A waffle widget is also used as a battery indicator. It represents the battery percent in five stages using the read voltage levels by the INA219 monitoring sensor of the UPS. The percent value is calculated from the ratio of the current-voltage difference to the maximum voltage difference, multiplied by 100.

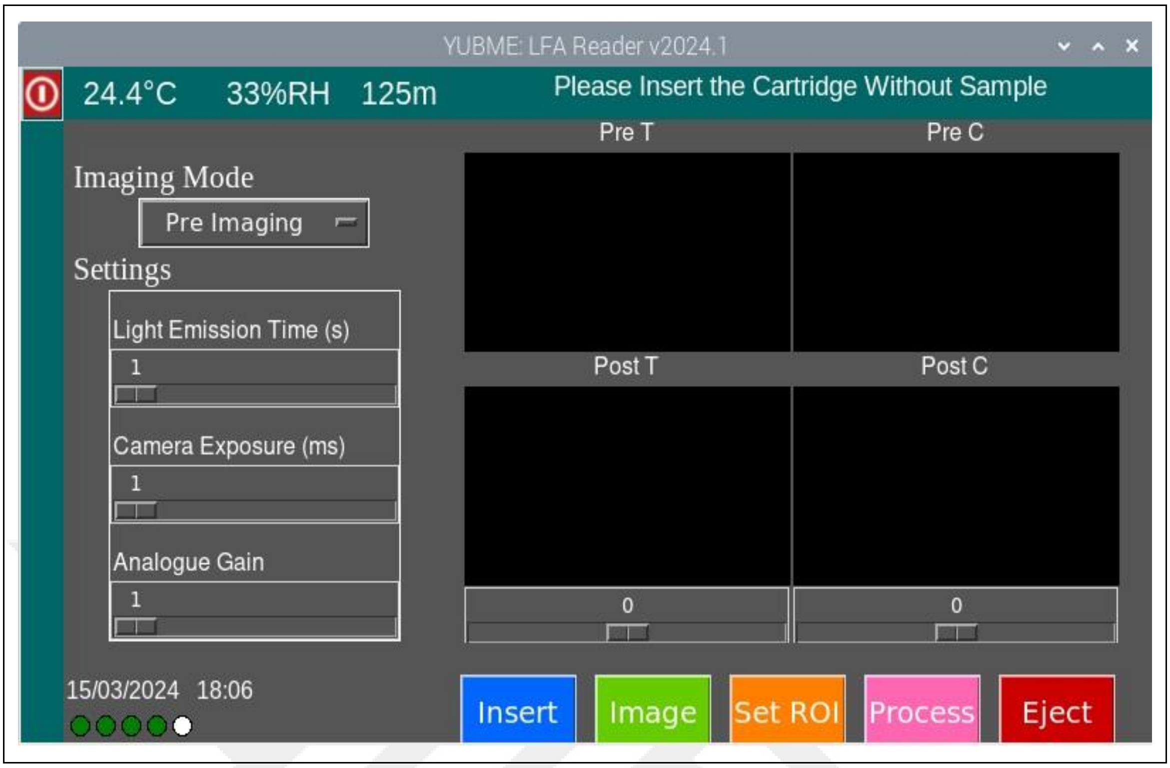

Figure 3.31. The graphical user interface of the final reader.

In the final optical reader, the IMX477 camera captures images with a higher resolution of 4056×3040 pixels. Since the imaging area of the camera with a 20° M12 lens is still larger than the target area, the images are cropped and saved as 1400×910 pixels. The camera chip captures images in RGGB Bayer format. The raw format saves 12-bit images in greyscale for representation, while the previous code saves 8-bit images in RGB format. By using Bayer transformation, the obtained image is converted to the 12-bit RGB format and saved. Each channel of the obtained image includes 12-bit data, so the overall RGB image is 48-bit. The pixel values within each channel can get values between 0 and 65520. Since the PIL library is not suitable for showing and saving this image format, they are represented and saved using the cv2 library. In the obtained 12-bit data, the higher-quality images with improved color resolution are aimed to be achieved. The exposure time range is scaled down from 10-300 ms to 1-30 ms because of the chip size differences in cameras and the smaller distance between the camera and the membranes. Other settings are configured, and the same operation steps for image capturing and processing are performed just like in the preliminary optical device. The ROIs in the imaged area are positioned by specified coordinates (x, y) and dimensions (width, height) to fit into these regions separately. These dimensions are modified to match the changed image area. The histogram plots representing pixel intensities within RGB channels are produced for both fluorescein sodium salt and rhodamine B images. The arrays obtained from the images are used to calculate mean intensities. The G channel and R channel are considered for fluorescein sodium salt and rhodamine B dyes, respectively, for mean value calculations. This section is developed for future experiments like in the preliminary optical reader.

The ImageJ open-source software is utilized to view and analyze the captured images in the final reader. For each 12-bit RGB image, a histogram is generated, with the x-axis maxing out at 65520, unlike the 255 maximum for 8-bit images. The pixel count axis is auto-scaled according to the maximum peak within the histogram of each channel. The mean, maximum, and minimum pixel values and standard deviation are calculated within the whole image. The ROI is set manually on the image, and the mean pixel value is calculated within the related channel instead of within the whole image. The mean value is calculated within the related channel by dividing the sum of the pixel values within the ROI by the area of the ROI. Some post-processing methods like image segmentation, filtering, or background subtraction can be applied to the captured images to enhance the interpretation of the results. The background subtraction is used to differentiate the fluorescence signal from the reflected excitation light or noise. For this aim, two images, under identical settings with the captured images of the fluorescent dyes, are captured on the related regions of both dyes using the control sample. The control sample does not include the fluorescent dyes to serve as the background on the images. The images of the corresponding concentration levels are evaluated based on this blank image. In this process, the blank image is subtracted from every image containing different concentrations of the dyes. In this process, the blank image of the fluorescein sodium salt is subtracted from the images captured for each concentration level of the fluorescein sodium salt. The blank image of the rhodamine B is subtracted from the images captured for each concentration level of the rhodamine B using Equation 3.3. The subtraction removes any uniform background noise, including the reflected excitation light from the power LEDs, enhancing the contrast and visibility of the specific fluorescence signal, which results in more accurate intensity and distribution of the fluorescent label.

$$Subtracted\ Image_{FS,RB} = Image\ with\ fluorescence_{FS,RB} - Blank\ image_{FS,RB} \tag{3.3}$$

3.3.12. Operating Procedure

The flowchart for the operating procedure of the final optical reader is shown in Figure 3.32. There are many similarities between the final and preliminary reader operations. Differently, on the graphical user interface, the sensor box also demonstrates the pressure measured, and the battery status is shown with the charge percent for the battery. The camera exposure time is now adjustable between 1 and 30 ms compared to the range of 10-300 ms in the preliminary reader. The final reader performs the same imaging steps as the preliminary reader. However, the camera is configured to capture a 12-bit RGB image rather than an 8-bit image while it benefits from the 12-bit RGGB Bayer imaging format.

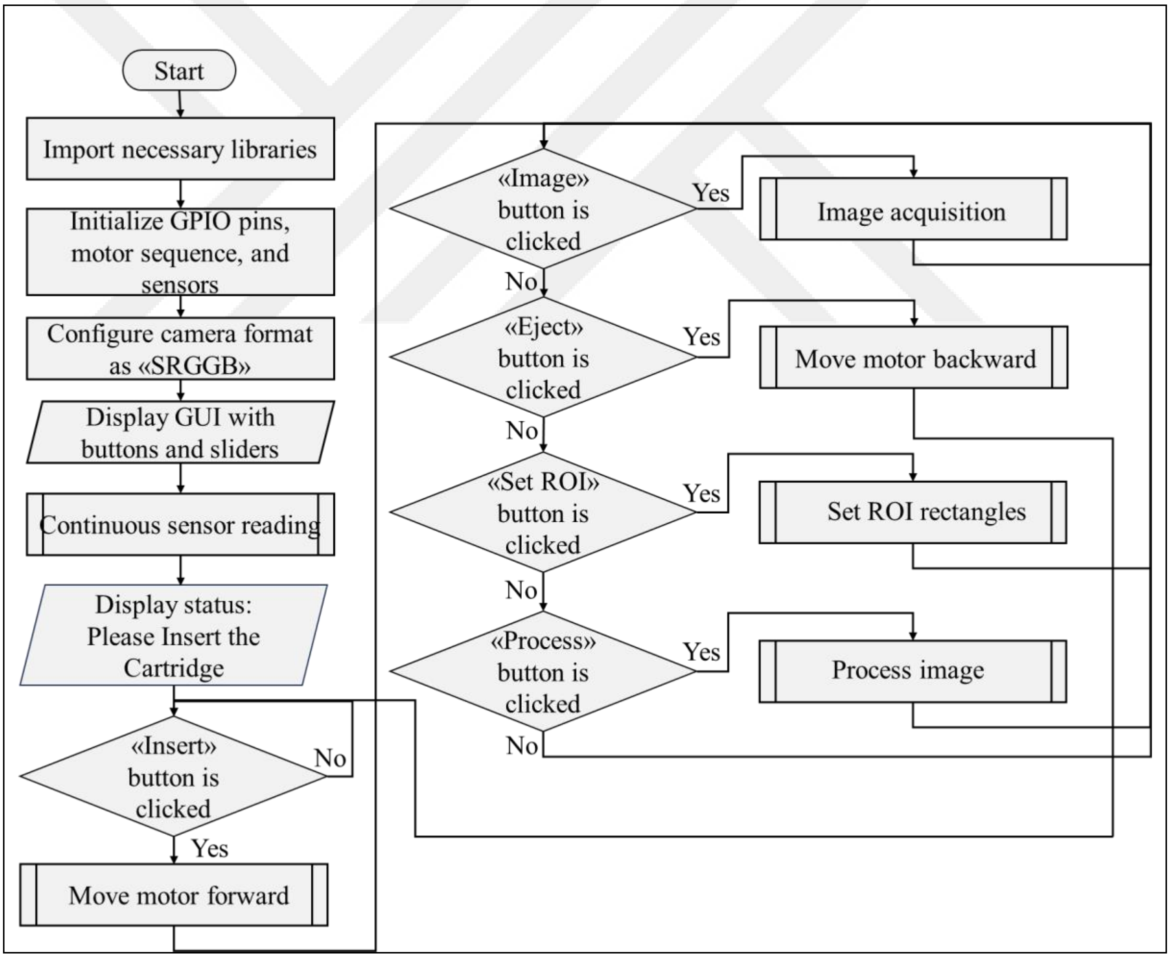

Figure 3.32. Flowchart for the working procedure of the final reader.

4. RESULTS

The results of the tests for the power LEDs and the optical filter and the images captured using the preliminary and the final readers are provided in separate sections.

4.1. TESTS WITH POWER LEDS

Figure 4.1 shows the electrical characteristics and light emission intensities of the 3W power LEDs tested for different DC supply voltages. For the 460 nm power LED, the supply voltage range is between 2.5 V and 3.3 V for regular operation, while it is from 2.1 V to 2.8 V for the 560 nm power LED. There is a strong linear correlation between the supply voltage and the emitted light intensity for both LEDs (R^2=0.9923 for the blue LED and R^2=0.9949 for the green LED). However, a strong non-linear correlation exists between the current and the emitted light intensity for the LEDs (R^2=0.9961 for the blue LED and R^2=0.9912 for the green LED).

Figure 4.2 shows the current and the emitted light wavelength for the power LEDs. The 460 nm LED emits light with center wavelengths from 464 nm to 459 while the current is set from 10 mA to 710 mA. The emitted light wavelength is fixed to 459 nm for the currents higher than 280 mA. On the other hand, the 560 nm LED emits light with center wavelengths from 580 nm to 558 nm while the current is set from 20 mA to 730 mA. The emitted light wavelength is fixed to 558 nm for the currents higher than 310 mA. The current flowing through a power LED has an impact on the wavelength of the light emitted by the LED, but it also determines the intensity of the light emitted. A higher current delivers a higher light intensity: The highest current of 710 mA is achieved for the 460 nm power LED when it is connected to a 3.3 V supply voltage, and the highest current of 730 mA is achieved for the the 560 nm power LED when it is connected to 2.8 V supply voltage (The readers developed house the 460 nm power LED for the excitation of the fluorescein sodium salt, and the 560 nm power LED for the excitation of the rhodamine B). Figure 4.3 shows the emission spectra of the LEDs when they are operated at these highest current ratings. The 460 nm LED provides a narrow emission spectrum concentrated between 445 nm and 475 nm with a peak at 459 nm. On the other hand, the 560 nm LED delivers a broader emission spectrum between 540 nm and 580 nm centered at 558 nm.

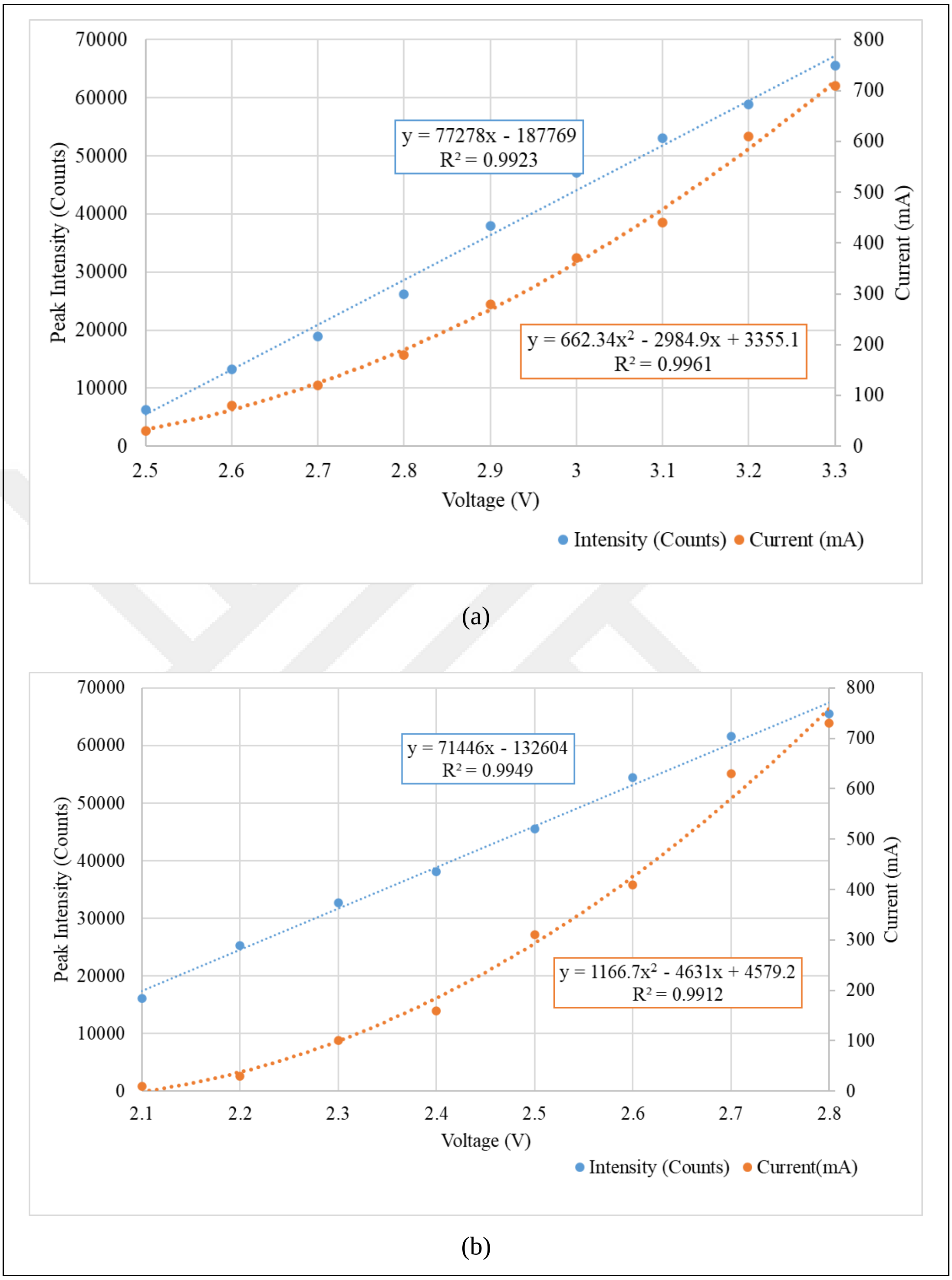

Figure 4.1. Electrical characteristics and light emission intensity by (a) the 460 nm LED and (b) the 560 nm LED.

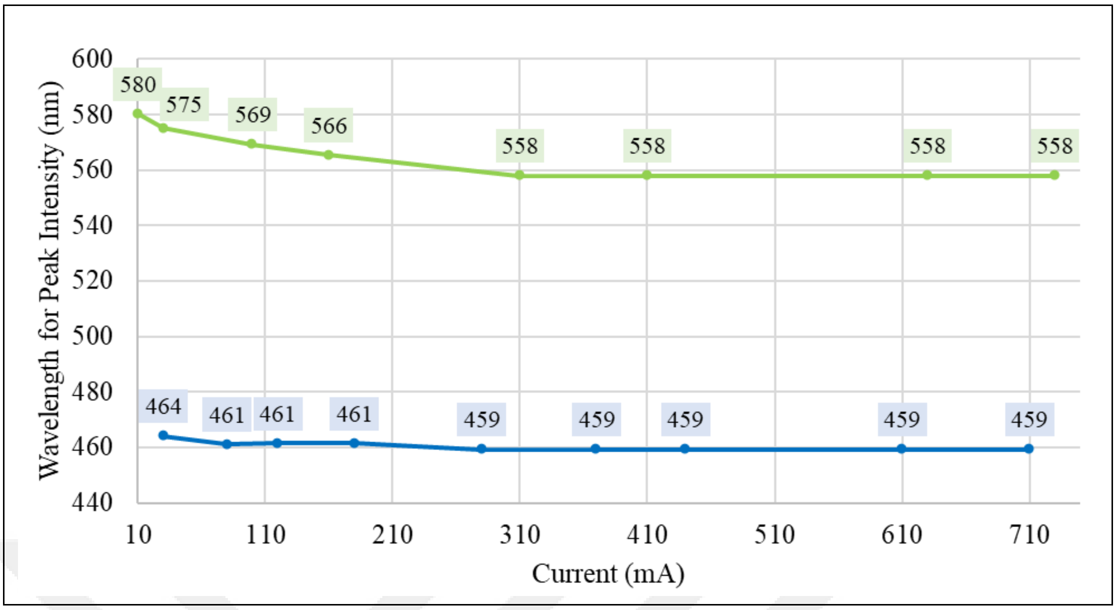

Figure 4.2. Plot for the current vs emitted light wavelength by (a) the 560 nm LED (green solid line), and (b) the 460 nm LED (blue solid line).

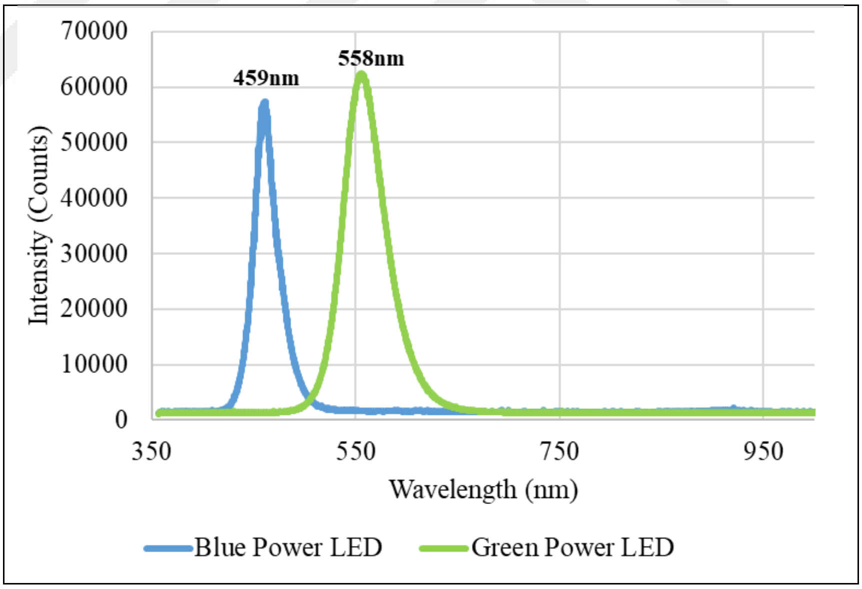

Figure 4.3. Emission spectra of the 460 nm LED (blue) and 560 nm LED (green).

4.2. TESTS WITH THE OPTICAL FILTER

Figure 4.4. shows the transmission curves for the optical dual band-pass filter obtained after testing and the curves reported in the datasheet of the filter. The test results describe that the filter has two distinct transmission bands, indicative of its capability to transmit light at two

specific wavelength ranges while attenuating the light at the remaining wavelengths. The first transmission band is at 512±23 nm and shows a sharp rise followed by a continuous slow rise and a fall in transmission, which indicates good filtering in detecting the light emitted by the fluorescein sodium salt dye (the center wavelength of the emitted light by the dye is at 515 nm). The second transmission band is at 630±91 nm and shows a sharp rise, a plateau, and a fall in transmission, which indicates remarkably good filtering in detecting the light emitted by the rhodamine B dye (the center wavelength of the emitted light by the dye is at 630 nm). The transmission curve obtained after testing and the transmission curve reported in the datasheet converge very well.

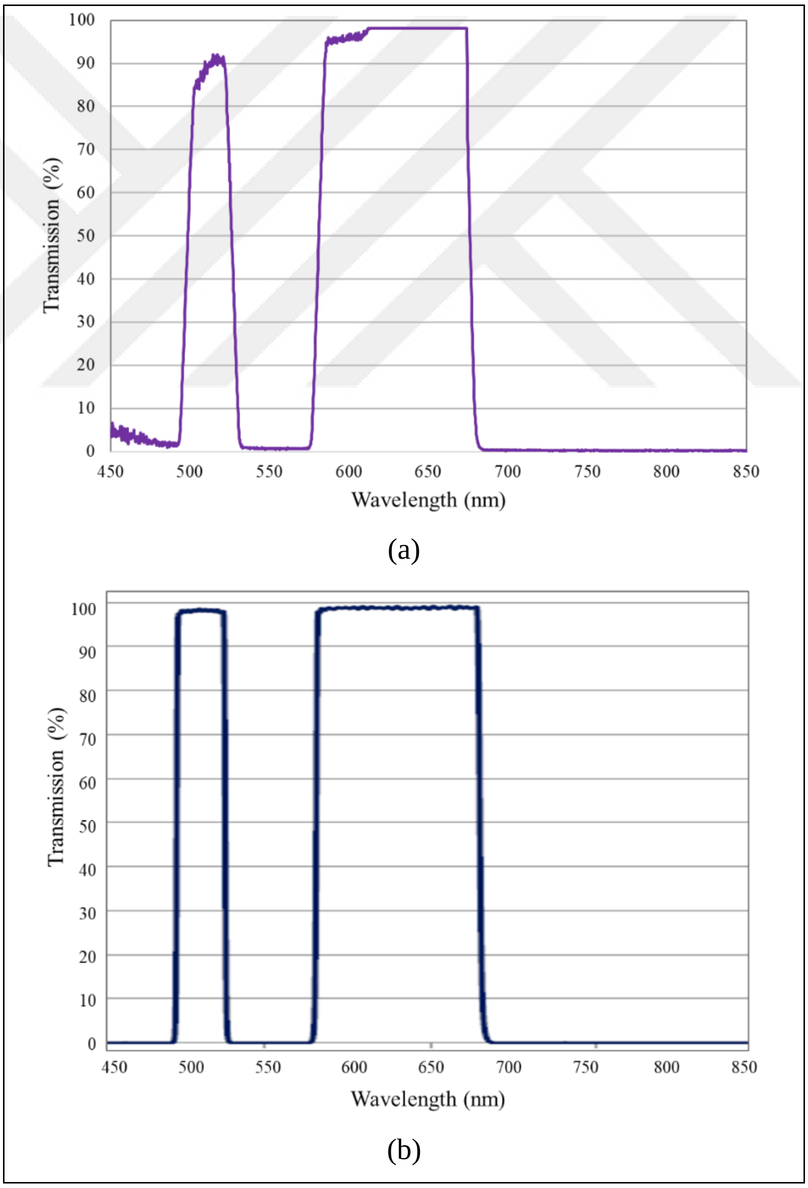

Figure 4.4. Transmission curves of the optical dual band-pass filter.

(a) The test result, and (b) The datasheet supplied.

4.3. EXAMPLE IMAGING

The imaging procedure is illustrated considering a membrane with 90 μM fluorescein sodium salt and rhodamine B dye drops. Figure 4.5 presents the 8-bit RGB images of the dyes captured with 1 ms camera exposure time, 1 s light emission time, and 1.0 analog gain. The content of the metadata file saved in a .txt file for each imaging is seen in Figure 4.6. The “SensorTimestamp” is the time in microseconds elapsed since the boot of the CMOS camera. The “ExposureTime” is the duration of the camera being exposed to light in microseconds. The “FocusFoM” gives the focus quality during imaging. The “ColorCorrectionMatrix” is the transformation matrix in estimating the standard RGB color space from the raw sensor color values. The “FrameDuration” is the total time from the start of one frame to the start of the next and is given in microseconds. The “AeLocked” is to lock the exposure settings at a desired level and is set to “True” to use the user-supplied exposure time. The “AnalogueGain” defines the amplification for the signal and is set to 1.0 for unity signal amplification. The “DigitalGain” determines the digitized signal amplification and is set to 1.0 for unity signal amplification. The “ColorTemperature” represents the color temperature of the light source in kelvin. The “ColorGain” is to balance the red and blue channels based on the color temperature of the light source. The “Lux” is the amount of light per unit area reaching the camera. The “SensorBlackLevels” is the level offset for each channel used for the calibration. The “ScalerCrop” is the sensor area in pixels that is read out and processed. The “LightOnTime” represents the light emission time and is set to 1 s by the user. The “EnvTemperature” and “EnvRelHumudity” are, respectively, the environment temperature and humidity that the membrane faces during imaging.

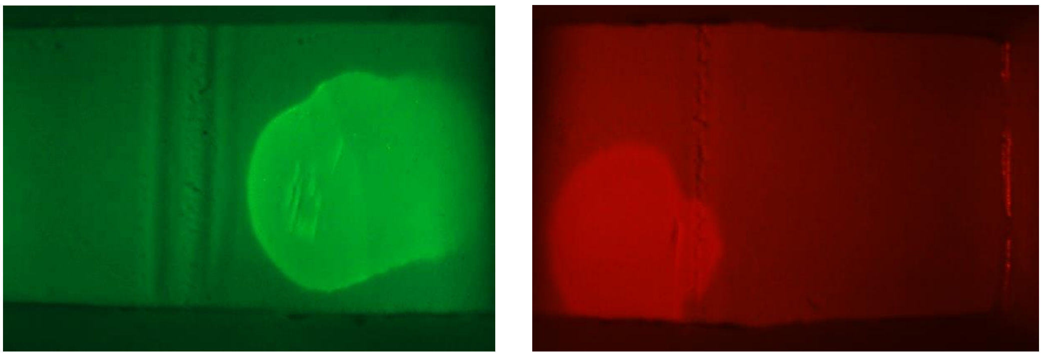

(a) (b)

Figure 4.5. Images captured for the (a) Fluorescein sodium salt, and (b) Rhodamine B.

```
SensorTimestamp: 347067932000
ExposureTime: 1000
SensorTemperature: 0.0
FocusFoM: 2176
ColourCorrectionMatrix: (2.1575498580932617, -1.1039637327194214,
 -0.05359601974487305, -0.3457588851451874,
 1.6122934818267822, -0.2665446400642395,
-0.02813815139234066, -0.7009111046791077, 1.7290493249893188)
FrameDuration: 100000
AeLocked: True
AnalogueGain: 1.0
ColourGains: (2.510904550552368, 1.656680941581726)
DigitalGain: 1.0
ColourTemperature: 4000
Lux: 821.1044921875
SensorBlackLevels: (4096, 4096, 4096, 4096)
ScalerCrop: (0, 0, 4056, 3040)
LightOnTime     (s): 1
EnvTemperature (oC):   20.6°C
EnvRelHumidity  (%):  36%RH
```

Figure 4.6. Contents of the metadata file.

Figures 4.7 and 4.8 show the mean and histogram plots of the imaged fluorescein sodium salt and rhodamine B generated by the reader for future analysis.

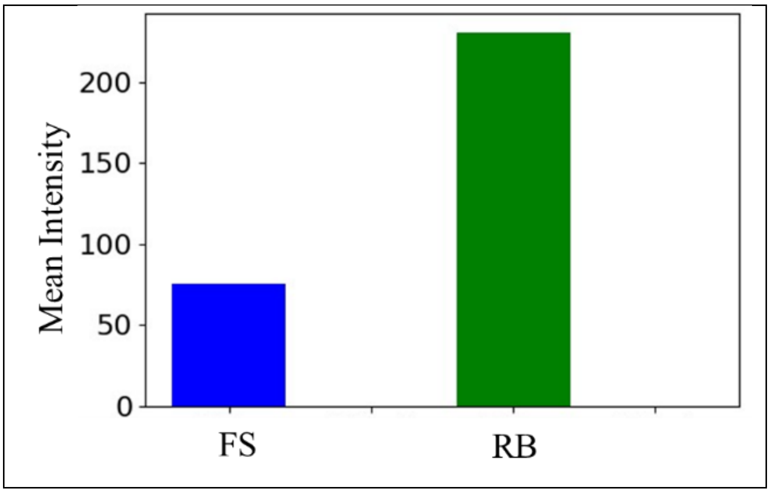

Figure 4.7. Plots for the mean intensity from fluorescein sodium salt, and rhodamine B images.

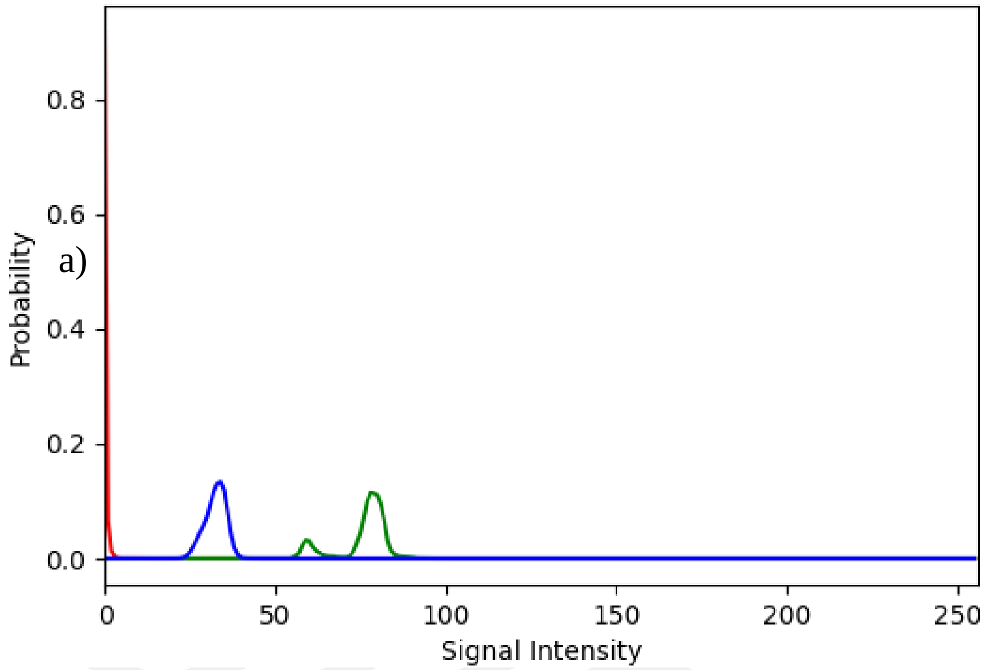

(a)

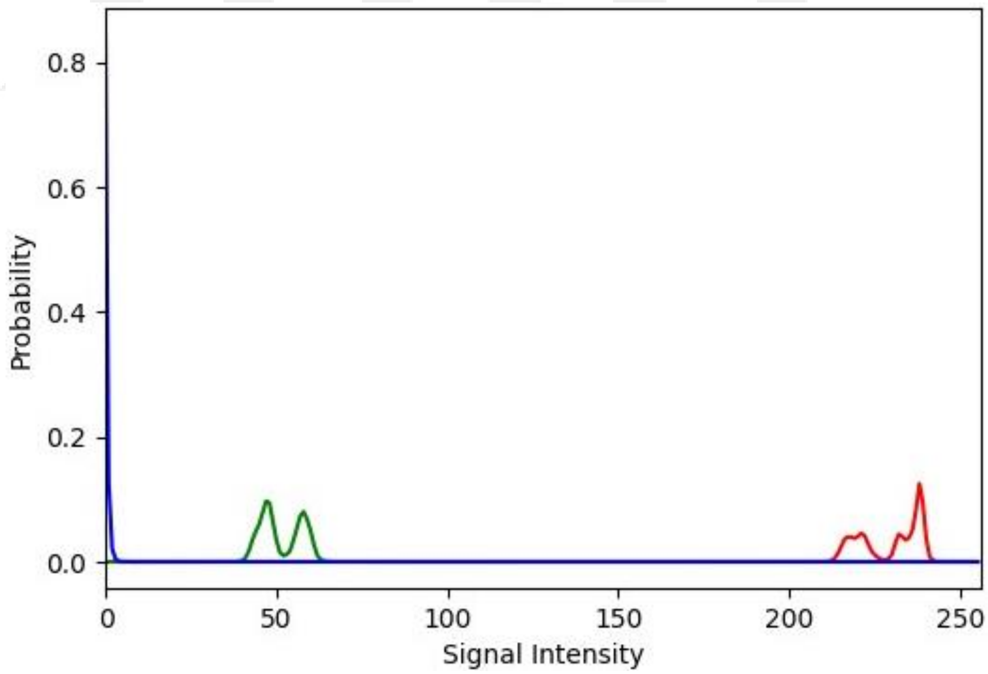

(b)

Figure 4.8. The image intensity histograms for the

(a) Fluorescein sodium salt, and (c) Rhodamine B images.

4.4. PRELIMINARY OPTICAL READER

The preliminary optical reader is with a weight of 0.93kg and dimensions of 15×14×23cm^3 (W×H×L). The reader is used to analyze the prepared fluorescein sodium salt and rhodamine B dyes. 1µL Fluorescein sodium salt and rhodamine B dyes with concentrations of 1000 µM, 100 µM, 10 µM, and 1 µM are dropped into the nitrocellulose membranes manually. The used membranes are blocked with 1% skim milk, and they are used for the first time. The membranes are next imaged using the preliminary optical reader device. The exposure time is set to 10 ms, the light emission time is set to 1 s, and the analog gain is set to 1.0 using the graphical user interface developed for the device. The 8-bit RGB images are captured for each concentration level. The membranes are also imaged with 30 ms exposure time, too. During imaging, the temperature and relative humidity are measured and recorded as 24.8°C and 29%, respectively, on average. All of the 8-bit RGB images captured are analyzed on ImageJ Software to generate histogram plots of each channel for the whole image and to estimate the mean intensity within a selected rectangular ROI on the image. Histogram plots for red, green, and blue channels are produced separately.

For the 1000 µM fluorescein sodium salt sample imaged using 10 ms exposure time, different shades of green color highlighting the fluorescein dye solution delivered by the membrane with darker-edge stains are observable on the image captured (Figure 4.9). The red channel histogram indicates a low mean intensity of 11±23. In the green channel, the mean intensity increases to 131±70, suggesting a brighter image with greater variability, which could be due to a combination of bright spots and darker areas. The blue channel histogram shows a mean pixel intensity of 65±38, indicating a moderate level of brightness and variation within the captured image. When imaging is repeated with 30 ms exposure time, a brighter image is obtained, and the mean intensity for all three channels is increased (Figure 4.10). The center of the dye stain is represented as white, which is a sign of saturation. In the red channel, the mean intensity is 26. In the green channel, the mean intensity increases to 192±85. The blue channel demonstrates an approximately doubled mean, 136±72, in the pixel intensity distribution.

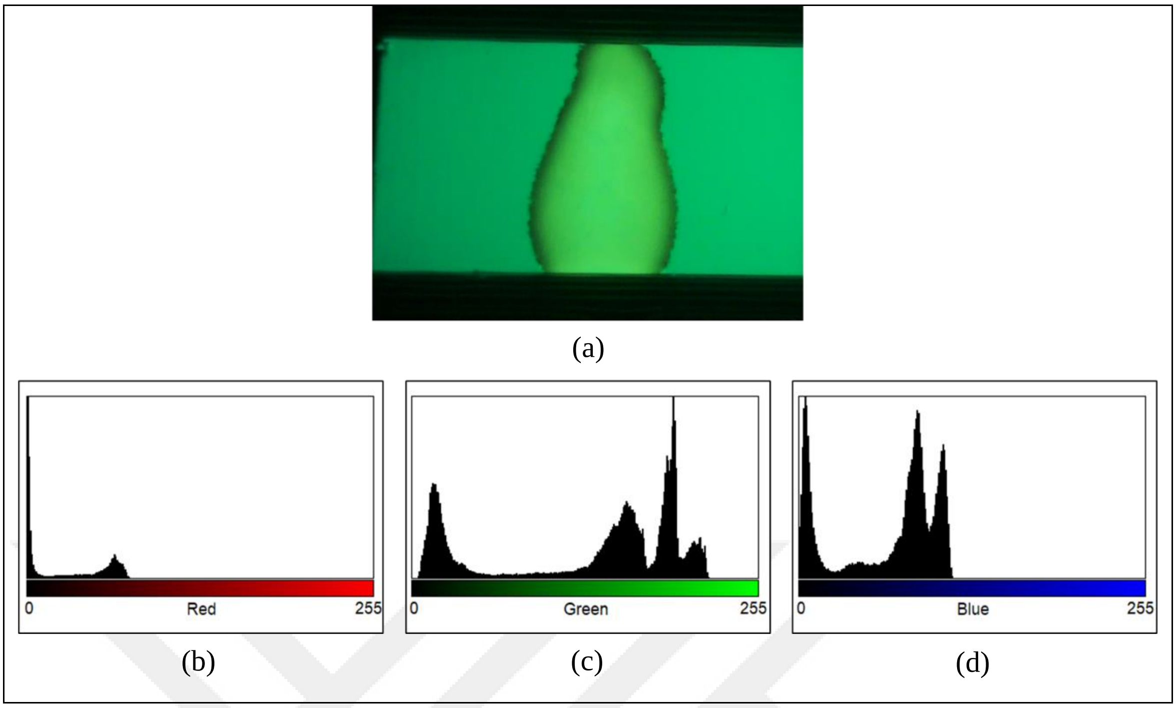

Figure 4.9. 1000 µM fluorescein sodium salt. (a) 8-bit image captured with 10 ms exposure time, and (b-d) RGB channel histograms.

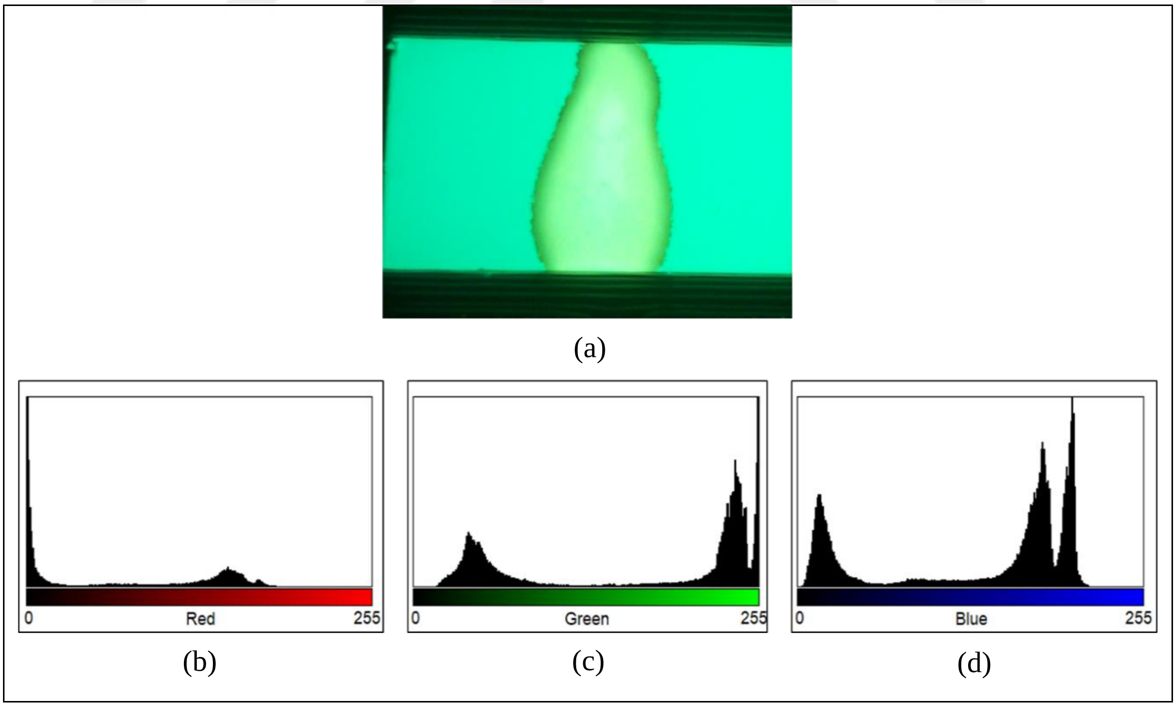

Figure 4.10. 1000 µM fluorescein sodium salt. (a) 8-bit image captured with 30 ms exposure time, and (b-d) RGB channel histograms.

For 100 μM concentration level at 10 ms camera exposure, the dye is distinguished from the background, especially on the edges of the stain (Figure 4.11). The red channel histogram shows a very low distribution of pixel intensities with a mean of 0.8±4. The mean intensity in the green channel is significantly higher at 139±70, reflecting the fluorescence emission. The blue channel has a mean pixel intensity of 74±40. When the sample is imaged with 30 ms camera exposure, the background and fluorescent parts are much brighter, and the stain edges become white-colored (Figure 4.12). The red channel has a low mean intensity of 5±26. In the green channel, the mean intensity is 199±83. The mean intensity value of 149±74 is observed in the blue channel.

For a 10 μM concentration level at 10 ms camera exposure, the delivered fluorescein sodium salt is slightly visible on the edges, as observed on the 8-bit RGB image (Figure 4.13). The red channel has a low level of signal intensity, 0.3±1. The histogram of the green channel shows a mean intensity value of 13±69, showing the spread of the intensities. The histogram for the blue channel reveals a mean pixel intensity of 70±39. When the exposure time of the camera is set to 30 ms, the fluorescent stain is barely seen on the image since the brightness of the whole image is increased (see Figure 4.14). The red channel mean intensity is 0.5±2, indicating a tight clustering of the intensity around the mean. The green channel displays a mean pixel intensity of 194±87, which is slightly greater than the measured value at 10ms exposure time. The histogram of the blue channel indicates a mean pixel intensity value of 143±73.

For 1 μM concentration of fluorescein sodium salt, the fluorescein sodium salt stain is not visible; the edges of the stain appear slightly on the 8-bit RGB image (see Figure 4.15). The histogram for the red channel presents a mean pixel intensity of 0.2, indicating a very low level of red intensity in the image. The green channel histogram indicates that the mean pixel intensity is 126±71, indicating a relatively wide spread of pixel intensities. The blue channel shows a mean pixel intensity of 67±40, indicating some variability in pixel intensity. In further imaging at 30 ms exposure time, the fluorescent part is not visible on the 8-bit RGB image (Figure 4.16). The mean intensity and standard deviation are 0.4±2, respectively, while the mode remains the same in the red channel. The green channel histogram shows an increased intensity of 187±90. A large number of pixels are saturated in the green channel. In the blue channel, the pixel intensity is 138±76.

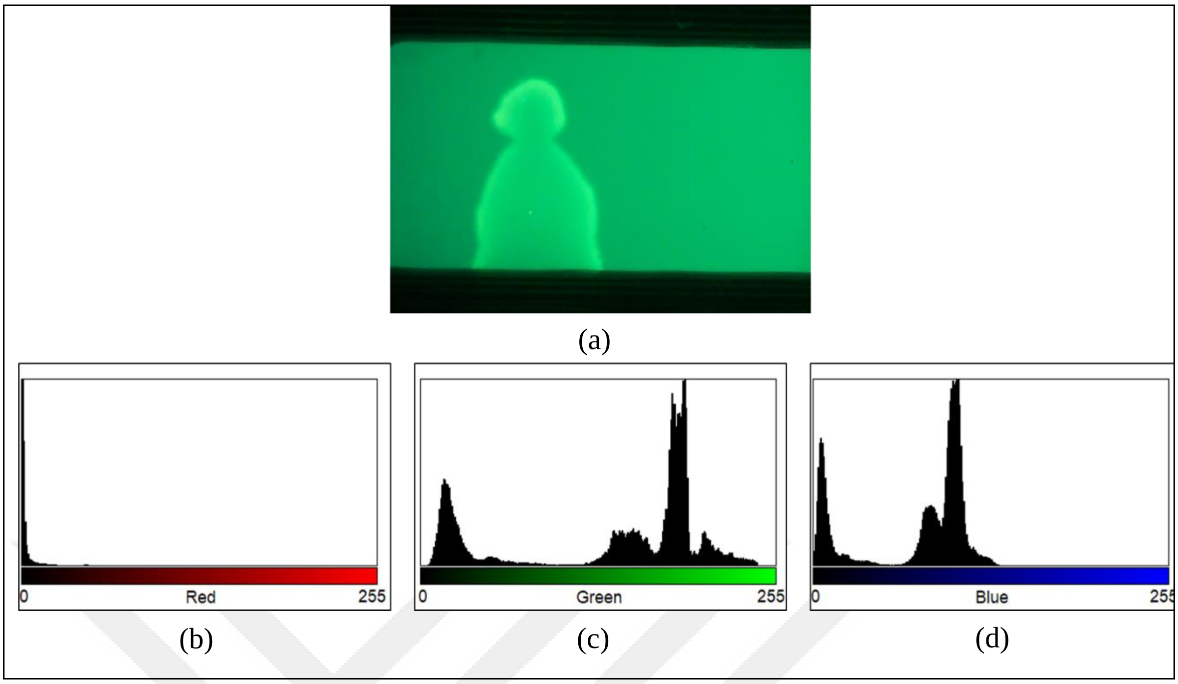

Figure 4.11. 100 µM fluorescein sodium salt. (a) 8-bit image captured with 10 ms exposure time, and (b-d) RGB channel histograms.

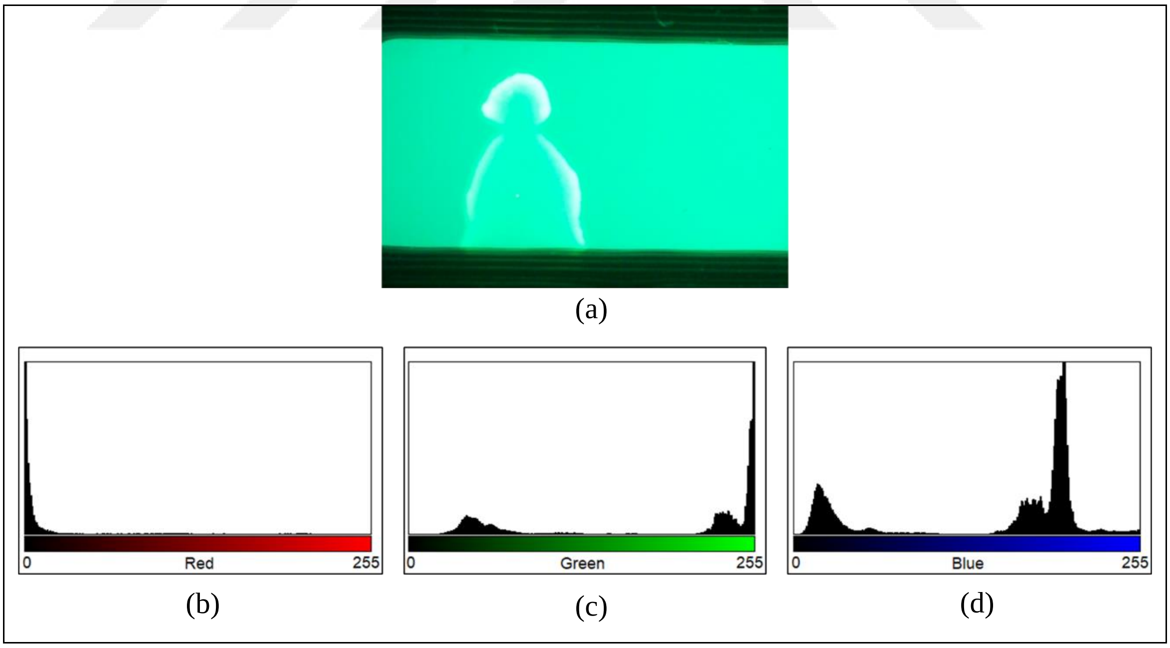

Figure 4.12. 100 µM fluorescein sodium salt. (a) 8-bit image captured with 30 ms exposure time, and (b-d) RGB channel histograms.

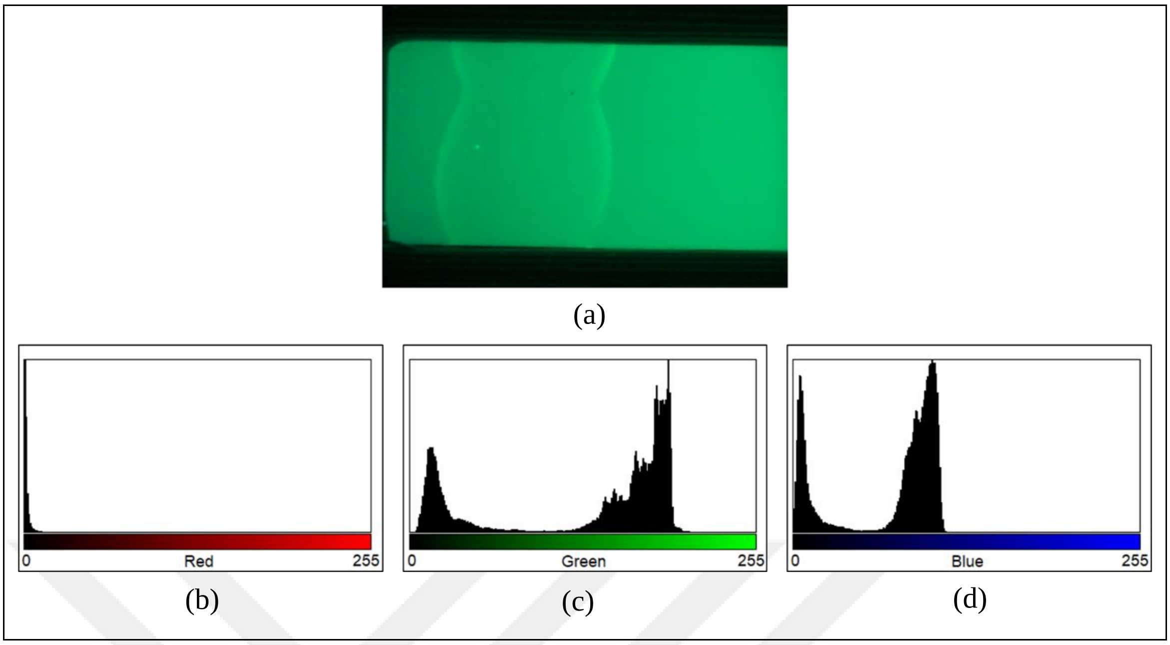

Figure 4.13. 10 μM fluorescein sodium salt. (a) 8-bit image captured with 10 ms exposure time, and (b-d) RGB channel histograms.

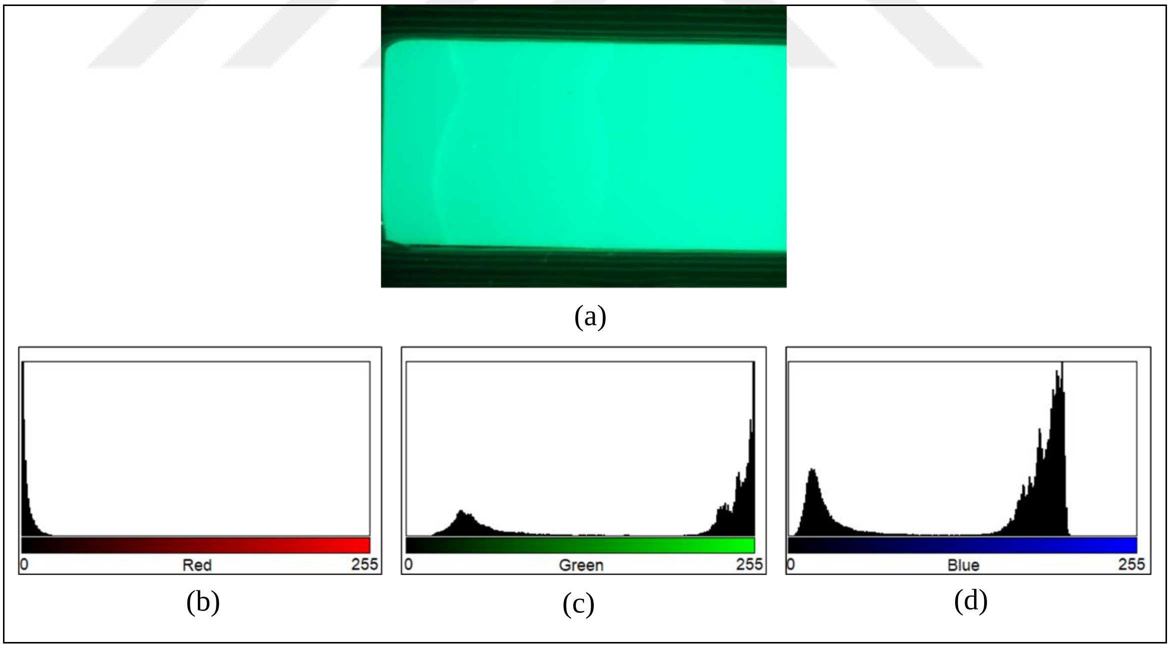

Figure 4.14. 10 μM fluorescein sodium salt. (a) 8-bit image captured with 30 ms exposure time, and (b-d) RGB channel histograms.

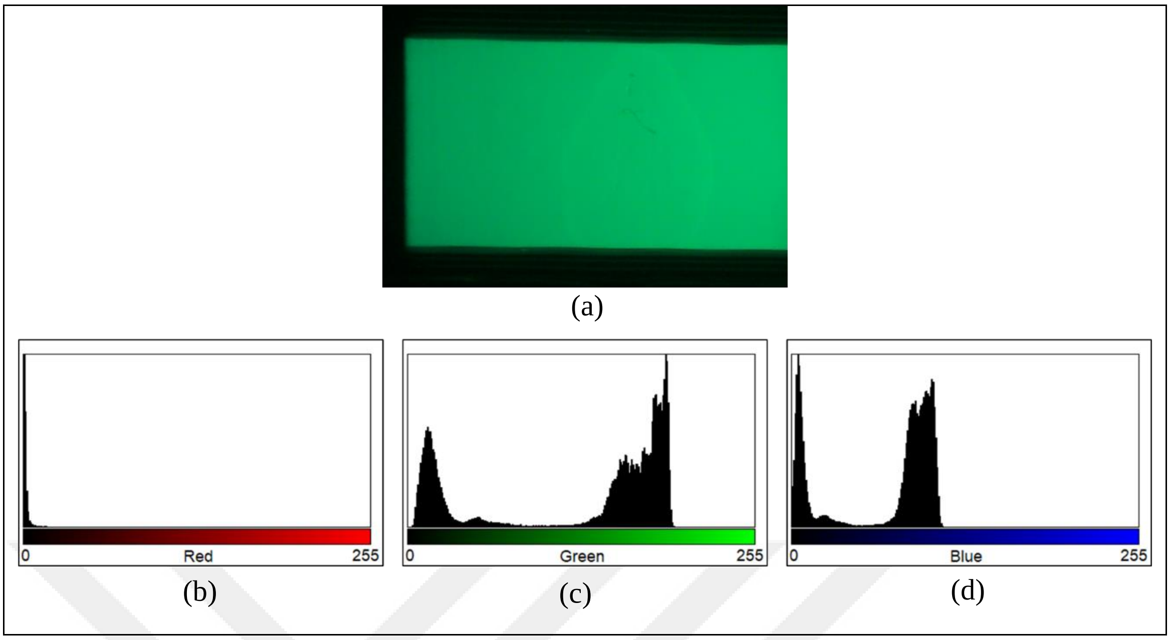

Figure 4.15. 1 μM fluorescein sodium salt. (a) 8-bit image captured with 10 ms exposure time, and (b-d) RGB channel histograms.

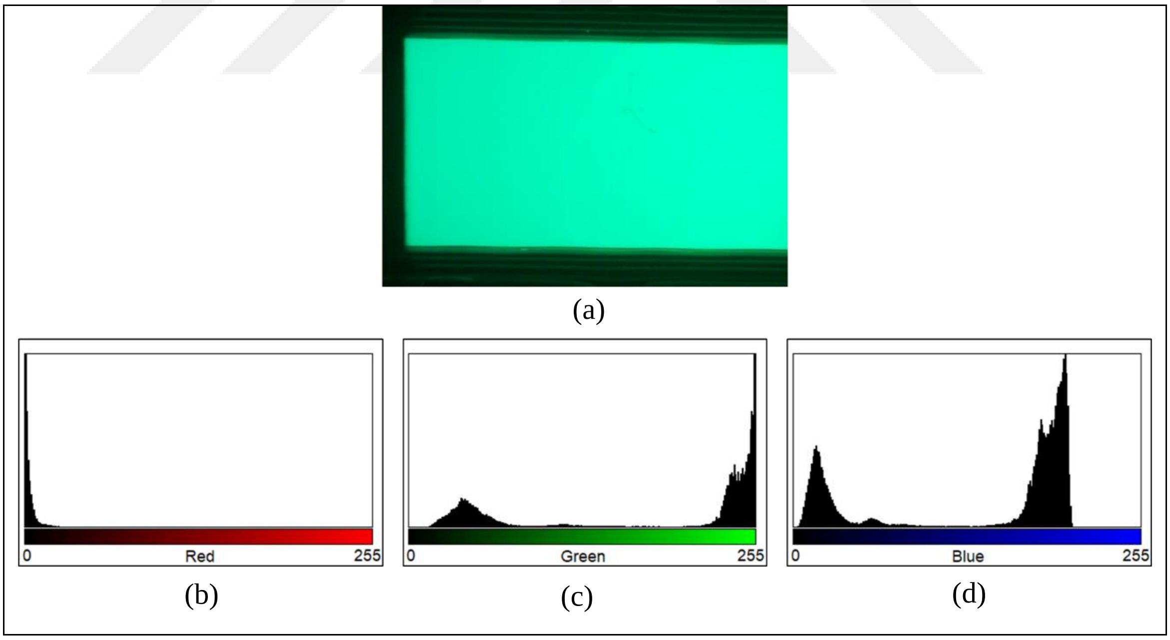

Figure 4.16. 1 μM fluorescein sodium salt. (a) 8-bit image captured with 30 ms exposure time, and (b-d) RGB channel histograms.

The images captured for different concentrations of the fluorescein sodium salt are further analyzed on ImageJ software to set rectangular ROIs and to assess the mean intensity values from the green channel for the ROIs. The ROI is positioned on the image to encompass the fluorescent parts of the nitrocellulose membrane, ensuring that the mean pixel intensity measurements reflect the fluorescence signal strength. The relationship between the fluorescein sodium salt concentration and the mean pixel intensity assessed for the images captured with 10 ms exposure time is seen in Figure 4.17. The mean intensity values for 1000 µM, 100 µM, 10 µM, and 1 µM are respectively 215, 205, 193, and 183. The nonlinear relationship between dye concentration and mean intensity indicates that the fluorescence intensity increases at a decreasing rate as the dye concentration increases. The same samples imaged at 30ms are also analyzed to show the relationship between fluorescein sodium salt concentration and mean intensity (Figure 4.18). The calculated mean values for 1000 µM, 100 µM, 10 µM, and 1 µM are 255, 255, 254, and 253. All of the intensities are higher when compared to the calculations for 10ms exposure time, and they are around the maximum pixel value of 255.

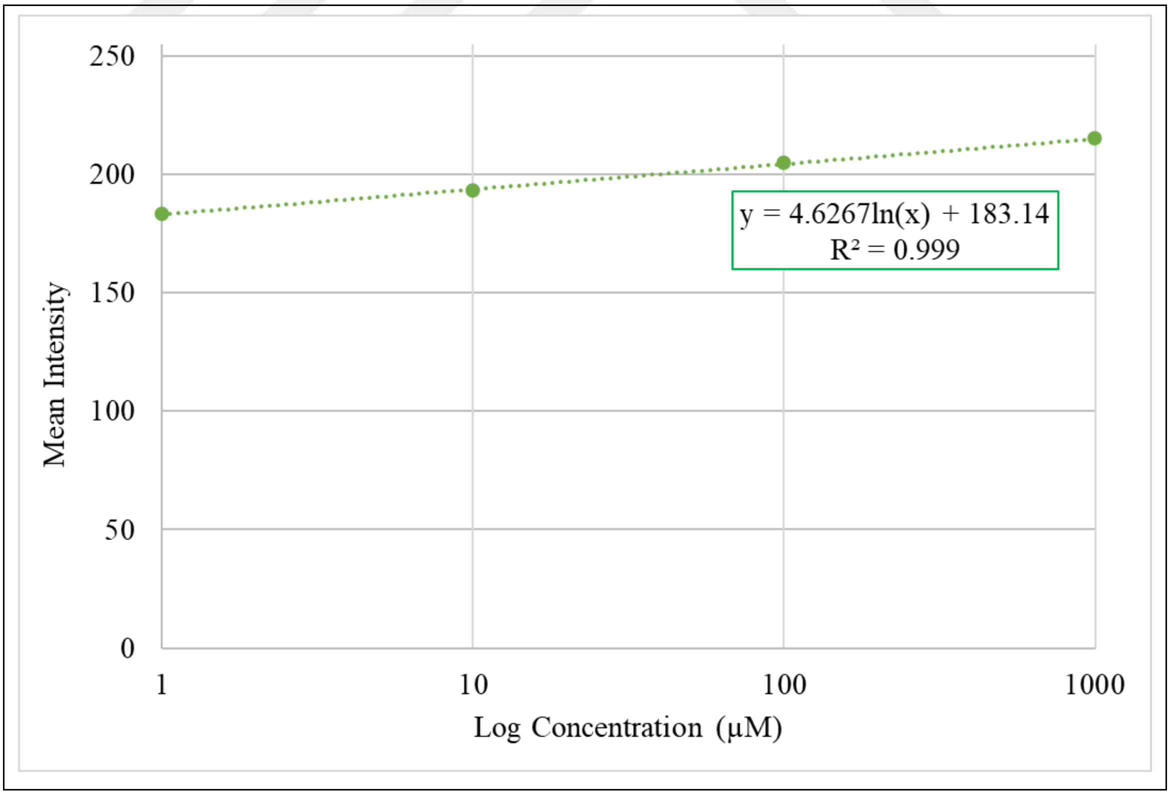

Figure 4.17. Mean intensity values with changing concentration of fluorescein sodium salt for the preliminary reader with 10 ms camera exposure time.

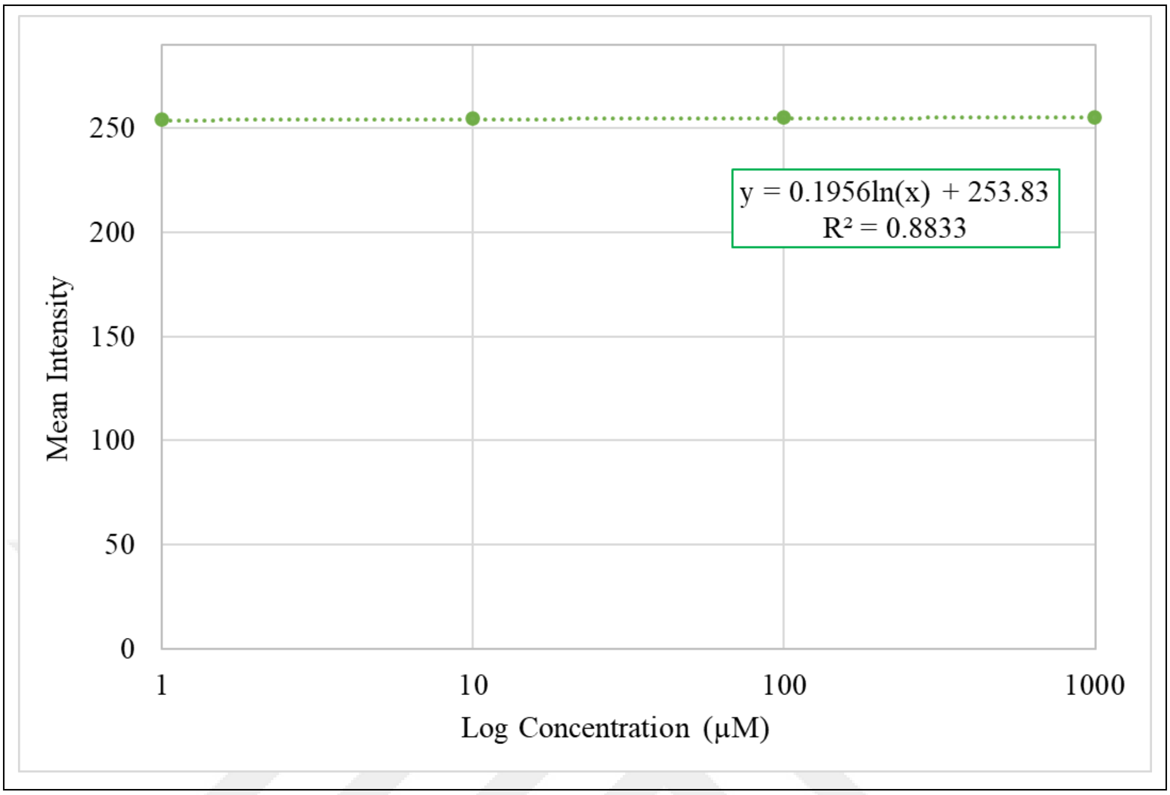

Figure 4.18. Mean intensity values with changing concentration of fluorescein sodium salt for the preliminary reader with 30 ms camera exposure time.

For 1000 µM concentration of rhodamine B imaged at 10 ms exposure time, the rhodamine B delivered to the membrane is clearly visible as red-colored on the yellowish background (see Figure 4.19). The histogram of the red channel exhibits the mean pixel intensity of 137±70, suggesting a relatively widespread in the intensity of values. The green channel has a mean pixel intensity of 98±55. A moderate level of signal is detected with a relatively broad distribution of intensity value. The histogram for the blue channel shows a mean pixel intensity of 0.4±1. This indicates a very low level of signal in the blue channel, with most pixels close to zero intensity. When the sample is imaged at 30 ms exposure time, the dye stain becomes lighter when compared to the image captured at 10 ms (Figure 4.20). The mean intensity value, 198, is closer to the upper limit of the scale in the red channel. For the green channel histogram, a mean intensity of 165±79 is calculated. In the blue channel histogram, a mean pixel intensity of 0.5±2, which is quite low, indicates that most pixels are near the dark end of the intensity spectrum. This would typically indicate minimal noise or variation across the captured image in the blue channel.

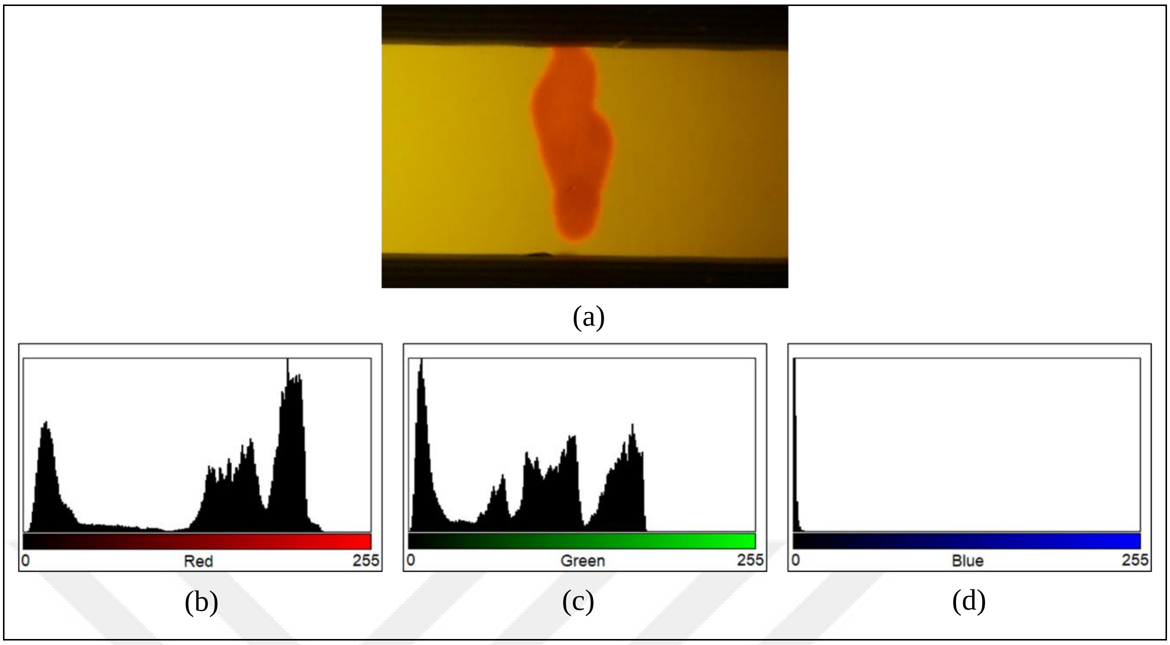

Figure 4.19. 1000 µM rhodamine B. (a) 8-bit image captured with 10 ms exposure time, and (b-d) RGB channel histograms.

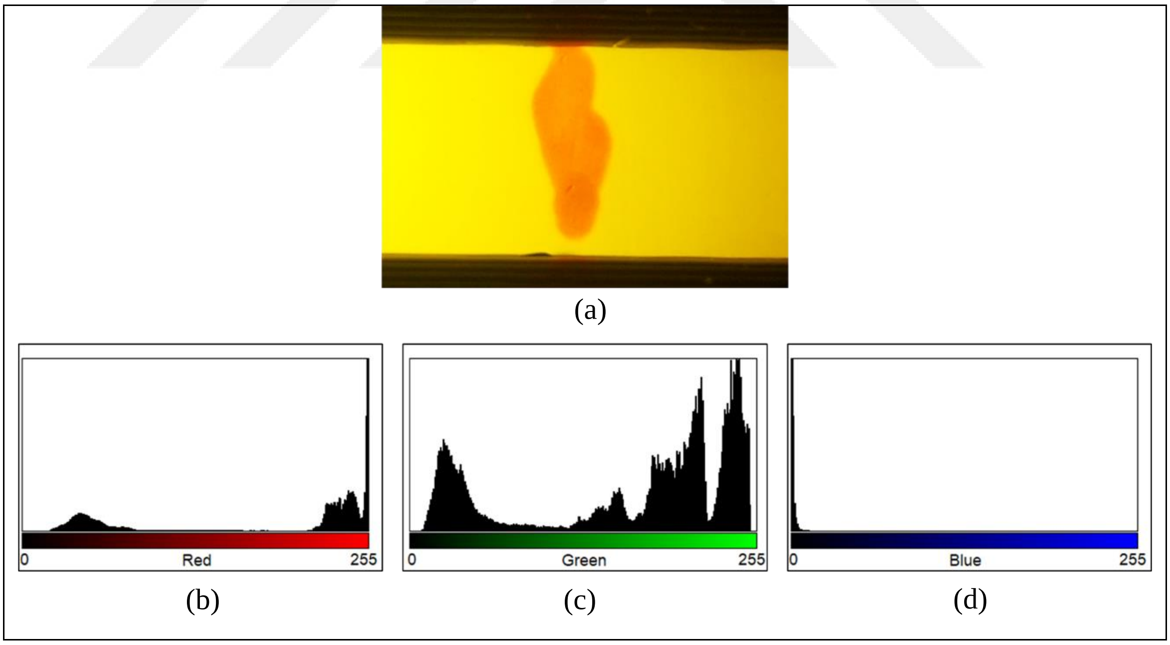

Figure 4.20. 1000 µM rhodamine B. (a) 8-bit image captured with 30 ms exposure time, and (b-d) RGB channel histograms.

For 100 µM concentration of rhodamine B at 10 ms exposure time, the fluorescent part of the rhodamine B is clearly visible with a light-red color (Figure 4.21). The red channel has a high mean intensity of 138±72. The mean intensity broadly distributed, demonstrates a relatively high signal within the imaged region. The mean intensity in the green channel is relatively low, 99±55. The histogram of the blue channel reveals a low mean pixel intensity of 0.4±2. The low mean intensity with narrow distribution indicates a minimal fluorescence response in the blue channel, consistent with the absorption and emission profile of rhodamine B. Dark pixels are dominant in the blue channel of the image. Raising the camera exposure time to 30 ms produces higher intensity levels for every channel (Figure 4.22). The rhodamine B stain is not clearly visible as most of the pixels are at the same value as the background. The histogram for the red channel shows a mean pixel intensity of 197±84, indicating a robust fluorescent response in the red channel. The green channel histogram displays a mean pixel intensity of 172±81. The histogram for the blue channel indicates a low mean pixel intensity of 0.6±2. This channel mostly includes darker pixels that are not related to the fluorescence signals.

For a 10 µM concentration of rhodamine B at 10 ms exposure time, the light-red colored stain is still distinguished from its background even though its visibility is diminished on the image (Figure 4.23). There is a wide range of pixel intensities with a mean value of 136±71 in the red channel. The histogram of the green channel shows a mean pixel intensity of 101±57, suggesting a fair distribution of pixel intensities around the mean, which indicates a moderate level of signal variation across the image. The mean intensity is lower than the red channel, which is expected since Rhodamine B has a red emission spectrum and would naturally exhibit lower intensity in the green channel. The lowest mean intensity of 0.4±1.3 is measured in the blue channel, reflecting the minimal signal detection. When the same sample is analyzed at 30 ms exposure time, the rhodamine B stain is hardly visible on the 8-bit RGB image (Figure 4.24). The mean pixel intensity in the red channel has significantly increased to 197±86. The mean pixel intensity in the green channel is 172±82. The histogram of the blue channel has a minimum mean pixel intensity of 0.6±3.0.

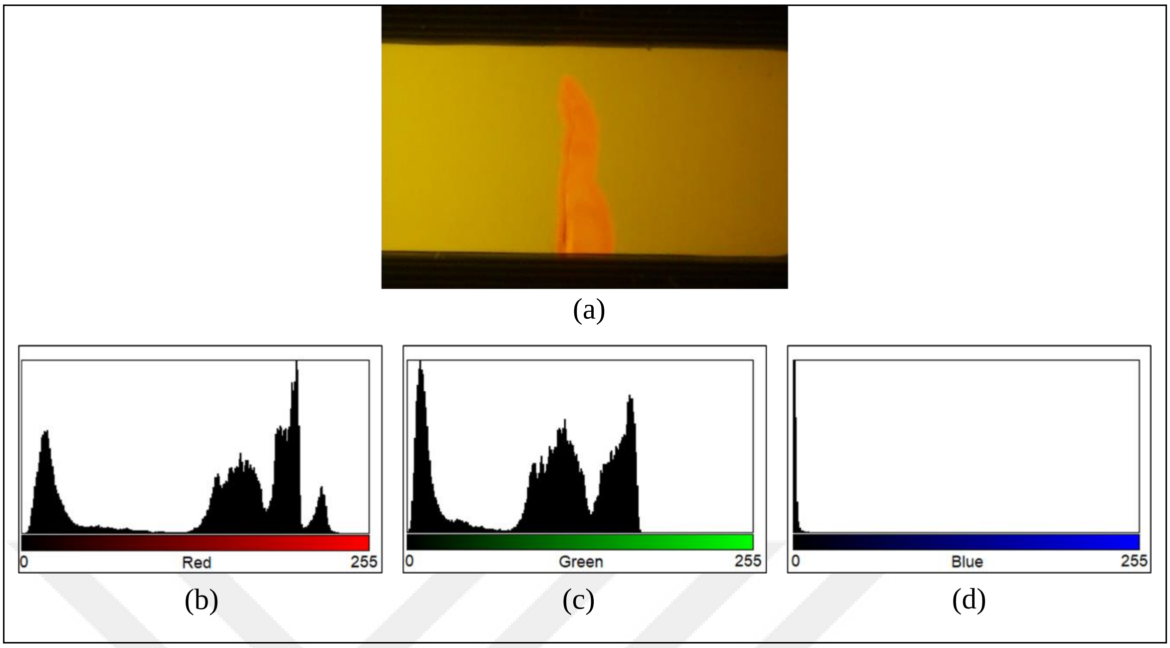

Figure 4.21. 100 µM rhodamine B. (a) 8-bit image captured with 10 ms exposure time, and (b-d) RGB channel histograms.

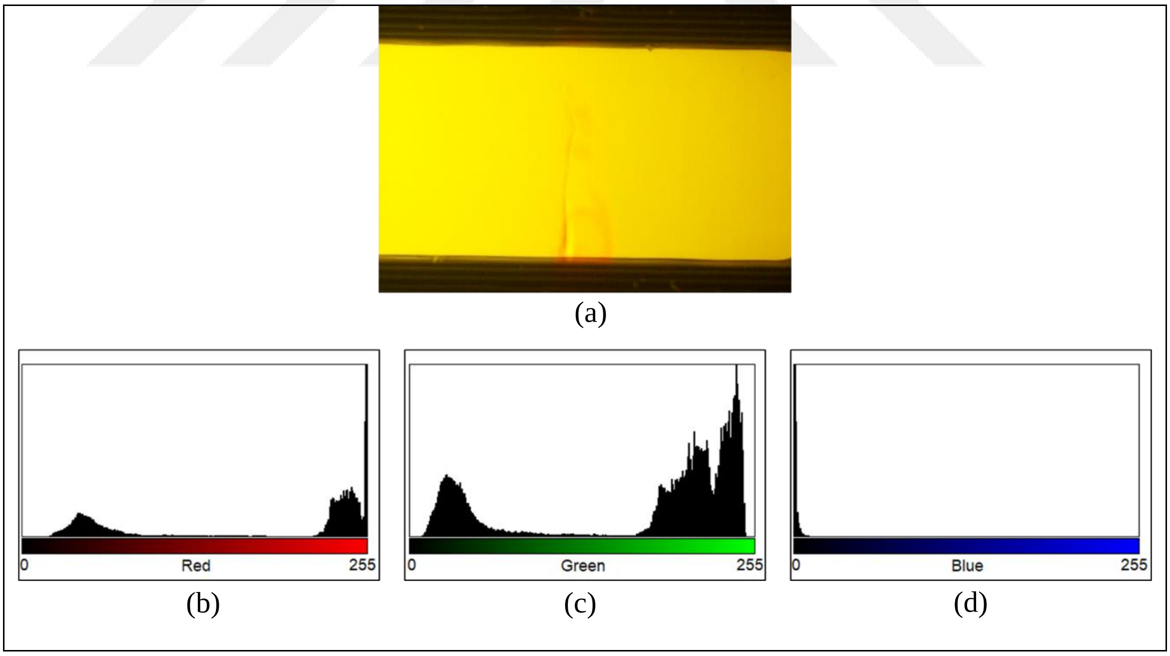

Figure 4.22. 100 µM rhodamine B. (a) 8-bit image captured with 30 ms exposure time, and (b-d) RGB channel histograms.

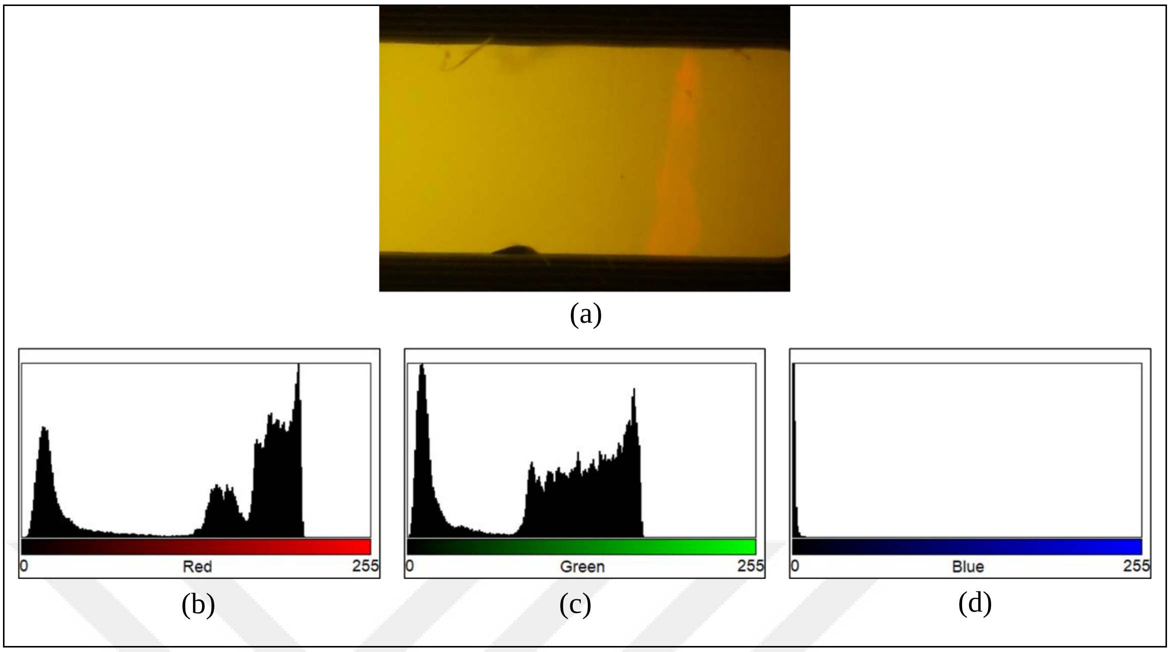

Figure 4.23. 10 μM rhodamine B. (a) 8-bit image captured with 10 ms exposure time, and (b-d) RGB channel histograms.

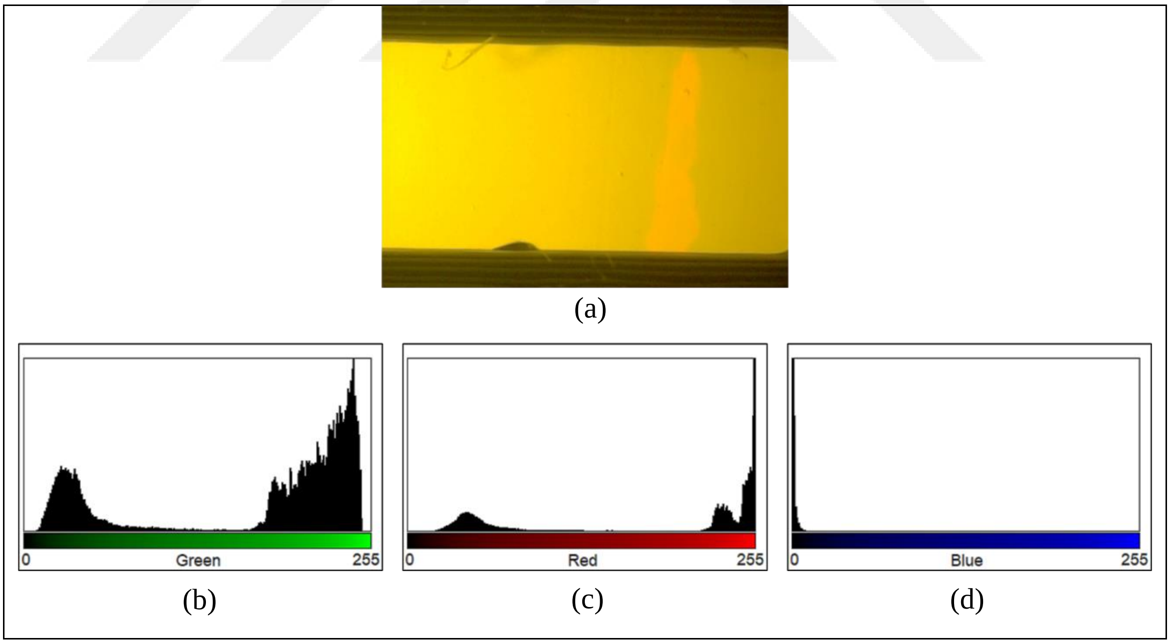

Figure 4.24. 10 μM rhodamine B. (a) 8-bit image captured with 30 ms exposure time, and (b-d) RGB channel histograms.

The lowest concentration level, 1 µM, measured at 10 ms camera exposure time, shows no visible rhodamine B fluorescence on the 8-bit RGB image (Figure 4.25). The histogram of the red channel exhibits a mean pixel intensity of 137±70. The green channel has a mean pixel intensity of 102±57. For the blue channel histogram, the mean pixel intensity is 0.4±1, indicating a narrow distribution of intensities close to the mean. At the 30 ms exposure time, there is not any visible sign of rhodamine B dye on the image (Figure 4.26). The histogram for the red channel reveals a significantly higher mean pixel intensity at 197±84, which indicates a wider spread of intensity values. The green channel also has a high mean pixel intensity of 173±82. The mean intensity in the blue channel is notably low at 0.5±2. According to the images of the rhodamine B, the red channel is dominant as it has the highest mean intensities for all concentrations, aligning with its emission spectrum. The rhodamine B dye images have greater mean intensities than the fluorescein sodium salt in general when compared to their mean intensities within whole images. Also, the effect of the 560nm excitation light of the rhodamine B is observed in the green channel of its captured 8-bit RGB images. The longer exposure of the camera leads to the saturation of the pixels, thereby limiting the sensor sensitivity to increasing concentrations of the dyes.

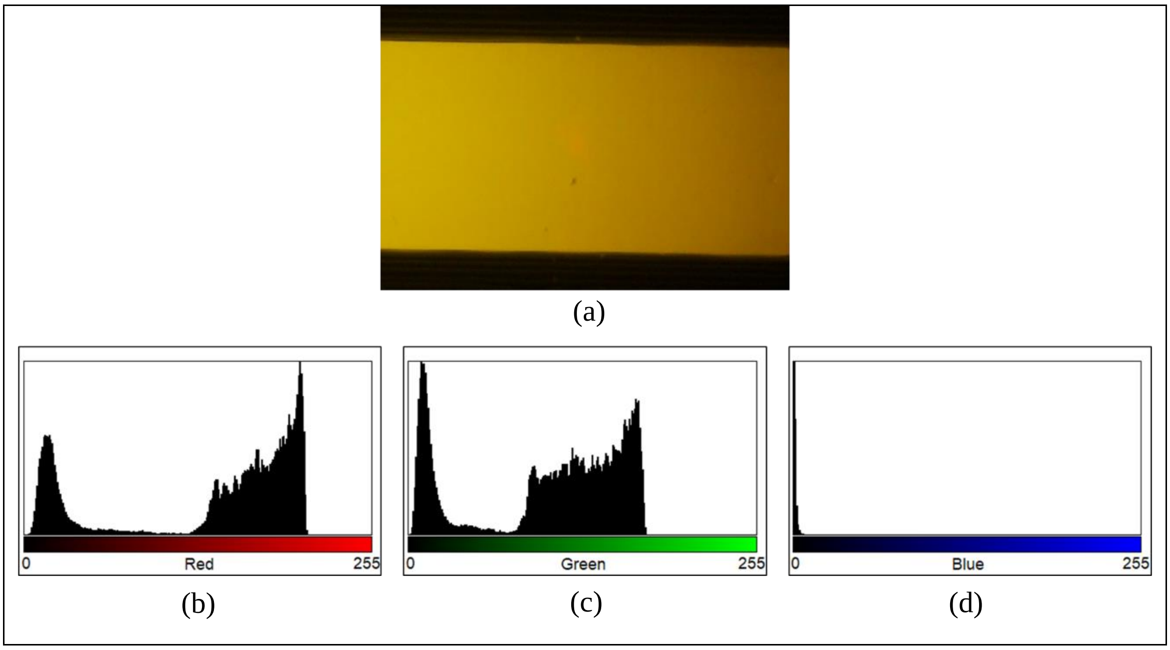

Figure 4.25. 1 µM rhodamine B. (a) 8-bit image captured with 10 ms exposure time, and (b-d) RGB channel histograms.

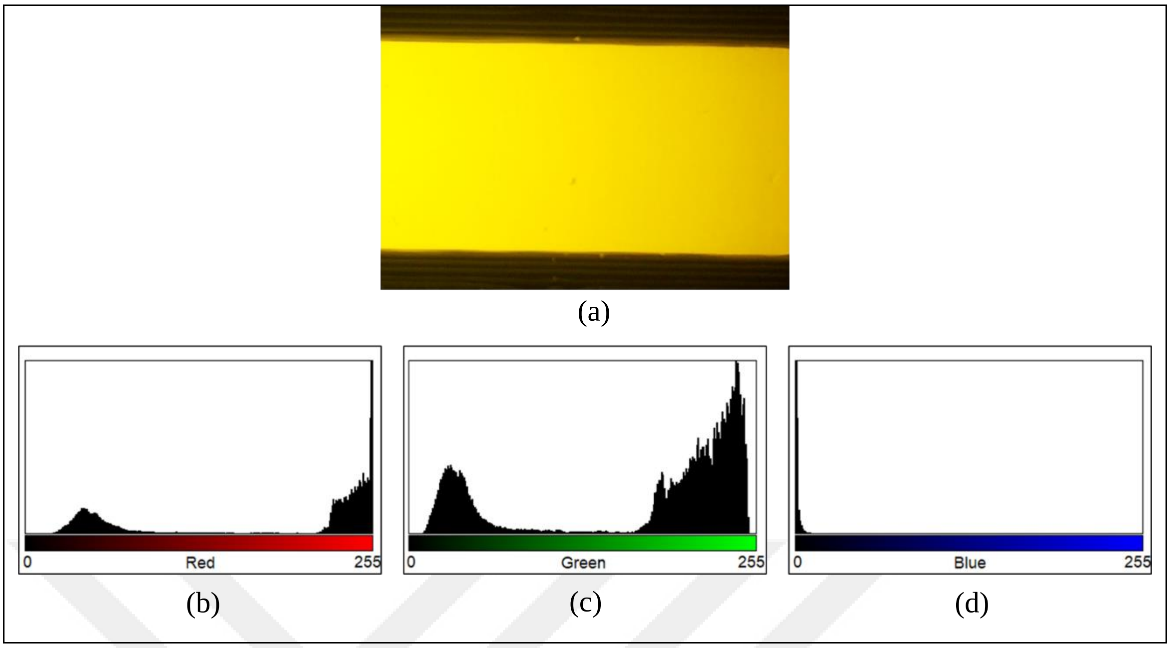

(a)

(b) (c) (d)

Figure 4.26. 1 μM rhodamine B. (a) 8-bit image with 30 ms exposure time, and (b-d) RGB channel histograms.

The image for each concentration level of Rhodamine B is further analyzed on ImageJ to set ROI rectangles and calculate the mean values of the red channels within the ROIs. During the analysis, the ROI has been strategically positioned to determine the rhodamine B signal strength. The relationship between the concentration of rhodamine B (μM) and the mean pixel intensity within the set ROI for a 10 ms camera exposure time is illustrated in Figure 4.27. The calculated mean values for 1000 μM, 100 μM, 10 μM, and 1μM are 193, 220, 193, and 191. The light intensity emitted by rhodamine B increases with the concentration until a point of 100 μM, after which further increases in concentration (1000 μM) lead to a decline in detected light intensity. The relationship between the concentration of rhodamine B (μM) and the mean pixel intensity in the red channels within the set ROIs for a 30 ms camera exposure time is exhibited in Figure 4.28. The calculated mean values for 1000 μM, 100 μM, 10 μM, and 1μ M are respectively 254, 255, 252, and 254. The mean intensities of the red channels increase for each concentration level when compared to the calculations for the images captured at 10ms exposure time, and they are around the maximum upper limit of the scale of 255. The presence of high pixel values, around 255, near the saturation point suggests that some regions of the image may be reaching or exceeding the camera's capacity to record incremental increases in fluorescence due to more photon capture. The measured mean values in the green channel are greater than the mean intensity values of the whole images for every concentration level of the fluorescein sodium salt dye. Also, the mean values in the red channel are larger than the mean values measured for the whole image for every concentration level of the rhodamine B dye. The measured mean values of the related channels within the ROIs on the images of both dyes are illustrated in Figure 4.29. for comparison. The mean intensity of the fluorescein sodium salt, 183, is smaller than the mean intensity of the rhodamine B, 191, at 1 μM concentration. The fluorescein sodium salt and rhodamine B dyes have an equal mean intensity, 193, within their related channels at 10 μM concentration. When 100 μM concentration is analyzed, the rhodamine B dye has a significantly greater mean intensity, 220, than the fluorescein sodium salt, 205. At 1000 μM concentration level, the mean intensity of the fluorescein sodium salt, 215, is larger than the rhodamine B dye's mean intensity, 193.

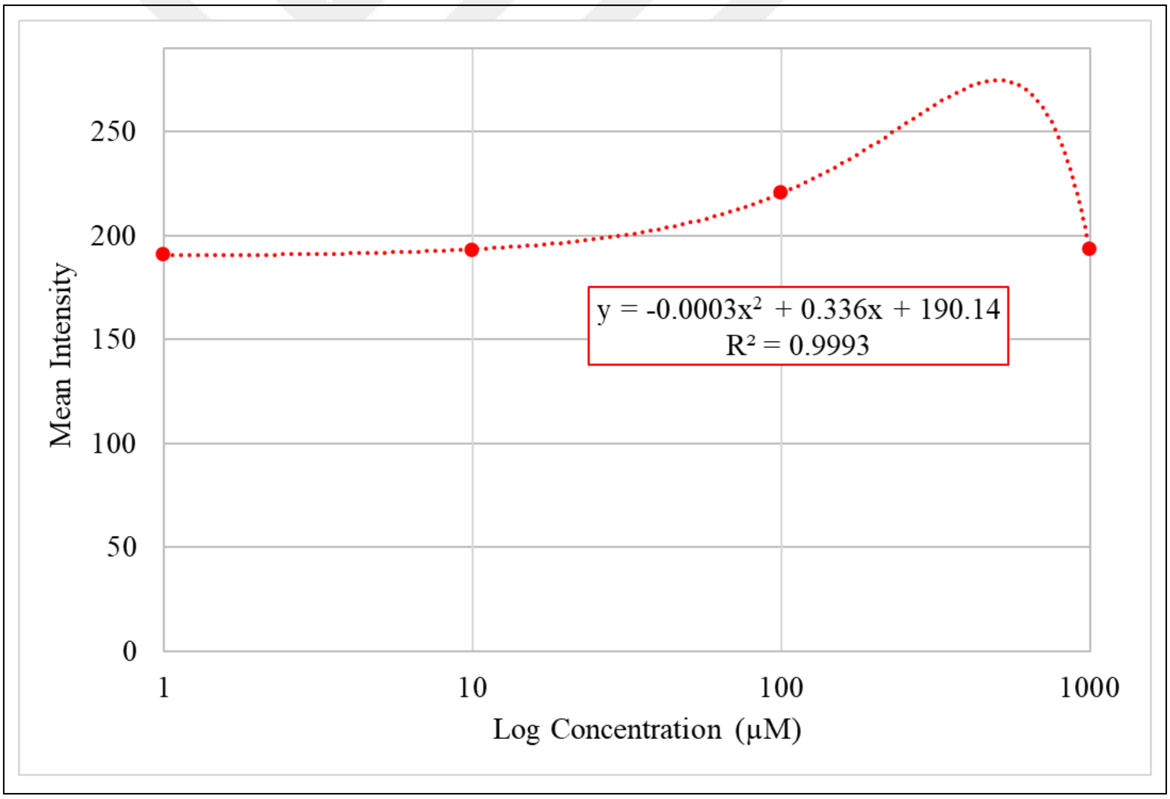

Figure 4.27. Mean intensity values with changing concentration of rhodamine B for the preliminary optical reader at 10 ms camera exposure time.

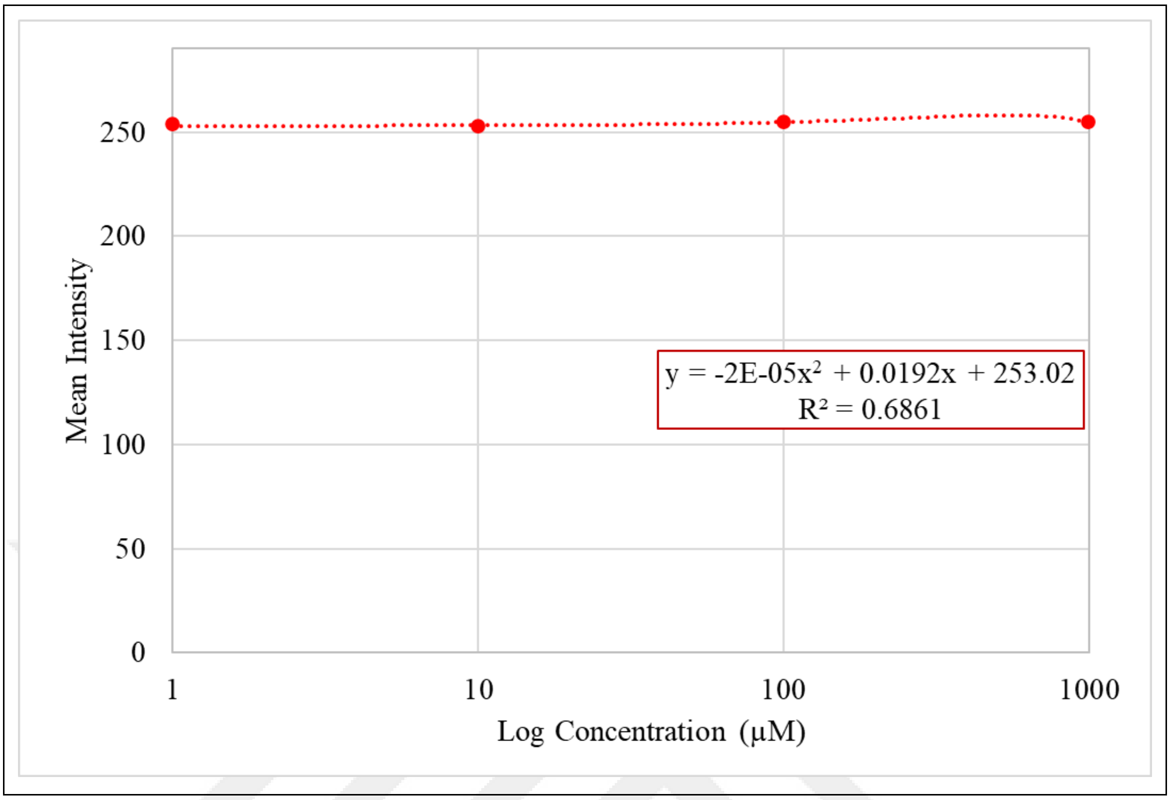

Figure 4.28. Mean intensity values with changing concentration of rhodamine B for the preliminary optical reader at 30 ms camera exposure time.

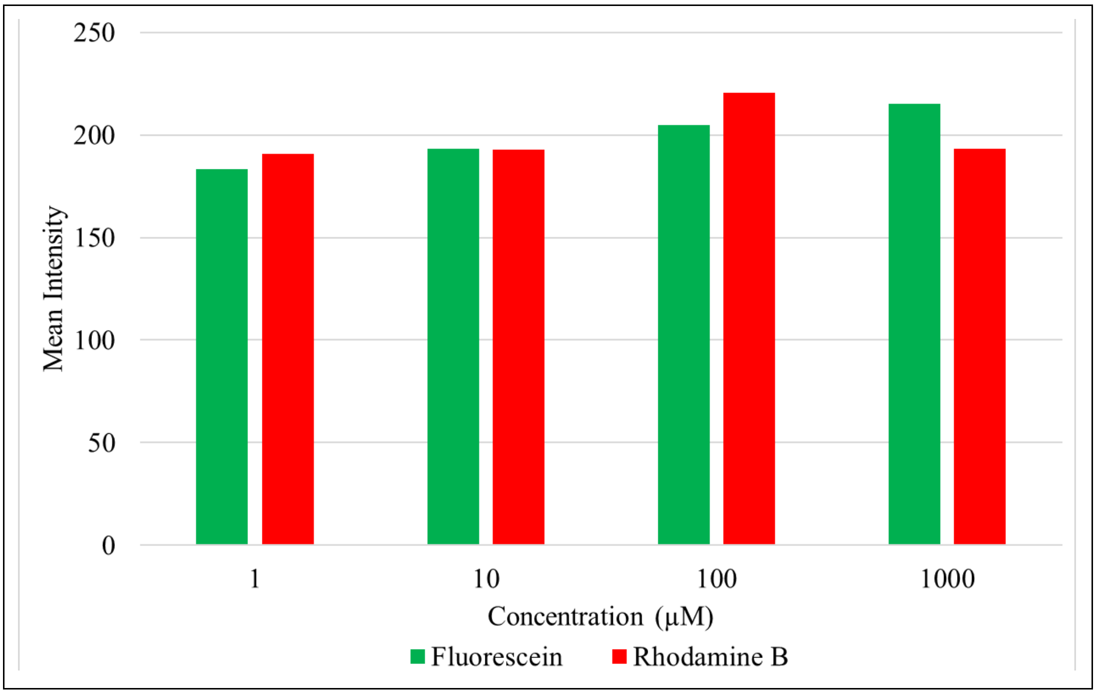

Figure 4.29. Bar plot of ROI mean intensity for fluorescein sodium salt and rhodamine B at varying concentrations.

The subtracted images of the 100 µM fluorescein sodium salt and rhodamine B are exhibited in Figure 4.30. In the resultant images, the fluorescent parts for fluorescein sodium salt and rhodamine B dyes are highly emphasized from their background.

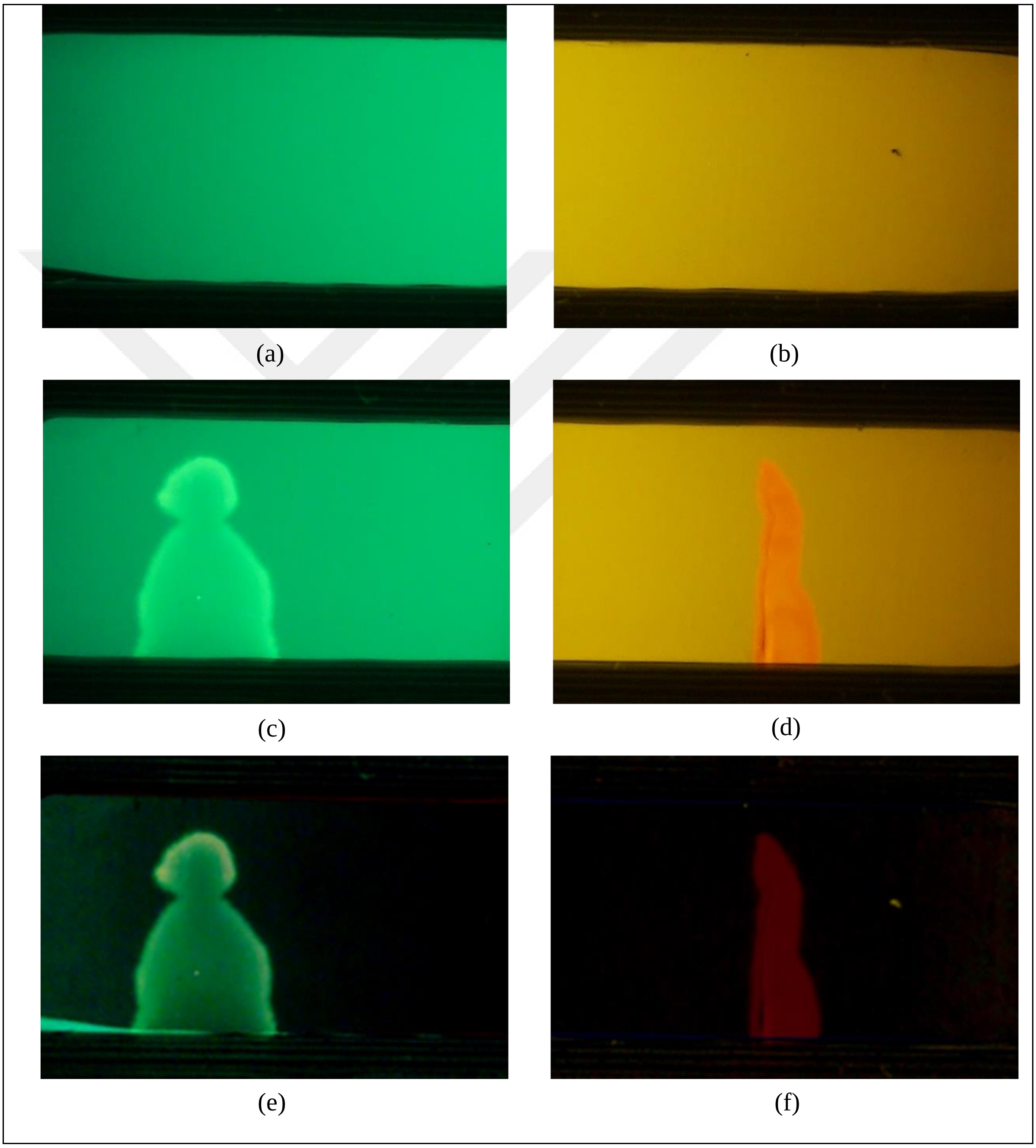

Figure 4.30. Example for 8-bit image subtraction. (a, b) Blank images for fluorescein sodium salt and rhodamine B, (c, d) Captured images for 100µM fluorescein sodium salt, and rhodamine B, (e, f) Resultant subtracted images.

4.5. FINAL OPTICAL READER

The final optical reader weighs 1.05 kg and is 24 cm (H) × 13 cm (W) × 14 cm (D) in size. It is tested with fluorescein sodium salt and rhodamine B with the concentrations of 0.1 μM, 1 μM, and 10-100 μM with 10 μM increments. The amount of 1 μL of each concentration level is dropped onto the membranes, and the reader images them. The auto-white balance and auto-exposure time settings of the camera are disabled, and 12-bit RGB image acquisition is set by default. The exposure time of 10 ms, light emission time of 1s, and analog gain of 1 are set using the GUI. (During imaging, the reader detects 23.5 °C temperature, 27 % relative humidity, and 137 m altitude).

For 90 μM concentration of the fluorescein sodium salt, the fluorescence emission detected is much brighter and is clearly distinguished from its background (Figure 4.31). The histograms for each channel of the captured 12-bit RGB image are produced using ImageJ software. A low mean pixel intensity, 8915±4742, is measured for the red channel. The pixels in the red channel are mostly composed of dark pixels. The average mean pixel intensity for the green channel is 30812±18183, which is significantly higher than what is observed in the red channel. There are saturated pixels having a maximum value of 65520 within the whole image. The histogram of the blue channel represents the mean intensity of 13944±5806. The findings above are in agreement with the emission spectrum of the fluorescein sodium salt that typically emits in the green region when excited by the 460nm light. For the 60 μM concentration of the fluorescein sodium salt, the fluorescent region is clearly visible on the 12-bit RGB image (Figure 4.32). Three histograms for each channel of the image are evaluated. The histogram of the red channel has a mean pixel intensity of 6646±2452, which is within the lower range of the scale. The mean pixel intensity in the green channel is 22025±8663. The channel effectively captures the strong fluorescence emission from the fluorescein sodium salt, even if it is lower than the one measured for the 90 μM concentration. The blue channel has a medium mean pixel intensity of 11226±4532, which is weaker than the green channel.

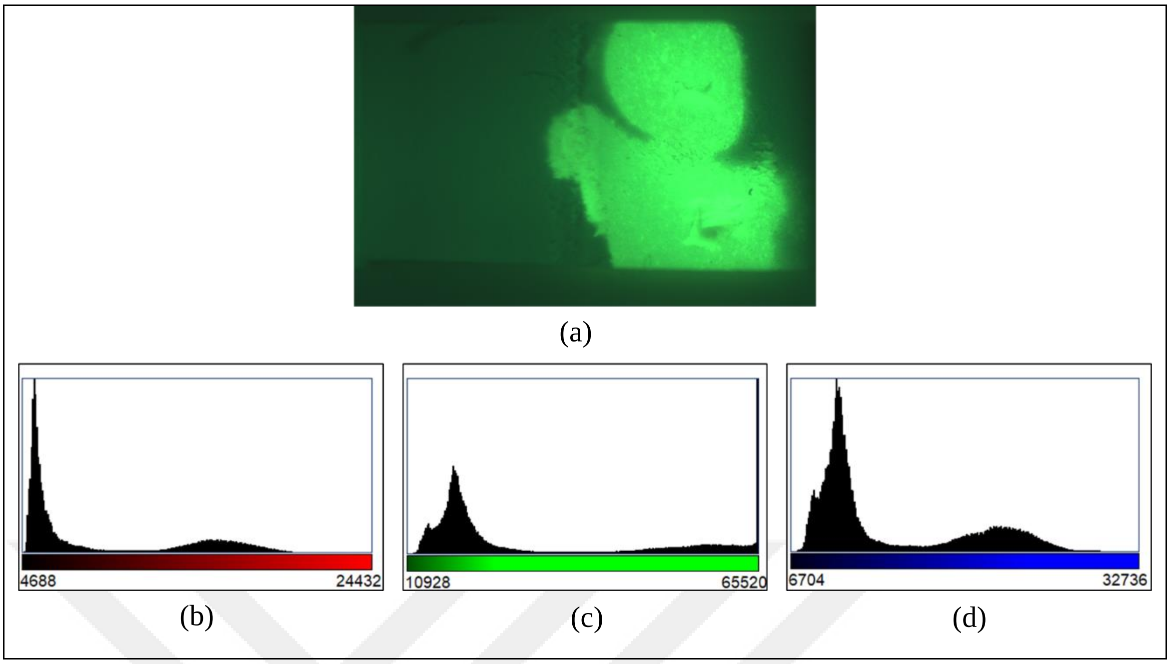

Figure 4.31. 90 µM fluorescein sodium salt. (a) 12-bit image, and (b-d) RGB channel histograms.

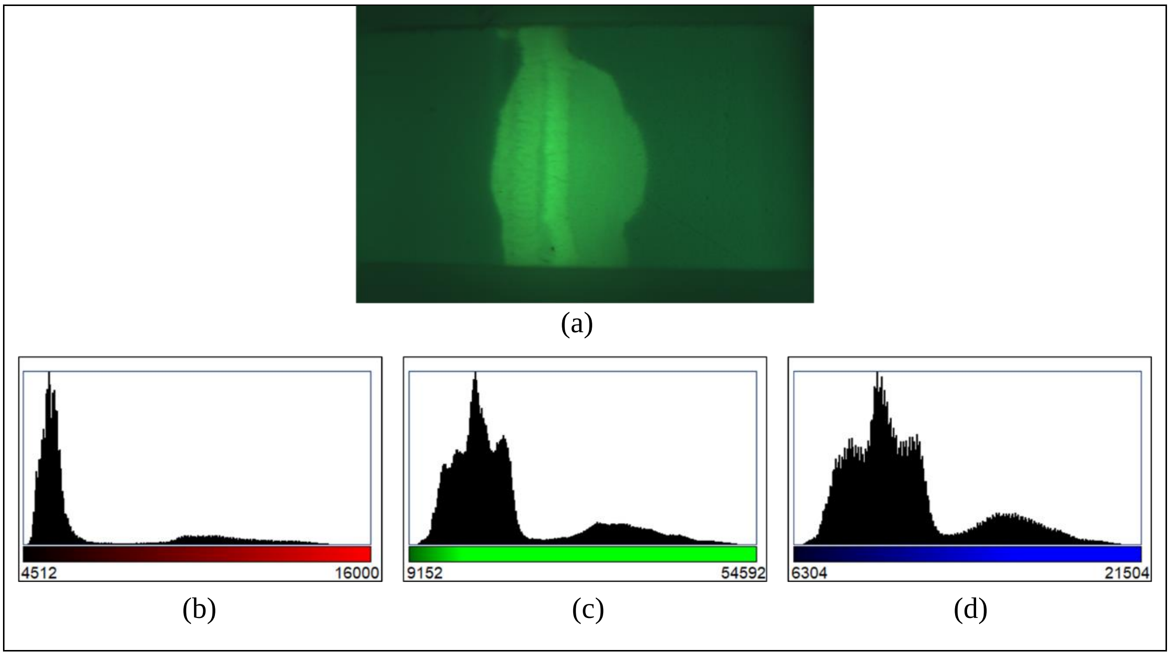

Figure 4.32. 60 µM fluorescein sodium salt. (a) 12-bit image, and (b-d) RGB channel histograms.

For the 30 μM concentration of the fluorescein sodium salt, the fluorescent region is visible on the 12-bit RGB image, but the stain of the dye is lighter-green colored (Figure 4.33). Its brightness is decreased when compared to the higher concentration levels. The red channel histogram exhibits a smaller mean pixel intensity of 5895±1336. The mean intensity, 18656±5395, is much greater than in the red channel. This indicates a strong signal detected by the green channel that aligns with the peak emission of the fluorescein sodium salt. The mean intensity value in the blue channel is 10094±1957.

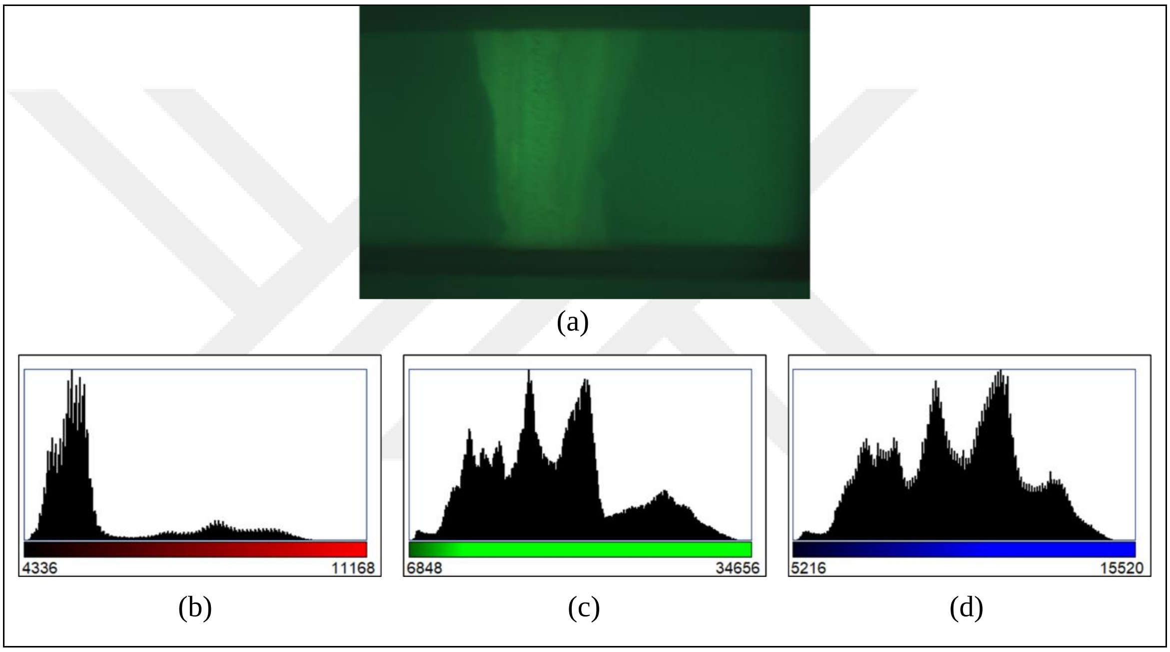

Figure 4.33. 30 μM fluorescein sodium salt. (a) 12-bit image, and (b-d) RGB channel histograms.

For a 10 μM concentration of fluorescein sodium salt, it is very difficult to differentiate the fluorescent region from the background on the 12-bit RGB image (Figure 4.34). The green color of the fluorescent region is nearly the same as the background tone, so it is very hard to differentiate the fluorescence visually. The red channel has a mean pixel intensity of 5619±684, which is on the lower end of the 12-bit scale. The histogram of the green channel shows a mean intensity of 18785±3182. The blue channel has a mean pixel intensity of 10318±1261. These mean intensities align with the green light emission by the fluorescein sodium salt.

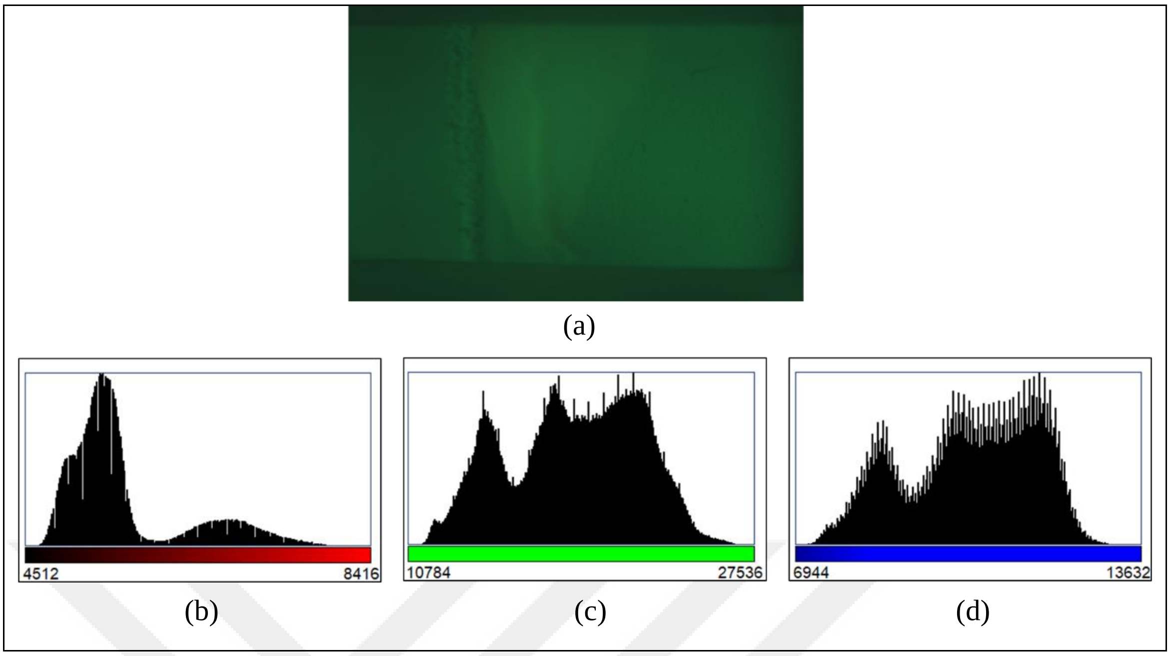

Figure 4.34. 10 µM fluorescein sodium salt. (a) 12-bit image, and (b-d) RGB channel histograms.

The 12-bit RGB image for each concentration level of the fluorescein sodium salt is further analyzed on the ImageJ software. The ROI rectangles are set on the fluorescent regions of the images, and the mean pixel intensities of the green channel are calculated within the ROIs. The relationship between the concentration of fluorescein sodium salt and the mean pixel intensity in the green channel within the set ROI for a 10 ms camera exposure time is seen in Figure 4.35. There is a quadratic relationship between the mean pixel intensity and the concentration of the fluorescein sodium salt. The mean intensity slowly increases until 20 µM concentration and continues increasing at a higher rate of 70 µM. There is not much difference in the mean pixel intensities between 70 µM and 80 µM. The mean intensity value peaks at 90 µM, which decreases to a lower intensity value at 100 µM. However, there is a linear relationship between mean intensities in the green channel and fluorescein sodium salt concentrations between 10 µM and 90 µM, as seen in Figure 4.36.

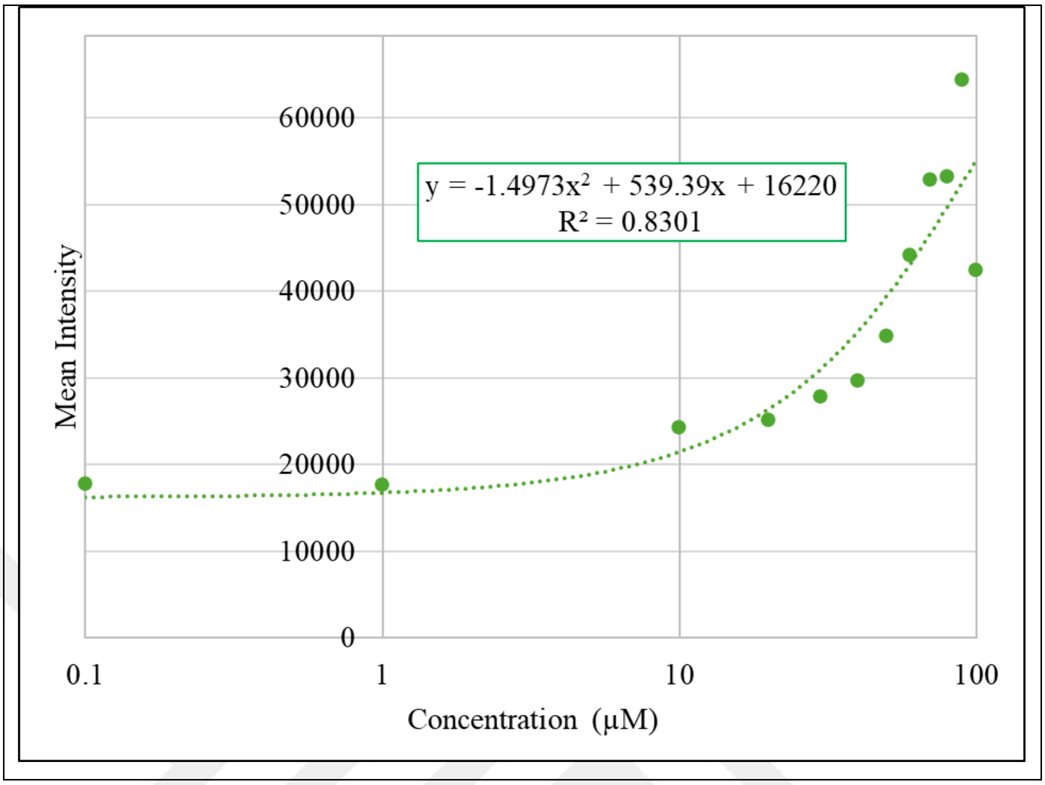

Figure 4.35. Mean intensity values with changing concentrations of fluorescein sodium salt for the final reader.

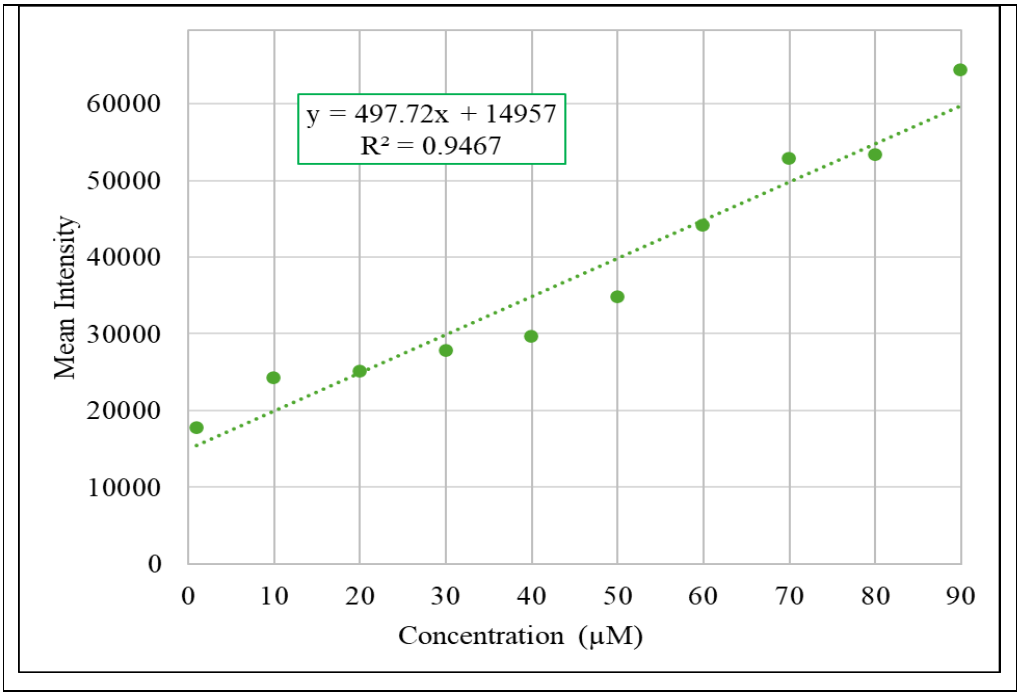

Figure 4.36. Mean intensity values for low concentrations of fluorescein sodium salt for the final reader.

The histograms for each channel of the captured 12-bit RGB images at 10ms exposure time are generated on ImageJ software. For an 80 µM concentration of rhodamine B, the fluorescent region is obviously detectable from the background on the image (Figure 4.37). The rhodamine B dye is observed as red-colored on a yellowish background. The mean intensity for the red channel is 31953±9112, which is a high value, suggesting that the image is quite bright and there is a significant amount of fluorescence signal. This aligns with the red-light emission of rhodamine B dye. The mean pixel intensity for the green channel is 27957±6763, reflecting that the image overall is bright. This also suggests that the green (560 nm) excitation light is absorbed by the dye. The mean intensity for the blue channel is 7257±850. This is considerably lower compared to the red and green channels. This suggests that the fluorescence emission captured in the blue channel is less intense, which is consistent with the emission spectrum of the rhodamine B rhodamine. For the 60 µM concentration of rhodamine B, the rhodamine B stain is clearly visible in the image. The bright fluorescence emission from the rhodamine B stain is distinguished from its background (Figure 4.38). The histogram of the red channel has a high mean intensity of 33387±10212, suggesting a wide distribution of intensity values. The mean signal intensity in the green channel is 28631±6948, which is less than the mean value in the red channel, aligning with expectations as Rhodamine B emits in the red spectrum. For the blue channel, the mean intensity is 7305±836, which is substantially lower than the red and green channels and with a narrower spread. For the 40µM concentration of rhodamine B, the rhodamine B stain is visible, but its visibility seems affected by the physically damaged membrane (Figure 4.39). The histogram of the red channel shows the mean intensity of 32946±7942. A strong signal is detected in this channel with a broad distribution of pixel intensities. However, the mean intensity is less and narrower than for the 60 µM concentration. The green channel has a mean pixel intensity of 28743. There is a moderate level of signal in this channel resulting from the excitation light. The lowest mean pixel intensity value is found in the blue channel, 7349. For the 20 µM rhodamine B concentration, the visibility of the rhodamine B is decreased on the 12-bit RGB image (Figure 4.40). The rhodamine B stain is light-pink colored and moderately differentiated from its background. The measured mean pixel intensity in the red channel is 31989±6628. The histogram of the green channel shows a mean intensity of 28261±5405, which is less than that of the red channel. The mean pixel intensity in the blue channel is 7311±710. The blue channel captures the least fluorescence from rhodamine B.

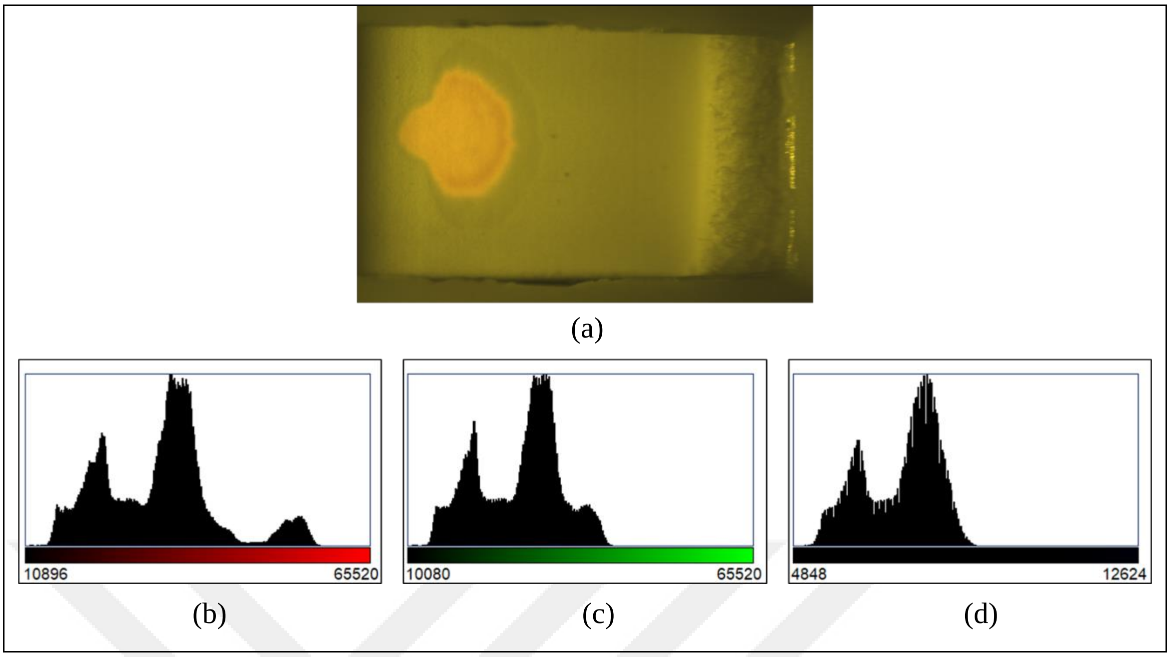

Figure 4.37. 80 µM rhodamine B. (a) 12-bit image, and (b-d) RGB channel histograms.

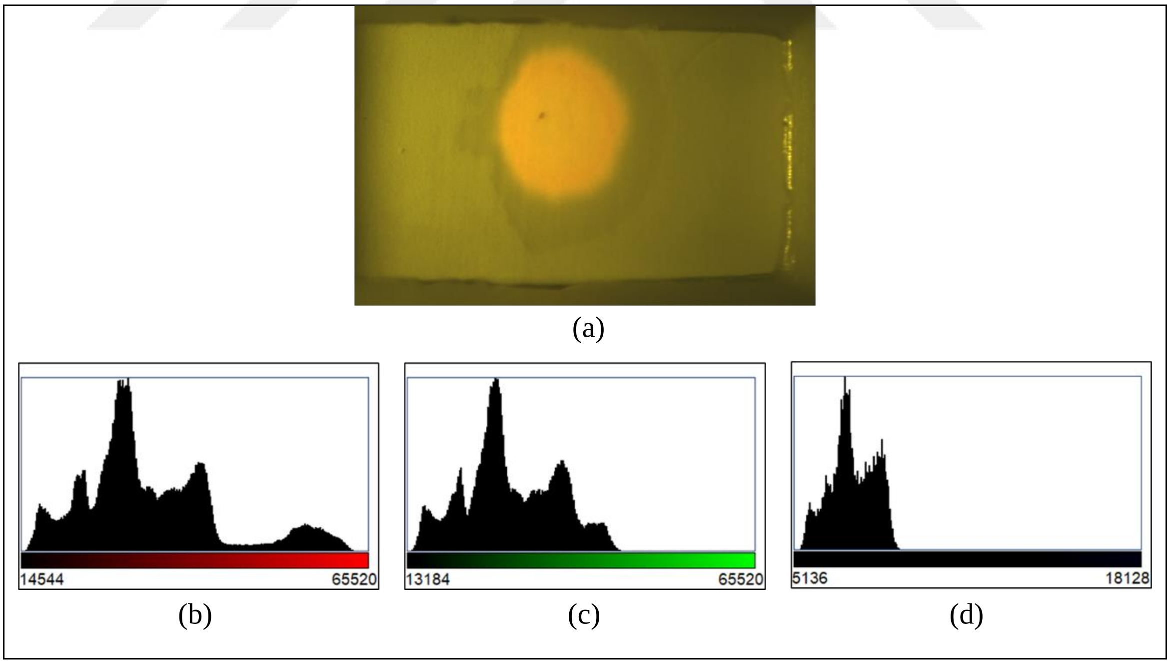

Figure 4.38. 60 µM rhodamine B. (a) 12-bit image, and (b-d) RGB channel histograms.

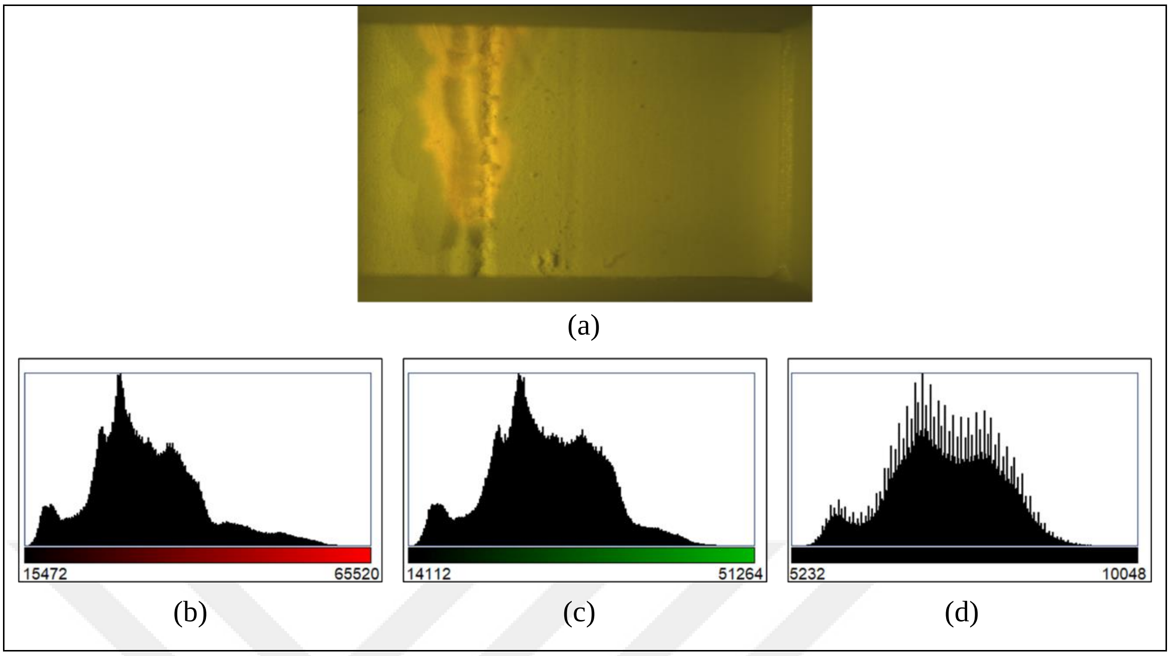

Figure 4.39. 40 μM rhodamine B. (a) 12-bit image, and (b-d) RGB channel histograms.

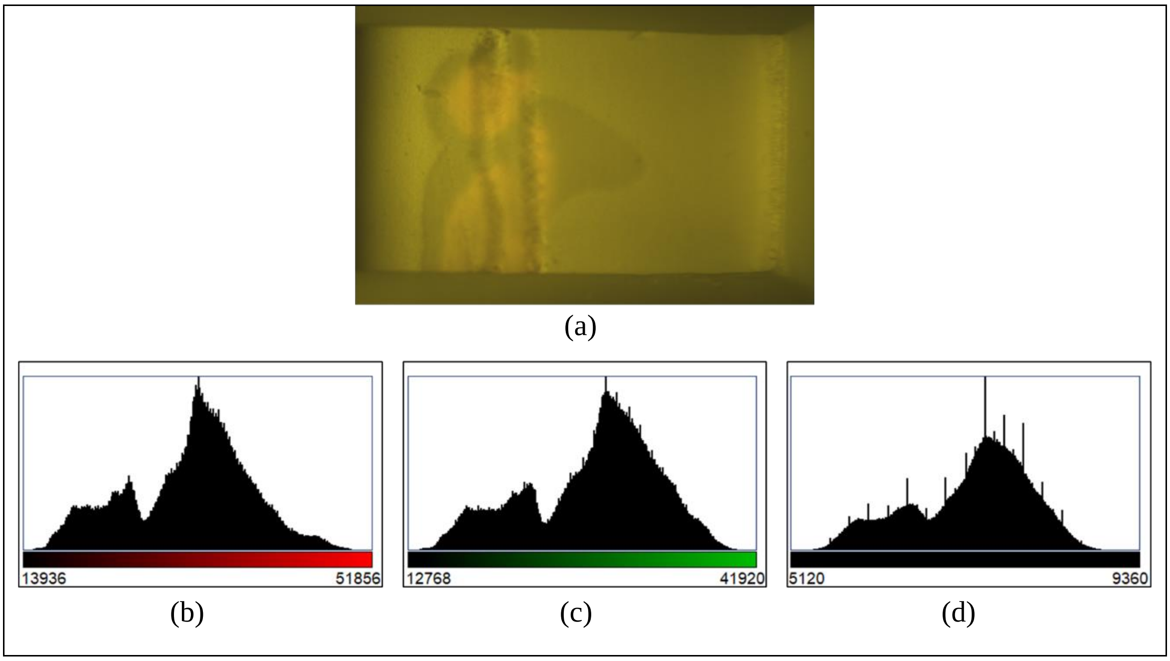

Figure 4.40. 20 μM rhodamine B. (a) 12-bit image, and (b-d) RGB channel histograms.

The 12-bit RGB image for each concentration level of rhodamine B is further analyzed on the ImageJ software. The ROI rectangles are set on the fluorescent parts of the nitrocellulose membranes, and the mean pixel intensities of the red channel are calculated within the ROIs. The relationship between the concentration of rhodamine B and the mean pixel intensity in the red channel within the set ROI for a 10 ms camera exposure time is illustrated in Figure 4.41. The plot shows a quadratic relationship between the concentration of rhodamine B and the mean pixel intensity of the red channel. Initially, the mean intensity increases with the increasing concentration, but beyond a certain point, the curve inverts, and the intensity value starts to decrease with increasing concentration. For 0.1 µM and 1µM concentration levels, the mean intensity values are near to each other. It starts an increasing trend until 60 µM and begins to drop from that point. The peak value of the mean intensity is achieved at 60 µM concentration of rhodamine B. The linear relationship between mean intensities in the red channel and rhodamine B concentrations is observed between 10 µM and 60 µM (Figure 4.42).

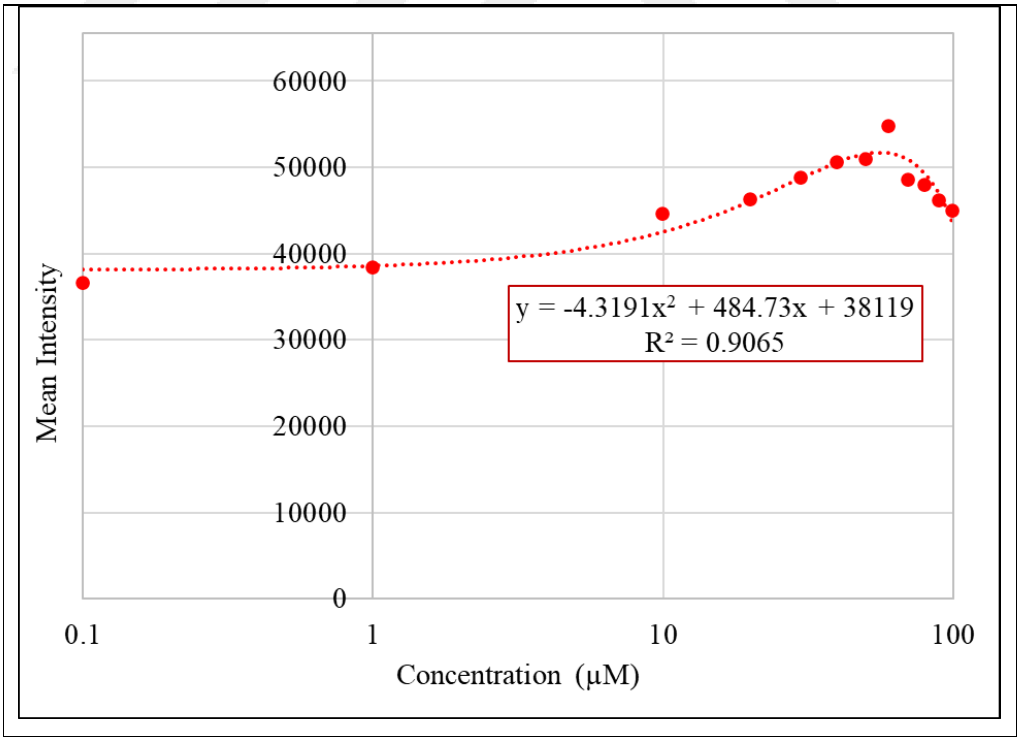

Figure 4.41. Mean intensity values for different concentrations of rhodamine B from the final reader.

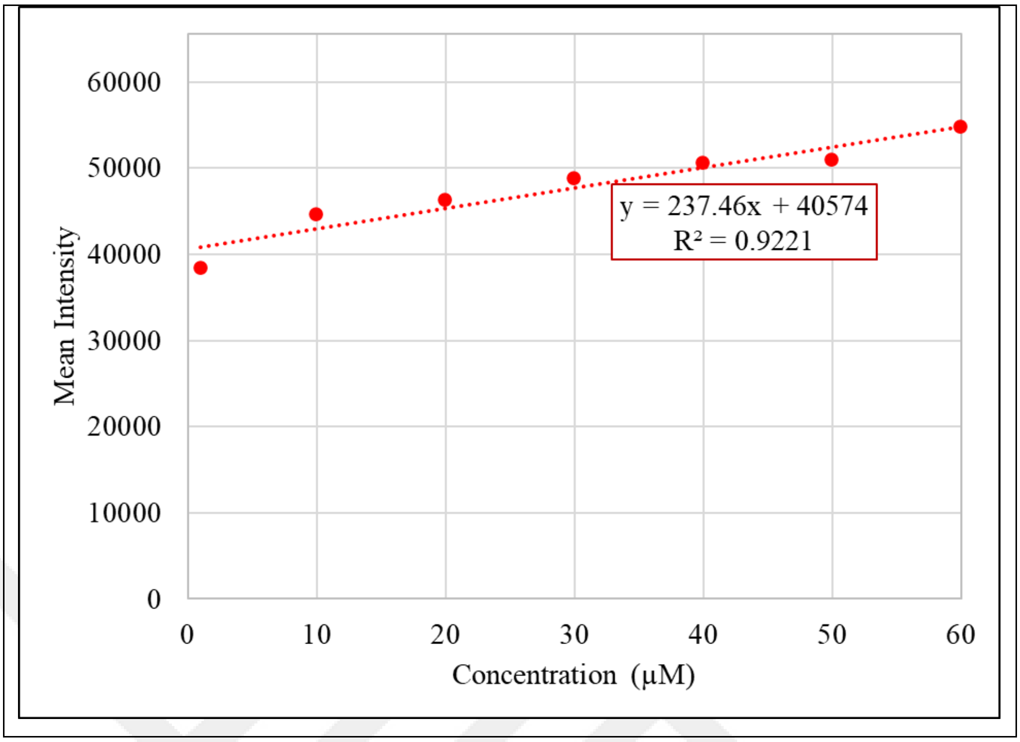

Figure 4.42. Mean intensity for low concentrations of rhodamine B from the final reader.

Table 4.1 lists the results for the mean intensity measurements. The mean intensity values within the whole image are smaller than the mean intensity values within the ROIs for all concentration levels of both fluorescent dyes. The mean values within the set ROIs are considered for comparing the fluorescein sodium salt and rhodamine B as they are aimed to encompass the fluorescent parts on the images (Figure 4.43). The mean intensity of the green channel within the set ROI on the fluorescein sodium salt image rises until reaching the concentration level of 90 µM. After that point, the mean intensity suddenly decreases to 42433 at 100 µM concentration of fluorescein sodium salt. The mean intensity of the red channel within the set ROI on the rhodamine B image increases with the increasing concentration until the 60µM concentration level. The mean intensity reaches its peak at 60 µM concentration and falls slightly when the concentration increases further. The mean intensities for rhodamine B become less than for fluorescein sodium salt.

Table 4.1. Mean intensity measurement results.

	Fluorescein Sodium Salt Green Channel		Rhodamine B Red Channel	
Concentration (µM)	Whole Image	ROI	Whole Image	ROI
0.1	17482±2703	17768	29981±5877	36600
1	17414±2985	17669	30840±6280	38394
10	18785±3182	24273	31388±6067	44542
20	18362±3730	25117	31989±6628	46288
30	18656±5395	27814	28901±9022	48735
40	20343±4210	29690	32946±7942	50523
50	20054±5655	34796	31373±8351	50880
60	22025±8663	44170	33388±10212	54762
70	27630±15291	52863	33417±10354	48525
80	25593±9832	53282	31953±9112	47937
90	30813±18183	64374	31692±7764	46171
100	22137±9720	42433	33697±10029	44917

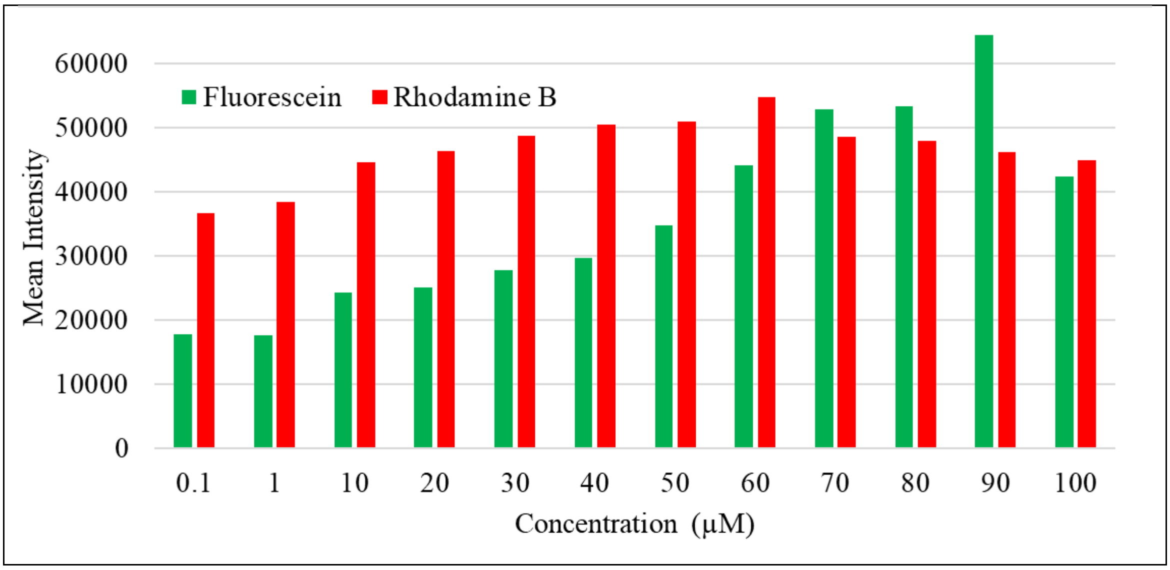

Figure 4.43. Bar plot of ROI mean intensity.

The examples of the post-processed images by subtracting the corresponding blank images from the 100µM fluorescein sodium salt and rhodamine B are demonstrated in Figure 4.44.

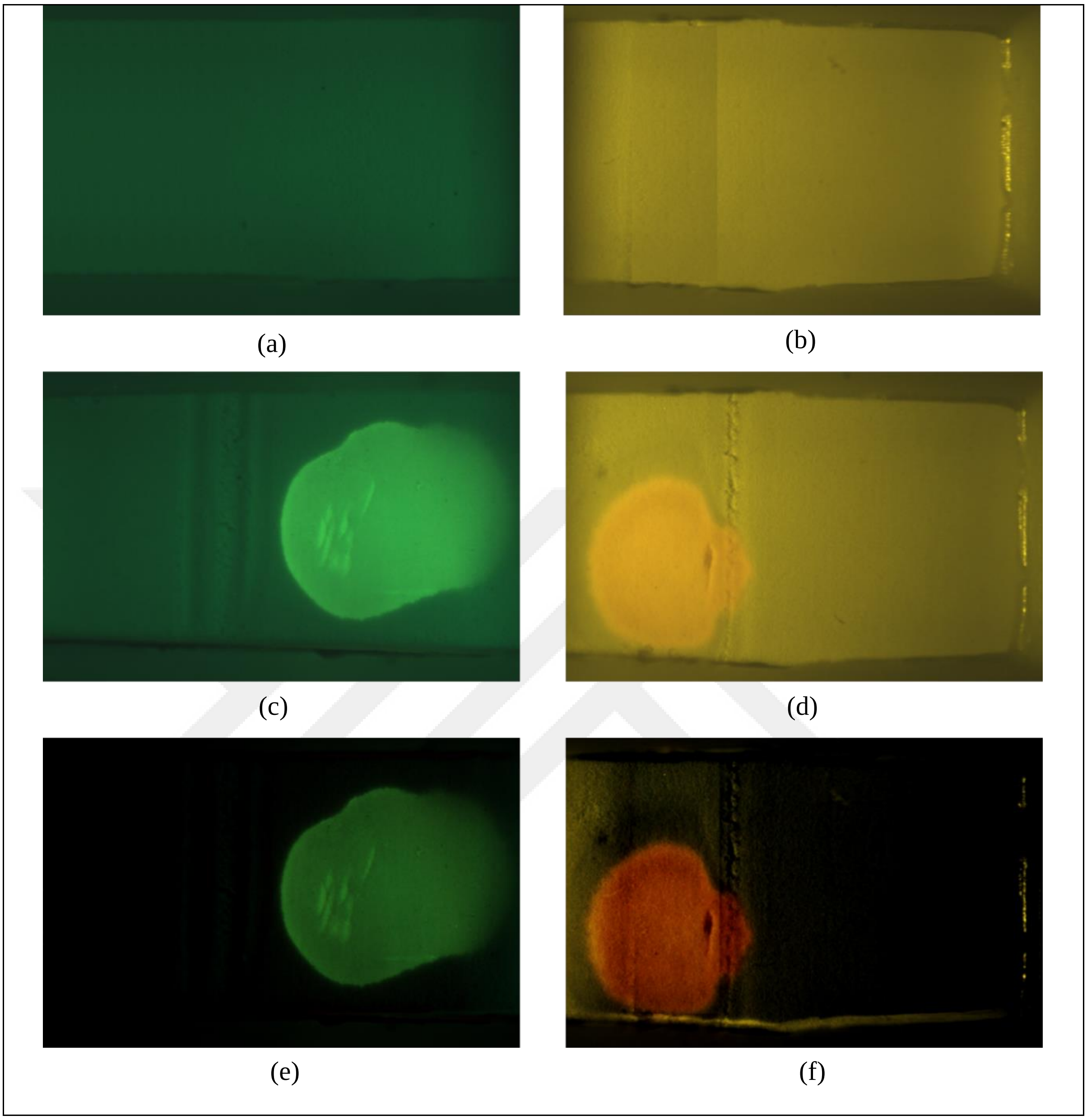

Figure 4.44. Image subtraction. (a, b) Control, (c, d) Test, and (e, f) Resultant subtracted images for fluorescein sodium salt, and rhodamine B samples.

4.6. COST ANALYSIS

The costs of the preliminary and final optical readers are analyzed to determine the financial feasibility and cost-effectiveness. During analysis, direct costs, including the electronic components and the materials to fabricate the devices, are considered (see Table 4.2). The final optical device costs approximately 20% more when compared to the cost of the preliminary due to the use of advanced components.

Table 4.2. Cost analysis.

Component	Piece	Preliminary Device ($)	Final Device ($)
Minicomputer	1	67 (4 GB RAM)	92 (8 GB RAM)
CMOS Camera Module	1	41 (Sony IMX219)	121 (Sony IMX477)
Camera Lens	1	-	3 (20° M12)
Touch-Screen Display	1	51 (HDMI)	40 (DSI)
Optical Filter	1	319	319
460 nm 3W Power LED	1	1	
560 nm 3W Power LED	1	8	
Power LED Collimator	2	1 (Beads)	1 (5°)
Step Motor, Motor Driver, and Position Sensor	1	4	
Real-Time Clock	1	8	
Temperature-Humidity Sensor	1	6 (HTU21D)	7 (BME280)
Step-Down Voltage Regulator Module	2	2	
Step-Up Voltage Regulator Module	1	-	1
Power Adapter	1	11 (5.1V 3A)	12 (8.4V 2A)
Uninterruptible Power Supply Module	1	-	23
2500 mAh Li-ion Battery	2	-	8
On/Off Power Switch, Cooling Fan, Aluminum Heatsink, Cables	1	9	
PLA Material	1	20	23
	TOTAL ($)	**548**	**682**

5. DISCUSSION

The development of a low-cost optical reader for imaging lateral flow assays with nitrocellulose membranes induced by fluorescein sodium salt and rhodamine B dyes has been aimed in the current study. The attempts result in two readers: a preliminary optical reader and a final optical reader. Both devices house two power LEDs as the light source, which generate light to excite the dyes on a nitrocellulose membrane, an optical dual-band pass filter to pass the light emitted by the dyes when excited, and a CMOS camera to capture the filtered light, temperature, humidity, and pressure sensors to monitor the environment conditions, a minicomputer to control the operation of the reader, and complementary electronic components. The final reader builds upon the strengths of the preliminary reader with significant improvements in imaging quality, light detection sensitivity, and device portability by employing a higher-resolution camera, better light control circuitry, and an uninterruptable power supply unit with high-capacity batteries. The final reader is less prone to light intensity saturation at high dye concentrations and may be beneficial for a wider range of imaging applications for the lateral flow assays requiring high sensitivity.

The 460 nm power LED emits light with a wavelength of 460±15 nm and does not converge with the 488 nm center excitation wavelength of the fluorescein sodium salt dye. This might lower the light emission efficiency of the fluorescein sodium salt dye. The power LEDs have a broad range of emission wavelengths, especially the 560nm power LED with a full width at half-maximum of 40nm. The power LEDs, which are the cheapest light sources, are not produced to emit light of a single wavelength like in the lasers. However, the light emission bands of the used power LEDs should be as narrow as possible for specificity to the fluorescent dyes. The 560nm power LED with a broad emission band may have an impact on the efficient excitation of rhodamine B. The power LEDs are expected to emit a stable wavelength based on the production material, and only the emitted light intensity should change by altering the voltage levels. However, the utilized power LEDs emit lights of longer wavelengths at the lower currents controlled by the voltage levels. This problem is majorly observed in the 560nm power LED emitting the wavelengths from 580nm to 558nm by the increased flowing current. The peak wavelength becomes stable after a threshold level is reached for the LED. Therefore, the drops in the voltage levels resulting from the over-use of the batteries may decrease the output voltages of the regulators, and the wavelengths of the 560nm power LED may shift toward the longer wavelengths. This could directly affect the absorption and emission of the rhodamine B dye. The exact current levels of the power LEDs cannot be measured when they are fed by the voltage regulators. The measured current values correspond to the currents flowing through the LEDs fed by the adjustable DC power supply, so there is a possibility to obtain slightly different current values for the LEDs fed by the voltage regulators. The power LEDs have different light intensities based on their lumens, although they both have 3W power. The 560nm power LED emits a more intense light when compared to the 460nm power LED. This causes changes in the illumination of the dyes. The overall brighter images of the rhodamine B dye, excited by the 560nm power LED, are perhaps caused by this issue. The minimum sensor responses to the changing concentration of rhodamine B can be explained by the high 560nm light intensity reaching the camera, resulting in the increase of all pixel values within the image. The power of the LEDs may not be adequate for the excitation of the fluorescent dyes, especially the rhodamine B. This also contributes to the low sensitivity of the reader to the changing concentrations. The more powerful LEDs with narrow emission bands can be used to improve the device's performance.

The fluorescein sodium salt dye emits light at a center wavelength of 515 nm that corresponds to greenish light, and therefore, the signal intensity is dominant for the green channel of the images acquired both by the preliminary and final reader. The broader and higher mean is the clue for the green channel capturing more fluorescence signals. The decreasing dye concentration causes a notable reduction in the green channel intensity. This indicates the sensitivity of the optical reader and its capability to differentiate between concentrations, which is critical for quantitative analysis. There is a moderate level of signal in the blue channel, resulting from the absorption of the 460 nm power LED. At lower concentrations, changes in concentration have a more noticeable effect on mean pixel intensity. At higher concentrations, the effect tapers off due to quenching effects or limitations by the CMOS camera.

The rhodamine B dye emits light at a center wavelength of 630 nm, which is observed as red light. Therefore, the fluorescence of the dye is dominant in the red channel of the images captured by both the preliminary and final reader. When the dye concentration increases, the mean intensity in the red channel initially follows an ascending trend. However, after reaching a certain concentration, the intensity diminishes, which could indicate the occurrence of concentration quenching at high concentrations of the dye, which occurs when the dye molecules are so densely packed that their energy is non-radiatively transferred to neighboring molecules or is absorbed, thus decreasing fluorescence emission. The moderate level of the signal in the green channel may be caused by the absorption of the 560 nm green excitation light, and the signal is possibly strengthened by some passing wavelengths of the excitation light. The smaller intensity values exist near the dark end of the intensity spectrum of the blue channel. The higher camera exposure time increases all pixel intensities for both dyes because of more photon capturing and results in overexposure, which leads to some of the details being lost in the brightest areas of the images. In the preliminary reader, the camera tends to saturate for all concentration levels of rhodamine B, so the response of the camera to the increasing concentration of the dye is less sensitive.

The imaging is performed only once for each concentration of the dyes due to limited resources for the membrane. Vibration could adversely impact the optical components, so the device should be stable when it is running. The settings of the image acquisition, including camera exposure time, light emission time, and gain, ought to be evaluated to enhance the sensitivity and performance of the reader device. Subtracted imaging offers remarkably increased contrast and facilitates the interpretation of the fluorescing regions on the assay. However, it is affected by the physical damages given to the assay.

The higher quality 12-bit RGB images by the final optical reader provide more detailed information. The final reader allows for a high dynamic range, capturing a broad spectrum of intensity values from very dim to very bright, which is critical for capturing the full range of fluorescence intensities without saturation or loss of details. Similar to the preliminary reader, the green channel of the image captured by the final reader is the most informative channel for fluorescein sodium salt. The mean pixel intensity rises with the increasing fluorescein sodium salt concentration, but at the highest levels, it drops due to the concentration quenching or inhomogeneity problems. The optimal concentration level of fluorescein sodium salt may be 90μM for imaging by the final optical reader, since the mean pixel intensity peaks at this level. The rhodamine B emission is dominant in the red channel like in the preliminary reader. Increasing the concentration of rhodamine B leads to increased fluorescence intensity, up to a point where it starts decreasing, which is a typical fluorescence behavior. The lower concentrations of the dyes, that are 0.1 μM and 1 μM, may not be sufficient for the fluorescence emission. The mean pixel intensity increases with the higher concentrations of rhodamine B and reaches its maximum at 60 μM concentration, which may be the optimal concentration level for imaging in the final reader. It is lower than the determined optimal concentration of fluorescein sodium salt, 90 μM. These concentration levels are in agreement with the findings reported in the literature, which that state 6-100 μM concentration of fluorescent dyes are adequate for fluorescence emission detection [39, 41, 141, 150].

At high dye concentrations, the intensity decreases remarkably. This may be due to the decrease in fluorescence intensity of the dye explained by the "quenching effect". The quenching effect may happen through various mechanisms. One common mechanism is static quenching, which occurs when the fluorescent dye and a quencher molecule form a non-fluorescent complex before the dye is excited. This reduces the number of dye molecules available for excitation and subsequent fluorescence. Another mechanism is dynamic quenching, where the quencher interacts with the excited state of the dye, transferring energy from the dye to the quencher without light emission. This effectively reduces the fluorescence intensity as the energy is dissipated non-radiatively.

The final optical reader outputs 12-bit images, which offer a higher sensitivity especially at higher concentrations of the dyes, when compared to the 8-bit images by the preliminary reader. The sensitivity to changing concentrations of the dyes is increased when compared to the preliminary reader. Moreover, the absence of saturation across the entire dynamic range indicates that the data are reliable and that the imaging conditions are well set for capturing the fluorescence without the risk of pixel saturation. Therefore, the system is suitable for quantitative analysis of the changing fluorescein sodium salt concentration. The detection sensitivity of the final optical reader can be improved further by using optical filters more specific to excitation and emission from the dyes and by utilizing a light source more to increase the fluorescence emission by the dyes. The use of subtracted images may be beneficial to emphasize the fluorescein sodium salt and rhodamine B dyes in the images.

The limitations in the current study are inspired in terms of dye solution, light source, collimator, optical filter, camera, imaging protocol, and mechanical parts. Dye solutions with different concentrations are prepared using the serial dilution technique, but the solutions are not vortexed; instead, they are mixed manually using a pipette. This may lead to some inhomogeneity in the solutions, while the tiny droplets of the main stock or base solution left on the pipette may hinder the concentration level targeted. On the other hand, the solutions are loaded onto the membranes using a pipette. Consequently, the locations, dispersions, and homogeneity of the fluorescent dyes dispensed on the membranes may be different. The use of a dispenser device may overcome the problems and may lead to better performance by the developed readers.

The light sources of the readers are two power LEDs, which generate very intense light at certain wavelengths but the center wavelength may change due to the current delivered to the LED. This instability may be due to the quality of the construction, semiconductor material, and thermal management of the LED. The construction quality may differ from production batch to batch, even though handled by the same company. Beads collimators are used in the preliminary reader while 5-degree collimators are employed in the final reader for homogenous light emission by the LEDs. Use of different type of collimators can affect the scattering aspect of the photons from the LEDs, so the homogeneity of the light exposure may be different in the readers developed.

The optical dual band-pass filter passes the light with two distinct wavelength ranges and works fine in detecting the light emission by fluorescein sodium salt since the center wavelength of the light emitted by the dye lies within one of the ranges. However, the filter has limited detection capability for rhodamine B due to the fact that the dye emits light at a center wavelength out of the ranges. On the other hand, the light emitted by one power LED is within the range, and therefore, some portions of the light may pass through the filter and reach the camera. This results in a yellowish background on the images captured by the camera. A dual band-pass filter tailored to detect light emission by the dyes while suppressing the excitation light emitted by the LEDs may overcome this limitation, but production of such a filter may be quite costly and infeasible. Alternatively, two separate band-pass filters with two distinct passing wavelength ranges can be used for the implementation but this may require an extra moving mechanism to position each filter for each dye during imaging, which may lead to undesirable time delays during imaging.

The CMOS cameras deliver very high imaging resolution, which leads to high detectability of the fluorescent particles of the dyes on the assay. However, the detectability may be improved further by a magnification lens positioned in front of the camera that can lead to more detail imaging for the homogeneous dispersion of the dyes on the membrane. On the other hand, the cameras provide high sensitivity to the green light during imaging when operated with the Bayer RGGB encoding pixel format. This makes the cameras more sensitive to greenish light emission by fluorescein sodium salt dye than to reddish light emission by rhodamine B dye. The sensitivity may be improved further by using an RRGG encoding pixel format, but the format has not been supported by the cameras, possibly due to some technical issues.

The imaging protocol includes the waiting period which is the time required for the solution to be sufficiently absorbed by the membrane and set to 15 minutes. Use of a different waiting time may change the fluorescence emission efficient of the dyes leading to an optimum efficiency. The imaging is performed for the same light exposure time and camera exposure time for all the solutions. Fluorescence emission rates of the dyes are different so the use of dedicated times to image a specific dye may result in higher quality images. On the other hand, the light exposure time is managed by turning on the initially off power LED for a given time and then turning it off. Power LEDs may need some time after turning on to emit light with a stable intensity and the short light exposure time used may have distorted the light intensity. On the other hand, the imaging is performed only once for a sample and repetitive imaging of the same sample may reduce error on the intensity measurements and subsequently improve the performance of the readers developed.

Mechanical parts of the readers are produced using a 3D-printing technology and PLA filament material. The 3D-printed technology may exhibit millimetric differences in the dimensions of the parts produced. This may obstruct the orientation geometry of the optical components and consequently hinder the proper illumination of the assays. The PLA material may result in reflective surfaces, and undesirable reflected light to the camera. A material with less reflectivity may be employed to avoid this problem.

In the future, we plan to perform complementary experiments to determine the optimum imaging parameters. Additional experiments will be carried out to optimize the volume of a single drop and the waiting time. Validation studies with a larger number of dye-loaded membranes are also scheduled.

6. CONCLUSION

Lateral flow assays are a type of diagnostic test to detect the presence or absence of a target analyte in a sample for the detection of various diseases in many different settings such as point-of-care. They are induced by many different fluorescent dyes, and among them, fluorescein sodium salt and rhodamine B are the most common ones. In detecting and quantification of the emitted fluorescence by the dyes, fluorescence-based optical readers are used. Available commercial readers usually need specialized equipment, environment, and trained personnel, which increases the cost of the reader and makes it impractical for portable use. There is a need for low-cost and portable fluorescence-based optical readers for the detection of the fluorescent dyes of the lateral flow membranes.

In the current study, a low-cost and portable optical reader has been developed targeting high-quality and sensitive imaging of the fluorescein sodium salt and rhodamine B dyes, making it versatile for the detection of various diseases labeled by these dyes. The reader benefits from an uncomplicated implementation and cost-effective electronic components and materials. Offering a good detection sensitivity, the reader may be beneficial for identifying subtle changes in fluorescence of both low and high concentrations of fluorescein sodium salt and rhodamine B dyes, expanding its applicability in a variety of settings, from clinical laboratories to point-of-care applications.

REFERENCES

1. Mansfield MA. Nitrocellulose membranes for lateral flow immunoassays: a technical treatise. In: Wong R, Tse H, editors. Lateral Flow Immunoassay. Humana Press; 2009. Available from: https://doi.org/10.1007/978-1-59745-240-3_6.
2. Jia P, Li Z, Wang X, Xu F, You M, Feng S. Performance improvement of lateral flow assay using heterogeneous nitrocellulose membrane with nonuniform pore size. Int Commun Heat Mass Transfer. 2023 Apr;143:106729. Available from: https://doi.org/10.1016/j.icheatmasstransfer.2023.106729.
3. Ngom B, Guo Y, Wang X. Development and application of lateral flow test strip technology for detection of infectious agents and chemical contaminants: a review. *Anal Bioanal Chem*. 2010; pp. 1113-1135.
4. Lazo Jara MD, Contreras Alvarez LA, Guimarães MCC, Antunes PWP, de Oliveira JP. Lateral flow assay applied to pesticides detection: recent trends and progress. *Environ Sci Pollut Res*. 2022;29:46487-46508.
5. Xing G, Sun X, Li N, Li X, Wu T, Wang F. New advances in lateral flow immunoassay (LFI) technology for food safety detection. *Molecules*. 2022;27(19):6596. doi:10.3390/molecules27196596.
6. Van Stappen T, Bollen L, Vande Casteele N, Papamichael K, Van Assche G, Ferrante M, Vermeire S, Gils A. Rapid test for infliximab drug concentration allows immediate dose adaptation. *Clin Transl Gastroenterol*. 2016 Dec;7(12):e206. doi:10.1038/ctg.2016.62. PMCID: PMC5288585. PMID: 27929524.
7. Li Z, Wang P. Point-of-care drug of abuse testing in the opioid epidemic. *Arch Pathol Lab Med*. 2020;144(11):1325-1334. doi:10.5858/arpa.2020-0055-RA.
8. Denizli A, Pohanka M. Point-of-care diagnoses and assays based on lateral flow test. *Int J Anal Chem*. 2021;2021:6685619. doi:10.1155/2021/6685619.
9. Zhang D, Huang L, Liu B, Ni H, Sun L, Su E, Chen H, Gu Z, Zhao X. Quantitative and ultrasensitive detection of multiplex cardiac biomarkers in lateral flow assay with core-shell SERS nanotags. *Biosens Bioelectron*. 2018 May 30; 106:204-211. doi: 10.1016/j.bios.2018.01.062.
10. Ranganathan V, Srinivasan S, Singh A, DeRosa MC. An aptamer-based colorimetric lateral flow assay for the detection of human epidermal growth factor receptor 2 (HER2). *Anal Biochem*. 2020;588:113471. doi:10.1016/j.ab.2019.113471.

11. Zhang J, Tang L, Yu Q, Qiu W, Li K, Cheng L, Zhang T, Qian L, Zhang X, Liu G. Gold-platinum nanoflowers as colored and catalytic labels for ultrasensitive lateral flow MicroRNA-21 assay. *Sens Actuators B Chem*. 2021;344:130325.
12. Burrell CJ, Howard CR, Murphy FA. Laboratory diagnosis of virus diseases. *In: Fenner and White's Medical Virology. 5th ed. Cambridge*, *MA: Academic Press*; 2017. 135-54.
13. Wang C, Yang X, Zheng S, Cheng X, Xiao R, Li Q, Wang W, Liu X, Wang S. Development of an ultrasensitive fluorescent immunochromatographic assay based on multilayer quantum dot nanobead for simultaneous detection of SARS-CoV-2 antigen and influenza A virus. *Sens Actuators B Chem*. 2021;345:130372.
14. Liu H, Dai E, Xiao R, Zhou Z, Zhang M, Bai Z, Shao Y, Qi K, Tu J, Wang C, Wang S. Development of a SERS-based lateral flow immunoassay for rapid and ultra-sensitive detection of anti-SARS-CoV-2 IgM/IgG in clinical samples. *Sens Actuators B Chem*. 2021;329:129196.
15. Liu X, Zhang C, Liu K, Wang H, Lu C, Li H, Hua K, Zhu J, Hui W, Cui Y, Zhang X. Multiple snps detection based on lateral flow assay for phenylketonuria diagnostic. *Anal Chem*. 2018;90(5):3430-3436. doi: 10.1021/acs.analchem.7b05113.
16. Natarajan S, Joseph J, Vinayagamurthy B, Estrela P. A Lateral flow assay for the detection of leptospira lipl32 gene using CRISPR technology. *Sensors*. 2023;23(14):6544. https://doi.org/10.3390/s23146544.
17. O'Farrell B. Lateral flow immunoassay systems: evolution from the current state of the art to the next generation of highly sensitive, quantitative rapid assays. *In: The Immunoassay Handbook (Fourth Edition): Theory and Applications of Ligand Binding, ELISA and Related Techniques*; 2013. p. 89-107. doi:10.1016/B978-0-08-097037-0.00007-5.
18. Ren ML, Chen XL, Li CH, Xu B, Liu WJ, Xu HY, Xiong YH. Lateral flow immunoassay for quantitative detection of ractopamine in swine urine. *Biomed Environ Sci*. 2014 Feb;27(2):134-7. doi: 10.3967/bes2014.029. PMID: 24625406.
19. Boehringer HR, O'Farrell BJ. Lateral flow assays in infectious disease diagnosis. *Clin Chem*. 2022;68(1):52-58. doi:10.1093/clinchem/hvab194.
20. Vashist SK, Luppa PB, Yeo LY, Ozcan A, Luong JH. Emerging technologies for next-generation point-of-care testing. *Trends Biotechnol*. 2015;33:692–705.
21. Li Z, Chen H, Wang P. Lateral flow assay ruler for quantitative and rapid point-of-care testing. *Anal*. 2019;144:3314–3322.

22. Ye H, Xia X. Enhancing the sensitivity of colorimetric lateral flow assay (CLFA) through signal amplification techniques. *J Mater Chem B*. 2018;44.
23. Deng J, Yang M, Wu J, Zhang W, Jiang X. A self-contained chemiluminescent lateral flow assay for point-of-care testing. *Anal Chem*. 2018;90(15):9132-9137. doi:10.1021/acs.analchem.8b01543.
24. Khodadadi M, Chang L, Trabuco JRC, Vu BV, Kourentzi K, Willson RC, Litvinov D. PCB-based magnetometer as a platform for quantification of lateral-flow assays. *Sensors*. 2019;19(24):5433. https://doi.org/10.3390/s19245433.
25. Zhan Y, Fei R, Lu Y, Wan Y, Wu X, Dong J, Meng D, Ge Q, Zhao X. Ultrasensitive detection of multiple Alzheimer's disease biomarkers by SERS-LFA. *Analyst*. 2022;(18).
26. Perju A, Wongkaew N. Integrating high-performing electrochemical transducers in lateral flow assay. *Trends Anal Bioanal Chem*. 2021;413:5535-5549.
27. Chen Y, Fu Q, Xie J, Wang H, Tang Y. Development of a high sensitivity quantum dot-based fluorescent quenching lateral flow assay for the detection of zearalenone. *Trends Anal Bioanal Chem*. 2019;411:2169-2175.
28. Wang C, Shen W, Rong Z, Liu X, Gu B, Xiao R, et al. Layer-by-layer assembly of magnetic-core dual quantum dot-shell nanocomposites for fluorescence lateral flow detection of bacteria. *Nanoscale*. 2020;2(2).
29. Gumus E, Bingol H, Zor E. Lateral flow assays for detection of disease biomarkers. *J Pharm Biomed Anal*. 2023 Feb 20;225:115206. doi: 10.1016/j.jpba.2022.115206.
30. Bose A, Thomas I, Kavitha G, Abraham E. Fluorescence spectroscopy and its applications: A Review. *International Journal of Advances in Pharmaceutical Analysis*. 2018;08(01):01-08.
31. Shin YH, Gutierrez-Wing MT, Choi JW. Recent progress in portable fluorescence sensors. *J Electrochem Soc*. 2021;168(1):017502. DOI: 10.1149/1945-7111/abd494.
32. Pilavaki E, Parolo C, Mckendry R, Demosthenous A. Wireless paper-based biosensor reader for the detection of infectious diseases at the point of care. *In: 2016 IEEE SENSORS*. 2016. p. 1–3.
33. Hui YY, Tang YX, Azuma T, Lin HH, Liao FZ, Chen QY, Kuo JH, Wang YL, Chang HC. Design and implementation of a low-cost portable reader for thermometric lateral flow immunoassay. *J Chin Chem Soc*. 2022. Advance online publication. DOI: 10.1002/jccs.202200124.

34. Mudanyali O, Dimitrov S, Sikora U, Padmanabhan S, Navruz I, Ozcan A. Integrated rapid diagnostic test reader platform on a cell phone. *Lab Chip*. 2012;12(15):2678-2686.
35. Shah MI, Joseph J, Sanne US, Sivaprakasam M. PhoneQuant: A smartphone-based quantitative immunoassay analyser. *2017 39th Annual International Conference of the IEEE Engineering in Medicine and Biology Society (EMBC)*. 2017. doi:10.1109/embc.2017.8037794.
36. Ilesh Shah M, Joseph J, Rajagopalan A, Sivaprakasam M. ImageQuant: An image-based quantitative immunoassay analyzer. *2017 IEEE International Symposium on Medical Measurements and Applications (MeMeA)*. 2017. doi:10.1109/memea.2017.7985913.
37. Saisin L, Amarit R, Somboonkaew A, Gajanandana O, Himananto O, Sutapun B. Significant sensitivity improvement for camera-based lateral flow immunoassay readers. *Sensors*. 2018;18(11):4026. DOI: 10.3390/s18114026.
38. Ulep TH, Yoon JY. Challenges in paper-based fluorogenic optical sensing with smartphones. *Nano Convergence*. 2018;5:14.
39. Huttunen A, Aikio S, Kurkinen M, Mäkinen J-T, Mitikka R, Kivim L. Portable low-cost fluorescence reader for lfa measurements. *IEEE Sensors Journal*. 2020;20(17):10275-10282. DOI: 10.1109/JSEN.2020.2992894.
40. Yeo SJ, Kang H, Dao TD, Cuc BT, Nguyen ATV, Tien TTT, Hang NLK, Phuong HVM, Thanh LT, Mai LQM, Rah Y, Yu K, Shin HJ, Chong CK, Choi HS, Park H. Development of a smartphone-based rapid dual fluorescent diagnostic system for the simultaneous detection of influenza A and H5 subtype in avian influenza A-infected patients. *Theranostics*. 2018;8(22):6132-6148. DOI: 10.7150/thno.28027.
41. Bheemavarapu LP, Shah MI, Joseph J, Sivaprakasam M. Multi-cartridge fluorescence reader for quantitative immunoassays. *In: Proceedings of the 2019 IEEE International Symposium on Medical Measurements and Applications (MeMeA)*; 2019. p. 5447-5450. DOI: 10.1109/MeMeA.2019.8780526.
42. Rosenstein RW, Bloomster TG. Solid-phase assay employing capillary flow. *US Pat.* 1989;4,855,240.
43. May K, Prior ME, Richards I. Capillary immunoassay and device therefore comprising mobilizable particulate labeled reagents. *US Pat*. 1997;5,622,871.
44. O'Farrell B. Evolution in lateral flow–based immunoassay systems. in: wong r, tse h, editors. lateral flow immunoassay. *Humana Press*; 2009. p. 1-33. DOI: https://doi.org/10.1007/978-1-59745-240-3_1.

45. Koczula KM, Gallotta A. Lateral flow assays. *Essays Biochem*. 2016 Jun;30;60(1):111-120. DOI: https://doi.org/10.1042/EBC20150012.
46. Soh JH, Chan HM, Ying JY. Strategies for developing sensitive and specific nanoparticle-based lateral flow assays as point-of-care diagnostic device. *Nano Today*. 2020 Feb;30:100831. DOI: https://doi.org/10.1016/j.nantod.2019.100831.
47. Bahadır EB, Sezgintürk MK. Lateral flow assays: principles, designs, and labels. *TrAC Trends in Analytical Chemistry*. 2016 Sep;82:286-306. DOI: https://doi.org/10.1016/j.trac.2016.06.006.
48. Hu Q, Wei Q, Zhang P, Li S, Xue L, Yang R, Wang C, Zhou L. An up-converting phosphor technology-based lateral flow assay for point-of-collection detection of morphine and methamphetamine in saliva. *Analyst*. 2018;19.
49. Ahmed SR, Chand R, Kumar S, Mittal N, Srinivasan S, Rajabzadeh AR. Recent biosensing advances in the rapid detection of illicit drugs. *TrAC Trends in Analytical Chemistry*. 2020 Oct;131:116006. DOI: https://doi.org/10.1016/j.trac.2020.116006.
50. Fan L, Yang J, Wu J, Li F, Yan W, Tan F, Zhang M, Draz MS, Han H, Zhang P. Deeply-dyed nanobead system for rapid lateral flow assay testing of drugs at point-of-care. *Sensors and Actuators B: Chemical*. 2022 Jul 1;362:131829. DOI: https://doi.org/10.1016/j.snb.2022.131829.
51. Lee S, Oncescu V, Mancuso M, Mehta S, Erickson D. A smartphone platform for the quantification of vitamin D levels. *Lab Chip*. 2014;8.
52. Vemulapati S, Rey E, O'Dell D, Mehta S, Erickson D. A Quantitative point-of-need assay for the assessment of vitamin d3 deficiency. *Sci Rep*. 2017 Oct 26;7(14142). DOI: 10.1038/s41598-017-14532-1.
53. Khelifa L, Hu Y, Jiang N, Yetisen AK. Lateral flow assays for hormone detection. *Lab Chip*. 2022;22:2451-2475. DOI: 10.1039/D1LC00960E.
54. Cao XE, Kim J, Mehta S, Erickson D. Two-color duplex platform for point-of-care differential detection of malaria and typhoid fever. *Anal Chem*. 2021 Sep 1;93(36):12175-12180. DOI: 10.1021/acs.analchem.1c03298.
55. Sastre P, Pérez T, Rueda P, et al. Development of a duplex lateral flow assay for simultaneous detection of antibodies against African and classical swine fever viruses. 2016;28(5):DOI: 10.1177/1040638716654942.

56. Le TT, Chang P, Benton DJ, McCauley JW, Iqbal M, Cass AEG. Dual recognition element lateral flow assay toward multiplex strain-specific influenza virus detection. *Anal Chem*. 2017 May 30;89(12):6781-6786. DOI: 10.1021/acs.analchem.7b01149.
57. Safenkova IV, Panferov VG, Panferova NA, Varitsev YA, Zherdev AV, Dzantiev BB. Alarm lateral flow immunoassay for detection of the total infection caused by the five viruses. *Talanta*. 2019 Apr 1;195:739-744. DOI: https://doi.org/ 10.1016/j.talanta.2018.12.004.
58. Cao Y, Chen Z, Li X, Li Z, Lin G, Liu T, Wu Y. Dual-color quantum dot-loaded nanoparticles based lateral flow biosensor for the simultaneous detection of gastric cancer markers in a single test line. *Analytica Chimica Acta*. 2022 Jul 25;1218:339998. DOI: https://doi.org/10.1016/j.aca.2022.339998.
59. Xing KY, Shan S, Liu DF, Lai WH. Recent advances of lateral flow immunoassay for mycotoxins detection. *TrAC Trends in Analytical Chemistry*. 2020 Dec;133:116087. DOI: https://doi.org/10.1016/j.trac.2020.116087.
60. Gondhalekar C, Biela E, Rajwa B, et al. Detection of E. coli labeled with metal-conjugated antibodies using lateral-flow assay and laser-induced breakdown spectroscopy. *Anal Bioanal Chem*. 2020;412:1291–1301. DOI: https://doi.org/10.1007/s00216-019-02347-3.
61. Cheng J, Yang G, Guo J, Liu S, Guo J. Integrated electrochemical lateral flow immunoassays (eLFAs): *recent advances*. Analyst. 2022;147(4).
62. Aksoy S, Dulda A, Ertaş G. Emerging technologies for fluorescence-based optical test strip readers. *Avrupa Bilim Ve Teknoloji Dergisi*. 2023;(49):16-24. Available from: https://doi.org/10.31590/ejosat.1265098.
63. Kasetsirikul S, Shiddiky MJA, Nguyen N-T. Challenges and perspectives in the development of paper-based lateral flow assays. *Microfluid Nanofluid*. 2020 Feb 12;24(1):17.
64. Calucho E, Parolo C, Rivas L, Álvarez-Diduk R, Merkoçi A. Nanoparticle-based lateral flow assays. I*n: Comprehensive Analytical Chemistry*, Volume 89; 2020. p. 313-359. doi: 10.1016/bs.coac.2020.04.011.
65. Amerongen A, Veen J, Arends H, Koets M. Lateral flow immunoassays. *Handbook of Immunoassay Technologies: Approaches, Performances, and Applications*; 2018:157-182.

66. Sadeghi P, Sohrabi H, Hejazi M, Jahanban-Esfahlan A, Baradaran B, Tohidast M, Majidi MR, Mokhtarzadeh A, Tavangar SM, de la Guardia M. Lateral flow assays (LFA) as an alternative medical diagnosis method for detection of virus species: The intertwine of nanotechnology with sensing strategies. *Trends Analyt Chem*. 2021 Dec;145:116460. doi: 10.1016/j.trac.2021.116460.
67. Ince B, Sezgintürk MK. Lateral flow assays for viruses diagnosis: Up-to-date technology and future prospects. *TrAC Trends in Analytical Chemistry*. 2022 Dec;157:116725. doi: 10.1016/j.trac.2022.116725.
68. Sotnikov DV, Zherdev AV, Dzantiev BB. Lateral flow serodiagnosis in the double-antigen sandwich format: theoretical consideration and confirmation of advantages. *Sensors*. 2021;21(1):39. https://doi.org/10.3390/s21010039.
69. Chen X, Miao X, Ma T, Leng Y, Hao L, Duan H, et al. Gold nanobeads with enhanced absorbance for improved sensitivity in competitive lateral flow immunoassays. *Foods.* 2021;10(7):1488.
70. Jing J, Wang Z. Research advance of lateral flow assay labels. *Sheng Wu Yi Xue Gong Cheng Xue Za Zhi*. 2018 Aug 25;35(4):661-664. doi: 10.7507/1001-5515.201703005.
71. Bishop JD, Hsieh HV, Gasperino DJ, Weigl BH. Sensitivity enhancement in lateral flow assays: a systems perspective. *Lab Chip*. 2019;19:2486-2499. DOI: 10.1039/C9LC00104B.
72. Parolo C, Sena-Torralba A, Bergua JF, Calucho E, Fuentes-Chust C, Hu L, Rivas L, Álvarez-Diduk R, Nguyen EP, Cinti S, Quesada-González D, Merkoçi A. Tutorial: design and fabrication of nanoparticle-based lateral-flow immunoassays. *Nat Protoc*. 2020;15:3788-3816.
73. Wang Z, Zhao J, Xu X, Guo L, Xu L, Sun M, Hu S, Kuang H, Xu C, Li A. An overview of nanoparticles-based quantitative lateral flow assay. *Small Methods*. 2021 Dec 2. doi: 10.1002/smtd.202101143.
74. Huang C, Wen T, Shi F-J, Zeng X-Y, Jiao Y-J. Rapid detection of IgM antibodies against the SARS-CoV-2 virus via colloidal gold nanoparticle-based lateral-flow assay. *ACS Omega*. 2020;5(21):12550-12556. doi:10.1021/acsomega.0c01554.
75. Porras JC, Bernuz M, Marfa J, Pallares-Rusiñol A, Martí M, Pividori MI. Comparative study of gold and carbon nanoparticles in nucleic acid lateral flow assay. *Nanomaterials*. 2021;11(3):741. doi:10.3390/nano11030741.

76. Fang B, Xiong Q, Duan H, Xiong Y, Lai W. Tailored quantum dots for enhancing sensing performance of lateral flow immunoassay. *TrAC Trends in Analytical Chemistry*. 2022 Dec;157:116754. doi: 10.1016/j.trac.2022.116754.
77. He W, You M, Li Z, Cao L, Xu F, Li F, Li A. Upconversion nanoparticles-based lateral flow immunoassay for point-of-care diagnosis of periodontitis. *Sensors and Actuators B: Chemical*. 2021;334.
78. Huang Y, Liu H, Chen W, Nieh M-P, Lei Y. Genetically engineered bio-nanoparticles with co-expressed enzyme reporter and recognition element for IgG immunoassay. *Sensors and Actuators Reports*. 2019;1:100003.
79. Chen L, Wang H, Guo T, Xiao C, Liu L, Zhang X, Liu B, Li P, Liu A, Li B, Li B, Mao Y. A rapid point-of-care test for dengue virus-1 based on a lateral flow assay with a near-infrared fluorescent dye. *Journal of Immunological Methods*. 2018 May;456:23-27.
80. Natarajan S, Su F, Jayaraj J, Shah MII, Huang Y. A paper microfluidics-based fluorescent lateral flow immunoassay for point-of-care diagnostics of non-communicable diseases. *Analyst*. 2019;21.
81. Fan R, Zhang W, Jin Y, Zhao R, Yang C, Chen Q, He L, Chen Y. Lateral flow immunoassay for 5-hydroxyflunixin based on near-infrared fluorescence molecule as an alternative label to gold nanoparticles. *Microchimica Acta*. 2020;187:368.
82. Kim K, Kashefi-Kheyrabadi L, Joung Y, Kim K, Dang H, Chavan SG, Lee MH, Choo J. Recent advances in sensitive surface-enhanced Raman scattering-based lateral flow assay platforms for point-of-care diagnostics of infectious diseases. *Sensors and Actuators B: Chemical*. 2021;329:129214.
83. Jin Y, Chen Q, Luo S, He L, Fan R, Zhang S, Yang C, Chen Y. Dual near-infrared fluorescence-based lateral flow immunosensor for the detection of zearalenone and deoxynivalenol in maize. *Food Chemistry*. 2021;336:127718.
84. Goux HJ, Vu BV, Wasden K, Alpadi K, Kumar A, Kalra B, Savjani G, Brosamer K, Kourentzi K, Willson RC. Development of a quantitative fluorescence lateral flow immunoassay (LFA) prototype for point-of-need detection of anti-Müllerian hormone. *Practical Laboratory Medicine*. 2023;35:e00314.
85. Natarajan S, Jayaraj J, Prazeres DMF. A cellulose paper-based fluorescent lateral flow immunoassay for the quantitative detection of cardiac troponin I. *Biosensors*. 2021;11(2):49.

86. Ranjan S, Jain S, Bhargava A, Shandilya R, Srivastava RK, Mishra PK. Lateral flow assay-based detection of long non-coding RNAs: A point-of-care platform for cancer diagnosis. *J Pharm Biomed Anal*. 2021 Sep 10;204:114285. doi:10.1016/j.jpba.2021.114285.
87. Schmidt C, Borcherding H, Thiele T, Schedler U, Werner F, Rödiger S, Roggenbuck D, Schierack P. Fluorescence-encoded poly(methyl methacrylate) nanoparticles for a lateral flow assay detecting IgM autoantibodies in rheumatoid arthritis. *Anal Biochem*. 2021 Nov 15;633:114389. doi:10.1016/j.ab.2021.114389.
88. Wang C, Shi D, Wan N, Yang X, Liu H, Gao H, Zhang M, Bai Z, Li D, Dai E, Rong Z, Wang S. Development of spike protein-based fluorescence lateral flow assay for the simultaneous detection of SARS-CoV-2 specific IgM and IgG. *Analyst*. 2021;12.
89. Sena-Torralba A, Pallás-Tamarit Y, Morais S, Maquieira Á. Recent advances and challenges in food-borne allergen detection. *TrAC Trends in Analytical Chemistry*. 2020 Nov;132:116050. doi:10.1016/j.trac.2020.116050.
90. Zhang R, Liao T, Wang X, Zhai H, Yang D, Wang X, Wang H, Feng F. Second near-infrared fluorescent dye for lateral flow immunoassays rapid detection of influenza A/B virus. *Analytical Biochemistry*. 2022 Oct 15;655:114847. doi:10.1016/j.ab.2022.114847.
91. Jiang N, Ahmed R, Damayantharan M, Ünal B, Butt H, Yetisen AK. Lateral and vertical flow assays for point-of-care diagnostics. *Advanced Healthcare Materials*. 2019 May 13;8(9):1900244. doi:10.1002/adhm.201900244.
92. Hong JM, Lee H, Menon NV, Lim CT, Lee LP, Ong CWM. Point-of-care diagnostic tests for tuberculosis disease. *Sci Transl Med*. 2022 Apr 6;14(639). DOI: 10.1126/scitranslmed.abj4124.
93. Ragavan KV, Kumar S, Swaraj S, Neethirajan S. Advances in biosensors and optical assays for diagnosis and detection of malaria. *Biosensors and Bioelectronics*. 2018 May 15;105:188-210. doi: 10.1016/j.bios.2018.01.037.
94. Ma Z, Guo J, Jiang L, Zhao S. Lateral flow immunoassay (LFA) for dengue diagnosis: recent progress and prospect. *Talanta*. 2024 Jan 15;267:125268. doi: 10.1016/j.talanta.2023.125268.
95. Wang D, He S, Wang X, Yan Y, Liu J, Wu S, Liu S, Lei Y, Chen M, Li L, Zhang J, Zhang L, Hu X, Zheng X, Bai J, Zhang Y, Zhang Y, Song M, Tang Y. Rapid lateral

flow immunoassay for the fluorescence detection of SARS-CoV-2 RNA. *Nature Biomedical Engineering*. 2020;4(12):1150-1158.

96. Pei F, Feng S, Hu W, Liu B, Mu X, Hao Q, Cao Y, Lei W, Tong Z. Sandwich mode lateral flow assay for point-of-care detecting SARS-CoV-2. *Talanta*. 2023 Feb 1;253:124051. DOI: 10.1016/j.talanta.2022.124051.
97. Hu R, Liao T, Ren Y, Liu W, Ma R, Wang X, Lin Q, Wang G, Liang Y. Sensitively detecting antigen of SARS-CoV-2 by NIR-II fluorescent nanoparticles. *Nano Res*. 2022 May 10;15:7313-7319.
98. Wang D, He S, Wang X, Yan Y, Liu J, Wu S, Liu S, Lei Y, Chen M, Li L, Zhang J, Zhang L, Hu X, Zheng X, Bai J, Zhang Y, Zhang Y, Song M, Tang Y. Rapid lateral flow immunoassay for the fluorescence detection of SARS-CoV-2 RNA. *Nat Biomed Eng*. 2020 Dec 3;4:1150-1158.
99. Sharma A, Tok AIY, Lee C, Ganapathy R, Palaniappan A, Liedberg B. Magnetic field assisted preconcentration of biomolecules for lateral flow assaying. *Sensors and Actuators B: Chemical*. 2019 Apr 15;285:431-437.
100. DeSousa JM, Jorge MZ, Lindsay HB, Haselton FR, Wright DW, Scherr TF. Inductively coupled plasma optical emission spectroscopy as a tool for evaluating lateral flow assays. *Analytical Methods*. 2021;18.
101. Qu Z, Wang K, Alfranca G, de la Fuente JM, Cui D. A plasmonic thermal sensing based portable device for lateral flow assay detection and quantification. *Nanoscale Research Letters*. 2020;15:10.
102. De Souza Sene I, Costa V, Cavalcante Brás D, de Oliveira Farias EA, Nunes GE, Bechtold IH, et al. A point of care lateral flow assay for rapid and colorimetric detection of interleukin 6 and perspectives in bedside diagnostics. *J Clin Med Res*. 2020;2(2):1-16. doi: https://doi.org/10.37191/Mapsci-2582-4333-2(2)-032.
103. Rahbar M, Wu Y, Subramony JA, Liu G. Sensitive colorimetric detection of interleukin-6 via lateral flow assay incorporated silver amplification method. *Front Bioeng Biotechnol*. 2021;9:778269. doi: 10.3389/fbioe.2021.778269.
104. Kim HT, Jin E, Lee MH. Portable chemiluminescence-based lateral flow assay platform for the detection of cortisol in human serum. *Biosensors*. 2021;11(6):191. https://doi.org/10.3390/bios11060191.

105. Chabi M, Vu B, Brosamer K, Smith M, Chavan D, Conrad JC, Willson RC, Kourentzi K. Smartphone-read phage lateral flow assay for point-of-care detection of infection. *Analyst*. 2023;148(4):740-747.

106. Li Y, Ma X, Wang W, Yan S, Liu F, Chu K, Xu G, Smith ZJ. Improving the limit of detection in portable luminescent assay readers through smart optical design. Published online October 10, 2019. DOI: 10.1002/jbio.201900241.

107. Kim S, Kim D, Kim S. A rapid real-time quantification in hybrid paper-polymer centrifugal optical devices. *Biosensors and Bioelectronics*. 2019 Feb 1;126:200-20. doi: 10.1016/j.bios.2018.10.064.

108. Deng X, Linnartz J-PMG, Long X, Zhou G. Reading analysis for barcode scanner with interference from led-based lighting. *IEEE Access*. 2019;7:96787-96798. doi: 10.1109/ACCESS.2019.2930328.

109. Rebelo R, Barbosa AI, Caballero D, Kwon IK, Oliveira JM, Kundu SC, Reis RL, Correlo VM. 3D biosensors in advanced medical diagnostics of high mortality diseases. *Biosensors and Bioelectronics*. 2019 Apr 1;130:20-39. doi: 10.1016/j.bios.2018.12.057.

110. Chen CH, Fu YC, Lee YT, Hsieh KS, Shen CF, Cheng CM. Efficacy of a paper-based interleukin-6 test strip combined with a spectrum-based optical reader for sequential monitoring and early recognition of respiratory failure in elderly pneumonia—a pilot study. *Front Pharmacol*. 2023 May 5;14:1166923. doi: 10.3389/fphar.2023.1166923.

111. Cao XE, Yhombi SO, Wang R, Ren Y. A diagnostic platform for rapid, simultaneous quantification of procalcitonin and C-reactive protein in human serum. *EBioMedicine*. 2022;76(1):103867. doi:10.1016/j.ebiom.2022.103867.

112. Wang Y, Qin Z, Boulware DR, Pritt BS, Sloan LM, González IJ, Bell D, Rees-Channer RR, Chiodini P, Chan WCW, Bischof JC. Thermal contrast amplification reader yielding 8-fold analytical improvement for disease detection with lateral flow assays. *Anal. Chem*. 2016;88(23):11774-11782. doi:10.1021/acs.analchem.6b03406.

113. You DJ, Park TS, Yoon JY. Cell-phone-based measurement of TSH using Mie scatter optimized lateral flow assays. *Biosensors and Bioelectronics*. 2013 Feb 15;40(1):180-185. doi:10.1016/j.bios.2012.07.014.

114. Hofmann A, Reich P, Grabmann M, Glaser G, Rolapp A, Reinhard M, Schäfer E, Trübenbach M, Scholz F. Filterless TRF reader with CMOS sensor ASIC for lateral flow immunoassays. *IEEE Biomedical Circuits and Systems Conference*; 2021.

115. Ye H, Liu Y, Zhan L, Liu Y, Qin Z. Signal amplification and quantification on lateral flow assays by laser excitation of plasmonic nanomaterials. *Theranostics*. 2020;10(10):4359–4373. doi:10.7150/thno.44298. PMCID: PMC7150487. PMID: 32292500.

116. Zhang Z, Guo L, Sun H, Peng D, Zou H, Sun N, Zhang Q, Hao X. Rare earth orthoniobate photochromics with self-activated upconversion emissions for high-performance optical storage applications. *Journal of Materials Chemistry C*. 2021;(39).

117. Claus H. Ozone generation by ultraviolet lamps. *Photochemical & Photobiological Sciences*. 2021;20(2). doi:10.1111/php.13391.

118. Makkar RL, Aliya SS, Borse V, Srivastava R. Design and development of portable fluorescence reader using silicon photomultiplier (SiPM) sensor. *Optical Sensing and Detection V*. 2018;10680. doi:10.1117/12.2305846.

119. Hofmann A, Saft B, Reich P, Grabmann M, Gläser G, Trübenbach M. Lock-in pixel CMOS image sensor for time-resolved fluorescence readout of lateral-flow assays. *IEEE Transactions on Biomedical Circuits and Systems*. 2022;16(4).

120. Budidha K, Mamouei M, Baishya N, Qassem M, Vadgama P, Kyriacou PA. Identification and quantitative determination of lactate using optical spectroscopy—towards a noninvasive tool for early recognition of sepsis. *Sensors*. 2020;20(18):5402. https://doi.org/10.3390/s20185402.

121. Thapa D, Samadi N, Patel N, Tabatabaei N. Enhancement of sensitivity and detection limit of lateral flow immunoassays using lock-in thermography. *Biophotonics in Point-of-Care*. 2020;11361. https://doi.org/10.1117/12.2555274.

122. Raj S, McCafferty D, Lubrasky G, Johnston S, Skillen KL, McLaughlin J. Point-of-care monitoring of respiratory diseases using lateral flow assay and CMOS camera reader. *IEEE Journal of Translational Engineering in Health and Medicine*. 2022;10. doi:10.1109/JTEHM.2022.3193575.

123. Yang J, Lu Y. Atomically thin optical lenses and gratings. in: two-dimensional materials in nanophotonics. jenny Stanford publishing; 2019. p. 26. eBook ISBN: 9780429428777.

124. Hagen R, Fehr D, Spano F, Brambilla D, Bonmarin M. Portable multi-wavelength fluorescence measurement device. I*n: Proceedings of the 2022 IEEE International Workshop on Medical Measurement and Applications (MEMEA) IEEE*;2022.

125. Rajendran VK, Bakthavathsalam P, Bergquist PL, Sunna A. Smartphone detection of antibiotic resistance using convective PCR and a lateral flow assay. *Sensors and Actuators B: Chemical*. 2019 Nov 1;298:126849.

126. Nguyen VT, Song S, Park S, Joo C. Recent advances in high-sensitivity detection methods for paper-based lateral-flow assay. *Biosensors and Bioelectronics*. 2020 Mar 15;152:112015.

127. Cai X, Yu J, Song Y. Ultrasensitive lateral flow immunoassay for staphylococcal enterotoxin B using nanosized fluorescent metal-organic frameworks. *Nanoscale*. 2022;14(45):19287-19292. doi:10.1039/D2NR05018D.

128. Sena-Torralba A, Torné-Morató H, Parolo C, Ranjbar S, Farahmand Nejad MA, Álvarez-Diduk R, Idili A, Hormozi-Nezhad MR, Merkoçi A. A novel ratiometric fluorescent approach for the modulation of the dynamic range of lateral flow immunoassays. *Adv Mater Technol*. 2022;7(3):2101450. doi:10.1002/admt.202101450.

129. Xiao M, Tian F, Liu X, Zhou Q, Pan J, Luo Z, Yang M, Yi C. Virus detection: from state-of-the-art laboratories to smartphone-based point-of-care testing. *Adv Sci (Weinh)*. 2022 Apr 7;9(8):2105904. doi: 10.1002/advs.202105904.

130. Sena-Torralba A, Álvarez-Diduk R, Parolo C, Piper A, Merkoçi A. Toward next-generation lateral flow assays: *Integration of Nanomaterials. Chem Rev*. 2022 Sep 6;122(18):14881-14910. doi: 10.1021/acs.chemrev.1c01012.

131. Rajendran VK, Bakthavathsalam P, Jaffar Ali BM. Smartphone-based bacterial detection using biofunctionalized fluorescent nanoparticles. *Microchimica Acta*. 2014;181(15-16):1815-1821.

132. Jin B, Yang Y, He R, Park YI, Lee A, Bai D, Li F, Lu TJ, Xu F, Lin M. Lateral flow aptamer assay integrated smartphone-based portable device for simultaneous detection of multiple targets using upconversion nanoparticles. *Sensors and Actuators B: Chemical*. 2018 Dec 10;276:48-56. doi: 10.1016/j.snb.2018.08.074.

133. Rong Z, Wang Q, Sun N, Jia X, Wang K, Xiao R, Wang S. Smartphone-based fluorescent lateral flow immunoassay platform for highly sensitive point-of-care detection of Zika virus nonstructural protein 1. *Analytica Chimica Acta*. 2019 May 9;1055:140-147. doi: 10.1016/j.aca.2018.12.043.

134. Foysal KH, Seo SE, Kim MJ, Kwon OS, Chong JW. Analyte quantity detection from lateral flow assay using a smartphone. *Sensors*. 2019;19(21):4812.

135.Gong Y, Zheng Y, Jin B, You M, Wang J, Li X, Lin M, Xu F, Li F. A portable and universal upconversion nanoparticle-based lateral flow assay platform for point-of-care testing. *Talanta*. 2019 Aug 15;201:126-133. doi: 10.1016/j.talanta.2019.03.105.

136.Minagawa Y, Ueno H, Tabata KV, Noji H. Mobile imaging platform for digital influenza virus counting. *Lab Chip*. 2019;19:2678-2687. DOI: 10.1039/C9LC00370C.

137.Zheng Q, Wu H, Jiang H, Yang J, Gao Y. Development of a smartphone-based fluorescent immunochromatographic assay strip reader. *Sensors*. 2020;20:4521. doi:10.3390/s20164521.

138.Danthanarayana AN, Finley E, Vu B, Kourentzi K, Willson RC, Brgoch J. A multicolor multiplex lateral flow assay for high-sensitivity analyte detection using persistent luminescent nano phosphors. *Anal Methods*. 2020;3.

139.Bergua JF, Álvarez-Diduk R, Idili A, Parolo C, Maymó M, Hu L, Merkoçi A. Low-cost, user-friendly, all-integrated smartphone-based microplate reader for optical-based biological and chemical analyses. *Anal Chem.* 2022;94:1271-1285. doi:10.1021/acs.analchem.1c04491.

140.Choi SJ, Park Y, Lee EY, Kim S, Kim HS. Performance evaluation of lumipulse g1200 autoimmunoanalyzer for the detection of serum hepatitis b virus markers. *J Clin Lab Anal*. 2013 Feb 25. doi:10.1002/jcla.21584.

141.Borse V, Patil AS, Srivastava R. Development and testing of portable fluorescence reader (PorFloR™). *2017 9th International Conference on Communication Systems and Networks (COMSNETS)*; 201

142.Cai Y, Kang K, Li Q, Wang Y, He X. Rapid and sensitive detection of cardiac troponin I for point-of-care tests based on red fluorescent microspheres. *Molecules*. 2018;23(5):1102.

143.Kim HJ, Lee SG, Kim JH, Lee JS, Jang HC. Evaluation of the Gmate® fluorometer device for point-of-care HbA1c testing in patients with diabetes. *J Clin Lab Anal*. 2018;32(3):e22297.

144.Eom JS, Park YK, Kim JY. Comparison of the Gmate® fluorometer and the bio-rad d-10™ hemoglobin a1c analyzer for diagnosing diabetes. *J Clin Lab Anal*. 2020;34(7):e23308.

145.Pizzorno A, Padey B, Julien T, Trouillet-Assant S, Traversier A, Errazuriz-Cerda E, Fouret J, Dubois J, Gaymard A, Lescure F-X, Dulière V, Brun P, Constant S, Poissy J, Lina B, Yazdanpanah Y, Terrier O, Rosa-Calatrava M. Characterization and treatment of SARS-CoV-2 in nasal and bronchial human airway epithelia. *Cell Rep Med*. 2020;1(4):100059. doi: 10.1016/j.xcrm.2020.100059.

146. Lee J, Song JU, Kim YH. Diagnostic Accuracy of the Quidel Sofia rapid influenza fluorescent immunoassay in patients with influenza-like illness: a systematic review and meta-analysis. *Tuberc Respir Dis (Seoul)*. 2021 Jul;84(3):226-236. doi: 10.4046/trd.2021.0033.
147. Patel R, Babady NE. The clinical impact of SARS-CoV-2 variant detection with the Quidel Sofia 2 SARS antigen FIA assay. *J Clin Microbiol*. 2021;59(2):e02416-20.
148. Jing M, McLaughlin D, McNamee SE, Raj S, Mac Namee B, Steele D, Finlay D, McLaughlin J. A novel method for quantitative analysis of c-reactive protein lateral flow immunoassays images via CMOS sensor and recurrent neural networks. *IEEE J Transl Eng Health Med*. 2021;9:1-7. doi: 10.1109/JTEHM.2021.3130494.
149. Rong Z, Xiao R, Peng Y, Zhang A, Wei H, Ma Q, Wang D, Wang Q, Bai Z, Wang F, Sun M, Wang S. Integrated fluorescent lateral flow assay platform for point-of-care diagnosis of infectious diseases by using a multichannel test cartridge. *Sensors & Actuators: B. Chemical*. 2021;329:129193.
150. Durdabak DB, Dogan S, Demir Tekol S, Celik C, Ozalp VC, Guvenc Tuna B. Direct detection of viral infections from swab samples by probe-gated silica nanoparticle-based lateral flow assay. *ChemistryOpen*. 2023. doi:10.1002/open.202300120.
151. Raspberry Pi Foundation. Raspberry Pi 4 Model B [Internet]. Available from: https://www.raspberrypi.com/products/raspberry-pi-4-model-b/ [cited 2023 Sep 20].
152. Raspberry Pi Foundation. Raspberry Pi NoIR Camera [Internet]. Available from: https://www.raspberrypi.com/products/pi-noir-camera-v2/ [cited 2023 May 5].
153. SparkFun Electronics. SparkFun humidity and temperature sensor breakout - HTU21D [Internet]. Available from: https://www.sparkfun.com/products/retired/12064 [cited 2023 Dec 11].
154. Waveshare. 5inch HDMI LCD (H) [Internet]. Available from: https://www.waveshare.com/wiki/5inch_HDMI_LCD_(H) [cited 2023 Oct 11].
155. Texas Instruments. LM2596S voltage regulator [Internet]. Available from: https://www.ti.com/lit/ds/symlink/lm2596.pdf?ts=1704692355341 [cited 2023 Sep 7].
156. Waveshare Electronics. UPS HAT (B) [Internet]. Available from: https://www.waveshare.com/wiki/UPS_HAT_(B). [cited 2024 Jan 25].

157. National Semiconductor. LM2577 Step-Up Voltage Regulator [Internet]. Available from: https://www.elecrow.com/download/LM2577.pdf
158. Arducam. 77P High Quality Camera for Raspberry Pi [Internet]. Available from: https://www.arducam.com/product/b0240-arducam-imx477-hq-quality-camera/. [cited 2024 Jan 20].
159. Bosch Sensortec. Humidity sensor BME280 [Internet]. Available from: https://www.bosch-sensortec.com/products/environmental-sensors/humidity-sensors-bme280/.
160. Waveshare Electronics. 5-inch Capacitive Touch Display for Raspberry Pi, DSI Interface [Internet]. Available from: https://www.waveshare.com/5inch-dsi-lcd.htm.

APPENDIX A: PYTHON CODE FOR PRELIMINARY READER

```
from guizero import App, PushButton, Text, Picture, Box, Slider, TextBox, ListBox, Combo
import RPi.GPIO as GPIO
import time
from PIL import Image
from PIL.PngImagePlugin import PngInfo
from time import sleep
from picamera2 import Picamera2, Preview
from datetime import datetime
import pickle
import numpy as np
import matplotlib.pyplot as plt
import matplotlib.patches as patches
import os
from subprocess import call
# pip3 install imageio
import imageio.v3 as iio
# Temperature-humidity sensor
import board
from adafruit_htu21d import HTU21D
import threading
# Initialize the HTU21D sensor which uses board.SCL and board.SDA
i2c = board.I2C(); sensor = HTU21D(i2c)
# Camera opens when the code starts
picam2 = Picamera2()
camera_config = picam2.create_still_configuration(main={"size": (3280, 2464)})

crop_B = (980, 1040, 980+620, 1040+430)
crop_G = (1620, 1040, 1620+620, 1040+430)
#camera_config_B = picam2.create_still_configuration(main={"size": (3280, 2464)},lores={"size":
(640, 480)},
#                                    display="lores", controls={"ScalerCrop": (980, 1040, 620, 430)})
#camera_config_G = picam2.create_still_configuration(main={"size": (3280, 2464)},lores={"size":
(640, 480)},
#                                    display="lores", controls={"ScalerCrop": (1620, 1040, 620, 430)})
controls_config = {"AwbEnable": 0, "AeEnable": 0, "ExposureTime": 100000, "AnalogueGain": 1};

# Define ROI coordinates and size (x, y, width, height)
x, y, width, height = 1432, 200, 400, 2064
stts   = 0
metadata=[]
wDIR = "/home/bme-rasp/Desktop/SA_IMG2/270224/"
image_path_B_PRE="x"
image_path_G_PRE="x"
image_path_B_POST="x"
image_path_G_POST="x"

# Button
def button_callback(channel):
    global stts; stts = 1; cleanup()
GPIO.setwarnings(False) # Ignore warning for now
```

```
GPIO.setmode(GPIO.BCM) # Use physical pin numbering
# GPIO pins for Strip Detector
button_pow = 6
button_pin = 5
GPIO.setup(button_pow, GPIO.OUT)
GPIO.output(button_pow, 1)
GPIO.setup(button_pin, GPIO.IN, pull_up_down=GPIO.PUD_DOWN) # Set pin 5 to be an input pin and set initial value to be pulled low (off)
GPIO.add_event_detect(button_pin,GPIO.RISING,callback=button_callback, bouncetime=200) # Setup event on pin 5 rising edge
# GPIO pin connected to the voltage regulator for Blue LED
BlueLED_pin  = 17; GPIO.setup(BlueLED_pin, GPIO.OUT, initial=GPIO.HIGH)
# GPIO pin connected to the voltage regulator for Green LED
GreenLED_pin = 27; GPIO.setup(GreenLED_pin, GPIO.OUT, initial=GPIO.HIGH)
# Motor configuration
step_sleep = 0.001; step_count = 1; step_count_e = 4096; direction = False
step_sequence = [[1, 0, 0, 1],
         [1, 0, 0, 0],
         [1, 1, 0, 0],
         [0, 1, 0, 0],
         [0, 1, 1, 0],
         [0, 0, 1, 0],
         [0, 0, 1, 1],
         [0, 0, 0, 1]]

# Setting up GPIO for motor driver
in1 = 19; in2 = 16; in3 = 26; in4 = 20
GPIO.setup(in1, GPIO.OUT)
GPIO.setup(in2, GPIO.OUT)
GPIO.setup(in3, GPIO.OUT)
GPIO.setup(in4, GPIO.OUT)

motor_pins = [in1, in2, in3, in4]
motor_step_counter = 0

def cleanup():
   GPIO.output(in1, GPIO.LOW)
   GPIO.output(in2, GPIO.LOW)
   GPIO.output(in3, GPIO.LOW)
   GPIO.output(in4, GPIO.LOW)

def power_off():
      cleanup()
      app.destroy()
      call("sudo shutdown -h now", shell=True)

# Function to read sensor data
def read_sensor_data():
   temperature = sensor.temperature ; temp_display.value = f"  {temperature:2.1f}Â°C  "
   humidity    = sensor.relative_humidity ; hum_display.value = f"{humidity:3.0f}%RH"
   current_time = datetime.now().strftime("%d/%m/%Y   %H:%M")
   date_display.value = current_time
   app.update()
```

```
# Function for continuous sensor reading
def continuous_sensor_reading():
    while True:
        read_sensor_data()
        time.sleep(2)


# Function for motor
def move_motor():
    global motor_step_counter
    global stts
    forward_counter = 0  # Counter for forward motion
    stts=0
    if GPIO.input(button_pin)==1:
        stts=1
    try:
        while stts==0:
            for _ in range(step_count):
                for pin in range(len(motor_pins)):
                    GPIO.output(motor_pins[pin], step_sequence[motor_step_counter][pin])

                motor_step_counter = (motor_step_counter + 1) % 8
                forward_counter += 1  # Count steps in the forward direction
                time.sleep(step_sleep)
    except KeyboardInterrupt:
        cleanup()
        app.destroy()
    cleanup()

def imaging(LEDpin, path, region, crop_area): #imaging(BlueLED_pin, camera_config_B,
"f"{wDIR}{timestamp}_G_{ExpTime}_PRE", 'T')
        global LightTime, wDIR
        # Setup the camera for T Line Imaging
        picam2.configure(camera_config)
        picam2.set_controls(controls_config)
        picam2.options["compress_level"] = 0
        picam2.start()
        time.sleep(8) # Wait 8 sec for camera to get ready
        #
        GPIO.output(LEDpin, GPIO.LOW)   # Turn the LED ON
        time.sleep(LightTime)
        #
        img = picam2.capture_request()       # Capture an image
        GPIO.output(LEDpin, GPIO.HIGH)  # Turn the LED OFF
        #
        stts_text.text_color = "white"; stts_text.value = region + " REGION imaging COMPLETED !"
        app.update()
        # Save the image
        image_path = path + ".png"
        img_f=img.make_image("main")
        img_f = img_f.crop(crop_area)
        #size_img = (620, 430)
        #img_f =img_f.resize(size_img)
        img_f.save(image_path)
```

```
        #img.save("main", image_path)
        time.sleep(2)

        # Gather metadata
        metadata = img.get_metadata()
        metadata.update({"LightOnTime     (s)": LightTime})
        metadata.update({"EnvTemperature (oC)": temp_display.value})
        metadata.update({"EnvRelHumidity  (%)": hum_display.value})

        # Generate txt file to store metadata
        data_path  = path + ".txt"
        with open(data_path, 'w') as file:
            for key, value in metadata.items():
                file.write(f"{key}: {value}\n")
        file.close()
        #
        img.release()   # Release the img heap
        picam2.stop()   # Stop picam2
        #img = Image.open(image_path)

def PRE_imaging():
    global image_path_B_PRE, image_path_G_PRE, ExpTime, timestamp, wDIR
    if stts == 0:
        stts_text.text_color = "yellow"
        stts_text.value      = "Insert the empty cartridge for PRE-IMAGING"
        app.update()
    else:
        stts_text.text_color = "white"
        stts_text.value      = "Performing PRE-IMAGING ..."
        app.update()
        time.sleep(1)
        ############ T Line Imaging
        stts_text.text_color = "white"; stts_text.value = "Imaging T REGION ..."
        app.update()
        image_path_B_PRE= f"{wDIR}{timestamp}_{ExpTime}_B_PRE"
        imaging(BlueLED_pin, image_path_B_PRE, 'T', crop_B)

        picture_b_nosample.image = image_path_B_PRE + ".png"
        app.update()

        ############ C Line Imaging
        stts_text.text_color = "white"; stts_text.value = "Imaging C REGION ..."
        app.update()
        image_path_G_PRE= f"{wDIR}{timestamp}_{ExpTime}_G_PRE"
        imaging(GreenLED_pin, image_path_G_PRE, 'C', crop_G)

        picture_g_nosample.image = image_path_G_PRE + ".png"
        app.update()

        # Eject the strip holder
        EjectHolder()

def POST_imaging():
    global image_path_B_POST, image_path_G_POST, ExpTime, timestamp, wDIR
```

```
    if stts == 0:
        stts_text.text_color = "red"
        stts_text.value      = "Insert the cartridge for POST-IMAGING"
        app.update()
    else:
        stts_text.text_color = "white"
        stts_text.value      = "Performing POST-IMAGING ..."
        app.update()
        time.sleep(1)

        ############ T Line Imaging
        stts_text.text_color = "white"
        stts_text.value      = "Imaging T REGION ..."
        app.update()

        image_path_B_POST= f"{wDIR}{timestamp}_{ExpTime}_B_POST"
        imaging(BlueLED_pin, image_path_B_POST, 'T', crop_B)

        picture_b.image = image_path_B_POST + ".png"
        app.update()

        ############ C Line Imaging
        stts_text.text_color = "white"; stts_text.value = "Imaging C REGION ..."
        app.update()
        image_path_G_POST= f"{wDIR}{timestamp}_{ExpTime}_G_POST"
        imaging(GreenLED_pin, image_path_G_POST, 'C', crop_G)

        picture_g.image = image_path_G_POST + ".png"
        app.update()

def test():
    global timestamp, ExpTime, LightTime, wDIR
    try:
        timestamp = datetime.now().strftime("%d%m%y_%H%M%S")
        LightTime      = int(float(slider_LightTime.value));
        ExpTime        = int(float(slider_CameraExp.value)); exposure_time = ExpTime * 10000
        analogue_gain  = float(slider_gain.value)
        controls_config["ExposureTime"]= exposure_time;
        controls_config["AnalogueGain"]= analogue_gain;

        mode_selector    = str(combo.value)

        if mode_selector == "Pre Imaging":
            picture_b_nosample.image = default_image_black
            picture_g_nosample.image = default_image_black
            PRE_imaging()
        else:
            picture_b.image = default_image_black
            picture_g.image = default_image_black
            POST_imaging()

    except KeyboardInterrupt:
        cleanup()
        app.destroy()
```

```
######## Image Processing
def C_UpdateROI(path):
    global Cx, Cy, Cw, Ch, wDIR
    x, y, width, height = 270, 65, 40, 280

    CROI_x = int(float(slider_CROIx.value))+20;

    ALLImg_C = iio.imread(uri=path + ".png")

    fig = plt.figure()
    plt.imshow(ALLImg_C)
    plt.gca().add_patch(patches.Rectangle((x+CROI_x, y), width, height, linewidth=2,
edgecolor='g', facecolor='none', figure=fig))
    plt.gca().text(40+x+CROI_x, 345, 'C', size=20, weight='bold', color='Green')
    plt.axis('off')
    plt.axis("tight")
    Cx=x+CROI_x; Cy = y; Cw=width; Ch=height
    # Save the image with the ROI rectangle
    roi_image_C_path = path +"_ROI.png"
    plt.savefig(roi_image_C_path, bbox_inches='tight', pad_inches=0)
    plt.close()

def T_UpdateROI(path):
    global Tx, Ty, Tw, Th, wDIR
    x, y, width, height = 270, 65, 40, 280

    TROI_x = int(float(slider_TROIx.value))+20;

    ALLImg_T = iio.imread(uri=path + ".png")

    fig = plt.figure()
    plt.imshow(ALLImg_T)
    plt.gca().add_patch(patches.Rectangle((TROI_x+x, y), width, height, linewidth=2,
edgecolor='b', facecolor='none', figure=fig))
    plt.gca().text(40+x+TROI_x, 345, 'T', size=20, weight='bold', color='Blue')
    plt.axis('off')
    plt.axis("tight")
    Tx=TROI_x+x; Ty = y; Tw=width; Th=height
    # Save the image with the ROI rectangle
    roi_image_T_path = path + "_ROI.png"
    plt.savefig(roi_image_T_path, bbox_inches='tight', pad_inches=0)
    plt.close()

def ROI():
    global image_path_B_PRE, image_path_G_PRE, image_path_B_POST,
image_path_G_POST, wDIR

    if os.path.exists(image_path_B_PRE + ".png"):
      T_UpdateROI(image_path_B_PRE)
      picture_b_nosample.image = image_path_B_PRE + "_ROI.png"
      C_UpdateROI(image_path_G_PRE)
      picture_g_nosample.image = image_path_G_PRE + "_ROI.png"
```

```
    if os.path.exists(image_path_B_POST + ".png"):
        T_UpdateROI(image_path_B_POST)
        picture_b.image        = image_path_B_POST + "_ROI.png"
        C_UpdateROI(image_path_G_POST)
        picture_g.image = image_path_G_POST + "_ROI.png"

    app.update()

def processing():
    global image_path_B_PRE, image_path_G_PRE, image_path_B_POST,
image_path_G_POST, wDIR
    global Tx, Ty, Tw, Th, Cx, Cy, Cw, Ch
    global values, timestamp

    SImean_TLine_Pre = SImean_CLine_Pre = SImean_TLine_Post = SImean_CLine_Post = 0

    values = [SImean_TLine_Pre, SImean_TLine_Post, SImean_CLine_Pre, SImean_CLine_Post]

    if os.path.exists(image_path_B_PRE + ".png"):
        Img = iio.imread(uri=image_path_B_PRE + ".png")
        TImg_ROI = Img[Ty:Ty+Th, Tx:Tx+Tw, :]
        hist(TImg_ROI, image_path_B_PRE)
        mean_stat(TImg_ROI, 0, 1)

        Img = iio.imread(uri=image_path_G_PRE + ".png")
        CImg_ROI = Img[Cy:Cy+Ch, Cx:Cx+Cw, :]
        hist(CImg_ROI, image_path_G_PRE)
        mean_stat(CImg_ROI, 2, 0)
        with open(image_path_B_PRE + "_C_PRE.txt", 'w') as f:
            f.write("T_PRE Mean Value: " + str(values[0]) + "\nT ROI: " + str(slider_TROIx.value)
                + "\nC_PRE Mean Value: " + str(values[2]) + "\nC ROI: " + str(slider_CROIx.value))


    if os.path.exists(image_path_B_POST + ".png"):
        Img = iio.imread(uri=image_path_B_POST + ".png")
        TImg_ROI = Img[Ty:Ty+Th, Tx:Tx+Tw, :]
        hist(TImg_ROI, image_path_B_POST)
        mean_stat(TImg_ROI, 1, 1)

        Img = iio.imread(uri=image_path_G_POST + ".png")
        CImg_ROI = Img[Cy:Cy+Ch, Cx:Cx+Cw, :]
        hist(CImg_ROI, image_path_G_POST)
        mean_stat(CImg_ROI, 3, 0)

        with open(image_path_B_POST + "_C_POST.txt", 'w') as f:
            f.write("T_POST Mean Value: " + str(values[1]) + "\nT ROI: " + str(slider_TROIx.value)
+
            "\nC_POST Mean Value: " + str(values[3])+ "\nC ROI: " + str(slider_CROIx.value))


    # Create the bar plot
    plt.figure(figsize=(6, 4))
    plt.xticks(fontsize=16)
    plt.yticks(fontsize=16)
```

```
    labels = ['T-Pre', 'T-Post', 'C-Pre', 'C-Post']
    plt.bar(labels, values, color=['blue', 'blue', 'green', 'green'])
    plt.ylabel('Average SI', fontsize=20)
    #plt.title('Mean SI Comparison', fontsize=22)

    # Save the plot as an image
    mean_plot_path = f"{wDIR}mean_val_{timestamp}.png"
    plt.savefig(mean_plot_path)

def hist(Img, path):

    #Img = iio.imread(uri=path + ".png")

    # tuple to select colors of each channel line
    colors = ("red", "green", "blue")

    plt.figure(figsize=(6, 4))
    plt.xlim([0, 256])
    # create the histogram plot, with three lines, one for
    # each color
    for channel_id, color in enumerate(colors):
        histogram, bin_edges = np.histogram(
        Img[:, :, channel_id], bins=256, range=(0, 256), density=True)
        plt.plot(bin_edges[0:-1], histogram, color=color)

    plt.title("Histogram")
    plt.xlabel("Signal Intensity")
    plt.ylabel("Probability")

    plt.savefig(path + "_HST.png")

#n:values array order, c:channel id
def mean_stat(Img, n, c):
    global values
    numpydata   = np.asarray(Img[:,:,c])
    values[n] = np.mean(numpydata)
    print(values[n], n)

def EjectHolder():
  global motor_step_counter
  global stts
  backward_counter = 0  # Counter for backward motion
  direction = True
  #m       = int(float(text_chron.value))
  #countdown(0, int(m), 0)
  try:
    if GPIO.input(button_pin)==1:
      stts_text.text_color = "white"
      stts_text.value      = "The holder is being ejected ..."
      app.update()

      for _ in range(step_count_e):
        for pin in range(len(motor_pins)):
```

```
                GPIO.output(motor_pins[pin], step_sequence[motor_step_counter][pin])

            motor_step_counter = (motor_step_counter - 1) % 8
            backward_counter += 1  # Count steps in the backward direction
            time.sleep(step_sleep)

        stts_text.text_color = "red"
        stts_text.value      = "Load the holder for post imaging!"
        app.update()

        stts = 0
    except KeyboardInterrupt:
        cleanup()
        app.destroy()
        pwm.stop()
    cleanup()

# Create a function to start the motor
def start_motor():
    insert_button.disable()

    stts_text.text_color = "white"
    stts_text.value      = "Reader waits for positioning the cartridge.."
    app.update()
    move_motor()

    insert_button.enable()
    stts_text.value = "Press 'Test' to start acquisition"
    app.update()

def countdown():
    global timer
    if timer > 0:
        timer -= 1
        time_display.value = f'{timer//60}:{timer%60:02d}'
        app.after(1000, countdown)  # Schedule this function to be called again after 1 second
    else:
        start_button.enable()  # Re-enable the start button when the countdown ends

def start_timer():
    global timer
    start_button.disable()  # Disable the start button to prevent multiple presses
    timer = 0
    try:
        timer = int(minutes_input.value) * 60  # Convert minutes to seconds
        countdown()
    except ValueError:
        time_display.value = "Enter a valid number!"
        start_button.enable()  # Re-enable the start button if there's a ValueError

######################################################################
#Create the GUI and the master of the GUI
default_image_black    = f"/home/bme-rasp/Desktop/seda_rpi/black.png"
default_image_path_off = f"/home/bme-rasp/Desktop/seda_rpi/power2.png"
```

```
app = App(title = "YUBME: LFA Reader v2024.1", width=1024, height=768, bg=(85,85,85),layout="grid")

######################################################################
# 1st Column
Col1 = Box(app,layout="auto", width=50, height=760, grid=[0,0], align="top"); Col1.bg=(0,102,102)
#
poweroff_bttn = PushButton(Col1, image=default_image_path_off, command=power_off)

######################################################################
# 2nd Column
Col2 = Box(app,layout="grid", width=300, height=860, grid=[1,0], align="top");
#
sensor_box= Box(Col2,layout="auto", width=300, height=56, grid=[0,0]); sensor_box.bg=(0,102,102)
#dSpace0  = Box(Col2,layout="grid", grid=[0,0]); dSpace0.bg=(0,102,102)
dSpace02  = Text(sensor_box,text=" ", width=5, align="left")
temp_display = Text(sensor_box, text=" -- Â°C ", color="white", size=18, font="Arial",align = "left")
dSpace03  = Text(sensor_box,text=" ", width=6, align = "right")
hum_display  = Text(sensor_box, text=" -- %RH", color="white", size=18, font="Arial",align = "right")

# Listbox for img acquisition mode
imagingmode_text = Text(Col2,text=" \n Imaging Mode", font="Times New Roman", size=19, color="white", align="left", grid= [0,2])
combo_box = Box(Col2,layout="grid", width=300, height=56, grid=[0,3]);
combo_box.set_border(1,"white")
combo = Combo(combo_box, options=["Pre Imaging", "Post Imaging"], width=20, grid=[0,1])
combo.text_color ="white"; combo.text_size= 14
#
dSpace01  = Box(Col2,layout="grid", height=30, grid=[0,3])
setting_text  = Text(Col2,text=" \n Settings", font="Times New Roman", size=19, color="white", align="left", grid= [0,4])

#
exp_gain_box = Box(Col2,layout="grid", grid=[0,5])
exp_gain_box.set_border(1,"white")

#
# Slider for Light Emission Time (1 - 10s)
LightTime = Text(exp_gain_box, text=" \nLight Emission Time (s)", size=16, color="white", align="left", grid= [0,2])
slider_LightTime = Slider(exp_gain_box, width=220,height=30,start=1,end=10, grid=[0,3])
slider_LightTime.bg=(85,85,85)
slider_LightTime.text_color="white"

# Slider for Camera Exposure Time (1000 - 2000ms)
CameraExp = Text(exp_gain_box, text=" \nCamera Exposure (ms)", size=16, color="white", align="left", grid= [0,4])
slider_CameraExp = Slider(exp_gain_box, width=220,height=30,start=1,end=30, grid=[0,5])
slider_CameraExp.bg=(85,85,85)
```

```
slider_CameraExp.text_color="white"

# Slider for Gain (1-10)
gain = Text(exp_gain_box, text=" \nAnalogue Gain", size=16, color="white", align="left",
grid=[0,6])
slider_gain = Slider(exp_gain_box, width=220,height=30,start=1,end=5, grid=[0,7])
slider_gain.bg=(85,85,85)
slider_gain.text_color="white"
#
Space4 = Text(exp_gain_box, text=" ",width=15,height=0,grid=[0,8])

#
#timer_text= Text(Col2, text=" \n Countdown Timer (mins)", font="Times New Roman", size=19,
color="white", align="left", grid=[0,6])

#timer_box= Box(Col2,layout="grid",width=280,height=80, grid=[0,7])
#timer_box.set_border(1,"white")
#textjh = Text(timer_box, text=" \nTimer (mins)",color="white", size=16, align="left", grid=[0,0])
#start_button = PushButton(timer_box, command=start_timer, text="Start", grid=[1,1])
#start_button.text_color="white"
#start_button.text_size=15
#minutes_input = Slider(timer_box, width=200,height=25,start=1,end=60, grid=[0,1]) # Default
value is 15 minutes
#minutes_input.text_color="white"
#minutes_input.bg=(85,85,85)
#
#time_display = Text(timer_box, text="0:00", color="white", size=14, grid=[0,2])
#
Space4 = Text(Col2, text=" ",width=15,height=5,grid=[0,8])

date_display = Text(Col2, text=" ", color="white", size=15, font="Arial",align = "left", grid=[0,9])

######################################################################
# 3th Column
Col3 = Box(app,layout="auto", grid=[3,0], align="top")
# Status Box
stts_box    = Box(Col3, layout="auto", width=674, height=56, grid=[0,0]); stts_box.bg=(0,102,102)
stts_message = "Please Insert the Cartridge Without Sample"
stts_text   = Text(stts_box, text=stts_message, size=17, color="white", font="Arial", align="top")
# Picture Box
picture_box = Box(Col3,layout="grid", width=630, height=550, grid=[0,1])
#
text00 = Text(picture_box, text="Pre C", color="white", size=15, width=15, height=1, grid=[1,0])
text10 = Text(picture_box, text="Pre T", color="white", size=15, width=15, height=1, grid=[0,0])
#
picture_b_nosample = Picture(picture_box, image=default_image_black, width=310, height=215,
grid=[0,1])
picture_g_nosample = Picture(picture_box, image=default_image_black, width=310, height=215,
grid=[1,1])
#
text20 = Text(picture_box, text="Post C", color="white", size=15, width=15, height=1, grid=[1,2])
text12 = Text(picture_box, text="Post T", color="white", size=15, width=15, height=1, grid=[0,2])
#
picture_b = Picture(picture_box, image=default_image_black, width=310, height=215, grid=[0,3])
```

```
picture_g = Picture(picture_box, image=default_image_black, width=310, height=215, grid=[1,3])

#
#ROI_box= Box(exp_gain_box,layout="grid",width=280,height=100, grid=[0,9])
#C_ROI = Text(ROI_box, text="C ROI", size=16, color="white", align="left", grid=[0,2])
slider_CROIx = Slider(picture_box, width=310,height=18,start=-270,end=270, grid=[1,4])
slider_CROIx.bg=(85,85,85); slider_CROIx.text_color="white"
#T_ROI = Text(ROI_box, text=" \nT ROI", size=16, color="white", align="left", grid=[0,0])
slider_TROIx = Slider(picture_box, width=310,height=18,start=-270,end=270, grid=[0,4])
slider_TROIx.bg=(85,85,85); slider_TROIx.text_color="white"

#
#dSpace5 = Text(Col3, text=" ", width=3, height=1, grid=[0,1])
#
button_box = Box(Col3,layout="grid", grid=[0,2])
#
insert_button = PushButton(button_box, command=start_motor, text="Insert",
                        padx=20, pady=20, width=4, height=2, grid=[1,0])
insert_button.text_size=18; insert_button.text_color="white"; insert_button.bg= (0,102,254)
#
dSpace1 = Text(button_box, text=" ", width=1, height=0, grid=[2,0])
#
test_button   = PushButton(button_box, command=test, text="Image",
                        padx=20, pady=20, width=4, height=2, grid=[3,0])
test_button.text_size=18; test_button.text_color="white"; test_button.bg= (102,204,0)
#
dSpace2 = Text(button_box, text=" ", width=1, height=0, grid=[4,0])
#
ROI_button = PushButton(button_box, command = ROI, text="Set ROI",padx=20, pady=20,
width=4, height=2, grid=[5,0])
ROI_button.text_color="white"; ROI_button.text_size=18; ROI_button.bg= (255,128,0)
#
dSpace8 = Text(button_box, text=" ", width=1, height=0, grid=[6,0])
#
proc_button = PushButton(button_box, command = processing, text="Process",padx=20, pady=20,
width=4, height=2, grid=[7,0])
proc_button.bg= (255,102,178); proc_button.text_color="white"; proc_button.text_size=18
#
dSpace3 = Text(button_box, text=" ", width=1, height=0, grid=[8,0])
#
eject_button  = PushButton(button_box, command=EjectHolder, text="Eject",
                        padx=20, pady=20, width=4, height=2, grid=[9,0])
eject_button.text_size=18; eject_button.text_color="white"; eject_button.bg= (204,0,0)
#

######################################################################
# Temperature Humudity Thread
sensor_thread = threading.Thread(target=continuous_sensor_reading)
sensor_thread.daemon = True  # Thread will end when the main program quits
sensor_thread.start()
app.display()
######################################################################
```

APPENDIX B: PYTHON CODE FOR FINAL READER

```
from guizero import App, PushButton, Text, Picture, Box, Slider, TextBox, ListBox, Combo, Waffle
import RPi.GPIO as GPIO
import time

from PIL import Image
from PIL.PngImagePlugin import PngInfo

from time import sleep
from picamera2 import Picamera2, Preview
from datetime import datetime

import pickle
import numpy as np
import matplotlib.pyplot as plt
import matplotlib.patches as patches
import os
import cv2

from subprocess import call

# pip3 install imageio
import imageio.v3 as iio

# Temperature-humidity sensor
import board
import bme280
import smbus2
import threading

import adafruit_ina219

# Initialize the HTU21D sensor which uses board.SCL and board.SDA
i2c = board.I2C(); ina219 = adafruit_ina219.INA219(i2c, addr=0x42)


# Initialize the HTU21D sensor which uses board.SCL and board.SDA
port = 1
address = 0x76 # BME280 address. Other BME280s may be different
bus = smbus2.SMBus(port)

bme280.load_calibration_params(bus,address)

# Camera opens when the code starts
picam2 = Picamera2()

#camera_config = picam2.create_still_configuration(main={"size": (4056, 3040)})
camera_config = picam2.create_still_configuration(raw={'format':'SRGGB12'})

crop_G = (2178, 1120, 2178+1400, 1120+910)
crop_B = (528, 1120, 1928, 1120+910)
```

```
controls_config = {"AwbEnable": 0, "AeEnable": 0, "ExposureTime": 100000, "AnalogueGain": 1};

# Define ROI coordinates and size (x, y, width, height)
x, y, width, height = 1432, 200, 400, 2064


stts   = 0
metadata=[]


wDIR = "/home/bme/Desktop/seda/1303/"

image_path_B_PRE="x"
image_path_G_PRE="x"
image_path_B_POST="x"
image_path_G_POST="x"


# Button
def button_callback(channel):
   global stts; stts = 1; cleanup()

GPIO.setwarnings(False) # Ignore warning for now
GPIO.setmode(GPIO.BCM) # Use physical pin numbering

# GPIO pins for Strip Detector
button_pow = 6
button_pin = 5
GPIO.setup(button_pow, GPIO.OUT)
GPIO.output(button_pow, 1)

GPIO.setup(button_pin, GPIO.IN, pull_up_down=GPIO.PUD_DOWN) # Set pin 5 to be an input
pin and set initial value to be pulled low (off)

GPIO.add_event_detect(button_pin,GPIO.RISING,callback=button_callback,  bouncetime=200)  #
Setup event on pin 5 rising edge

# GPIO pin connected to the voltage regulator for Blue LED
BlueLED_pin  = 17; GPIO.setup(BlueLED_pin, GPIO.OUT, initial=GPIO.HIGH)

# GPIO pin connected to the voltage regulator for Green LED
GreenLED_pin = 18; GPIO.setup(GreenLED_pin, GPIO.OUT, initial=GPIO.HIGH)

# Motor configuration
step_sleep = 0.001; step_count = 1; step_count_e = 4096; direction = False
step_sequence = [[1, 0, 0, 1],
                 [1, 0, 0, 0],
                 [1, 1, 0, 0],
                 [0, 1, 0, 0],
                 [0, 1, 1, 0],
                 [0, 0, 1, 0],
                 [0, 0, 1, 1],
                 [0, 0, 0, 1]]
```

```
# Setting up GPIO for motor driver
in1 = 19; in2 = 16; in3 = 26; in4 = 20
GPIO.setup(in1, GPIO.OUT)
GPIO.setup(in2, GPIO.OUT)
GPIO.setup(in3, GPIO.OUT)
GPIO.setup(in4, GPIO.OUT)

motor_pins = [in1, in2, in3, in4]
motor_step_counter = 0

def cleanup():
   GPIO.output(in1, GPIO.LOW)
   GPIO.output(in2, GPIO.LOW)
   GPIO.output(in3, GPIO.LOW)
   GPIO.output(in4, GPIO.LOW)

def power_off():
       cleanup()
       app.destroy()
       call("sudo shutdown -h now", shell=True)


P0 = 1013.25 #average sea level pressure in hPa

# Function to read sensor data
def read_sensor_data():
   bme280_data = bme280.sample(bus,address)
   humidity  = bme280_data.humidity ; hum_display.value = f"{humidity:3.0f}%RH"
   temperature = bme280_data.temperature ; temp_display.value = f"  {temperature:2.1f}Â°C  "
   temp = temperature + 273.15 # convert to Kelvin
   pressure =  bme280_data.pressure

   #calculate altitude from pressure using barometric formula
   altitude = ((P0 / pressure)**(1 / 5.257)-1) * (temp / 0.0065)   ; pres_display.value = f"
{altitude:.0f}m  "

   current_time = datetime.now().strftime("%d/%m/%Y   %H:%M")
   date_display.value = current_time
   app.update()

# Initialize variables for the moving average filter
#N = 10
#voltage_readings = []

# Function to update the battery level indicator
def update_battery_indicator(percentage):
   # Calculate how many squares to fill based on the percentage
   filled_squares = int(round(percentage * 5 / 100))  # Assuming 5 squares for 0-100%
   for i in range(5):
      if i < filled_squares:
         battery_indicator.set_pixel(i, 0, "green")
      else:
         battery_indicator.set_pixel(i, 0, "white")
```

```
# Adjusted battery display update function
def update_battery_display():
    #global voltage_readings

    bus_voltage = ina219.bus_voltage
    #print(bus_voltage)
    #bus_voltage = 8.4
    #voltage_readings.append(bus_voltage)

    #if len(voltage_readings) > N:
    #    voltage_readings = voltage_readings[-N:]

    #avg_voltage = sum(voltage_readings) / len(voltage_readings)
    percent = (bus_voltage - 6) / (8.4 - 6) * 100
    percent = max(0, min(100, percent))

    # Update the battery level indicator based on the calculated percentage
    update_battery_indicator(percent)

# Function for continuous sensor reading
def continuous_sensor_reading():
    while True:
        read_sensor_data()
        update_battery_display()
        time.sleep(2)

# Function for motor
def move_motor():
    global motor_step_counter
    global stts
    forward_counter = 0  # Counter for forward motion
    stts=0
    if GPIO.input(button_pin)==1:
        stts=1
    try:
        while stts==0:
            for _ in range(step_count):
                for pin in range(len(motor_pins)):
                    GPIO.output(motor_pins[pin], step_sequence[motor_step_counter][pin])

                motor_step_counter = (motor_step_counter + 1) % 8
                forward_counter += 1  # Count steps in the forward direction
                time.sleep(step_sleep)
    except KeyboardInterrupt:
        cleanup()
        app.destroy()
    cleanup()

def imaging(LEDpin, path, region, crop_area, picture): #imaging(BlueLED_pin, camera_config_B,
"f"{wDIR}{timestamp}_G_{ExpTime}_PRE", 'T')
        global LightTime, wDIR
        # Setup the camera for T Line Imaging
        picam2.configure(camera_config)
```

```
    picam2.set_controls(controls_config)
    picam2.options["compress_level"] = 0
    picam2.start()
    time.sleep(8) # Wait 8 sec for camera get ready
    #
    GPIO.output(LEDpin, GPIO.LOW)   # Turn the LED ON
    time.sleep(LightTime)
    #
    # Gather metadata
    metadata = picam2.capture_metadata()
    metadata.update({"LightOnTime     (s)": LightTime})
    metadata.update({"EnvTemperature (oC)": temp_display.value})
    metadata.update({"EnvRelHumidity  (%)": hum_display.value})

    # Capture an image
    img = picam2.capture_array("raw").view(np.uint16)
    GPIO.output(LEDpin, GPIO.HIGH)  # Turn the LED OFF
    #
    stts_text.text_color = "white"; stts_text.value = region + " REGION imaging COMPLETED !"
    app.update()

    # Save the image
    img = img * 16;        image_path = path + ".png"

    img_rgb = cv2.cvtColor(img, cv2.COLOR_BAYER_RGGB2RGB)
    img_rgb=img_rgb[crop_area[1]:crop_area[3],crop_area[0]:crop_area[2]]
    cv2.imwrite(image_path,img_rgb)

    picture.image = image_path
    app.update()

    image_path_12 = path + "12BIT" + ".png"

    img = Image.fromarray(img)
    img = img.crop(crop_area)
    img.save(image_path_12)
    #cv2.imwrite(image_path,img)
    time.sleep(2)

    # Generate txt file to store metadata
    data_path  = path + ".txt"
    with open(data_path, 'w') as file:
        for key, value in metadata.items():
            file.write(f"{key}: {value}\n")
    file.close()

    #img.release()   # Release the img heap
    picam2.stop()   # Stop picam2


def PRE_imaging():
    global image_path_B_PRE, image_path_G_PRE, ExpTime, timestamp, wDIR
    if stts == 0:
        stts_text.text_color = "yellow"
```

```
        stts_text.value      = "Insert the empty cartridge for PRE-IMAGING"
        app.update()
    else:
        stts_text.text_color = "white"
        stts_text.value      = "Performing PRE-IMAGING ..."
        app.update()
        time.sleep(1)
        ############ T Line Imaging
        stts_text.text_color = "white"; stts_text.value = "Imaging T REGION ..."
        app.update()
        image_path_B_PRE= f"{wDIR}{timestamp}_{ExpTime}_B_PRE"
        imaging(BlueLED_pin, image_path_B_PRE, 'T', crop_B, picture_b_nosample)

        ############ C Line Imaging
        stts_text.text_color = "white"; stts_text.value = "Imaging C REGION ..."
        app.update()
        image_path_G_PRE= f"{wDIR}{timestamp}_{ExpTime}_G_PRE"
        imaging(GreenLED_pin, image_path_G_PRE, 'C', crop_G, picture_g_nosample)

        #picture_g_nosample.image = image_path_G_PRE + ".png"
        #app.update()

        # Eject the strip holder
        #EjectHolder()

def POST_imaging():
    global image_path_B_POST, image_path_G_POST, ExpTime, timestamp, wDIR
    if stts == 0:
        stts_text.text_color = "red"
        stts_text.value      = "Insert the cartridge for POST-IMAGING"
        app.update()
    else:
        stts_text.text_color = "white"
        stts_text.value      = "Performing POST-IMAGING ..."
        app.update()
        time.sleep(1)

        ############ T Line Imaging
        stts_text.text_color = "white"
        stts_text.value      = "Imaging T REGION ..."
        app.update()

        image_path_B_POST= f"{wDIR}{timestamp}_{ExpTime}_B_POST"
        imaging(BlueLED_pin, image_path_B_POST, 'T', crop_B, picture_b)

        #picture_b.image = image_path_B_POST + ".png"
        #app.update()

        ############ C Line Imaging
        stts_text.text_color = "white"; stts_text.value = "Imaging C REGION ..."
        app.update()
        image_path_G_POST= f"{wDIR}{timestamp}_{ExpTime}_G_POST"
        imaging(GreenLED_pin, image_path_G_POST, 'C', crop_G, picture_g)
```

```
        #picture_g.image = image_path_G_POST + ".png"
        #app.update()

def test():
    global timestamp, ExpTime, LightTime, wDIR
    try:
        timestamp = datetime.now().strftime("%d%m%y_%H%M%S")
        LightTime      = int(float(slider_LightTime.value));
        ExpTime        = int(float(slider_CameraExp.value)); exposure_time = ExpTime * 1000
        analogue_gain   = float(slider_gain.value)
        controls_config["ExposureTime"]= exposure_time;
        controls_config["AnalogueGain"]= analogue_gain;

        mode_selector     = str(combo.value)

        if mode_selector == "Pre Imaging":
            picture_b_nosample.image = default_image_black
            picture_g_nosample.image = default_image_black
            app.update()
            PRE_imaging()
        else:
            picture_b.image = default_image_black
            picture_g.image = default_image_black
            app.update()
            POST_imaging()

    except KeyboardInterrupt:
        cleanup()
        app.destroy()

######## Image Processing
def C_UpdateROI(path):
        global Cx, Cy, Cw, Ch, wDIR
        x, y, width, height = 640, 100, 120, 670

        CROI_x = int(float(slider_CROIx.value));

        ALLImg_C = iio.imread(uri=path + ".png")

        fig = plt.figure()
        plt.imshow(ALLImg_C)
        plt.gca().add_patch(patches.Rectangle((x+CROI_x,     y),     width,     height,     linewidth=2,
edgecolor='g', facecolor='none', figure=fig))
        plt.gca().text(120+x+CROI_x, 855, 'C', size=20, weight='bold', color='Green')
        plt.axis('off')
        plt.axis("tight")
        Cx=x+CROI_x; Cy = y; Cw=width; Ch=height
        # Save the image with the ROI rectangle
        roi_image_C_path = path +"_ROI.png"
        plt.savefig(roi_image_C_path, bbox_inches='tight', pad_inches=0)
        plt.close()

def T_UpdateROI(path):
        global Tx, Ty, Tw, Th, wDIR
```

```
    x, y, width, height = 640, 100, 120, 670

    TROI_x = int(float(slider_TROIx.value));

    ALLImg_T = iio.imread(uri=path + ".png")

    fig = plt.figure()
    plt.imshow(ALLImg_T)
    plt.gca().add_patch(patches.Rectangle((TROI_x+x, y), width, height, linewidth=2,
edgecolor='b', facecolor='none', figure=fig))
    plt.gca().text(120+x+TROI_x, 855, 'T', size=20, weight='bold', color='Blue')
    plt.axis('off')
    plt.axis("tight")
    Tx=TROI_x+x; Ty = y; Tw=width; Th=height
    # Save the image with the ROI rectangle
    roi_image_T_path = path + "_ROI.png"
    plt.savefig(roi_image_T_path, bbox_inches='tight', pad_inches=0)
    plt.close()

def ROI():
    global image_path_B_PRE, image_path_G_PRE, image_path_B_POST,
image_path_G_POST, wDIR

    if os.path.exists(image_path_B_PRE + ".png"):
      T_UpdateROI(image_path_B_PRE)
      picture_b_nosample.image = image_path_B_PRE + "_ROI.png"
      C_UpdateROI(image_path_G_PRE)
      picture_g_nosample.image = image_path_G_PRE + "_ROI.png"

    if os.path.exists(image_path_B_POST + ".png"):
      T_UpdateROI(image_path_B_POST)
      picture_b.image     = image_path_B_POST + "_ROI.png"
      C_UpdateROI(image_path_G_POST)
      picture_g.image = image_path_G_POST + "_ROI.png"

    app.update()

def processing():
    global image_path_B_PRE, image_path_G_PRE, image_path_B_POST,
image_path_G_POST, wDIR
    global Tx, Ty, Tw, Th, Cx, Cy, Cw, Ch
    global values, timestamp

    SImean_TLine_Pre = SImean_CLine_Pre = SImean_TLine_Post = SImean_CLine_Post = 0

    values = [SImean_TLine_Pre, SImean_TLine_Post, SImean_CLine_Pre, SImean_CLine_Post]

    if os.path.exists(image_path_B_PRE + ".png"):
      Img = iio.imread(uri=image_path_B_PRE + ".png")
      TImg_ROI = Img[Ty:Ty+Th, Tx:Tx+Tw, :]
      hist(TImg_ROI, image_path_B_PRE)
      mean_stat(TImg_ROI, 0, 1)

      Img = iio.imread(uri=image_path_G_PRE + ".png")
```

```
        CImg_ROI = Img[Cy:Cy+Ch, Cx:Cx+Cw, :]
        hist(CImg_ROI, image_path_G_PRE)
        mean_stat(CImg_ROI, 2, 0)
        with open(image_path_B_PRE + "_C_PRE.txt", 'w') as f:
            f.write("T_PRE Mean Value: " + str(values[0]) + "\nT ROI: " + str(slider_TROIx.value)
                + "\nC_PRE Mean Value: " + str(values[2]) + "\nC ROI: " + str(slider_CROIx.value))

    if os.path.exists(image_path_B_POST + ".png"):
        Img = iio.imread(uri=image_path_B_POST + ".png")
        TImg_ROI = Img[Ty:Ty+Th, Tx:Tx+Tw, :]
        hist(TImg_ROI, image_path_B_POST)
        mean_stat(TImg_ROI, 1, 1)

        Img = iio.imread(uri=image_path_G_POST + ".png")
        CImg_ROI = Img[Cy:Cy+Ch, Cx:Cx+Cw, :]
        hist(CImg_ROI, image_path_G_POST)
        mean_stat(CImg_ROI, 3, 0)

        with open(image_path_B_POST + "_C_POST.txt", 'w') as f:
            f.write("T_POST Mean Value: " + str(values[1]) + "\nT ROI: " + str(slider_TROIx.value)
+
            "\nC_POST Mean Value: " + str(values[3])+ "\nC ROI: " + str(slider_CROIx.value))


    # Create the bar plot
    plt.figure(figsize=(6, 4))
    plt.xticks(fontsize=16)
    plt.yticks(fontsize=16)

    labels = ['T-Pre', 'T-Post', 'C-Pre', 'C-Post']
    plt.bar(labels, values, color=['blue', 'blue', 'green', 'green'])
    plt.ylabel('Average SI', fontsize=20)
    #plt.title('Mean SI Comparison', fontsize=22)

    # Save the plot as an image
    mean_plot_path = f"{wDIR}mean_val_{timestamp}.png"
    plt.savefig(mean_plot_path)

def hist(Img, path):

    #Img = iio.imread(uri=path + ".png")

    # tuple to select colors of each channel line
    colors = ("red", "green", "blue")

    plt.figure(figsize=(6, 4))
    plt.xlim([0, 256])
    # create the histogram plot, with three lines, one for
    # each color
    for channel_id, color in enumerate(colors):
        histogram, bin_edges = np.histogram(
        Img[:, :, channel_id], bins=256, range=(0, 256), density=True)
        plt.plot(bin_edges[0:-1], histogram, color=color)
```

```
    plt.title("Histogram")
    plt.xlabel("Signal Intensity")
    plt.ylabel("Probability")

    plt.savefig(path + "_HST.png")

#n:values array order, c:channel id
def mean_stat(Img, n, c):
    global values
    numpydata   = np.asarray(Img[:,:,c])
    values[n] = np.mean(numpydata)
    print(values[n], n)

def EjectHolder():
  global motor_step_counter
  global stts
  backward_counter = 0  # Counter for backward motion
  direction = True
  #m       = int(float(text_chron.value))
  #countdown(0, int(m), 0)
  try:
    if GPIO.input(button_pin)==1:
      stts_text.text_color = "white"
      stts_text.value      = "The holder is being ejected ..."
      app.update()

      for _ in range(step_count_e):
        for pin in range(len(motor_pins)):
          GPIO.output(motor_pins[pin], step_sequence[motor_step_counter][pin])

        motor_step_counter = (motor_step_counter - 1) % 8
        backward_counter += 1  # Count steps in the backward direction
        time.sleep(step_sleep)

    stts_text.text_color = "red"
    stts_text.value      = "Load the holder for post imaging!"
    app.update()

    stts = 0
  except KeyboardInterrupt:
    cleanup()
    app.destroy()
    pwm.stop()
  cleanup()

# Create a function to start the motor
def start_motor():
  insert_button.disable()

  stts_text.text_color = "white"
  stts_text.value      = "Reader waits for positioning the cartridge.."
  app.update()
  move_motor()
```

```
    insert_button.enable()
    stts_text.value = "Press 'Test' to start acquisition"
    app.update()

def countdown():
    global timer
    if timer > 0:
        timer -= 1
        time_display.value = f'{timer//60}:{timer%60:02d}'
        app.after(1000, countdown)  # Schedule this function to be called again after 1 second
    else:
        start_button.enable()  # Re-enable the start button when the countdown ends

def start_timer():
    global timer
    start_button.disable()  # Disable the start button to prevent multiple presses
    timer = 0
    try:
        timer = int(minutes_input.value) * 60  # Convert minutes to seconds
        countdown()
    except ValueError:
        time_display.value = "Enter a valid number!"
        start_button.enable()  # Re-enable the start button if there's a ValueError


####################################################################
#Create the GUI and the master of the GUI
default_image_black    = f"/home/bme/Desktop/seda/black.png"
default_image_path_off = f"/home/bme/Desktop/seda/power2.png"

app = App(title = "YUBME: LFA Reader v2024.1", width=800, height=480, bg=(85,85,85),layout="grid")

####################################################################
# 1st Column
Col1 = Box(app,layout="auto", width=30, height=480, grid=[0,0], align="top"); Col1.bg=(0,102,102)
#
poweroff_bttn = PushButton(Col1, image=default_image_path_off, command=power_off)

####################################################################
# 2nd Column
Col2 = Box(app,layout="grid", width=270, height=445, grid=[1,0], align="top");
#
sensor_box= Box(Col2,layout="auto", width=270, height=35, grid=[0,0]); sensor_box.bg=(0,102,102)
#dSpace02  = Text(sensor_box,text=" ", width=1, align="left")
temp_display = Text(sensor_box, text=" -- Â°C ", color="white", size=16, font="Arial",align = "left")
dSpace03  = Text(sensor_box,text=" ", width=1, align = "left")
hum_display  = Text(sensor_box, text=" -- %RH", color="white", size=16, font="Arial",align = "left")
dSpace04  = Text(sensor_box,text=" ", width=1, align = "left")
pres_display = Text(sensor_box, text=" -- m", color="white", size=16, font="Arial", align = "left")
```

```
# Listbox for img acquisition mode
imagingmode_text = Text(Col2,text=" \n Imaging Mode", font="Times New Roman", size=16,
color="white", align="left", grid= [0,2])
combo_box = Box(Col2,layout="grid", width=270, height=5, grid=[0,3]);
combo_box.set_border(1,"white")
combo = Combo(combo_box, options=["Pre Imaging", "Post Imaging"], width=12, grid=[0,1])
combo.text_color ="white"; combo.text_size= 12
#
#dSpace01  = Box(Col2,layout="grid", height=2, grid=[0,3])
setting_text  = Text(Col2,text=" Settings", font="Times New Roman", size=16, color="white",
align="left", grid= [0,4])

#
exp_gain_box = Box(Col2,layout="grid", width=270, height=150, grid=[0,5])
exp_gain_box.set_border(1,"white")

#
# Slider for Light Emission Time (1 - 10s)
LightTime = Text(exp_gain_box, text=" \nLight Emission Time (s)", size=12, color="white",
align="left", grid= [0,2])
slider_LightTime = Slider(exp_gain_box, width=200,height=12,start=1,end=10, grid=[0,3])
slider_LightTime.bg=(85,85,85)
slider_LightTime.text_color="white"

# Slider for Camera Exposure Time (1000 - 2000ms)
CameraExp = Text(exp_gain_box, text=" \nCamera Exposure (ms)", size=12, color="white",
align="left", grid= [0,4])
slider_CameraExp = Slider(exp_gain_box, width=200,height=12,start=1,end=30, grid=[0,5])
slider_CameraExp.bg=(85,85,85)
slider_CameraExp.text_color="white"

# Slider for Gain (1-10)
gain = Text(exp_gain_box, text=" \nAnalogue Gain", size=12, color="white", align="left",
grid=[0,6])
slider_gain = Slider(exp_gain_box, width=200,height=12,start=1,end=5, grid=[0,7])
slider_gain.bg=(85,85,85)
slider_gain.text_color="white"

#
Space4 = Text(Col2, text=" ",width=8,height=1,grid=[0,8])

date_display = Text(Col2, text=" ", color="white", size=12, font="Arial",align = "left", grid=[0,9])

#####################################################################
# 3th Column
Col3 = Box(app,layout="auto", width=500, height=480, grid=[3,0], align="top")
# Status Box
stts_box    = Box(Col3, layout="auto", width=500, height=35, grid=[0,0]); stts_box.bg=(0,102,102)
stts_message = "Please Insert the Cartridge Without Sample"
stts_text   = Text(stts_box, text=stts_message, size=14, color="white", font="Arial", align="top")
# Picture Box
picture_box = Box(Col3,layout="grid", width=475, height=347, grid=[0,1])
#
```

```
text10 = Text(picture_box, text="Pre T", color="white", size=12, width=10, height=1, grid=[0,0])
text00 = Text(picture_box, text="Pre C", color="white", size=12, width=10, height=1, grid=[1,0])
#
picture_b_nosample = Picture(picture_box, image=default_image_black, width=230, height=132,
grid=[0,1])
picture_g_nosample = Picture(picture_box, image=default_image_black, width=230, height=132,
grid=[1,1])
#
text12 = Text(picture_box, text="Post T", color="white", size=12, width=15, height=1, grid=[0,2])
text20 = Text(picture_box, text="Post C", color="white", size=12, width=15, height=1, grid=[1,2])
#
picture_b = Picture(picture_box, image=default_image_black, width=230, height=132, grid=[0,3])
picture_g = Picture(picture_box, image=default_image_black, width=230, height=132, grid=[1,3])

#
#ROI_box= Box(exp_gain_box,layout="grid",width=280,height=100, grid=[0,9])
#C_ROI = Text(ROI_box, text="C ROI", size=16, color="white", align="left", grid=[0,2])
slider_CROIx = Slider(picture_box, width=225,height=12,start=-580,end=580, grid=[1,4])
slider_CROIx.bg=(85,85,85); slider_CROIx.text_color="white"
#T_ROI = Text(ROI_box, text=" \nT ROI", size=16, color="white", align="left", grid=[0,0])
slider_TROIx = Slider(picture_box, width=225,height=12,start=-580,end=580, grid=[0,4])
slider_TROIx.bg=(85,85,85); slider_TROIx.text_color="white"

#
dSpace5 = Text(Col3, text=" ", width=3, height=1, grid=[0,1])
#
button_box = Box(Col3,layout="grid", width=480, height=75, grid=[0,2])
#
insert_button = PushButton(button_box, command=start_motor, text="Insert",
                     padx=12, pady=10, width=4, height=1, grid=[1,0])
insert_button.text_size=15; insert_button.text_color="white"; insert_button.bg= (0,102,254)
#
dSpace1 = Text(button_box, text=" ", width=1, height=0, grid=[2,0])
#
test_button   = PushButton(button_box, command=test, text="Image",
                     padx=12, pady=10, width=4, height=1, grid=[3,0])
test_button.text_size=15; test_button.text_color="white"; test_button.bg= (102,204,0)
#
dSpace2 = Text(button_box, text=" ", width=1, height=0, grid=[4,0])
#
ROI_button = PushButton(button_box, command = ROI, text="Set ROI",padx=12, pady=10,
width=4, height=1, grid=[5,0])
ROI_button.text_color="white"; ROI_button.text_size=15; ROI_button.bg= (255,128,0)
#
dSpace8 = Text(button_box, text=" ", width=1, height=0, grid=[6,0])
#
proc_button = PushButton(button_box, command = processing, text="Process",padx=12, pady=10,
width=4, height=1, grid=[7,0])
proc_button.bg= (255,102,178); proc_button.text_color="white"; proc_button.text_size=15
#
dSpace3 = Text(button_box, text=" ", width=1, height=0, grid=[8,0])

#
eject_button  = PushButton(button_box, command=EjectHolder, text="Eject",
```

```
                    padx=12, pady=10, width=4, height=1, grid=[9,0])
eject_button.text_size=15; eject_button.text_color="white"; eject_button.bg= (204,0,0)
#
#battery_display = Text(button_box, text=" -- % ", color="white", size=18, font="Arial",grid= [9,1],
align ="right")

battery_indicator = Waffle(Col2, width=5, height=1, dim = 13, color="white", dotty=True,
grid=[0,10], align ="left")

###########################################################################
# Temperature Humudity Thread
sensor_thread = threading.Thread(target=continuous_sensor_reading)
sensor_thread.daemon = True  # Thread will end when the main program quits
sensor_thread.start()

battery_thread = threading.Thread(target=update_battery_display)
battery_thread.daemon = True  # Thread will end when the main program quits
battery_thread.start()
app.display()
###########################################################################
```

APPENDIX C: TECHNICAL DRAWINGS FOR PRELIMINARY

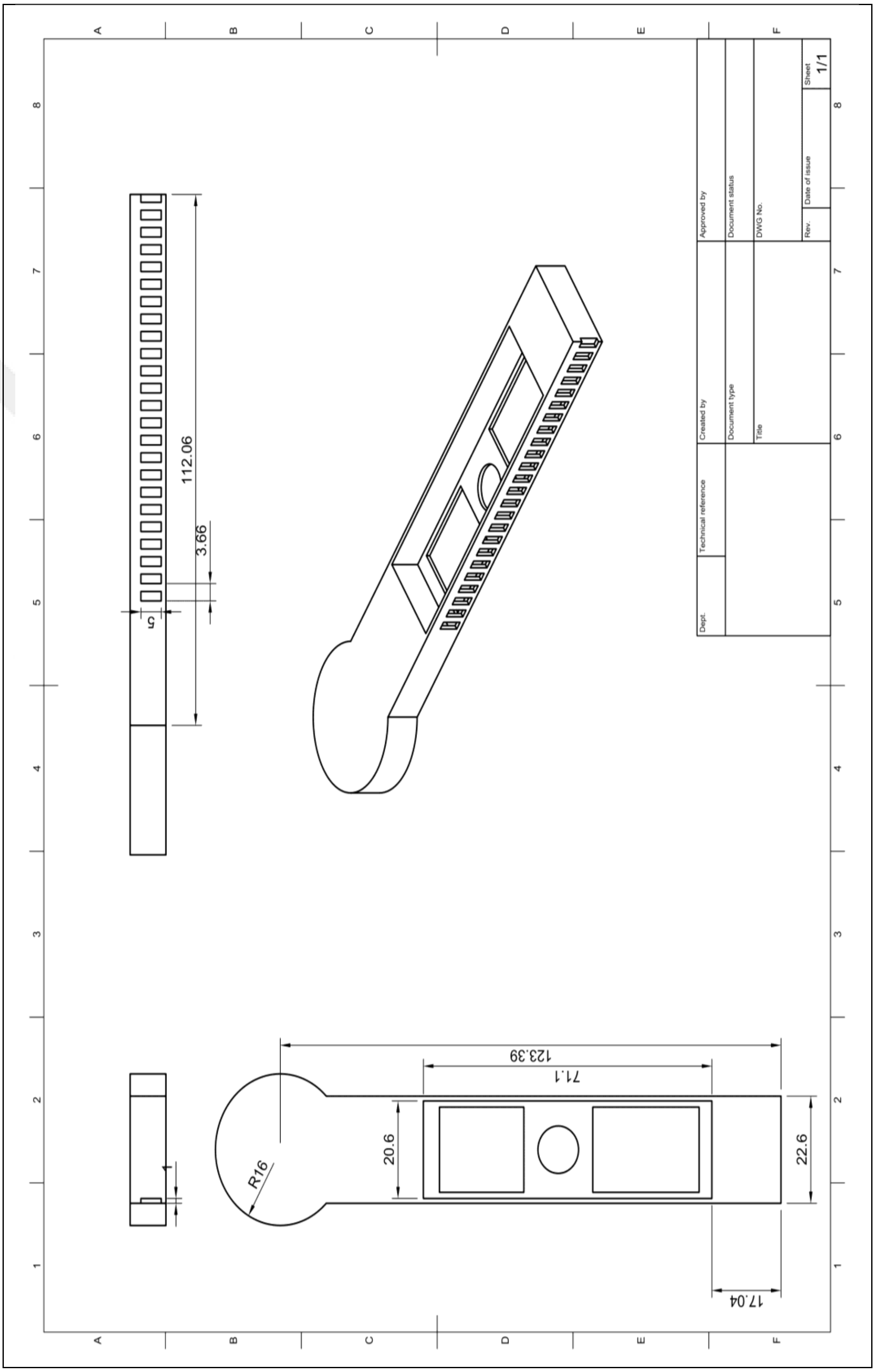

Figure C.1. Cassette holder.

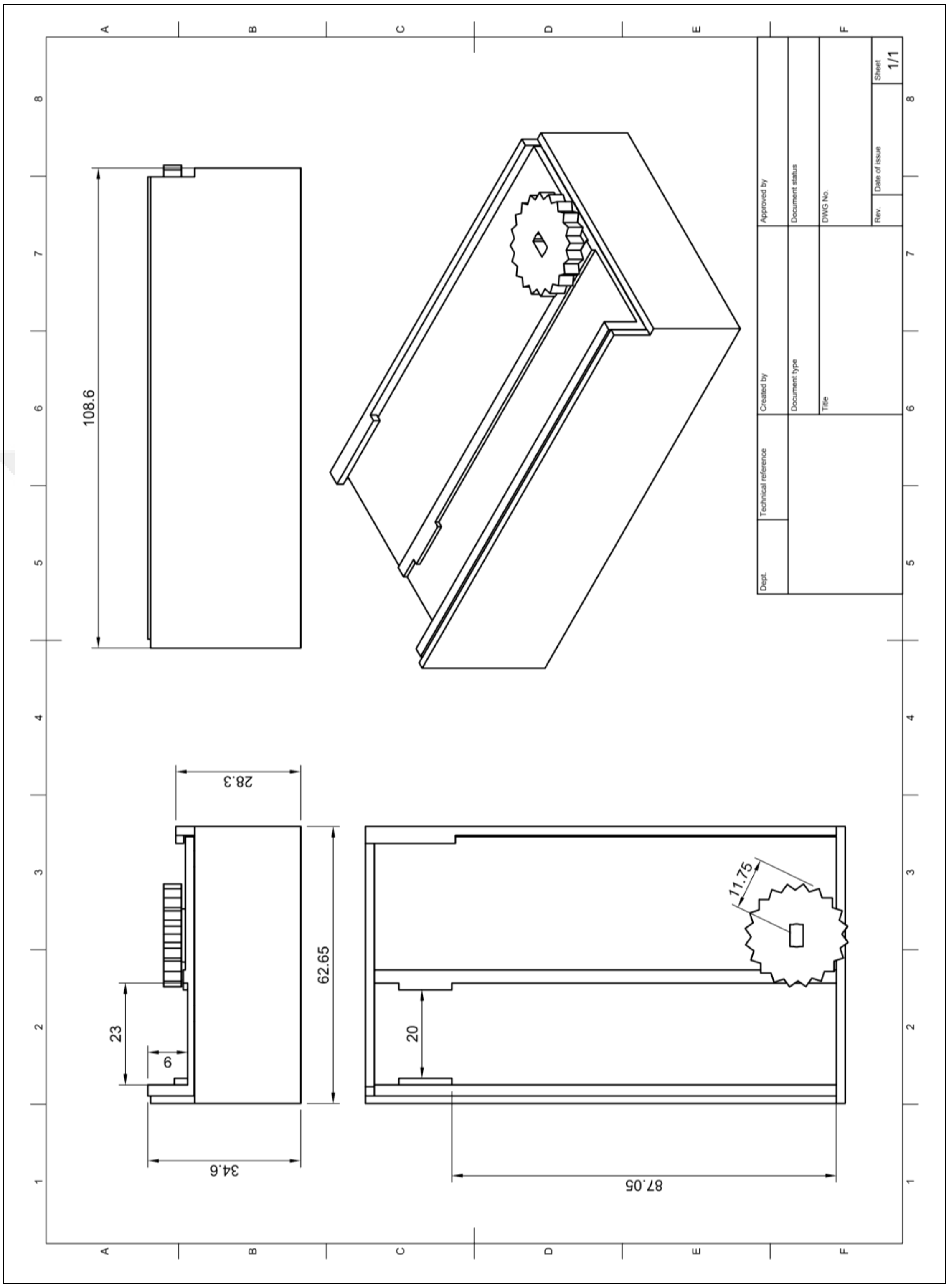

Figure C.2. Motorized sliding tray.

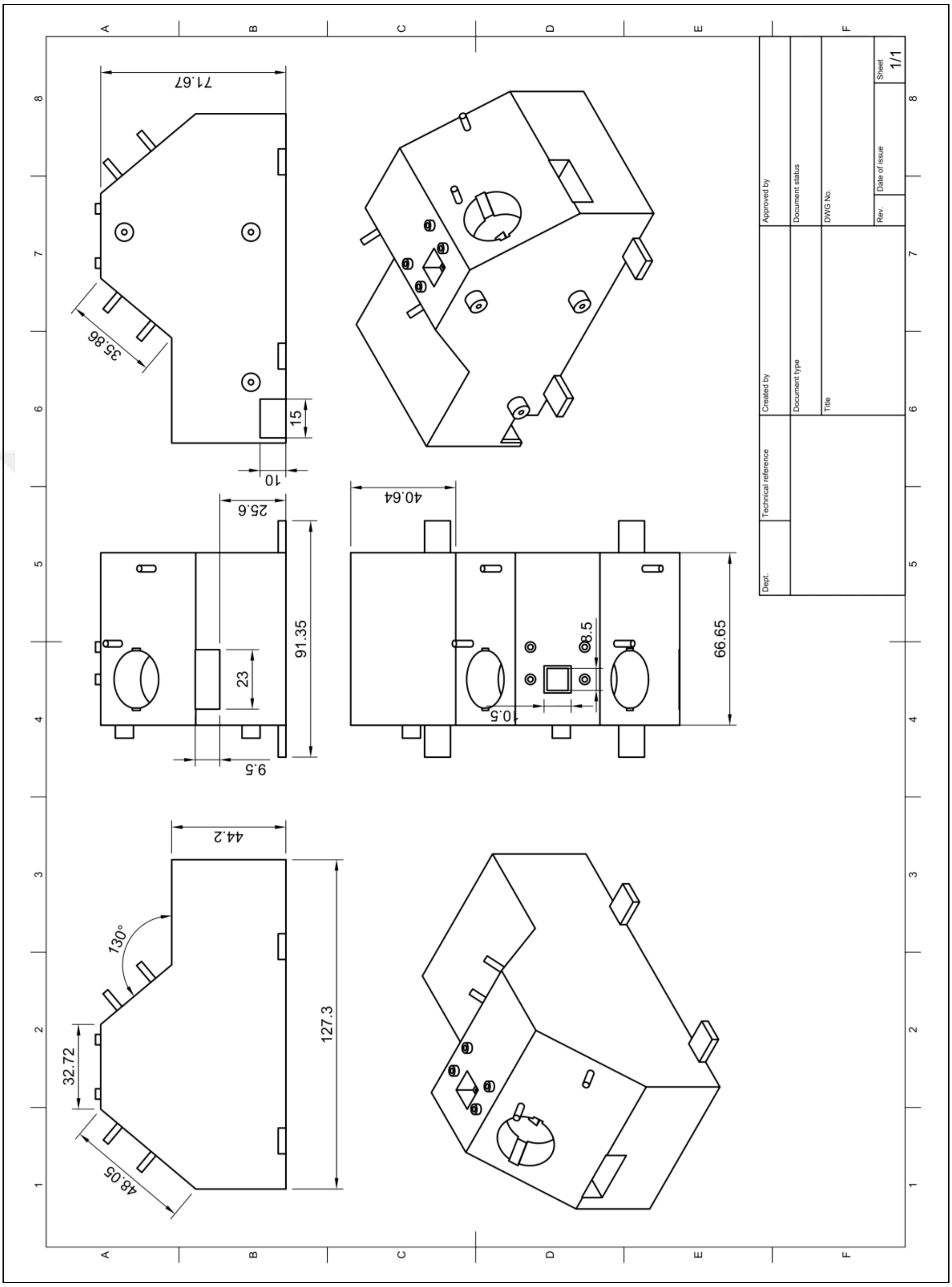

Figure C.3. Darkroom.

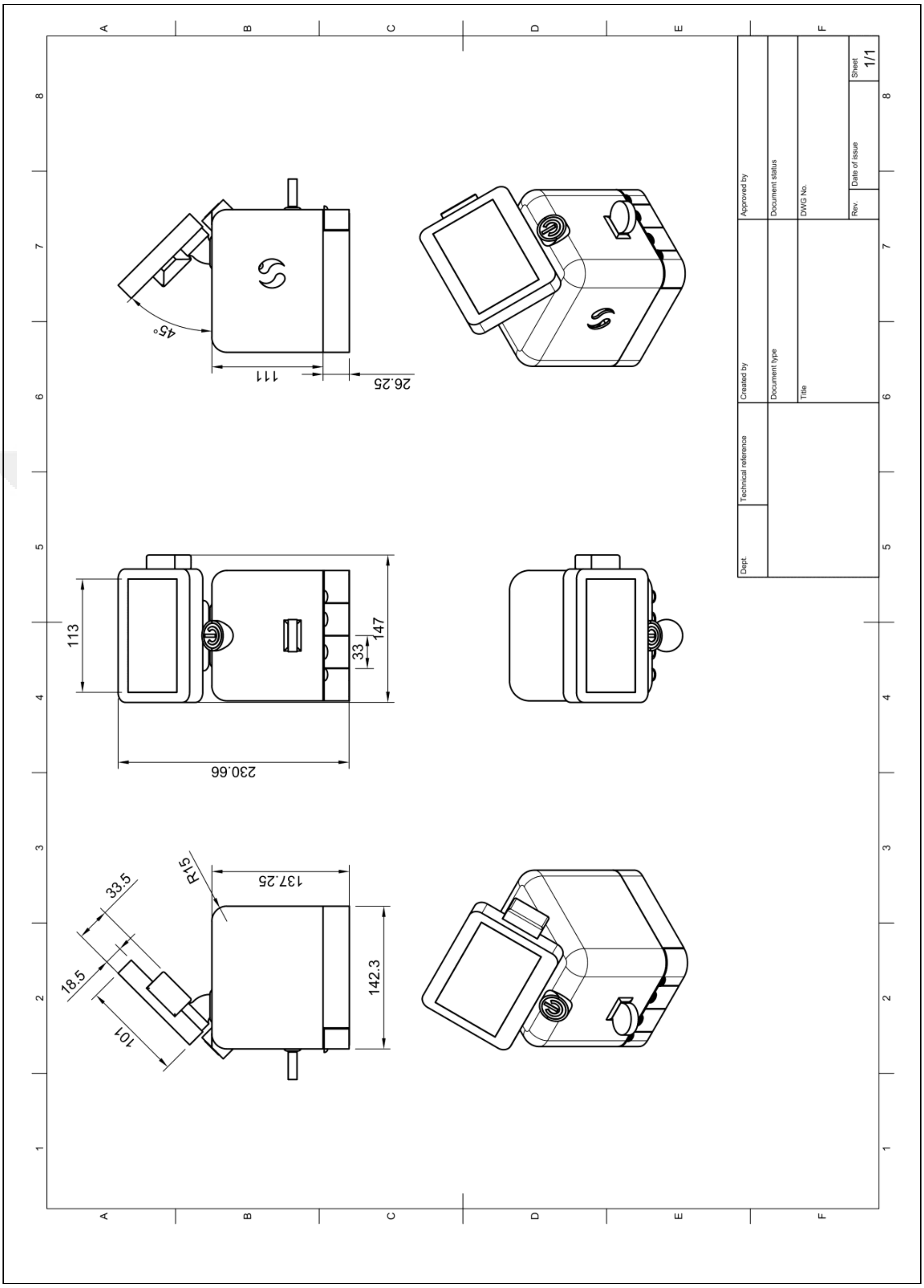

Figure C.4. Preliminary optical reader enclosure.

APPENDIX D: TECHNICAL DRAWINGS FOR FINAL

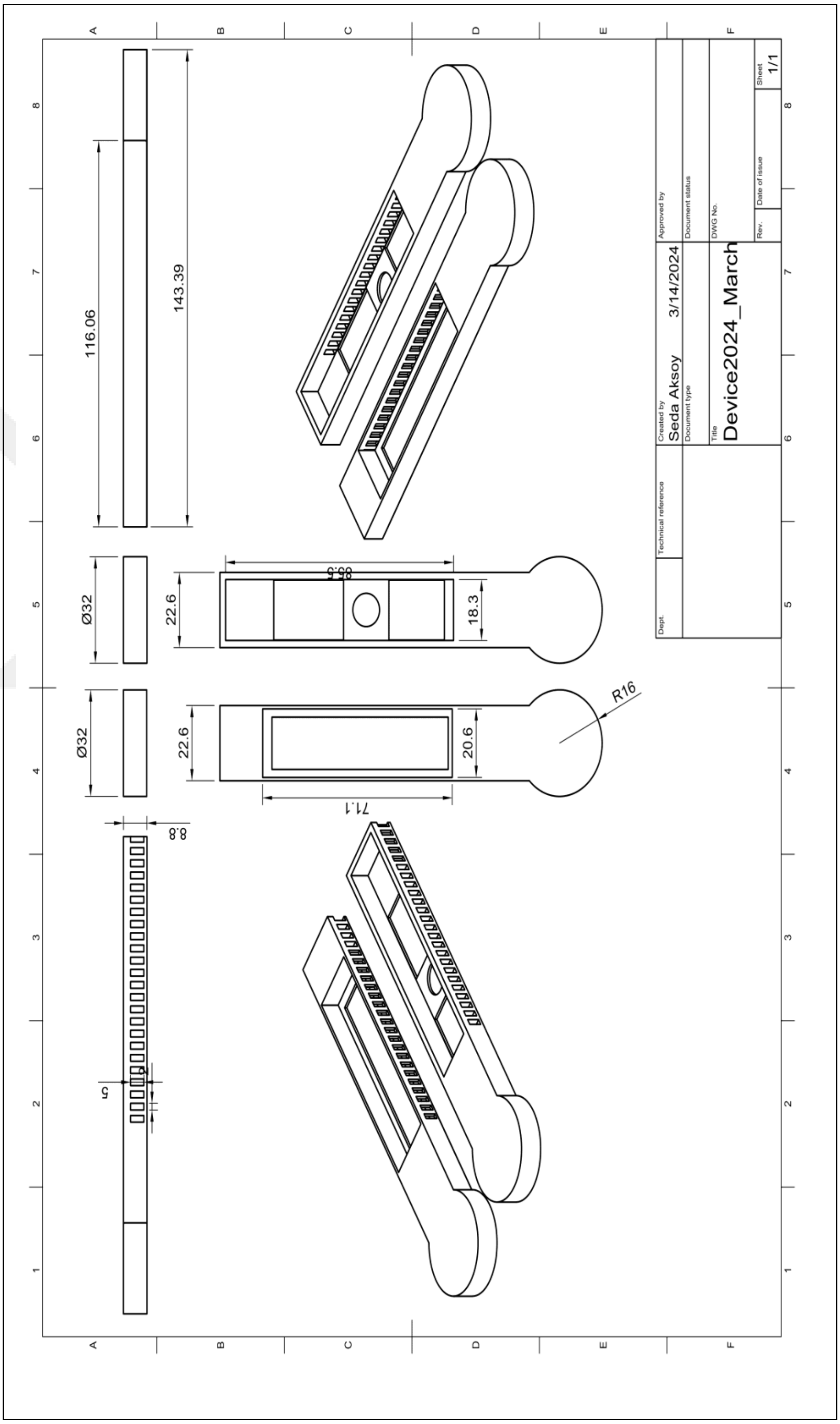

Figure D.1. Final cassette holder.

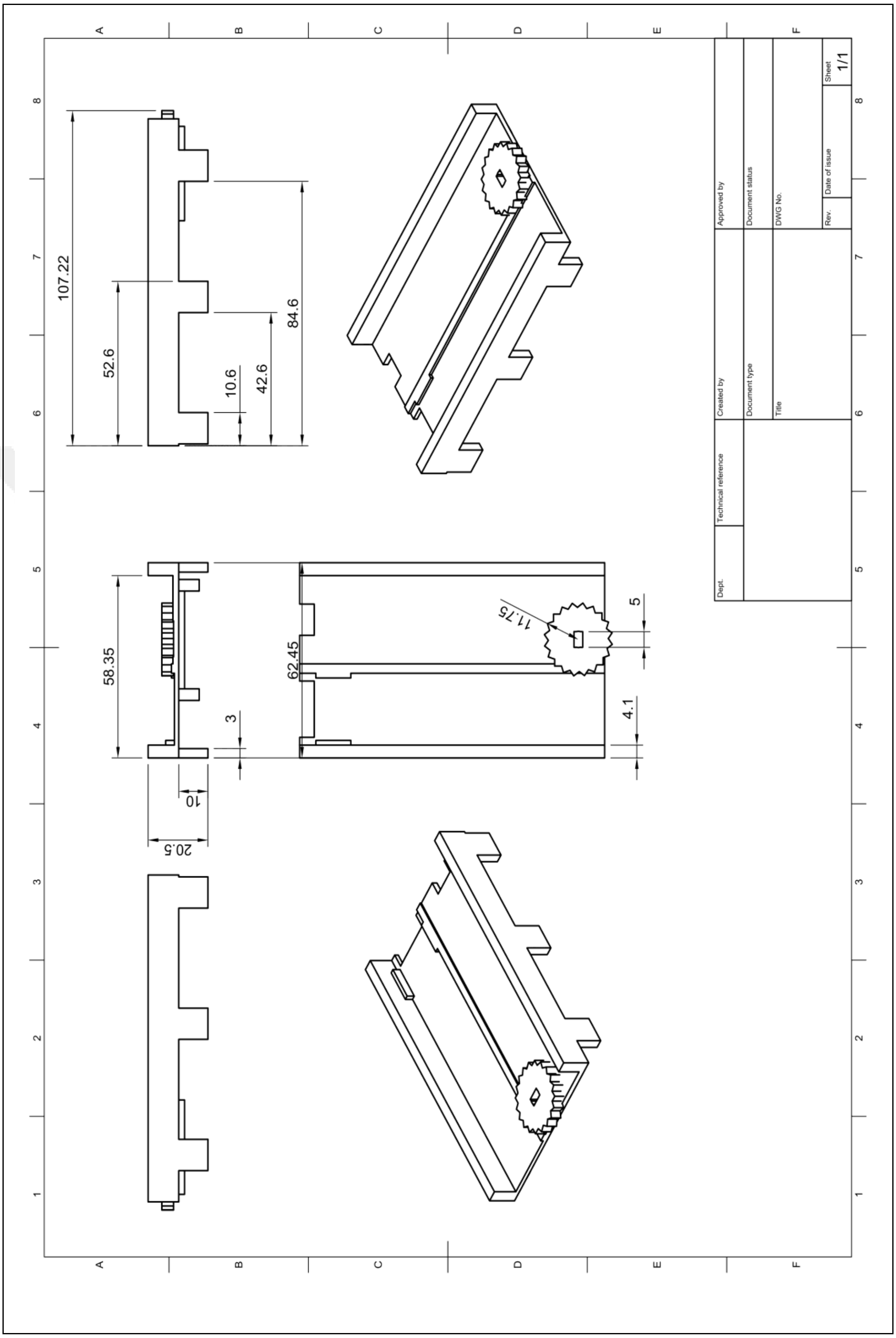

Figure D.2. Final motorized sliding tray.

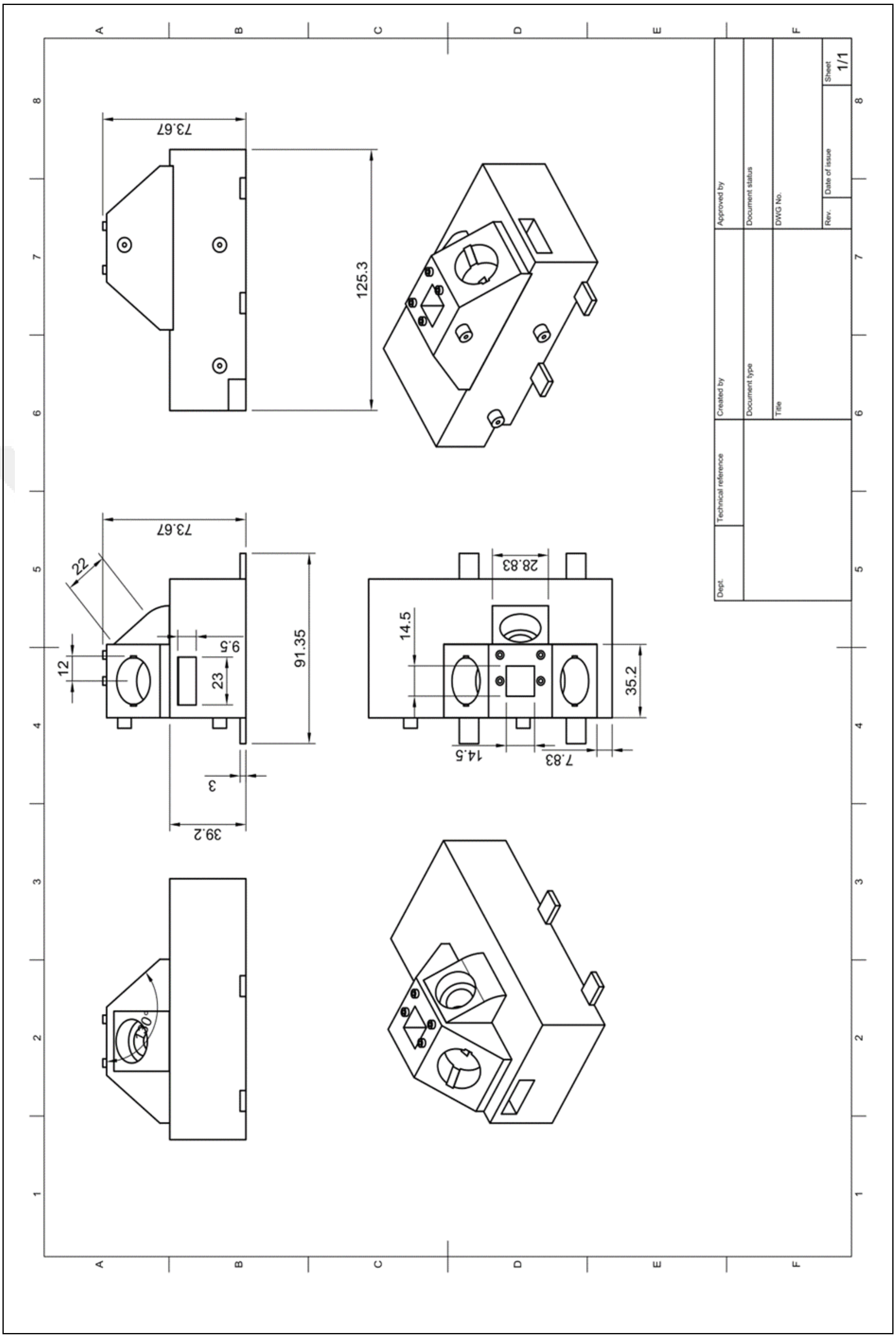

Figure D.3. Final darkroom.

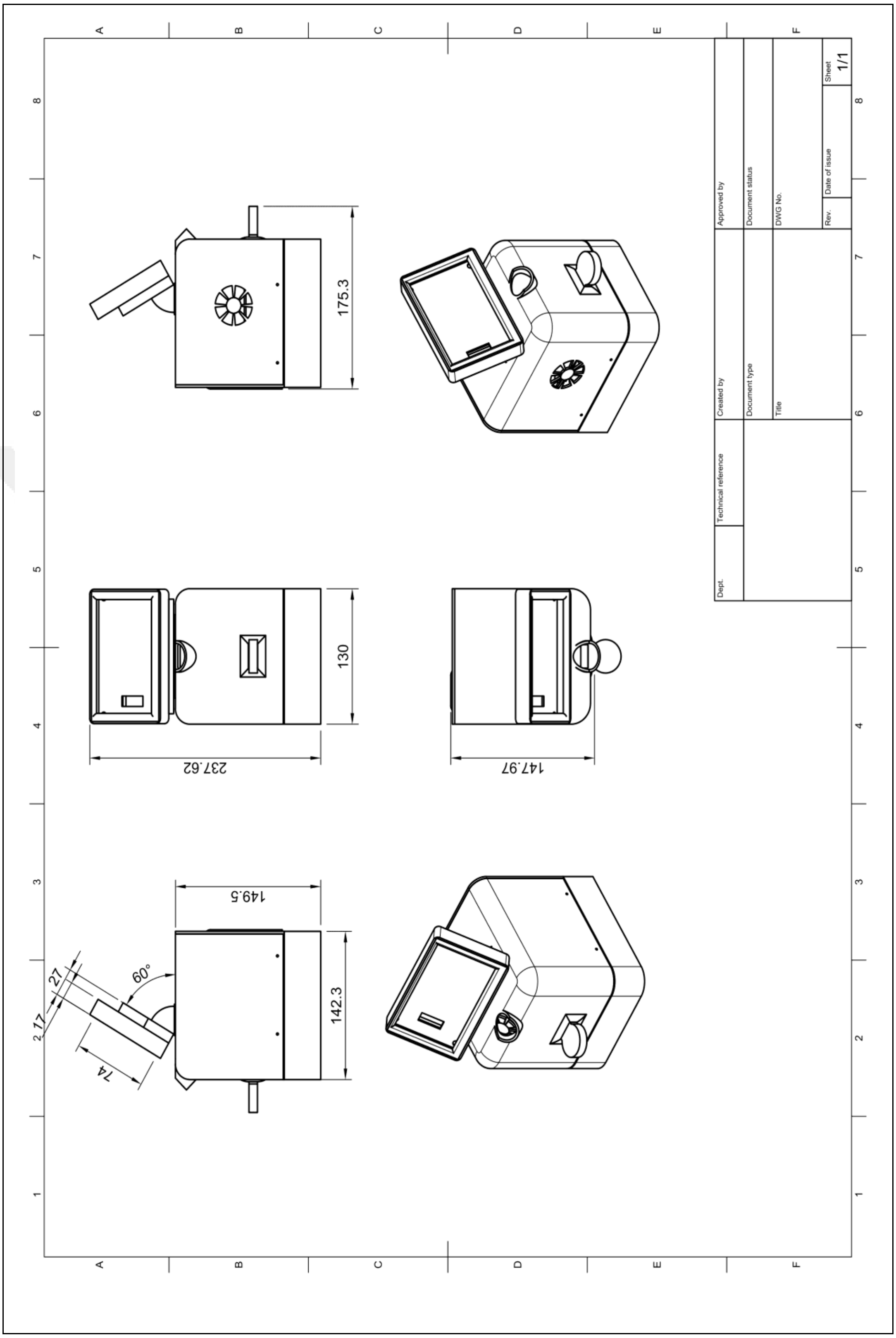

Figure D.4. Final optical reader enclosure.